THE USE OF METEOSAT SATELLITE DATA FOR SPATIAL RAINFALL ESTIMATIONS AND HYDROLOGICAL SIMULATIONS

ALWARD NAWAZISH SIYYID

Submitted for the degree of Doctor of Philosophy

The University of Aston in Birmingham

March, 1993

THE UNIVERSITY OF ASTON IN BIRMINGHAM

The Use of Meteosat Satellite Data for spatial Rainfall Estimations and Hydrological Simulations

Alward Nawazish Siyyid

Submitted for the Doctor of Philosophy 1992

SUMMARY

Satellite information, in combination with conventional point source measurements, can be a valuable source of information. This thesis is devoted to the spatial estimation of areal rainfall over a region using both the measurements from a dense and sparse network of rain-gauges and images from the meteorological satellites. A primary concern is to study the effects of such satellite assisted rainfall estimates on the performance of rainfall-runoff models.

Low-cost image processing systems and peripherals are used to process and manipulate the data. Both secondary as well as primary satellite images were used for analysis. The secondary data was obtained from the in-house satellite receiver and the primary data was obtained from an outside source. Ground truth data was obtained from the local Water Authority.

A number of algorithms are presented that combine the satellite and conventional data sources to produce areal rainfall estimates and the results are compared with some of the more traditional methodologies. The results indicate that the satellite cloud information is valuable in the assessment of the spatial distribution of areal rainfall, for both half-hourly as well as daily estimates of rainfall.

It is also demonstrated how the performance of the simple multiple regression rainfall-runoff model is improved when satellite cloud information is used as a separate input in addition to rainfall estimates from conventional means. The use of low-cost equipment, from image processing systems to satellite imagery, makes it possible for developing countries to introduce such systems in areas where the benefits are greatest.

Keywords: Meteorological Satellites

Areal Rainfall Estimation

Rainfall-Runoff models

Multiple Regression

Low-cost

In the Name of Allah
Most Compassionate and Most Merciful

Dedication

To my parents, family and friends, for their love and encouragement

ACKNOWLEDGEMENTS

There are a number of people who have helped during the course of this work and in the production of this thesis.

I would like to thank my supervisors Dr J. Elgy and Dr. T.R.E. Chidley and advisor Dr. G. Collins for their generous advice and guidance on this project. Thanks are also due to Dr. M. Salim of University of Central England, Dr. Chris England of Imperial College, London and the staff at the National Rivers Authority for the provision of technical data. Credit is also due to all members of the Remote Sensing Unit (past and present) for their assistance and friendship, especially Dr. D. Flach (Space Technology Systems) for help in software development.

Finally, I would like to thank Space Technology Systems for the funding and the Department of Civil Engineering for the use of facilities.

Alward Nawazish Siyyid : March 1993.

Contents

List of figures

List of Tables

List of Plates

CHAPTER 1

1. Introduction

1.1 General

The study of hydrological cycle is of paramount importance to civil and environmental engineers, geologists, and other earth scientists because of the environmental significance of floods and droughts, water supply, drainage, erosion, and water quality issues. Although water covers three quarters of the worlds surface, only a small percentage is in the form suitable for human use and consumption (inland lakes, rivers, snow caps and precipitation, etc). In addition, it is also the most widely and heavily exploited natural resource. Shortages of water, in terms of either volume or quality of supply, or both, have been traditionally severe in many parts of the world, especially in Africa where severe droughts in recent years have been the focus of much World attention and is responsible for great loss of human life and misery. Concerns on the shortages of water have also arisen in areas which were previously thought to be immune to such crises. Examples include parts of northwest Europe during the summer of 1976 and parts of USA in early 1970's and forcing some of the Water Authorities in England to ban use of hose pipes and other non essential water activities. At the other extreme some parts of the world are under constant threats of floods where proper knowledge and understanding of the movement of water through the hydrological cycle are of vital importance for safeguard of life and property.

1.2 The Hydrological Cycle

The basic components of the hydrological cycle are shown in fig. 1.1 for a typical river basin catchment. The movement of water through various phases of the hydrological cycle is erratic in time and space and very complex. However, under certain simplifying assumptions, the catchment response to rainfall, evaporation and infiltration can be modelled mathematically. Such Rainfall-runoff models forecast catchment response in terms of river flows on the basis of current information on rainfall, evaporation, infiltration etc. (Anderson & Burt, 1985; Singh, 1989). Such models usually require vast amounts of data for calibration purposes and therefore found new impetus in the 70's and 80's with the wide spread use of digital computers. Among these, the Stanford Watershed model (Crawford & Linsley, 1966), Pitman model (Pitman, 1976) and more recently the SHE model (Beven et al, 1980) have found widespread use.

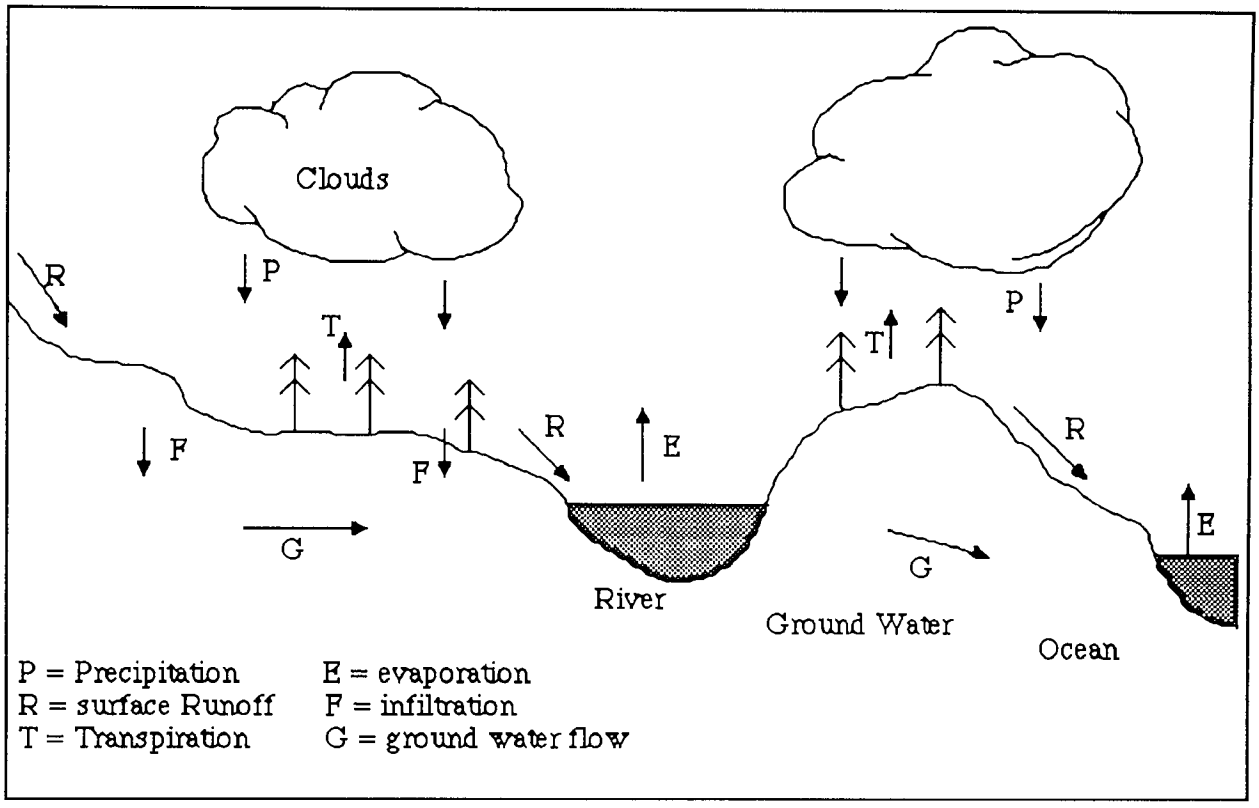

Fig 1.1 The hydrological cycle

1.2.1 Application of Satellite data in hydrology

Many of the parameters of hydrological interest are continuous in nature but can only be monitored traditionally as point data samples from a network of data stations saptially and temporally distributed within the catchment. Such networks are expensive to install and monitor. Therefore most hydrological regimes throughout the world are still devoid of suitable data sets for effective monitoring (see section 1.3).

With the advent of satellite remote sensing platforms, new possibilities of studying and monitoring hydrological parameters were opened. A satellite views the catchment as a whole and due to differences in the spectral response, many of the catchment characteristic of hydrological interests can be monitored and measured such as:

* Rainfall estimates from sequential thermal infrared and visible data, that provide information on cloud extent, temperature, thickness and height.

* Snow cover and amount, that forms vital information for hydrological regimes in which snow melt is the major contribution to river flow.

* Land-use, land cover, stratigraphy and soil type from high resolution Landsat and Spot images. Slope factors and elevations can also be assessed from stereo Spot satellite images.

* Surface Water assessments and quality monitoring

* Estimates of evapotranspiration.

* Drainage pattern and therefore sub-catchment boundaries for distributed models.

In addition, satellites are vital in an efficient data relay systems (Deutch et al, 1979; Goodison et al, 1985a, 1985b).

Definition and assessment of each of the above variables using satellite data boasts a subject area on their own. Among these, Rainfall has been of particular interest. Unlike many other hydrological parameters, it is highly discontinuous both spatially and temporally, it may fall from cloud systems with lifetimes of several days or only a few hours, it can fall from rapidly moving systems or very localised, relatively static ones; instantaneous rainfall may vary from fractions of millimetres per hour to over 100 mm per hour and the variation of rainfall intensity can be large from storm to storm and region to region (Sumnar, 1988).

1.3 Rainfall Monitoring: The present situation

Conventional rain-gauges are still operationally the major source of rainfall information in most parts of the world (Barrett & Martin, 1981). Weather radar is also used but their use has not become widespread due to the high costs involved. Rain-gauges provide point data samples of rainfall estimates and therefore the accuracy of rainfall estimates depend upon their network density and distribution. Tables 1.1 and 1.2 gives a guide to the minimum rain-gauge networks for monthly and daily rainfall estimates in relation to the size of the study area.

Unfortunately, rain-gauge densities fall well below the minimum required in most arid and semi arid areas and much of the developing World. In addition, these minimum values are derived assuming uniform networks of rain-gauges. In most cases the distribution of rain-gauges is such that majority of the rain-gauges are located near populated areas for easy access and maintenance. In general terms, the land regions of greatest deficiency include most of the arid and semi arid regions, most major mountain regions, and extensive humid regions in the tropics.

Table 1.1 World Meteorological Organization recommended minimum rain-gauge densities for different types of topographic and geographic area and daily rainfall amounts (from Sumnar, 1988).

Nature of Area	Area per gauge (km^2)	
	Normal tolerance	Maximum tolerance
Small mountainous islands with irregular precipitation	25	-
Mountainous regions in temperate, Mediterranean & Tropical areas	100 to 250	250 to 2000
Flat regions in temperate, Mediterranean & Tropical areas	600 to 900	900 to 3000
Arid and polar areas	1500 to 10000	-

Table 1.2 Minimum numbers of rain-gauges required for the adequate estimation of monthly rainfall (From Sumnar, 1988).

Area (sq. km)	No. of rain-gauges
100	5
200	6
500	8
1000	10
2000	13
5000	17
10000	20
25000	25
50000	29
100000	33
500000	36

In addition to the problems associated with rain-gauge densities, errors and ambiguity also arises in transforming point values of rainfall into total volumetric estimates of catchment rainfall and its distribution. Methods of transformation are based on various mathematical

interpolation routines. Among these methods, the Arithmetic mean, the Theissen polygons, the Reciprocal distance square method and the Isohyetal methods are the most common (Shaw, 1988; Sumnar, 1988). The choice of the method used depends on the study area, facilities available and personal preferences.

Ground based radars have also been used operationally for more than two decades in conjunction with calibrating rain-gauges. Radar has the advantage of providing areal extent of the rainfall field and can be operated continuously in time. However, there are problems associated with it that stem from the less than full understanding of the relationship between backscattered energy of the radar beam and rainfall drop-size, attenuation and absorption of the radar beam with distance and problems associated with signal calibrations and geography. Partly due to these reasons but perhaps mainly due to the costs of installation and running and maintenance, use of radar data has not become widespread outside the more advance nations of the Western world.

Satellites also have the potential to estimate rainfall and considerable efforts have been made towards this end in the past two decades (Barrett & Martin, 1981). Satellites provide greater temporal and spatial resolution and are also relatively cost effective. On the other hand they cannot detect rainfall directly and must infer it through observations of clouds tops and their properties and therefore rely heavily on the accuracy of calibrating rain-gauges or radar data. Most of the studies in this respect are from the meteorological point of view rather than hydrological.

1.4 Aim and Objectives

The main question to be answered was "How can geostationary satellite data in the form of infrared and visible images be used to improve rainfall estimates in order to improve the performance of rainfall-runoff models ?". Within this broad outline, more specific questions can be identified:

1) Firstly the relationship between the clouds observed in the satellite images and observed rainfall needed to be established. Initial investigations for such relationships were based on a review of the available literature. In addition, to gain a better understanding of the various satellite rainfall estimation techniques described in the literature, some of them were tested using local data. This is important in view of the study area which is in the mid-latitudes while most techniques were developed over tropical regions.

2) If it can be established that satellites provide useful information about catchment rainfall, the next step would be to design and test an objective methodology of

rainfall estimation, using satellite as well as ground truth data, so that improved rainfall estimates can be made. This requires comparisons with more traditional interpolation methodologies such as Theissen polygons and Arithmetic mean based on rain-gauges alone.

3) The next stage would be to investigate the effect of improvements in rainfall estimates due to satellite data on the performance of a rainfall-runoff model. This would require an understanding of rainfall-runoff models and the degree to which they are dependant on rainfall estimates. In addition, any improvement in the performance must be measured against the costs incurred. To be of practical interest, satellite data should be cost effective.

1.5 Outline of the thesis

Chapter 2 reviews critically some of the techniques developed using satellite observations to estimate rainfall. The methodologies, although essentially employing the same properties of clouds observed in satellite images, differ in their approach according to climatology, economics, ground truth data and means of statistical analysis.

Chapter 3 highlights the essential features of the Meteosat satellite. A brief discussion is presented on the methods deployed for information acquisition, pre-processing and dissemination by the European Space Agency (ESA). The description of the study area and acquisition of satellite and ground data are also presented. Satellite and ground data are two distinctive form of data and methods developed to make them compatible are discussed in some depth.

In chapter 4, some of the methodologies presented in chapter 2 were applied to the data collected for this study, in order to assess the merits of these methodologies as well as gain insight in the association of satellite observations and ground observed rainfall. The experienced gained from this preliminary investigation lead to the development of two techniques which attempt to combine satellite as well as ground data for the estimation of areal rainfall and are the subject of chapters 5 and 6. The first technique concerned itself with half-hour rainfalls and the corresponding individual satellite images while the other looked into daily rainfall accumulations daily cloud durations. Comparisons are presented with other conventional methods of estimating areal rainfall in order to assess the importance of satellite data.

In chapter 7, hydrological investigations were carried out over two different catchments which shows that satellite data can be of most use if related directly to river flow observations rather than indirectly via improving the areal rainfall estimates.

Chapter 8 discusses the results obtained in perspective and suggestions for future work and chapter 9 draws the thesis to conclusion.

CHAPTER 2

2. Literature Review

2.1 Introduction

Satellites have been launched to fulfil a large number of purposes, including international surveillance, telecommunications, geological and geophysical surveys, and crucially weather observations (Sumnar, 1988, Atlas & Thiele, 1981).

The advent of satellites and their ability to observe clouds and their properties (such as temperature, area, movement etc.) in real time made it possible to observe and estimate rainfall fields and amounts from a new perspective. Rainfall is an essential parameter in a number of meteorological and hydrological fields. Climatological and general circulation studies, validation of numerical weather prediction models and river runoff models need accurate information on precipitation. Major beneficiaries of a rainfall estimation technique based on satellite data would therefore be regions where conventional networks of rain-gauges are considered inadequate.

Subjective cloud identification using the range of imagery available is a relatively straight forward task for a skilled meteorologist. His decision is largely based on the observed cloud morphology, knowledge of weather systems and associated cloud formations, the extent of cloud shadows at ground level, its temperature and its thickness and so on. However, matching observed cloud type and distribution against ground level precipitation is quite complex due to the extremely variable nature of rainfall. Satellite imagery from weather satellites is available for the visible, infrared and microwave portions of the spectrum. Of the three, use of visible and infrared imagery is the most widespread (D' Souza & Barrett, 1988).

Numerous satellite rainfall estimation techniques have been developed over the past two decades. Many were developed and subsequently modified for particular needs in particular areas. These methods may be conveniently split under the following heads (After Barrett & Herschy, 1986):

1. Cloud indexing method - Identifying possible precipitating clouds on the basis of morphology.

2. The 'Life History' method - The sequencing of time-lapsed images to identify cloud development - especially developed for tropical areas and convective clouds.

3. Bispectral methods - Use of infrared and visible imagery in combination to distinguish the height and mode of development of possible precipitating clouds.

4. Climatological methods - For large scale mapping.

5. Textural methods - The textural properties of clouds are also investigated in addition to spectral signatures.

Description of these different approaches are presented. A brief description of the use of microwave sensor on the satellite for rainfall estimation is also presented for the sake of completion although it is still in developmental stage.

2.2 Cloud Indexing Method

This method (as the name suggests) depends on the use of visible or infrared imagery to identify "Cloud Type", and in particular those which characteristically are associated with precipitation at the ground, and relate the areas determined for possible precipitation-bearing clouds via empirical indices, to precipitation amounts over medium to long term durations. The technique involves an initial calibration period in which cloud imagery is analysed (nephanalysis) and related to ground observed rainfall to derive the empirical elements of an equation which is used to estimate rainfall amounts (Barrett, 1970).

Major cloud categories that can be identified from satellite imagery subjectively and are usually associated with rainfall (Barrett & Curtis, 1974, 1982; Barrett, 1974) are as follows:

1. Cirriform

2. Stratiform

3. Stratocumulus

4. Cumuliform

5. Cumulonimbus

2.2.1 The Bristol / BIAS Method

The initial cloud indexing method from Bristol was formulated in an attempt to use satellite data for rainfall mapping for unit periods of time (initially one month) for a large region (Barrett, 1970). Cloud indices based on cloud area, type and altitude on a grid square bases are derived and related through a table of "Meteorological Expectations" to

probabilities and intensities of resultant rainfall (see table 2.1) so that (Barrett & Martin, 1981, Barrett, 1979):

$$R = f\{ c, i(a) \} \qquad \text{eq.2. 1}$$

where R is total rainfall, c is cloud area, i is cloud type and a is the altitude. The resultant cloud indices are weighted by local synoptic weather reports and are related over time to available rain data from gauge (or radar if available) over the same period. These cloud indices are than translated into rainfall estimates through region specific regressions. An example of such regression equation is shown in fig.2.1 (Barrett; 1970, 1973, 1977a, 1977b).

BIAS (Bristol / NOAA interactive schemes) was initiated with an intention to produce techniques on the lines of Bristol method but which would be implemented on an interactive image processing system so that the routine aspects could be handled by a computer leaving only the interpretive aspects to a skilled analyst.

To automate the rainfall estimation process, a "Global regression" curve is constructed for immediate deployment in any new area. Also a "meteorological floating" scheme was devised to modify estimates whenever and wherever local station reports are available. Bias has been applied to N & S America, Europe and Asia, as well as within Africa (Barrett, 1986; Barrett & Kidd, 1988). Verifications tests carried out in America were found to be 5-25% closer to reported values than those obtained by isohyetal procedures (Moses and Barrett, 1986).

Table 2.1 Rainfall probabilities and intensities as related to satellite-observed states of the sky (From Barrett, 1970).

States of the sky	Assigned prob. of Rainfall (relative scale range 0-1.0)	Assigned intensities of rainfall (realtive scale range 0-1.0)
Cumulonimbus	.9	.8
Stratiform	.5	.5
Cumuliform	.1	.2
Stratocumuliform	.1	.01
Cirriform	.1	.01
Clear Skies	-	-

Fig. 2.1 Regression of 'precipitation coefficients' (cloud indices) versus precipitation observations for 29 stations in the Tropical Far East, March-June 1966. From Barrett, 1970.

2.2.2 Kilonsky-Ramage Method

This technique, pioneered by Kilonsky & Ramage (1976), permits an estimation to be obtained for the spatial distribution of rainfall over tropical oceans simply by integrating over a period of time the incidence of very bright clouds from visible images. The reasoning is simply that in tropical ocean areas most rainfall events are associated with convectional clouds which, because of their depth, appear very bright in satellite images. This hypothesis was tested by comparing the monthly frequencies of highly reflective clouds over coral islands in the pacific ocean with monthly rainfall measured at these islands. Over 820 station months of data were considered in arriving at the regression equation (fig.2.2):

$$Y = 62.6 + 37.4X \qquad \text{eq.2.2}$$

where Y - estimated rainfall for a month

X - no. of days during a month with highly reflective clouds.

The y intercept of 62.6 indicates that in the case of zero occurrence of highly reflective clouds, the station will still register a minimum of 62.6 mm of rainfall. Garcia (1981) justified the inclusion of a positive intercept with an explanation that it compensates for the occurrence of highly reflective cloud over stations between satellite observations.

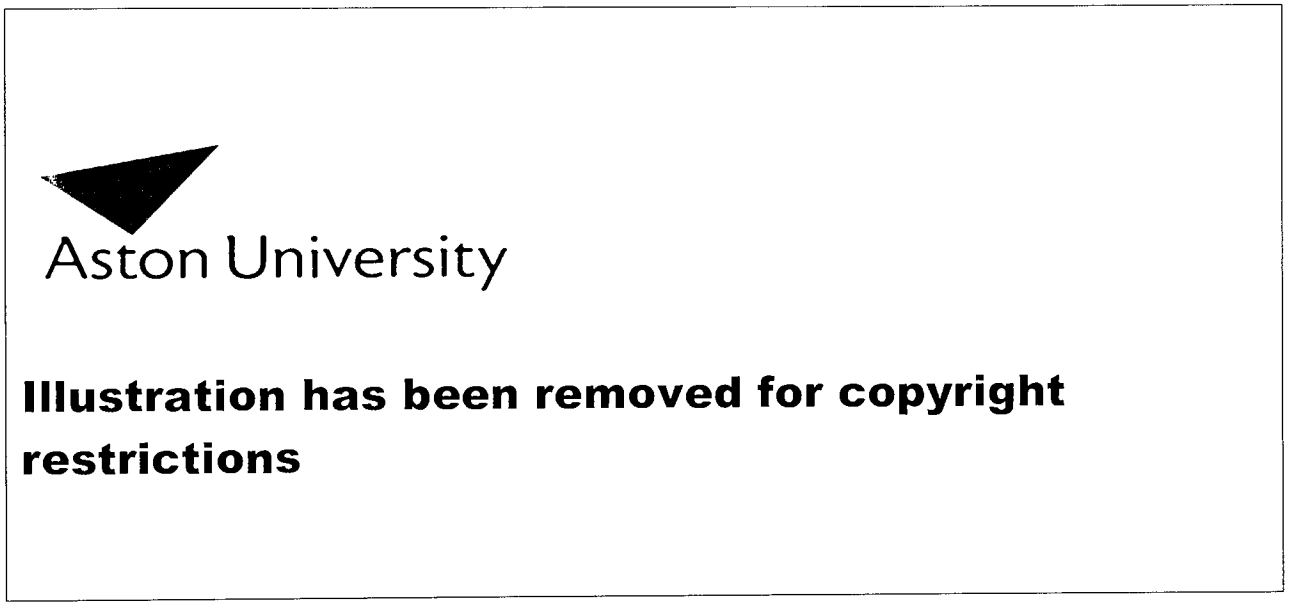

Fig. 2.2 Relationship between monthly observed rainfall totals on Pacific Ocean coral islands and the number of days with highly reflective cloud at the same locations and for the same months, as determined from NESS polar-orbiting satellite Mercator mosaics. The straight line is the least-squares best fit. From Kilonsky and Ramage, 1976.

Garcia attempted this technique for the Atlantic ocean during the period of the Global Atmospheric Tropical Experiment (GATE). He compared his estimates of rain with those of Griffith et al (1978) over 1^{o} grid square. Agreement was better for ocean areas alone than for ocean and land. Over the ocean his estimates tended to be larger by 20% for the GATE period.

Kilonsky and Ramage technique has the advantage of being simple to use and easy to implement. The disadvantage is that it relies on subjective assessment of highly reflective clouds which is very dependent on the analyst and available only during the daytime. Also, the representation of island rainfall for the ocean needs to be properly established.

2.2.3 Statistical Averaging Method

An alternative and simpler approach but one which provides estimates of daily rainfall over larger areas, is that pioneered by Follansbee (1973). The method involves the identification of the areal extent of, three main cloud types with which precipitation is most frequently associated; Cumulonimbus, large cumulus and nimbostratus. Here:

$$R = \frac{K_1A_1 + K_2A_2 + K_3A_3}{A_0} \qquad \text{eq.2.3}$$

where A_0 = area of study

A_1, A_2, A_3 = areas covered by individual cloud types

K_1, K_2, K_3 = empirical constants related to each cloud type

Initially the values of these weights were very similar to the cloud indices used by Barrett in his study of the tropical east. However, Follansbee used them as expressions of total daily rainfall, whereas Barrett had used them as dimensionless weighting factors.

The method was tested in tropical and subtropical areas with varied success. These trials revealed that :

1. Estimation of a single rainfall value obscured spatial distribution of rainfall over that area.

2. There is no flexibility in the method due to fixed nature of cloud indices.

In the modified methods, additional cloud weighting factors were introduced to take care of local effects (Follansbee & Oliver, 1975), convective nature of clouds, etc. Sampling cloud fields twice (day time visible and night time infrared) to account for diurnal variation was found to be of some success, particularly in semi arid regions. Later the method was modified and extended to mid-latitude regions (Follansbee, 1976).

Several other researchers have used the cloud indexing method for different regions. Callis and Lecomte (1987) have tried the method over the Sahelian countries of Africa. They used six-hour satellite images to calculate mean percentage convective cloud cover to form cloud indices which when calibrated against daily rainfall amounts, gave rise to region-specific regression equation. Davis et al (1971) used nine basic cloud types/formation characteristics with autumn/winter and spring/summer 12-hourly precipitation rates for a number of drainage basins in the U.S.A. The nine were, in decreasing order of precipitation intensity :

1. Bright Shield (vortical).

2. Bright band

3. Extensive convection

4. Shield fringe, desiccated shield

5. Broken dissipating band

6. Limited convection

7. Multilayered, disorganized

8. Single layered, disorganized

9. Clear or mostly clear

All these methods, although simple in perspective suffer from one major drawback; i.e. the method of recognizing cloud types is highly subjective. An analyst must have the experience and capability to recognize different types of clouds on the satellite imagery. Also, opinions on percentages of cloud cover vary from analyst to analyst. There have been attempts to objectively identify cloud types (Hawkins; 1980, Desbois et al; 1982, Parikh; 1977) with limited success. Also, the process of cloud type recognition does not lend itself easily to automation and where it is achieved (eg. BIAS, section 2.2.1), improvement in results are not significant in relation to the increased cost.

2.3 Life History Methods

2.3.1 The Griffith / Woodley technique (GWT)

Griffith & Woodley (1973) (Griffith et al, 1976, 1978, 1985, Woodley et al, 1979,1980, Augustine et al, 1981a, 1981b) developed a rainfall estimation technique based on the assumption that the evolution of clouds on the satellite images and the corresponding radar echoes approximated the simple model of fig. 2.3 in which both clouds and echoes grow to a maximum size and decay. The method is based on brightness (visible imagery) or temperature (infrared imagery) as parameters for identifying raining clouds, cloud area as the measure of the extent of the rain area and stage of development as an indicator of rain intensity.

Thresholds of 80 counts for visible and 253 K for infrared were used to define the cloud area individually. These were the optimized values obtained to give maximum correlation between cloud area and rainfall.

Fig. 2.3 An idealized schematic history of a cloud on a satellite image and its associated radar echo, in which cloud area has been defined by a threshold value and not by the visual edge. Most clouds dissipate through fragmentation rather than by the simple contraction shown here. From Griffith et. al., 1978.

Complete histories of several Florida cloud areas were obtained using satellite and radar observations to derive the empirical relationship between cloud area and rainfall. The relationships are as depicted in fig. 2.4 for visible and infrared imagery respectively. Here cloud masses viewed by the infrared or visible imagery having thresholds of ≥ 80 and ≤ 253 K respectively are related to associated radar echoes. After the determination of respective precipitation areas, all measurements for a particular cloud are normalised to the maximum area achieved by the cloud system. The ratios A_c/A_m and A_e/A_m are shown in fig. 2.4, where A_c is cloud area, A_e is the radar echo area and A_m is the maximum cloud area achieved.

From these parameters rainfall is calculated on cloud by cloud basis. It employs the relationship between rainfall volume and radar echo area of the type:

$$R_v = I * A_e \qquad \text{eq.2.4}$$

where R_v is the volumetric rainfall, A_e is the radar echo area and I is the empirical constant which can be derived for any area providing the radar data is available. From the complete histories of the subject cloud masses on the satellite photographs, the maximum cloud area (A_c) is determined for each cloud, the ratio A_c/A_m is calculated for each picture and A_e/A_m values are read from the curves in fig. 2.4. The left portion of fig. 2.4 applies to clouds growing in size while the right portion applies to clouds decreasing in size. Knowing the value of A_e/A_m and A_m, the value of A_e is obtained depending on the stage of development of the cloud mass (increasing or decreasing) and the type of imagery (visible or infrared). Consequently, rain volume is obtained using eq. 2.4.

The technique was applied to different locations (Griffith et al, 1976) with varying degrees of accuracies. The error and scatter of hourly estimates were found to be relatively large but both decreased as estimates were accumulated.

The method over the years has been applied extensively. Woodley et al (1980) applied it to the GATE area with the added modification that rainfall is inversely proportional to the cloud temperature. Therefore, three temperature ranges bounded by lower limits of 253 K, 223 K and 213 K were used instead of a single temperature threshold of 253 K. Comparison with radar and gauge measurements generally showed good agreement with overall average rain volumes, generally within a few percent.

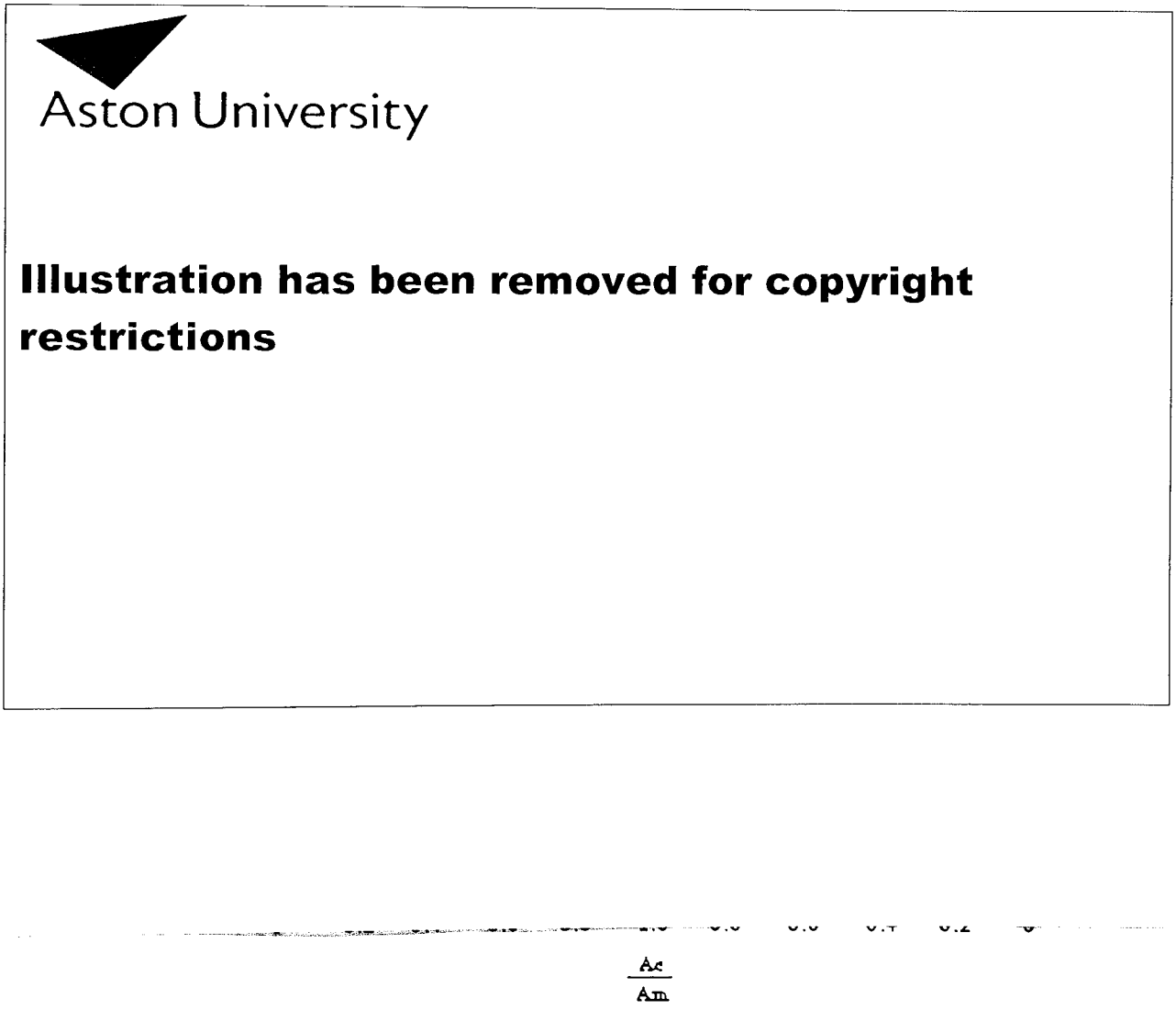

Fig. 2.4 Cloud and echo area relationships for Florida. Both cloud and echo area (A_c and A_c) are normalized to the relative maximum cloud area A_m. Data are averaged over intervals of 0.10 (A_c/A_m) Visible satellite data (top); infrared data (bottom). Infrared data have been stratified by maximum cloud area A_m. From Griffith et. al., 1978.

Griffith et al (1981) also applied the method to the extratropical area of the U.S. High Plains which showed that the technique is applicable to climatologically different regions but some adjustment is required to the satellite estimation using gauge readings.

Negri et al (1984) further explored the method in his studies and the major conclusions drawn were that the improvement in accuracy in the life history term of the GWT were not significant in relation to the extra complexity and computational effort. He proposes a simpler method of relating rainfall to the cloud area (A_c) and the infrared temperature thresholds eliminating the need to monitor cloud life cycles which can duplicate the GWT to the first order.

Recent modifications to the procedure is the so called streamlining of the technique (Griffith, 1987a, 1987b). The streamlined technique recognizes (as do other studies those by Stout et al, 1979; Lovejoy and Austin, 1979a,b ; Garcia, 1981; Negri et al, 1984) that the dependence of the inferred rainfall on the systems stage in its life-cycle is small compared with the dependence on cloud area alone. The streamlined technique is identical to GWT except that life cycle dependent terms are specified values from the life history relationships. For eq.2.4:

$$I = 16.7 \text{ mm/h}$$

$A_c/A_m=0.016$	$A_c < 2000$ km^2
$A_c/A_m=0.047$	$2000 < A_c < 10000$ km^2
$A_c/A_m=0.067$	$A_c > 10000$ km^2

Griffith found little difference in the two methods when compared with the rain-gauges but the streamlined technique required only 10% of the computation time as that of life history technique and therefore reducing the costs of the initial approach considerably. Nevertheless, the technique was developed for regions with frequent convective rainfall and is depended on the availability of radar data for calibrations and individual tracking of cloud entities requires substantial computing resources for operational use.

2.3.2 The Stout, Martin and Sikdar Technique

In the method developed by Stout et al. (1979), the volumetric rainfall is assumed to be a function of cloud area and the rate of change of cloud area. Rainfall is estimated as:

$$R_v = a_0 A_c + a_1 \frac{dA_c}{dt} \qquad \text{eq.2.5}$$

where R_v = volumetric rainfall

A_c = cloud area defined by visible and infrared threshold

a_0, a_1 = empirical constants

t = time

The method was developed to provide maps and tables of convective scale rainfall for the GATE outside the area covered by 5 cm shipboard radar.

The basis of this scheme was the observation that plots of cloud area and volumetric rainrate for particular clouds showed similar shapes (fig. 2.5), but that cloud area lagged behind rainfall. Implied here is the condition that there exist a visible or infrared count threshold which defines an area of a raining cloud closely related to production of rainfall.

To derive the empirical relationship of eq. 2.5, cloud area is defined by the threshold value of brightness (for visible images) and one of coldness (for infrared images). The corresponding volumetric rainfall rate is obtained from the radar measurements and the procedure is repeated for a cloud through its life cycle. The whole procedure is repeated for a number of chosen clouds and cloud area - rainrate pairs are used to calculate the constants a_0 and a_1 by a least square fit.

Rain estimation is made in a similar way using the derived equation to estimate volumetric rainfall rates for the interval used. Hourly comparison with calibrated radar in the GATE agreed well with correlations of 0.84, standard error 0.25 mm and the overall bias insignificant. The comparison was also made through 24h rainfall maps for two days. On both days the resolution of satellite and radar rain estimates was comparable and the magnitudes and orientation of the main centres were similar (Stout et al, 1979).

Wylie (1979) also employed this technique but found that he had to drop the areal change term and introduce a cloud model to account for different cloud environments in the mid-latitudes. This allowed the empirical relationships derived in GATE to be more applicable in other areas (eg. Montreal). Kruger et al. (1982) used a slightly modified automated version of this technique for estimating rainfall from a thunderstorm cell above the Germany/Switzerland border with relative success.

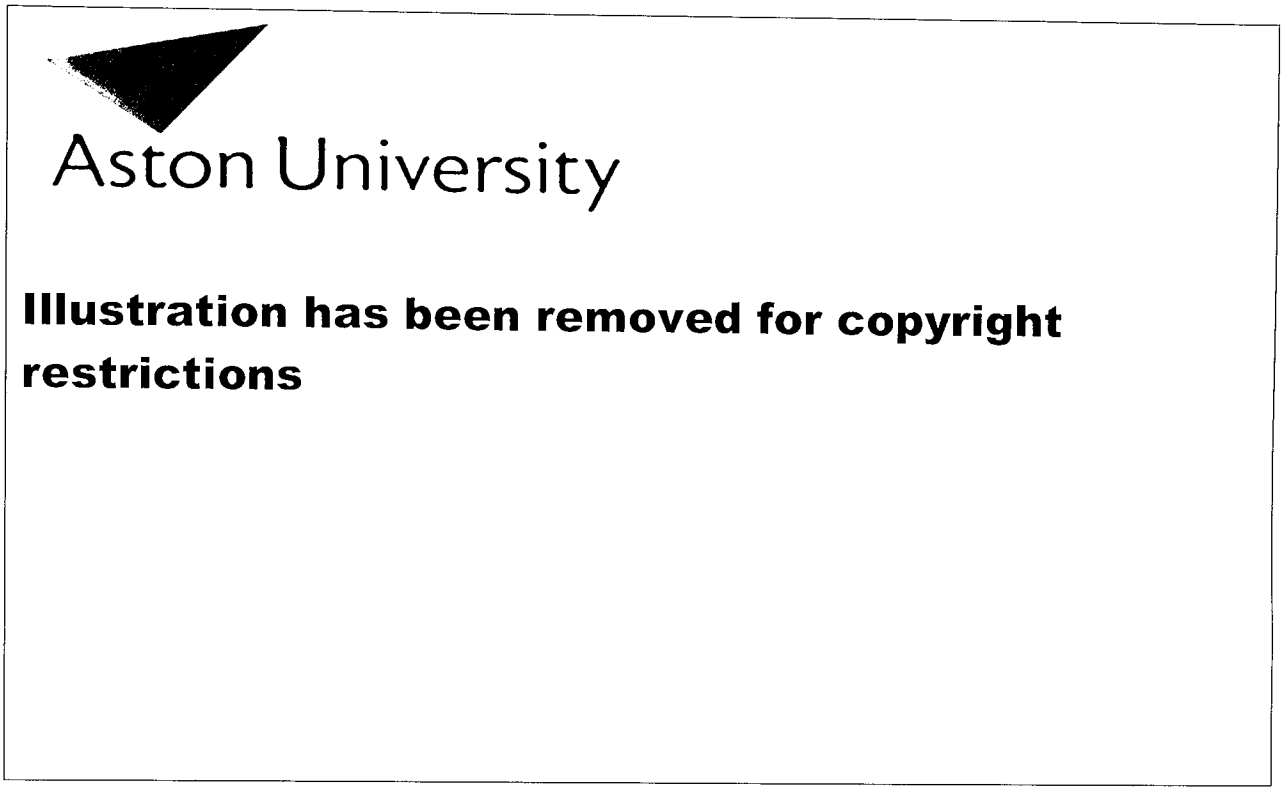

Fig. 2.5 The evolution of a typical cloud showing the linear relationship between the cloud area defined by visible and infrared images and volumetric rainfall (measured by radar, From Stout et. al., 1979).

2.3.3 Scofield & Oliver technique (Also called the Nesdis method)

This technique was originally developed to assist meteorologist in detecting flash flood producing rain storms which due to their intensity and extent cause widespread damage. Despite radar, rain-gauges and river gages, forecasters were handicapped by lack of information on the intensity and magnitude of the storms producing the floods. It is this kind of information which the method of Scofield & Oliver (1977) attempts to provide.

The technique is based on the following premises:

1. Bright clouds in the visible imagery produce more rainfall than darker clouds.

2. Bright clouds in the visible and clouds with cold tops in the infrared which are expanding in areal coverage produce more rainfall than those not expanding.

3. Decaying clouds produce little or no rainfall.

4. Colder clouds produce more rainfall than warm clouds.

5. Cold clouds becoming warmer produce little or no rainfall.

6. Merging of Cumulonimbus clouds increase rainfall rates.

7. Most of the significant rainfall occurs in the upwind portion of the convective system.

Based on these observations, a technique is developed which is presented as a decision tree (Scofield, 1987) in which point rainfall amounts are adjusted according to the presence or absence of a number of meteorological factors assessed from satellite and conventional data sources. These factors are related to observations described above and include items such as cloud shape, cloud area rate of change, atmospheric moisture etc.

Initially the technique only had three factors (Scofield & Oliver, 1977): cloud top temperature; overshooting top and mergers, but after it had been used for two years, other additional factors (Spayd,1986; Scofield, 1981, 1985) had been included. It was also modified to handle warm top clouds.

Tests of the technique involved rainfall over South and North Carolina. The location, movement and strength of the main rain area were very well reflected in 6h totals of satellite estimation. Six hour average rainfall agreed to within 0.38 cm of rain-gauge measurements and 24h rainfall was 0.13 cm away from gauge rainfall (Scofield & Oliver, 1977, McGinnis et al, 1979, Scofield, 1986).

Another verification study (Scofield, 1987) was made by comparing the total maximum rainfall estimates for a storm with the 2h rainfall. The results show the average error to be about 30 % and it increases as the magnitude of the event increases.

Various other researchers have used this technique for rainfall estimation with modifications to suit their own location and applications. Ingraham et al (1977) applied it in Venezuala and Columbia for water resources purposes. Mishra (Mishra et. al., 1988) used it in the Indian peninsula using the INSAT-1B satellite data. They found, from an independent data set, the percentage deviation of the rainfall estimates from actual lie between +111% to -43% and 85 % of the estimates lie within an error of ± 50%. Moses (1983) fitted empirical functions to the discrete values of cloud growth versus rainrate and shown ways in which a computer may be used to spread the process of making a rain estimate in flood-forecast situations.

2.4 Climatological Methods

These methods consist of those that have been designed to produce rainfall estimates over longer time periods (10 days or over).

2.4.1 The GOES Precipitation Index (GPI)

Arkin (1979) developed this method in which the fractional cloud cover colder than a certain temperature threshold was related to the accumulated precipitation. The scheme has been shown to be fairly reliable if it is integrated over an area larger than 150 * 150 km and over a longer time period than 24 hours (Richards and Arkin, 1981). In the present configuration, rainfall in 2.5 ^{o} latitude by 2.5 ^{o} longitude grid squares is estimated as a linear function of daily coverage of each grid square by cold cloud (defined as cloud with top temperature of less than 235 K), sampled at 3- hour intervals (Arkin & Meisener, 1987). Three years of precipitation index data produced from the American geostationary satellites have provided useful insights into spatial and annual variations in the diurnal cycle of large-scale tropical convective clouds and precipitation. Three month calender season estimates seem to show good overall correspondence with observed reports over the tropical oceans, but a general overestimate of areas of heavy rainfall and higher peak values during the rainy season over the Americas (Arkin and Meisner, 1987).

The precipitation index has also been incorporated into the range of routine products from the Meteosat geostationary satellite and this version is known as EPI (ESOC precipitation index) (Turpeinon et al, 1987, Turpeinon, 1986). In this version, an attempt has been made to include data from the upper tropospheric humidity (UTH) product readily available from the 6.3 micrometer water vapour channel of Meteosat, in order to account for the rate of humidity as emphasized by Adler and Mach (1984).

Verification results from country wide studies in several African states indicated that rainfall (5-day period averages) may be estimated in the tropical areas to a relatively high-level of correlation (about 0.7 correlation), while more sophisticated methods are required in the sub-tropics. Inclusion of UTH was found to be insignificant in the multiple regression analysis.

2.4.2 The Polar-orbiting Effective Rainfall Monitoring Integrative Technique (PERMIT)

As a major part of an EEC project concerned with the monitoring of pastureland ecosystems in the Sahel and mapping of cloud cover and rainfall, a simple, objective method was devised at the Bristol Remote Sensing Unit for rainfall estimation of 10-day, monthly or longer periods, using either polar-orbiting or geostationary satellite data, based on infrared temperature thresholding, climatic information and ground-station reports (if available).

Rainfall is said to be a function of cloud top temperature (area with infrared temperatures below 241K being deemed potential rain cloud), the number of raincloud days per pixel,

and a morphoclimatological weight (expressed as mean rainfall per rainday recalculated on a monthly basis); adjusted by synoptic weights related to rain-gauge data if available (Barrett & Power, 1986).

First-approximation rainfall fields are obtained as a product of the number of raincloud days and the morphoclimatic weight for each pixel. If required, these fields may be weighted by ground data to provide "Calibrated estimates". PERMIT has been applied to part of Western Sahel over two study periods, July 1985 and July 1986 (Barrett & Power, 1986, Barrett et al, 1986) with encouraging results showing "calibrated" satellite-derived spatial patterns similar to ground-reports for 10-day or monthly periods.

2.4.3 The TAMSAT Method

The Tropical Agriculture Meteorology Satellite Project (TAMSAT) at the University of Reading (Dugdale and Milford,1986, Dugdale et al, 1986, 1989) has been investigating the applicability of infrared imagery from Meteosat for the estimation of rainfall in the Sahel since 1981.

The basis of their technique is that in the Sahel most of the rainfall comes from thunderstorms which extend high in the atmosphere (Cumulonimbus cells) and therefore can be recognized in the infrared data by their cold tops. Furthermore, the longer an area is affected by thunderstorms, the more rain it will receive. In other words, the longer the cold cloud duration (CCD) over an area, the higher the amount of rainfall. To average out the variation in intensity of the individual showers, the CCD is measured over a 10 day period, which is likely to include several rainfall events.

The CCD is determined on pixel by pixel basis. Using the Meteosat infrared data, for each pixel a score is kept of the time that its temperature drops below a certain threshold temperature. The relation between CCD and rainfall is established by linear regression using rain-gauge measurements. The choice of the threshold temperature is important. It must be low enough to exclude warmer clouds which are not associated with heavy rainfall. There is no unique relationship between CCD and rainfall. It was found that the relationships varied for different months and for different bands of latitude (Carn et al, 1988). More work is currently being done to establish further the consistency of these results, and to show to what extent similar deductions can be made for other tropical areas. It was claimed that much of the scatter in the cloud duration / rainfall relationship arose from sampling errors caused by the use of a single rain-gauge to represent the areal rainfall over the pixel (Huygen et al, 1988). Work has also been carried out to introduce more factors such as latitude of a pixel and the cloud temperature itself in addition to a single CCD factor in a multiple regression model (more detail in chapter 6).

2.4.4 The FAO method

The remote sensing centre of the Food and Agriculture Organization (FAO) of the United Nations has been involved in the research and application of satellite based techniques for rainfall monitoring in Africa since the mid 1970's. These activities were carried out in the framework of FAO's programmes on Global Information and Early Warning on Food and Agriculture and on Desert-Locust Plague Prevention. In the current configuration, low resolution SDUS image data (usually between 3 and 6 per day) are analysed manually to produce probability maps of "precipitating clouds". The results are entered into a computer, calibrated by climatic background fields, and then used to provide 10 day and monthly images of estimated rainfall (Hielkema et al, 1986). The estimated rainfall for any period for any grid square is effectively calculated as the number of estimated raindays during that period, multiplied by a corresponding morphoclimatic weight for the same grid square. This weight is the average rainfall per rain day statistic calculated from climatic data of mean monthly rainfall and mean number of raindays.

Initial Verification studies have indicated that the estimates reflect the general spatial distribution of rainfall and that better correlations are obtained over longer periods of time (Hielkema et al, 1986).

2.5 Textural And Statistical Methods

These methods employ various other meteorological parameters in addition to spectral values of the visible and infrared images in order to distinguish between raining and not-raining clouds. Whitney and Herman (1979) used a total of 22 different parameters such as height, dew point data,infrared gradient etc. in a multiple regression analysis to find the best correlated parameters. Six different parameters were found giving a correlation coefficient of 0.8 but were also found to be heavily location dependent. Weiss and Smith (1987) focused their studies on the problem of discriminating areas of intense rainfall from light and non-raining areas within convective clouds using similar techniques. They employed 17 different parameters derived from the infrared imagery and using the technique of discriminant analysis found that the parameters : coldest top temperature, spatially averaged cloud top temperature and the change over time of average cloud top temperature worked best when overall convective activity was great. The method managed to identify the heavier rainfall events ($\geq$ 10 mm/h) from the more frequent light and no-rain events. Wu et. al. (1985) employed a pattern-recognition algorithm applied to single (infrared) or pair of images (visible and infrared). The algorithm classified rain into three classes, namely: 0.0-0.5 mm/h; 0.5-5.0 mm/h; and over 5.0 mm/h. Textural and radiance features over grid squares of 20 * 20 km were classified in a hierarchical decision tree. The radiance features included maxima, minima, and means; and the textural features included

edge strength per unit area; and the maxima and means of mean, contrast and angular second moment in four directions.(See also Lee & chin, 1983; Lee et. al., 1985 and section 4.3.3)

It was found that case studies that employed visible and infrared data identified correctly rain/no-rain in 90% of the cases (as verified by ground radar). 70% of the estimated rain pixels were correctly separated into classes 1 and 2. Specifically, the addition of texture features along with radiance features raised the skill score in identifying rain from 56% to 83%. However, output is in the form of digital images with 20x20 grid squares (rather than individual pixels). Also, Wu et. al. (1985) found that the best results were obtained for images with higher spatial resolution. Poorer results therefore may be expected at night-time when only infrared imagery (coarser spatial resolution than visible) is available.

2.6 Bispectral Methods

2.6.1 General

Cloud indexing, life history and the climatological methods discussed above make use of imagery from satellites in a way, which tend only to consider either visible or infrared images in their interpretation of rainfall fields or amounts. Infrared sensors provide information on the temperature and thus (indirectly) on heights of the tops of clouds. Visible sensors provide information on the thickness of clouds, their geometry and composition. By themselves these data sets sometimes fail to provide accurate information on where rain is falling and where not. Bispectral methods were designed to combine these two separate pieces of information with an assumption that the accuracies obtained in this way would be greater than using either of them separately. The following sections discusses some of the work done in that prospect.

2.6.2 The Lovejoy-Austin Method

The first major study on the estimation of rainfall with bispectral imagery was carried out by Lovejoy and Austin (1979a) in Montreal.

They developed a technique which concerned itself with the delineation of rain area rather than the rain amount. They argued that there is little or no information about the rainfall rate since visible and infrared wavelengths predominantly respond to abundance of cloud particles and not to the precipitation size particles. Rain area delineation however is of value too when used with synoptic charts and for short range forecasting.

They used the statistical pattern recognition approach to delineate rain areas. With radar as ground truth, they defined the following variables :

NN = Correctly classified no rain points

Nr = Incorrectly classified no rain points

RR = Correctly classified rain points

Rn = Incorrectly classified rain points

and defined a loss function:

$$f = \frac{Rn + Nr}{R + N} \qquad \text{eq.2.6}$$

Where $R = RR + Rn$

$N = Nn + Nr$

For a specific area (over which the coverage by the training radar is available), the probability of rain is derived by considering the bivariate frequency distribution in the visible / infrared domain of the raining and non-raining points (fig. 2.6). This probability field is optimized by minimizing eq.2.6 and adding an additional constraint that the scheme must classify approximately the same number of points into the rain category as there were radar-determined rainpoints, thus guaranteeing that the satellites-derived rain map had approximately the same area as the radar one. The optimized field for a particular day is also shown in fig. 2.6 with the corresponding rain map in fig. 2.7.

The probability of rainfall fields or the optimum boundary was found to be relatively insensitive to diurnal and day to day variation i.e. the field occupied the same position in the visible / infrared domain for each sequence examined. The method had been applied to both Montreal and GATE data and was found to show (RR / R = 0.65 for GATE, RR / R = 0.56 for Montreal) good results when compared to ground radar data with GATE data doing 20% better than the Montreal data. This is explained due to the presence of less low thick clouds and colder convection tops found in the tropical Atlantic of the GATE area. These results were limited to the range of radar training area but the accuracy decreases with distance outside that range (Tsonis & Isaac, 1985). One explanation is that the bivariate frequency distribution, and therefore the derived probabilities of rain, are representative of the air mass over the radar covered area but they become less and less representative as the air mass changes with distance. In a real time operation of such a scheme, weather radar data must be provided.

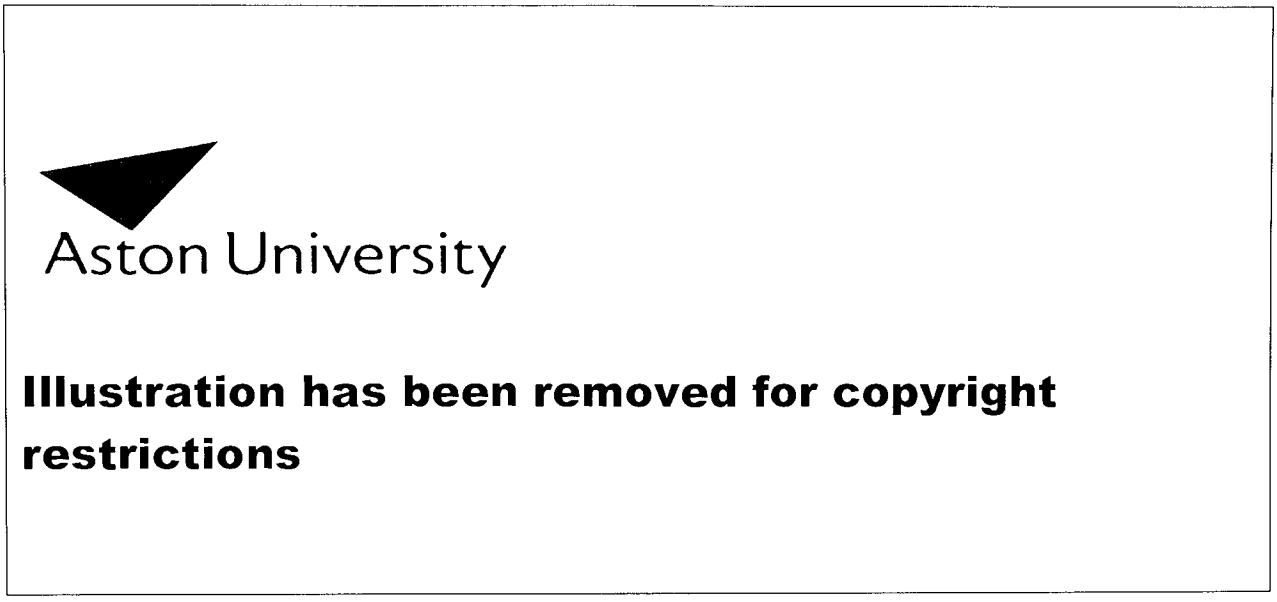

Fig. 2.6 The conditional probability of rain in percent. For any element this probability is as a percentage of all R plus all N. The 50% optimum boundary is sketched. From Lovejoy & Austin, 1979a.

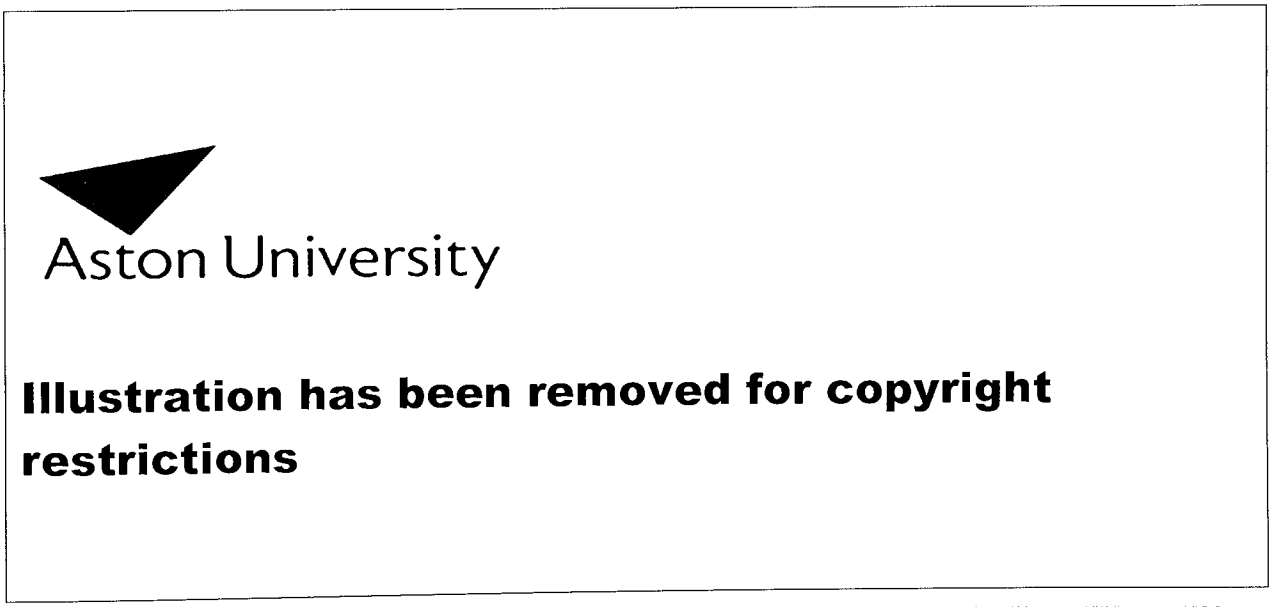

Fig 2.7 The satellite rain map produced when the optimum boundary of fig. 2.6 is applied to the same data. vertical lines are radar rain areas, horizontal lines are satellite rain areas. From Lovejoy & Austin, 1979a.

In a second study (Lovejoy and Austin, 1979b) the authors attempted to quantify the errors resulting from the rain area determination and the rain-rate determination from the satellite data. Radar echo area assumed to be equal to rain area, was correlated with volumetric rainrate (rain amount) and with echo average rain-rate for hourly periods and also for areas accumulated for up to 15 hours. For both samples, rain area was highly correlated with

rain amount (correlation coefficient = 0.9), but overall, area was weakly correlated with intensity (correlation coefficient = 0.1) thus giving support to the conclusion that determining rain area was indeed sufficient to achieve reasonable accuracy in an estimate of amount.

To assess the importance of rate, radar-area rain amounts defined as the product of echo-area and the sample mean rainrate (averaged separately for GATE and Montreal data) were calculated and compared with individually measured amounts. RMS differences, Bias (mean ratio) and error factor statistics all declined with increasing period. RMS errors for Montreal at 1 hour were 44% and 27% at 15 hour, and for GATE were 41% and 20% for one and fifteen hours respectively. These errors, originating in rate were found to be of the same magnitude as errors reported by the other techniques applied over the GATE study area (see Scofield and Oliver, 1977; Griffith et al, 1978 ; Stout et al, 1979 ; and Wylie, 1979).

2.6.3 Tsonis and Isaac Method

In recent years a series of papers were published by Tsonis and Isaac (Tsonis and Isaac, 1985; Tsonis, 1984 & 1987) in which they set out to provide a method which would be first step towards delineating instantaneous rain areas in the mid-latitudes from visible and infrared data alone. Radar data was used only for calibrating purposes. The objective was to use the work of Lovejoy and Austin (1979a,b) as the basis but without the use of coextensive radar data. The authors used normalised GOES-EAST visible and infrared images and using bivariate frequency analysis developed a clustering technique to differentiate between raining and non-raining areas. The analysis was based on the location of peak frequencies in the visible/infrared domain and it was found that these peaks can be associated with various classes present in the images (eg. land,water,snow/clear skies and clouds). The peaks found within the spectral range associated to clouds could further be divided into subclasses of "rain clouds" and "non-raining clouds" (fig. 2.8). The scheme was applied to another independent verifying sample. This provided encouraging results and the main conclusion that during daylight, the visible images contained more information about the rainfall as compared to the infrared images at mid-latitudes. However, in some instances, the infrared data were useful in the differentiation process between clouds that gave similar visible responses. The infrared data apparently contained as much information as the visible only when strong convection was present. The scheme was found to be more satisfactory in delineating instantaneous rain area in convective cases, suggesting that the method could also be applied in the tropics.

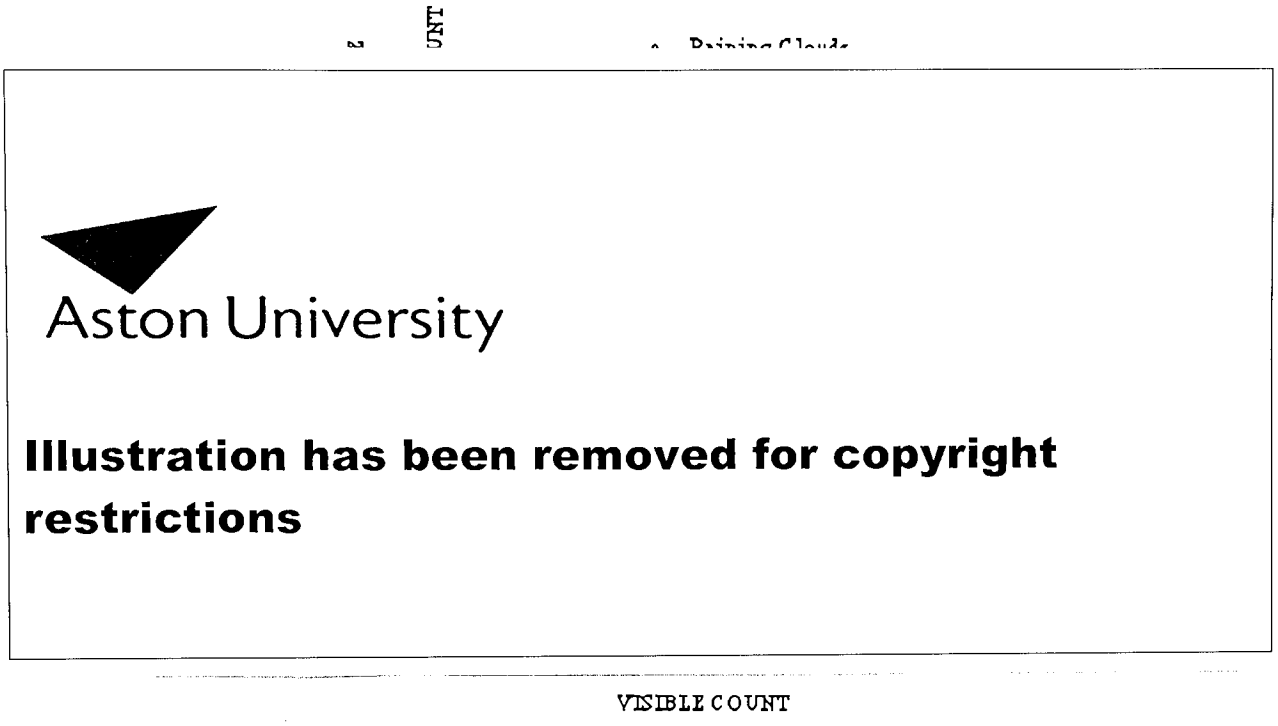

Fig 2.8 Scatter diagram of the peaks found in the bivariate analysis and their division into separate clusters. From Tsonis & Isaac, 1985.

Considering seven convective and eleven non-convective cases together, the resulting average probability of detection was 66% (range 33% to 81%) and the false alarm ratio was about 37% (ranging from 19% to 70%). The elimination of coextensive radar data in the detection process made the method simpler, more flexible and more universally applicable (Tsonis and Isaac,1985).

Tsonis (1987) adopted this method of delineating rain/no-rain areas for a sample of 25 cases over the Ontario area. A further approach was employed to extract the information within the delineated rain area to derive estimates of the intensity and type of precipitation using only the satellite data. The method involved the concept of the degree of matching between two-dimensional patterns, which could be measured by a spatially calculated cross correlation coefficient.

Results indicated, that although differing distributions of intensity inside a rain area could not be determined using this technique, it was possible to classify the overall rain system as convective or non-convective (in 23 out of 25 cases), and that rain areas themselves could be separated into two rain-classes: light to moderate (0-8 mm/h) and moderate-heavy (> 8 mm/h).

2.6.4 Other Bispectral Investigations

2.6.4.1 Bellon and Austin

Bellon and Austin (1986) investigated fourteen sequences of images during daylight hours in order to derive the relative accuracy of satellite rainfall estimation using both bispectral and monospectral methods. Both rain-gauge and radar data sets were used for ground truth and verification purposes. The study was conducted over approximately $3*10^5$ km^2 area with a gauge density of one gauge per 1900 km^2. For comparison of the satellite derived areal distribution of rainfall with gauge interpolated rainfall distribution, the weight equation of the form:

$$W_i = e^{-\frac{d_i}{y}} \qquad \text{eq.2.7}$$

where w_i is the relative contribution of gauge i to a point at distance d_i from the gauge.

was preferred over a simpler method of using Theissen polygons in which rainfall at a point is equal to rainfall at the nearest gauge. Y in the above equation is a scaling parameter and is the distance where w_i falls to 37% of its value at d=0. For convective cases, where stronger rainfall gradients are observed y is taken to be around 10 km, and for the stratiform cases where correlations are over wider distances y is taken to be approximately equal to 20 km.

Empirically derived rainfall rates as a function of normalised visible and infrared spectral values were used to derive rainfall estimates for verifying cases. Best results were obtained when rainfall rates were assumed to be the function of both visible and infrared data. Point comparisons over all the 14 sequences revealed CSI, POD and FAR (see chapter 4 for the description of these statistics) scores to be 50%, 70% and 35% respectively. Slightly improved scores were obtained when area averages satellite estimates were compared with interpolated gauge field.

In order to assess the relative accuracy of satellite estimates, rainfall pattern based on lower gauge densities are simulated by omitting a variable number of gages and then comparing the value at the unused gauge site with that of the interpolated field. By equating the satellite scores with the scores obtained from lower gauge densities fields, it was concluded that the accuracy of satellite rainfall measurements is similar to that of an interpolated field at a distance of approximately 40 km from the nearest gauge. This accuracy was equivalent to that of a network one third the density of full network where more than 50% of the area was deprived of a gauge within a 40 km radius. It must be noted here that these results were obtained for 2mm rainfall threshold, i.e. the statistical

figures indicate the relative skill of satellite data in delineating areas which have received equal to or more than 2mm of rainfall. This research was sponsored by the Canadian Forestry Service in order to determine the usefulness of satellite rainfall estimates over data sparse forested regions. Since the computation of forest fire indices essentially requires the knowledge of whether the ground is wet or dry, a map delineating areas of rainfall in excess of 2mm in the last 24 hours is a sufficient input. It was acknowledged that a satellite system, which basically has skill only in delineating the rain area, may well satisfy this requirement but not the needs of hydrologists.

2.6.4.2 ADMIT (Automatic Drought Monitoring Integrative Technique)

The University of Bristol submitted two different techniques: PERMIT (section 2.4.2) and ADMIT. This technique was originally developed for automated (objective) rainfall estimation over the continent of Africa based on Meteosat visible and infrared imagery for 5, 7, 10 days or longer periods. It consists of the delineation of daily rain/no-rain areas by visible/infrared bispectral thresholding during daylight hours and by related temperature thresholding during night time. The night-time temperature thresholding is constrained within dilated daytime rain/no-rain boundaries, thereby using indirectly the information relating to cloud thickness provided by the visible imagery, and so reducing problems of cirrus contamination. Multiday initial rainfall estimates are made by the multiplications of estimated numbers of raindays by maps of mean rainfall per rainday constructed for each period of application from climatological data sources. (Barrett & D'Souza, 1985, 1986a, 1986b, Barrett et al, 1988, D'Souza et al, 1988).

In its present configuration, ADMIT utilizes three pairs of daytime visible/infrared and three night-time infrared images per 24h period. It has been tested over the whole of Africa (at a reduced resolution) for January and July 1985, at full resolution over the Western Sahel during July 1985 and 1986, and over East Africa for July 1985 (D'souza, 1988, D'souza et al, 1988).

The only apparent difference between PERMIT and the ADMIT techniques is the use of visible imagery in ADMIT for delineation of rain areas.

Snidgers (1988) evaluated both these techniques and the TAMSAT technique of Milford and Dugdale (1986) and found none of the techniques giving overall better results than the other. The overall performance of the adjustment factors using conventional data sources were worse than the unadjusted indicating that the validity of adjustment based on observed rainfall has a rather limited spatial extent. The results from the ADMIT when compared to those from PERMIT indicated that the advantage of the use of visible channel data in addition to infrared is minor, atleast for the area and period of that study.

2.7 Use of Microwave Imagery

Finally some comments should be made concerning the use of Microwave imagery. Use of cloud indexing, life-history and Bispectral techniques yield measures of precipitation only indirectly, normally where it is also possible to calibrate the various measures of cloud morphology, with ground based precipitation observations. Microwave sensing provides a further means of obtaining a measure of surface precipitation directly. At the Microwave wavelengths, the atmosphere is nearly transparent where no precipitating clouds occur. Where there is a high humidity in the atmosphere and in particular where clouds are actively precipitating, higher microwave emmissivity occur.

Microwave technology has generally been applied to determine precipitation over the oceans where the change in emmissivity is more detectable due to precipitation against the background emmissivity caused by the ocean surface which is much more uniform. Over land, the changes in the emmissivity is not easily distinguishable due to variation caused by different land features and surface types (Fowler et al, 1979, Ferroro et al, 1988; Spencer & Goodman, 1988).

The advantage of a microwave technique as opposed to one based upon visible and infrared is that the microwave measurements respond directly to the column of rain, while the visible / infrared can only indirectly determine the presence and intensity of rain. The present disadvantages of microwave technique are the poor spatial resolution (25 km versus 2.5 km) and lack of global coverage. Future technology will undoubtedly improve the resolution of the microwave instruments and future satellite missions will provide near global coverage. For eg. the recently launched (June 1987) Special Sensor Microwave Imager (SSM/1) with its 1392-km swath width and near sun-synchronus polar orbit can provide twice daily coverage over a large portion of the earth (Barrett et al, 1987, 1989a, 1989b, Barrett & Kidd, 1988).

2.8 Summary and Discussion

As can be seen, researchers over the past two decades, since the launch of first weather satellites in space, have developed different techniques to extract maximum information from the satellite images. The techniques developed were influenced by various factors such as :

* Requirement of the end user

* Availability of satellite and ground truth data

* Quality of ground truth data

* Location and weather conditions that prevailed in the area of interest

* Size of the area concerned

* Type of processing equipment and manpower

In general methods have been developed which :

* may be manual, interactive or entirely automatic

* may produce short period estimates or they may produce daily, weekly, or monthly estimates of rainfall

* may vary spatially from pixel size (typically 5 x 5 km) to thousands of km^2

* may be based on infrared or visible or both combined

* may have variable image frequency

* may be verified against point or areal, rain amount or rainrate, daily, weekly or monthly rainfall totals

In view of the points mentioned above, comprehensive comparison of the above methods is difficult although general points can be made.

* Cloud indexing methods are designed to make rainfall estimates with small image data frequency (as few as 3 to 4 a day) and for weekly or longer periods. They rely on an expert analyst to assess the various parameters of cloud to derive the indices.

* The life-history methods were found to be highly complex and labour intensive and the increase in the accuracies were insignificant due to the life-history term in the equation and was subsequently abolished in favour of a simple correlation between cloud area and areal rainfall.

* Textural and statistical methods employed more sophisticated techniques of pattern recognition in their effort to distinguish between rain/no-rain points but while they show considerable promise, they also increase the complexity as well as the processing time required.

* The bispectral method of Lovejoy and Austin (1979a,b) is also fully automated, but this make no assessment of rainrate, only rain area. Also it must have atleast one calibration weather radar data within the area of interest.

One explanation for the limited success of all these methods lies in the nature of rainfall itself which is highly variable in its areal and temporal extent. Satellites at best can only observe cloud fields from the top and based on their radiance properties can infer if that particular cloud field is capable of producing rainfall. Problems arise when one tries to apportion rainfall amount to that particular cloud system and how it is distributed spatially and temporally. A cloud system with particular infrared and visible properties may produce rainfall ranging from little to very high amounts with high areal and temporal variability. This is why Tsonis (1988) and Hogg et al (1988) found that simple thresholding techniques for estimating rainfall from satellites perform as satisfactorily as more complicated ones. It also explains why estimates improve as compared to ground truth when averaged over long periods (daily or longer) and areas (typically 1000's of km^2).

To estimate the accuracies of satellite rainfall estimates, complicated statistical procedures have been employed by several researchers but very few have attempted to define the accuracy of their method in terms of equivalent rain-gauge density network. Griffith et al (1981) found that in statistical terms their technique is equivalent to a rain-gauge density of 2837 km^2/gauge for an area of 10000 km^2 and 700 km^2/gauge for an area of 2220 km^2; i.e in each case 3 to 4 rain-gauges in the area exhibit the same amount of error as the satellite method. Bellon and Austin (1986) similarly found a gauge density of 6000 km^2 / gauge for their study area of 100000 km^2. Very little work has been done to combine available ground truth data with the satellite data. The usual method that was employed was to adjust the satellites estimates using the rain-gauge data and not vice-versa i.e using satellite data to improve the rain-gauge estimate.

Chapter 3

3. Data Acquisition and Processing

3.1 Introduction

The impact of geosynchronous satellites in the field of meteorology has been commented on by many writers. The ability to observe weather features in remote regions which were previously void of observations has extended the capabilities of national weather forecasting offices throughout the world. Extraction of information from these multi-spectral images for the purpose of rainfall monitoring and estimation in the main involves identifying the area of interest on the images and relating the image data with the ground based observations which may be in the form of ground-based radar echo data or point rain-gauge readings.

However, prior to such analysis, the space-borne observations and the ground-based observations are required to be processed and integrated to a common format which involves: the acceptance of the image data; assessment of the spatial relationship between the image data and the ground-based map data and; processing of the ground-rainfall data.

This chapter reviews the Meteosat satellite system and the image products that are made available to the end user. This is followed by a description of the study area, data acquisition and an algorithm developed to spatially relate the satellite image data with the ground map data of the study area. Hardware and software considerations undertaken are also presented.

3.2 The Meteosat System

3.2.1 Historical Background

In the early seventies the European Meteorological Community decided to enter the field of space meteorology.

The prime purpose of the Meteosat Programme was to meet the needs of the European Meteorological services, however, it also represented Europe's contribution to two programmes set up by the WMO:

* firstly, the World Weather Watch (WWW), a permanent undertaking to monitor the status of the earth's atmosphere;

* secondly, the Global Atmospheric Research Programme (GARP) undertaken jointly with the International Council of Scientific Unions (ICSU).

The Meteosat Programme was initiated by the French space and meteorological authorities, who performed the feasibility studies and undertook the pre-development of the satellite's radiometer.

METEOSAT-1 was successfully launched on 23rd November 1977. The primary objectives of this satellite were to provide a useful daily contribution to the WWW and to prepare the system for participation in the first GARP Global Experiment. METEOSAT-1 successfully achieved both of these objectives and the system made substantial contribution to meteorology and other Earth Sciences in the two years of operation until a fault caused a failure of the imagery and dissemination missions in November 1979. METEOSAT-2 was launched as a replacement on 19th June, 1981 and provided routine images until August 1988. A refurbished METEOSAT-3, with performance characteristics similar to METEOSAT-2 was successfully launched on 15th June 1988. This was followed by METEOSAT-4 early in 1989 and this currently provides routine images.

The full Meteosat system is presented in fig 3.1. The two major components of the system are the satellite itself and the Ground system. The satellite is situated in a geostationary orbit at 35900 km and is located over the Gulf of Guinea, at the crossing between the Equator and the Greenwich meridian (0^{o}N,0^{o}E).The main components of the Ground Station are the Data Acquisition, Telecommand and Tracking Station (DATTS) and the Meteosat Ground Computer System (MGCS). The MGCS is located in the European Space Operations Centre (ESOC) in Darmstadt, Federal Republic of Germany, and DATTS is situated in open country about 40 km from Darmstadt.

3.2.2 The Meteosat Satellite

Meteosat is composed of a main cylindrical body containing most of the satellite subsystems, including the radiometer and its cylindrical surface is covered with N/P silicon solar cells which provide the electrical power.

The spacecraft has four main thruster motors and two smaller thrusters. All are fed by hydrazine propellant from spherical tanks having sufficient capacity for a five year lifetime in normal circumstances. This system is used to maintain Meteosat's attitude in space and can be used to make small changes in orbit - principally to move the satellite in its orbital plane to make fine adjustments to the longitude over which Meteosat is stationed. In operation these thrusters are activated by telecommands from the ground stations and normally such adjustments are required every few months.

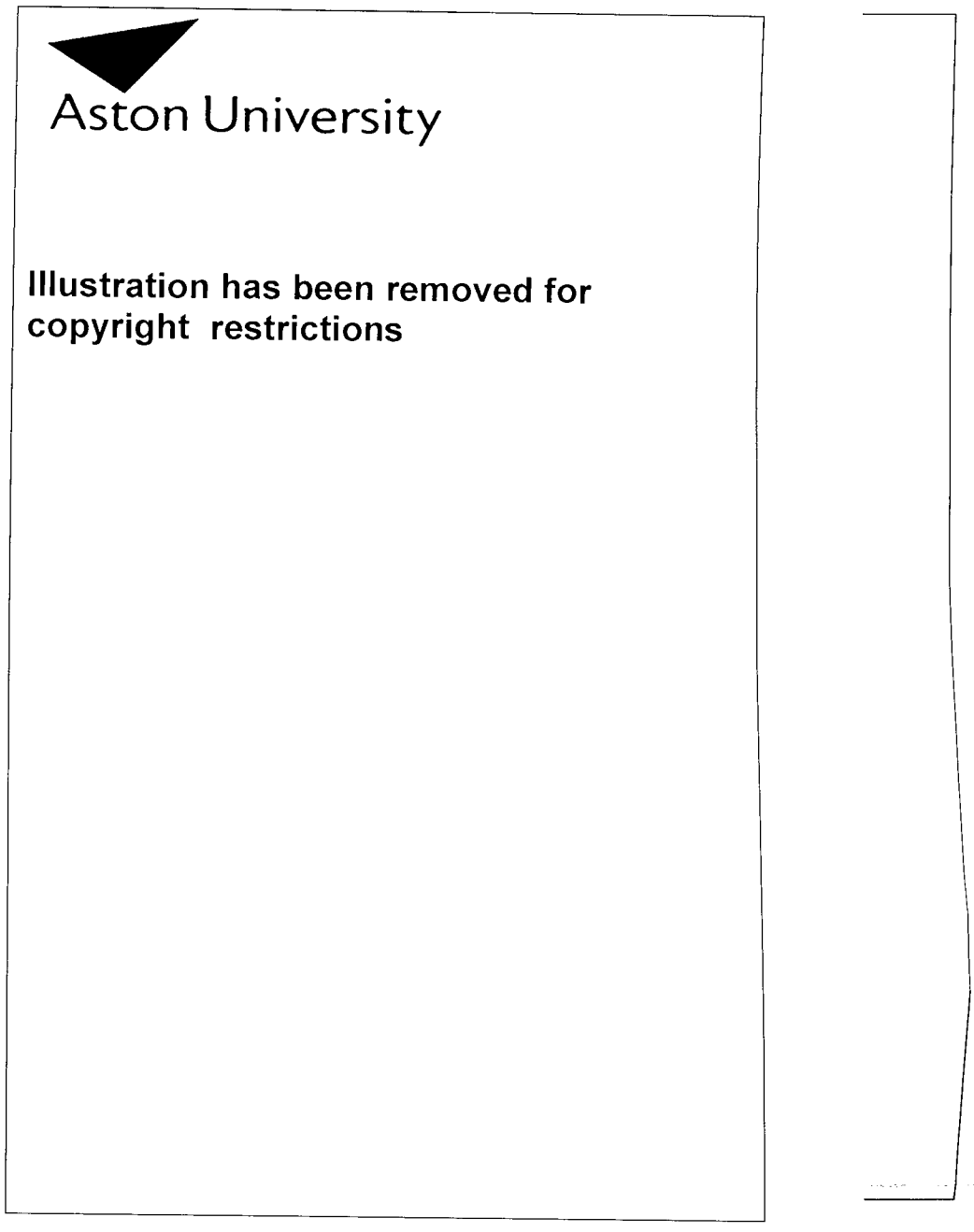

Fig. 3.1 The Meteosat System

The satellite has a comprehensive communication capabilities and operates in two distinct frequency bands. S-band (1670 - 2110 MHz) is used to transmit the raw image to the ground, to relay processed image data to user stations, for ranging (earth location) signals, for reception of telecommands and transmission of telemetry. UHF (402.0 - 402.2 MHz) is used to receive data from Data Collection Platforms (DCP).

In orbit the satellite spins at 100 rpm around its main axis, which is aligned nearly parallel to the earth's North-South direction.

3.2.3 The Meteosat Radiometer

The Four-channel, three-spectral-band high-resolution radiometer constitutes the main payload on board Meteosat. The instrument allows continuous imaging of the earth with radiance data from the full earth disc being acquired during a 25-minute period. This is followed by a five minute stabilization period, so that one set of images is available each half hour. The main Radiometer characteristics are summarised in table 3.1. An image consists of a raster of pixels and is telemetered line by line to the ground station. An East-West line of pixels are generated as the radiometer scans the Earth's disk due to the spinning motion of the satellite. A succession of lines is obtained by rotating the radiometer telescope stepwise from South to North synchronously with the satellite spin period.

Table 3.1 Radiometer Characteristics

Characteristics	Visible	Infrared	Water vapour
Spectral bands (μm)	0.5 - 0.9	5.7 - 7.1	10.5 - 12.5
Detector type	Si photodiodes	HgCdTe	HgCdTe
dimensions (μm)	250 x 250	70 x 70	70 x 70
field of view (mrad)	0.07	0.14	0.14
Detector temperature		90 K	90 K
Number of lines per image	5000	2500	2500
Telescope			
primary aperture		400 mm diameter	
secondary aperture		140 mm diameter	
focal length		3650 mm	

Each infrared image is composed of 2500 lines and 2500 picture elements (pixels) with the spatial resolution of 5 km at the subsatellite point. The visible image has twice the resolution with 5000 lines and 5000 pixels in each line since two visible channels are operated side by side.

3.2.4 Meteosat Ground Station

The Ground Station supports all activities required to control the spacecraft and ensure that the mission objectives are met. The functions of the ground station include spacecraft and payload control together with the collection, processing and redistribution of the data via the satellite or surface telecommunication links.

The raw image data are transmitted to the Data Acquisition, Tracking and Telemetry station (DATTS). DATTS is a primary means of communicating with Meteosat from the ground. The station acts as a complex relay station and communicates the Meteosat data by ground link to the Meteosat Ground Computer System (MGCS) and Meteosat Control Centre (MCC), both of which are located within the European Space Operation Centre (ESOC) in Darmstadt.

The station receives raw image data from the spacecraft at the normal rate of 166 kb/s but can also acquire the data in 'burst' mode at 2.7Mb/s should the spacecraft's onboard memory fail, necessitating transmission at the higher rate. This received data at DATTS is transmitted to MGCS via the Data Transmission Routing System (DTRS) which includes a ground link.

The MGCS is a large computer system used exclusively for the processing of Meteosat data and for control of the spacecraft. As well as the primary data link with the DATTS, the MGCS is also connected by a computer-to-computer link with the meteorological Global Telecommunication System (GTS). This allows parameters extracted from the image data to be transmitted to the user community. The link is also used in in the reverse direction, since conventional meteorological data are needed for the computations made within the MGCS, and some data received this way may also be disseminated via the spacecraft to the data user station.

The Meteosat Control Centre (MCC) is where all spacecraft and mission control function are carried out and the operation of the DATTS is monitored and controlled. Any parameter extraction is accomplished here.

The raw image data from the spacecraft are transmitted on a line by line basis to the DATTS, and from there transmitted by landline to the MGCS. When they arrive in the MGCS the data is pre-processed by the computer system prior to their use for dissemination, meteorological parameter extraction or archiving. The image processing consist of three stages:

* Raw image acceptance

* Image conditioning

* Image rectification

3.2.4.1 Raw Image Acceptance

The acceptance of the raw image data is accomplished by one of the Front End Processors (FEP) working in a real time mode, accepting and processing the data at a rate of one line every 0.6 seconds.

The image data arriving at the FEP are in line by line format in the original order as sampled by the satellite radiometer. Each line is composed of 48-bit words, containing interleaved visible, infrared and water vapour data. The main task of the FEP is to separate the raw image data into the different radiometric channels. The raw image data is also stored as a safety measure.

3.2.4.2 Image Conditioning

Conditioning of Meteosat images involves the removal of any defects that may arise due to faulty instrumentation. The software is designed to remove defects caused by optical errors in the radiometer; errors in the detector responses; errors caused by electronic filters etc. The parameters on which corrections are based are calculated on the main frame computer.

3.2.4.3 Image Rectification

The purpose of image rectification is to locate the image in terms of earth coordinates. This is necessitated by the fact that no geostationary satellite is truly fixed in position with respect to the earth. Minute changes in altitude, orbit position, spin speed and scan line start causes actual images to be deformed with respect to a reference image which is deemed to be taken under nominal conditions. These changes occur between images and to a lesser extent, within the space of one image. The deviation of actual image from the reference image is known as the deformation. The use of a mathematical model taking into account the spacecraft dynamics together with the measurements made on the received image provide a set of deformation vectors from which the geographical locations of the image pixels can be determined.

The image rectification completes the standard image processing and the image data is not changed in any way before final archiving, dissemination or parameter extraction.

3.2.5 Image Dissemination

The Meteosat dissemination system is the process whereby image data and other meteorological information are relayed via the spacecraft to the user community. This includes the relay of data using the Meteorological Data Dissemination feature incorporated on the operational Meteosat satellites.

Meteosat has dedicated two channels for the dissemination of a wide variety of data. Channel 1 operates at 1694.5 MHz and is used for digital transmissions (High resolution) and channel 2 operates at 1691.0 MHz for conventional analogue transmissions (WEFAX).

The WEFAX transmissions are in a format compatible with the transmissions from other geostationary meteorological satellites and the Automatic Picture Transmission (APT) of the polar orbiting meteorological satellites. These transmissions can be received by the simplest kind of receiving station known as Secondary Data User Station (SDUS). The high resolution digital data are in a format specific to Meteosat and are designed for the user requiring full resolution pre-processed data in a form suitable for local computer processing. Reception of high resolution dissemination data requires the more complex Primary Data User Station.

All transmissions pass along the route from the MGCS via the communications system and DATTS to Meteosat and hence to the user stations. The dissemination programme includes:

* Processed Meteosat High Resolution images.

* Processed messages from DCP's.

* Conventional meteorological charts and cloud top height extracted from the basic image data

* Administrative messages and system test formats.

After the image processing in the MGCS is completed, the images are cut into convenient formats (detailed in the following sections) and latitude and longitude grids and coastlines are added before transmission. In the case of WEFAX this information is superimposed on the actual image but with high resolution PDUS images it is added to the transmission as coded data, to be utilized as required by the individual user. Images from all three Meteosat spectral channels are included in the dissemination schedule, which is designed to include

formats covering the entire Meteosat field of view at least once every three hours and the European area every half an hour.

3.2.6 Primary Data User Stations (PDUS)

Local image processing is more generally associated with the use of PDUS, which receives digital images specifically designed for computer processing. Here the basic station consists of the antenna plus receiver and a frame synchronizer followed by a computer and associated peripheral devices (Fig. 3.2).

The image data transmitted is in the full raw data resolution of 2500 x 2500 pixels for the infrared and water vapour images and 5000 x 5000 pixels for the visible images.

The visible and water vapour images are coded in 6 bits grey-levels and the infrared in 8 bits grey-levels. The images are transmitted for user reception in two formats:

1. A - format

   The A-format represents the whole earth disc as seen by the Meteosat and is transmitted every hour.

2. B - Format

   B-format represents the European, North-Africa and Middle-Eastern regions and is disseminated every half hour (only daylight hours for the Visible).

Examples of these formats are depicted in fig 3.3. Further information relating to PDUS can be found in Meteosat system guide, vol 9 (ESA, 1981).

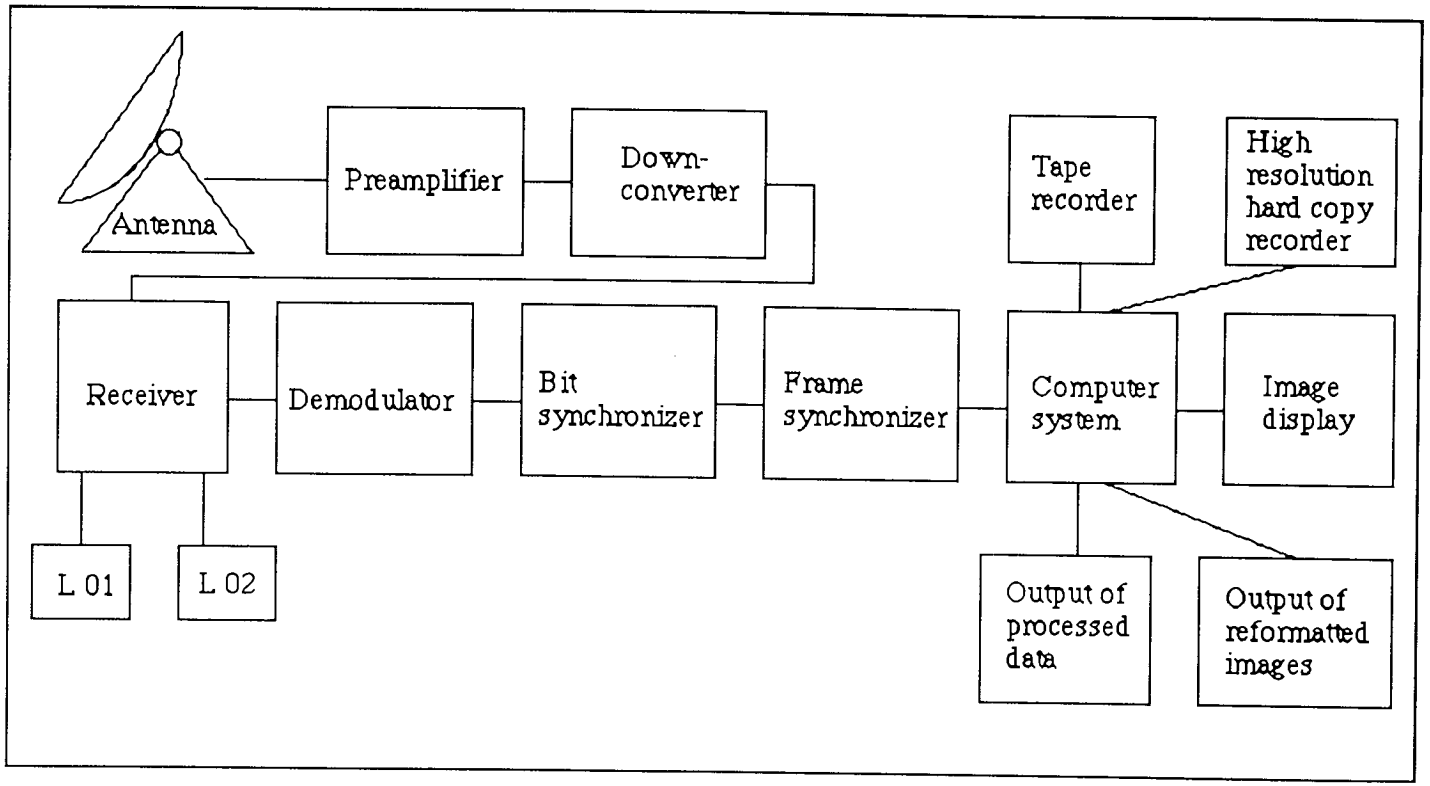

Fig 4.2 Block diagram of a typical Primary Data User Station

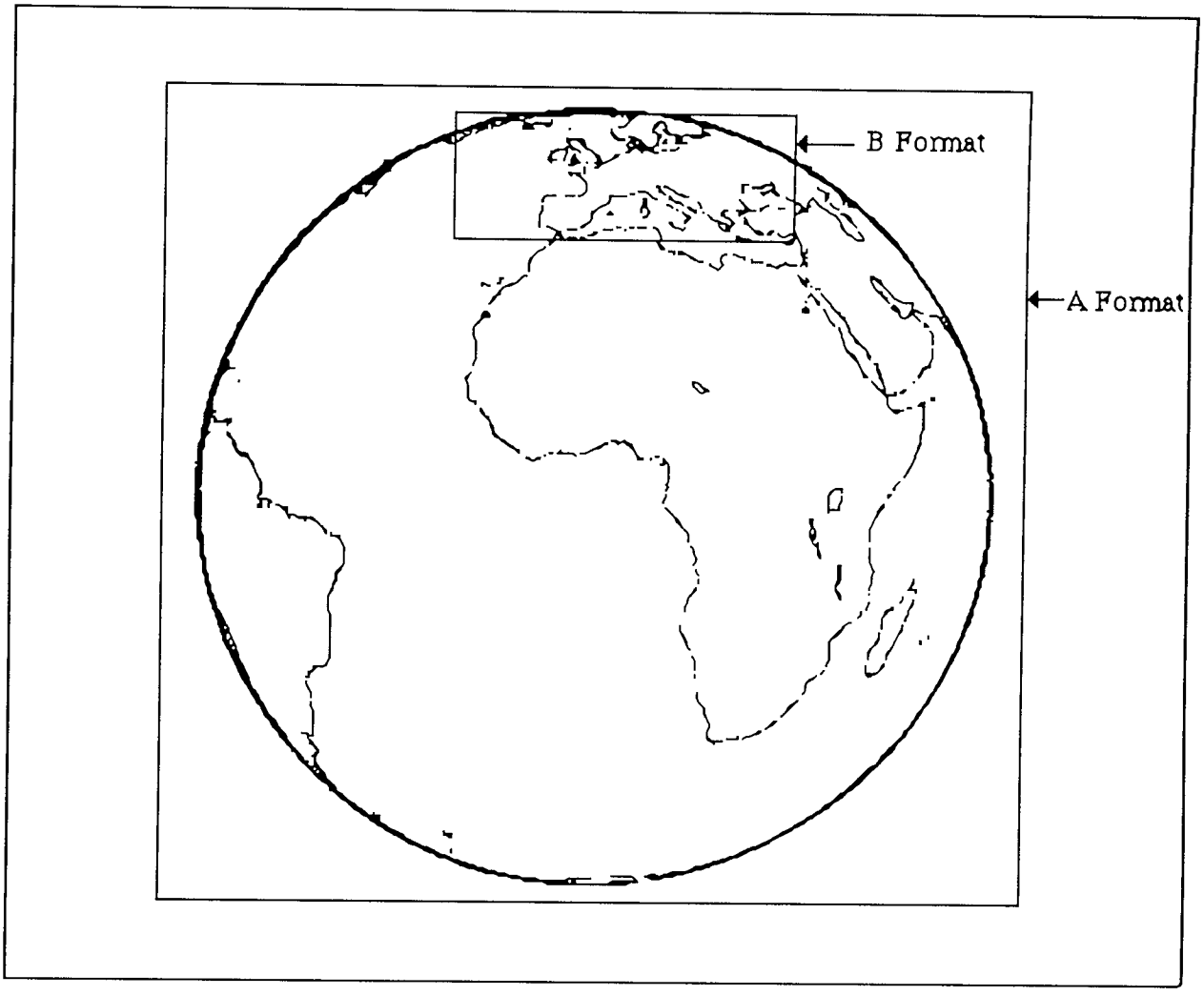

Fig. 3.3 High-Resolution (digital) PDUS image formats

3.2.7 Secondary Data User Stations (SDUS)

Basic configuration of the SDUS system is as depicted in fig. 3.4. The SDUS are generally used as display stations giving a rapid visual update of weather phenomena with no form of computer attachment. Although this is generally the case, a system can be developed incorporating a analogue to digital converter and a computer with image processing facilities which is normally associated with PDUS systems (Salim, 1989).

As indicated earlier, the images are sectored into formats. The visible images are transmitted in C-format as depicted in fig. 3.6 due to their high resolution. Infrared images are transmitted in the D-format as shown fig 3.5. The C02 and C03 in the visible and D2 in the infrared are available every half hour covering the British isles. Water vapour images are transmitted in E-formats which is the same as D-formats and their transmission rate is every 3 hours (ESA, 1980).

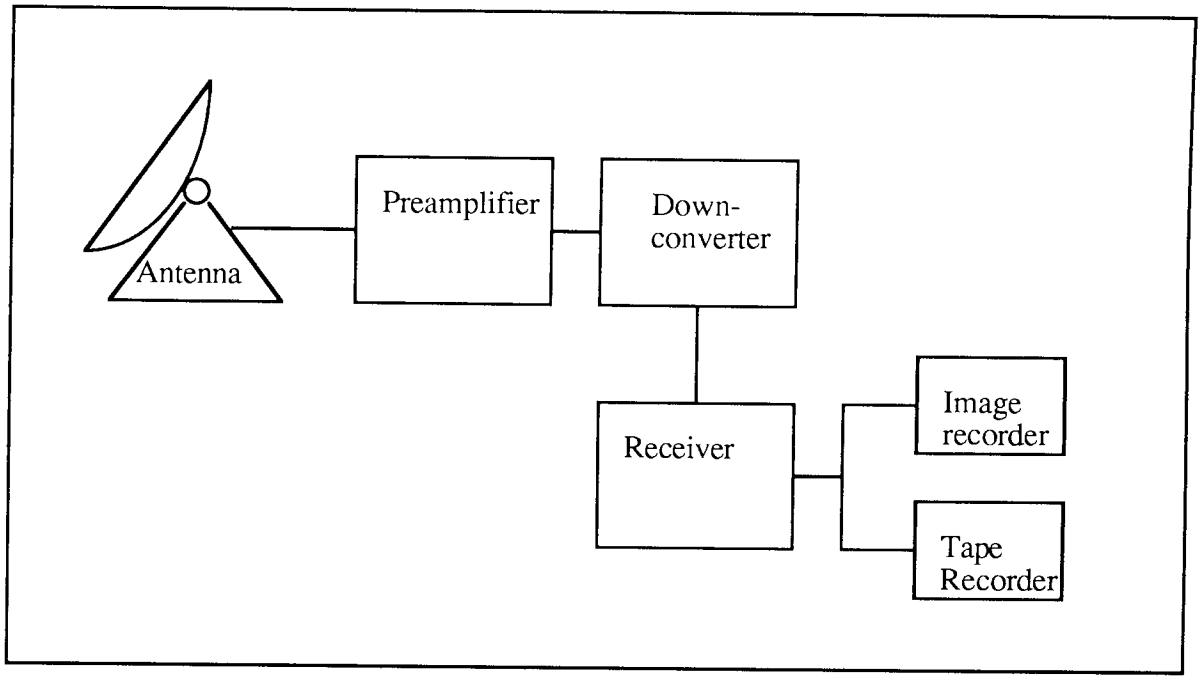

Fig. 3.4 Block Diagram of a typical Secondary Data User Station

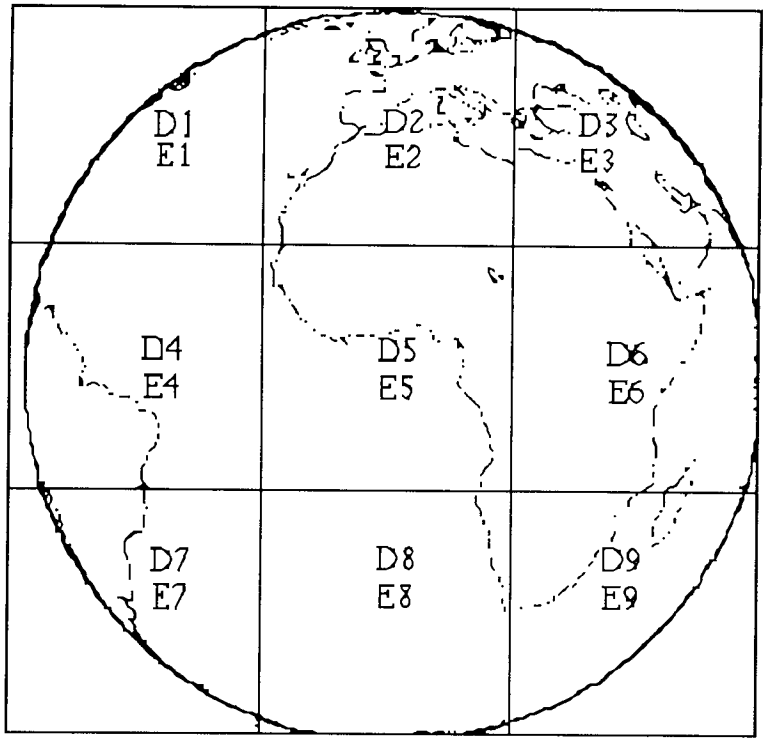

Fig. 3.5 Format for SDUS infrared dissemination

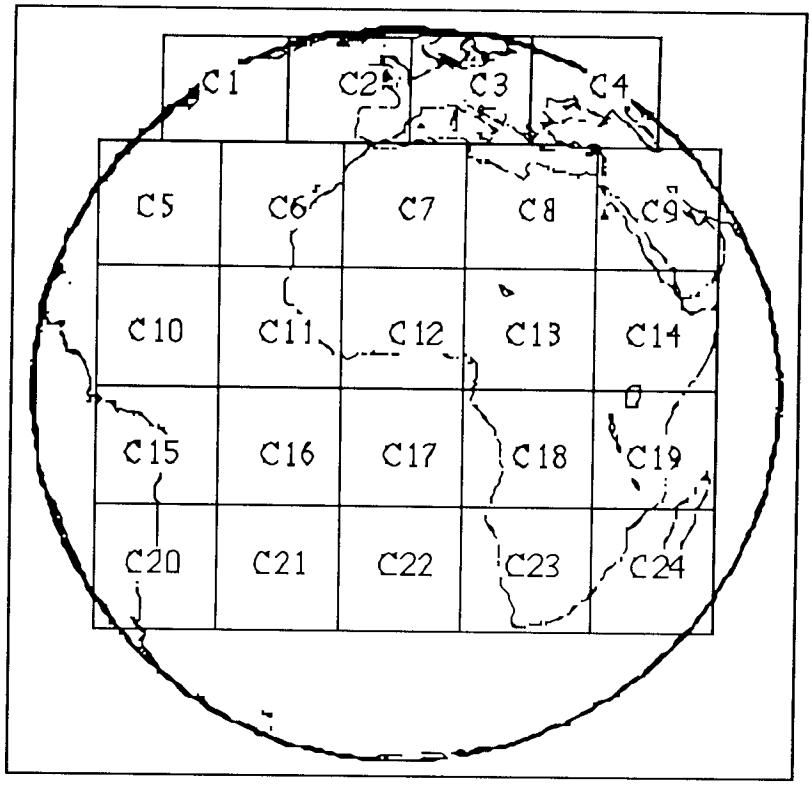

Fig. 3.6 Format for SDUS visible dissemination

3.3 University Of Aston SDUS Receiver Station

A SDUS receiver station was assembled in the Electrical Engineering Department of Aston University for research purposes. The system was developed by Dr. M. Salim (Salim, 1989) and is capable of capturing image data from WEFAX transmissions in digital form.

The whole system is under software control through the host IBM PC which on receiving the image signal, captures and displays the image line by line on the screen containing the 'PC VISION plus' graphics board. On completion of the transmission, the image can be stored for further analysis.

For the purposes of this research, sequences of day and night images were required for which it was essential that images can be archived automatically on to a storage device. The original software was acquired from the author and another module was added for the automatic capture and storage of the image data. The module would function satisfactorily when tested on its own but when tested in combination with the original software, the system crashed after storing few images. The detection of the fault was made more difficult due to the substantial complexity of the original software which consisted of modules based on the C language, Assembler language and the TSR's (Terminate and Stay Resident programs). The bug was finally traced to the use of some C Library input/output memory functions and was eliminated by the use of alternative library routines

(Salim, 1989). Laser disks with memory in excess of 200 Mb were used as storage devices for the images.

SDUS images have the advantage of being low-cost as compared to the high resolution PDUS system (SDUS system is approximately 1/10 the cost of PDUS system). It has also been shown that useful information exists in digitized SDUS images (Salim, 1989) and that there is good correlation between digitized SDUS images and the corresponding PDUS images (Tamayo et al, 1988).

3.4 Other Major Satellite Systems

In addition to geostationary satellite such as Meteosat, there are sun-synchronized polar orbital satellites. These satellites, due to there low orbits, provide very high resolution images but the frequency of images for any given area is restricted to two per month at the most. Table 3.2 gives basic details of some other geostationary and polar-orbital satellites.

Table 3.2 Details of major satellite Systems in operation

Name	Payload Sensors	Bands and Frequency	Reso-lution (km)	Swath	Orbit (km)	Cove-rage
GOES (Geostationary Operational Environmental Satellite USA, NOAA)	VISSR (Visible and Infrared Spin Scan Radiometer)	2 bands 0.55-0.70 10.5-12.6	0.9 0.9 0.9	Entire visible disk	36000 *GS	30 min
METEOSAT (European Space Agency)	VISSR (Visible and Infrared Spin Scan Radiometer)	3 bands 0.4-1.1 5.1-7.1 10.5-12.5	 2.5 5.0 5.0	Entire visible disk	36000 GS	30 min
NOAA (National Oceanic & Atmospheric Administration USA, NOAA)	AVHRR (Advance Very High Resolution Radiometer)	5 bands 0.58-0.68 0.74-1.1 3.55-3.93 10.3-11.3 11.5-12.5	1.09	1600	850 *SS	0.25 days

Name	Payload Sensors	Bands and Frequency	Reso-lution (km)	Swath	Orbit (km)	Cove-rage
MOS-1	MSP-1	4 bands	0.05	100	908	17
(Marine Observation /	(MESSR)	0.51-0.59			SS	days
Satellite Japan,	(Multispectral Electrically	0.61-0.69				
NASDA)	Self Scanning	0.73-0.80				
	Radiometer)	0.80-1.1				
	VTIR	4 bands		1500		
	(Visible and Thermal IR	0.5-0.7	0.9			
	Radiometer)	6.0-7.0	2.7			
		10.5-11.5	2.7			
		11.5-12.5	2.7			
	MSR	2 bands		317		
	(Microwave Scanning	23.8	32			
	Radiometer)	31.4 GHz	23			
DMSP	SSM/1	4 bands		1400	833	0.25
(Defence	(Special Microwave /	19.35,	12.5		SS	days
Meteorological,	Imager	37.0,	25.0			
Satellite Program		85.50,	12.5			
USA, U.S. Military)		22.23				
LANDSAT 5	MSS	4 bands	0.08	185	705	16
(NASA, USA)	(Multispectral Scanner)	0.5-0.6			SS	days
		0.6-0.7				
		0.7-0.8				
		0.8 1.1				
	TM	7 bands		185		
	(Thematic Mapper)	0.45-0.52	0.03			
		0.52-0.60	0.03			
		0.63-0.69	0.03			
		0.76-0.90	0.03			
		1.55-1.75	0.03			
		2.08-2.35	0.03			
		10.4-12.5	0.12			

Name	Payload Sensors	Bands and Frequency	Reso-lution (km)	Swath	Orbit (km)	Cove-rage
SPOT	2x HRV	4 bands		950	832	2.5
(Systeme Probatoire	(High Resolution	0.50-0.60	0.02		SS	days
d'Observation de la	Visible)	0.60-0.70	0.02			
Terre, CNES, France)		0.78-0.90	0.02			
		0.51-0.73	0.02			

*GS - geostationary Satellite

!SS - Sun-synchronous Satellite

3.5 Characteristic Of Meteosat Imagery

3.5.1 Visible Imagery

3.5.1.1 General

All substances emit or reflect electromagnetic radiation. The traditional view of the earth's disc from a satellite is that of a reflected visible radiation from the sun. Different components of the earth's surface and the clouds within the atmosphere reflect differing amounts of visible radiation and with differing combination of wavelengths within the visible portion of the spectrum (between 0.4 to 0.7 microns). Brighter elements are bright because they reflect proportionately more incident visible solar radiation, and colour is added when one wave length dominates over others. At this visible level, therefore, we see the conventional view of the earth and activity within its atmosphere. The Meteosat visible sensors measure the reflected solar radiation in this level and is quantified in 6-bits or 64 grey levels. If the source is of a resolution below the field of view of the sensor (2.5 km for the visible) then the radiances of all the objects within the field of view are integrated into a single response. Thus the radiometer is unable to detect any source which is less than the field of view of the scanner. Fig. 3.7 shows an example of a SDUS Meteosat visible image.

3.5.1.2 Normalization of Visible Imagery

The brightness (i.e the detected visible radiance) of a target depends on the reflectivity of the body, the intensity of the solar radiation, and the solar zenith angle. Changes in the detected radiance due to changes in the solar zenith angles within an image is negligible for small areas but its considerable from image to image corresponding to different times of the day. Fig 3.8 shows two visible images from the same day corresponding to 0800 and

1200 GMT respectively. It is evident from the two images that the 0800 image is less bright than the 1200 image due to different solar zenith angle (also known as sun elevation angle). This gives rise to the need for normalization of the visible imagery with respect to a reference image and the solar zenith angle.

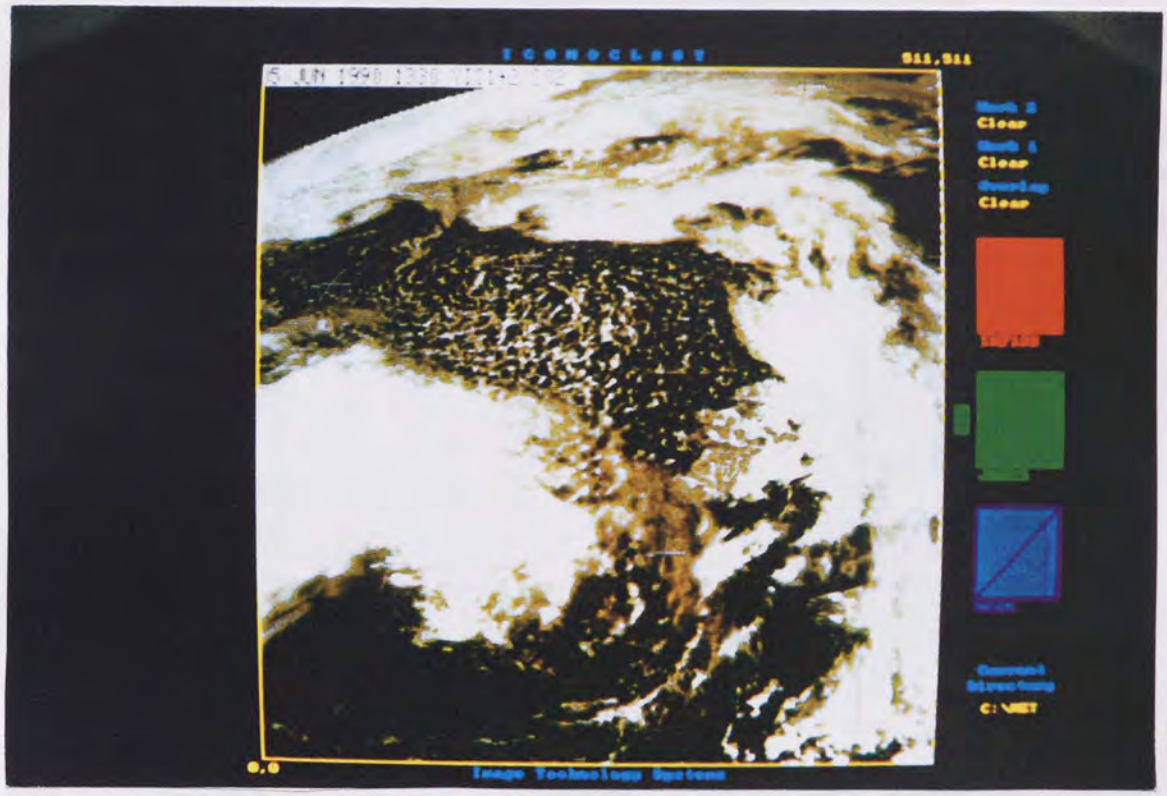

Fig. 3.7 An example of SDUS visible imagery

Lovejoy and Austin (1979a,b), in their normalization scheme, scaled the visible data linearly to occupy the full range of 25 visible levels that they adopted. The scheme used by Griffith et al (1978) was developed to normalize visible imagery for the relative angles between the Sun, sensor and the corresponding target. Martin and Howland (1986) used an empirical relationship of brightness correction as a function of solar zenith angle. Tsonis (1984) also recognized the need for normalization and used the reciprocal of the square of sine of the solar zenith angle as their normalization factor.

The normalization procedure used here is based on a simple procedure used by Doneud et. al.(1987) which involves the calculation of the solar zenith angle and assumes the earth disk to have properties of a Lambertian reflector which means that the reflecting surface is 'perfectly diffuse' (a perfectly diffuse surface reflects equally in all directions). Under this assumption, the radiance measured by the sensor is proportional to the cosine of the solar

zenith angle. Let D be the digital count value at a pixel location and ζ be the solar zenith angle. Therefore:

$$D(\zeta) = K * \cos(\zeta) \qquad \text{eq. 3.1}$$

where K is the constant of proportionality

Therefore the normalization of the visible imagery consisted of dividing the visible digital counts at each pixel location by the corresponding cosine of the solar zenith angle calculated at that pixel location. This can be calculated indirectly from other parameters such as the solar declination (a function of the day of the year), the hour-angle and the latitude. Fig 3.8 also shows the normalized 0800 image with respect to 1200 image.

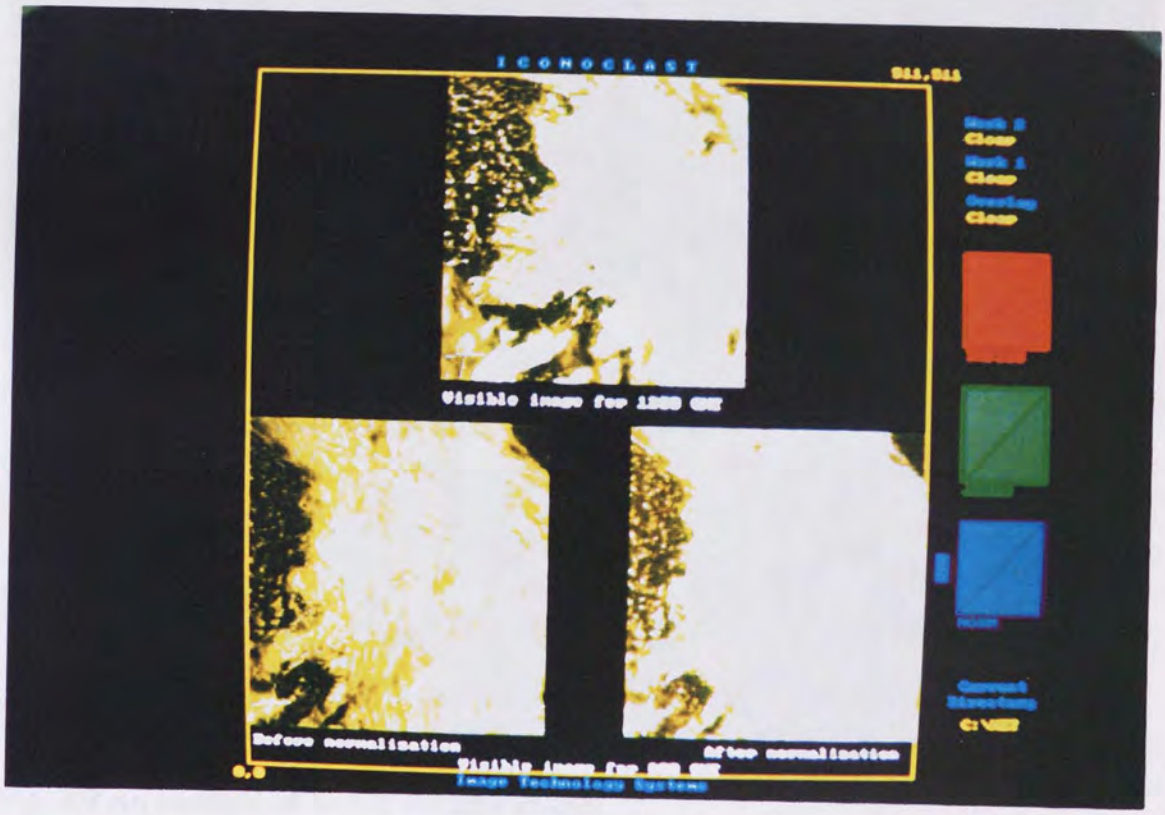

Fig. 3.8 Visible images for 0800 and 1200 GMT before normalization clearly showing the difference in radiance levels due to different solar zenith angle. 0800 is also shown after normalization.

3.5.2 Infrared Imagery

The components parts of the earth's surface and its atmosphere also emit, scatter and reflect radiation at other wavelengths--in other portions of the electromagnetic spectrum. Viewed from space the proportion of visible radiation emitted by the earth is small

compared to the heat it radiates, the infrared radiation. The wavelength and amount of infrared radiation emitted varies according to the temperature of the emitting body. The infrared radiation detected by the sensors takes place through 'atmospheric windows' where neither water vapour nor carbon dioxide absorb such radiation, so that it is allowed to escape to space. These windows occur at wavelengths of between 3.5 and 4.2 μm and 10.5 and 12.5 μm. Each pixel sampled by the radiometer is recorded as voltage and converted to a digital count and transmitted to ground on a scale 0-255. Thus the infrared image is a raster of pixels where each pixel has a value from 0-255 and these numbers may be converted to radiance values through calibration tables (explained in the next section). Fig. 3.9 shows an example of a SDUS Meteosat infrared image.

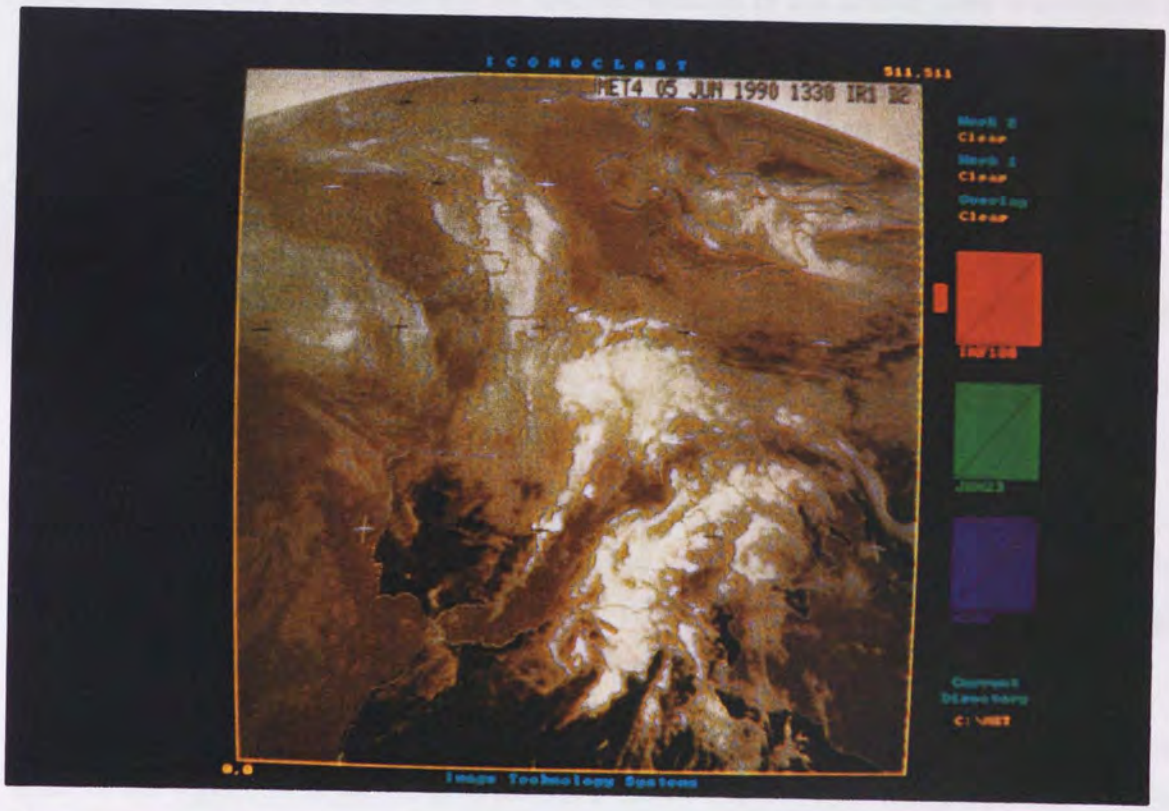

Fig. 3.9 An example of SDUS infrared images.

3.5.2.1 Calibration of Infrared Imagery

The infrared images are calibrated using the calibration coefficients that are routinely published by the European Space Operations Centre (ESOC) (ESOC, 1990). There are two calibration factors: the Fine Adjustment of Gain (FAG) which is used to compensate for radiometric instabilities (gradual degradation caused by contamination of the sensor due to ice formation) and Meteosat Information Extraction Centre (MIEC) factor which is used so that the sea surface temperatures derived from the infrared data give a zero bias when

compared to ship temperature data. These coefficients are used to convert pixel values to radiances which can then be converted to temperatures using the look up tables also published in the ESOC calibration reports.

In addition to infrared and visible images, Meteosat also disseminate water-vapour images. However, these have lower temporal resolution (every four hours) than the visible or infrared images and were therefore not considered in this study.

3.6 Description Of the Study Area

3.6.1 General

The study area chosen for this research is the Severn-Trent Catchment Area in the midlands. The map of the area and its relative position in the British Isles is as shown in fig. 3.10. The choice was based on the following factors:

* Rainfall data could be easily and inexpensively obtained from the Severn-Trent Water Authority (STWA) on computer compatible tapes and the area has a good network of short period rainfall gauging stations (total of 92 in number).

* The area of the catchment ($\cong$ 22176 km^2) was considered large enough for satellite applications.

* The area was local.

Rainfall systems in the region are predominantly cold frontal but are also frequented by convective type thunder storms and warm frontal systems. More rainfall is observed in the higher regions of the catchment as shown in fig. 3.11 which relates the annual average rainfall with the altitude using all the 92 rain-gauges.

Originally, the STWA was responsible for the archiving and distribution of hydrological data for the region. In 1988, the government published detailed plans to privatize the water industry in England and Wales. Under privatisation the environmental, regulatory, and policing functions of the water industry remained in the public sector under the auspices of the National Rivers Authority (NRA), while the operational aspects (the provisions of water services and sewage disposal) were transferred to new water services public liabilities companies (plcs). The privatisation of the water industry has resulted in substantial related changes within the individual Water Authorities. The rainfall data are now the responsibility of the NRA .

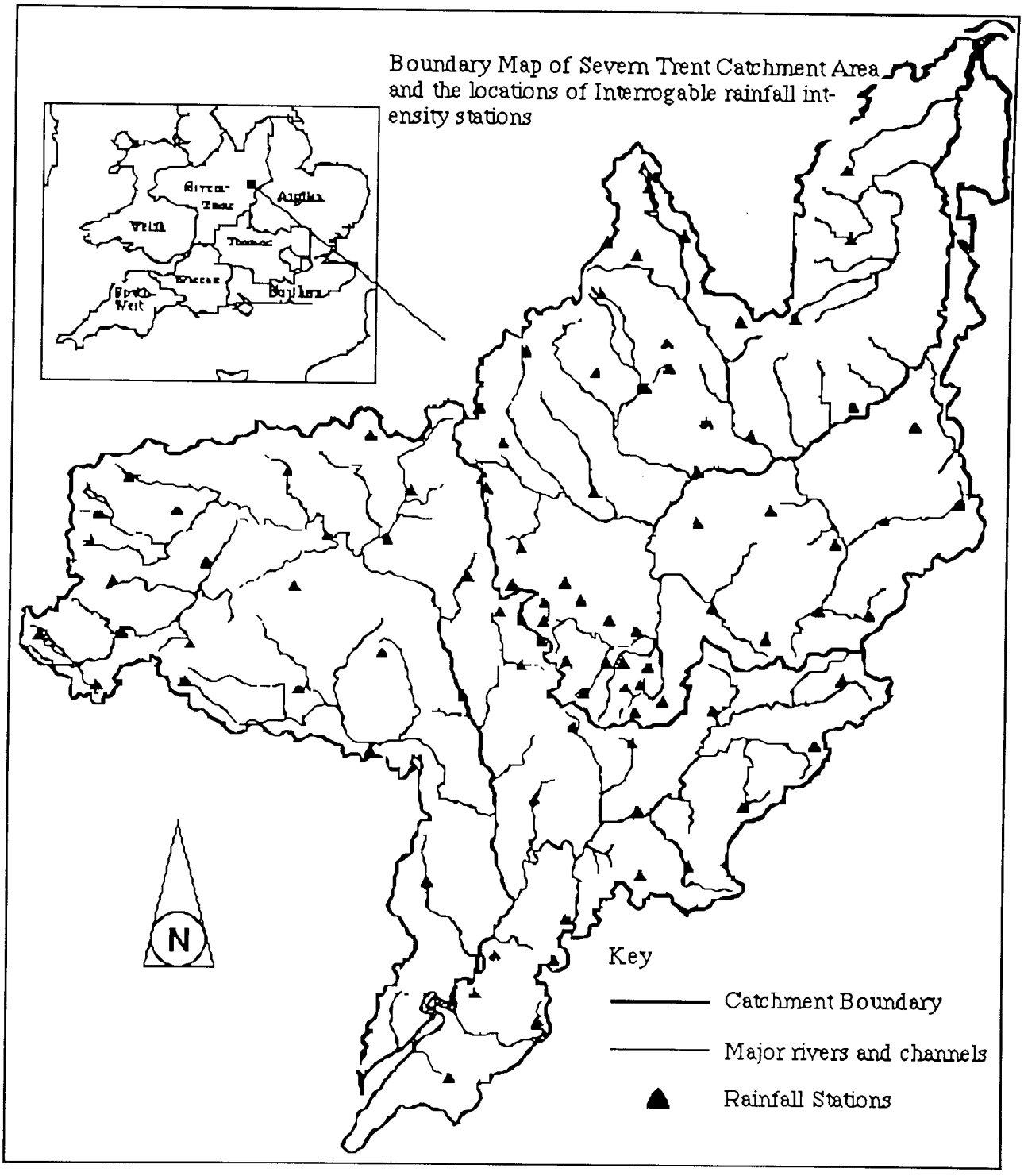

Fig. 3.10 Map of the Severn-Trent catchment area showing its relative position with respect to British Isles and the location of the rain-gauges.

3.6.2 Rain-gauge Network

NRA maintain an extensive hydrometric network in the Severn-Trent region. At 92 sites, rate of rainfall is measured automatically by tipping bucket rain-gauges connected to TG1150 outstation loggers. These are battery powered and have the capability of remote interrogation over telephone lines. Data from these stations is archived directly onto a

computer compatible tapes. The rain-gauges have a resolution of 0.5 mm and their distribution is also shown in fig. 3.10. For each rain-gauge, its location in terms of OS grid coordinates, its altitude and the annual average rainfall were obtained from the NRA and are given in their yearly publications of Hydrological Year book.

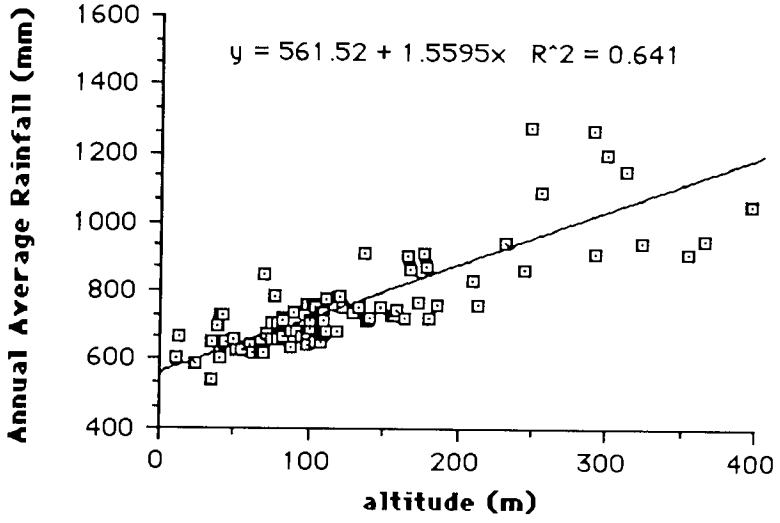

Fig. 3.11 Graph showing the relationship between annual rainfall and altitude.

3.7 Spatial Integration of Catchment Map and the Meteosat Images

3.7.1 General

The incoming multi-spectral images are captured and mapped on the image processing display screen. However, these images cannot be immediately analysed using computer algorithms as they are not in the form for direct analysis. An algorithm must be defined which relates the map of the study area to the raw image received. This would enable the retrieval of image information for any point on the map such as a rain-gauge.

3.7.2 The Catchment Map Data

The standard map of the Severn Trent catchment area was obtained from the Severn Trent Water Authority and is as shown in fig. 3.12. The map uses the Ordinance Surveys grid as its frame of reference and is based on Transverse Mercator Projection (Harley, 1975). It was transferred onto the computer using the videograph facility on the ITS-30 image processing system (Flack, 1989, Flach et al 1989).

The catchment boundary and the position of rain-gauges were stored in terms of vector coordinates using a scale of 500m to 1 pixel which was found to be adequate for the representation of catchment map on a 512 by 512 image frame. The processed map of the

catchment boundary and the rain-gauges are shown in fig. 3.13. The map is so defined such that the bottom left hand corner of the image correspond to OS grid coordinates of :

x = 280 km y = 170 km

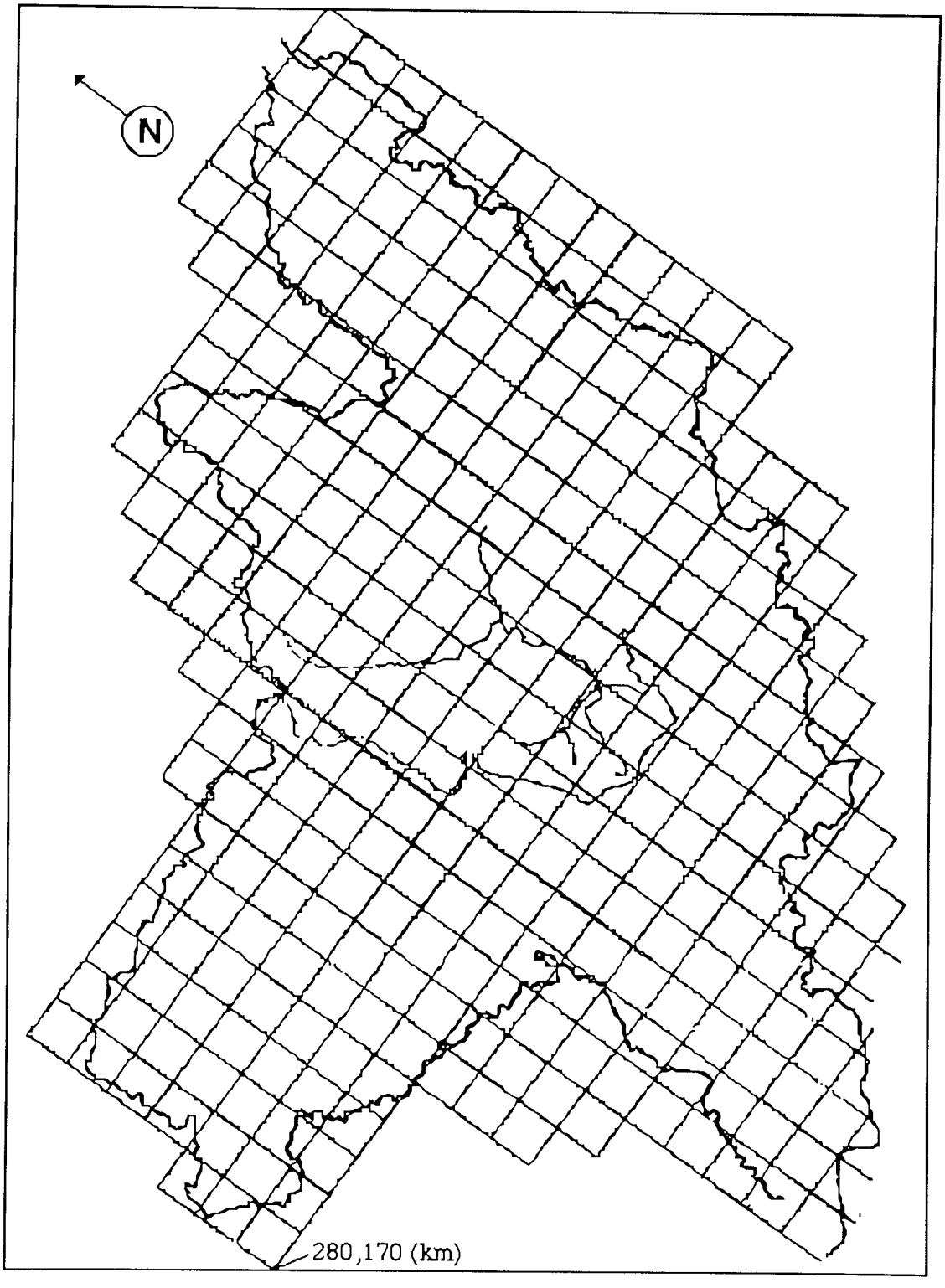

Fig. 3.12 Standard map of the Severn-Trent catchment area with the OS grid overlay as received from the STWA.

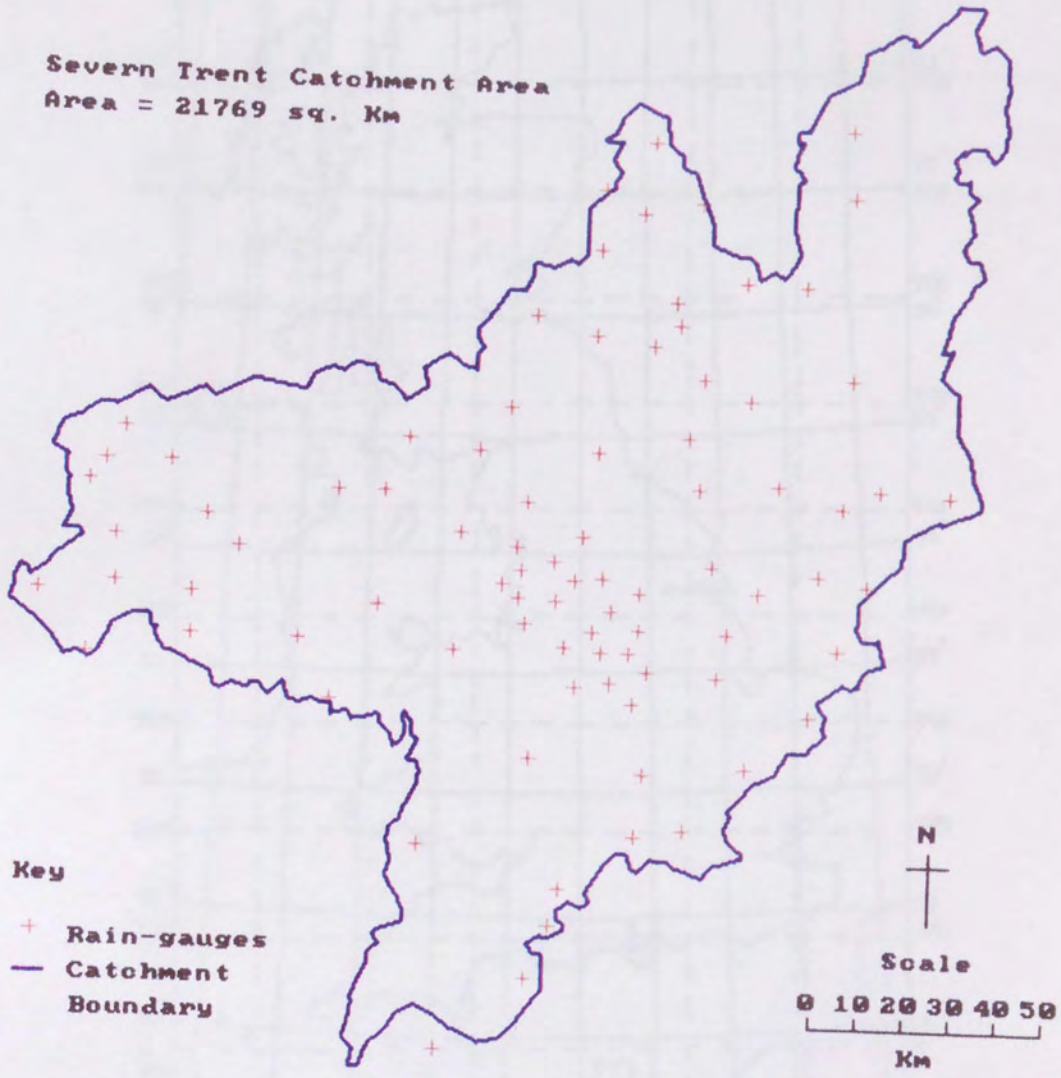

Fig. 3.13 Processed catchment map and the distribution of rain-gauges on the computer.

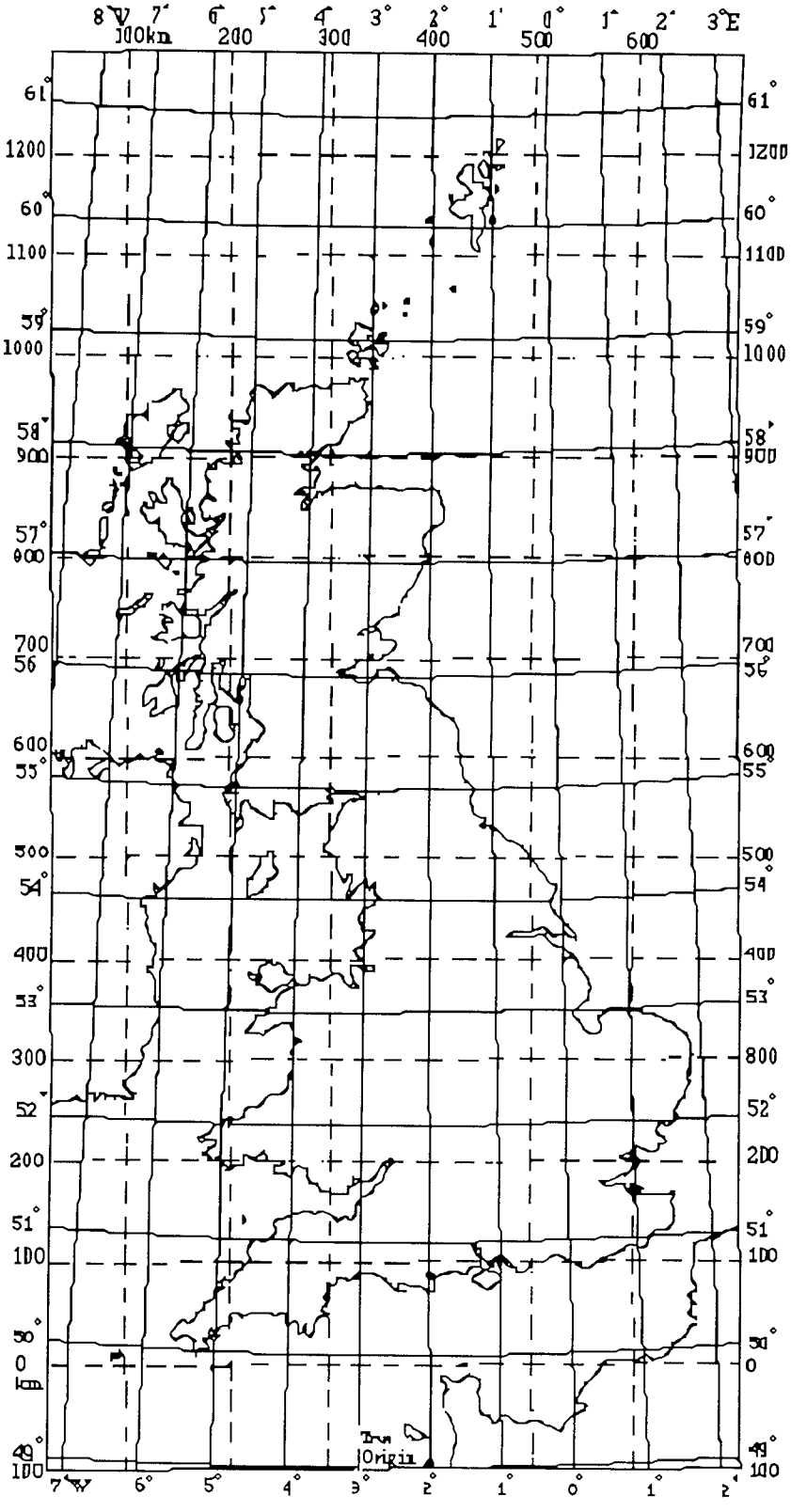

Fig. 3.14 Relationship of the Transverse Mercator graticule and the National Grid system on the Ordinance Survey maps. Continuous lines represent projection; broken lines the National Grid.

3.7.3 Definition Of OS Grid Coordinates As Longitudes (λ) And Latitudes (ϕ)

The Earth's surface is a three dimensional spheroid and can only be represented on a two dimensional flat surface by means of map projection equations.

Several methods for map projections are reported (Maling, 1973; Snyder, 1982) that locally stretch the earth's surface from a sphere to a flat plane. These projections deform the corrected area to some extent and different map projections distort the area of interest in different ways. The way maps are distorted is used to classify the type of projection.

The Transverse Mercator Projection is favoured for land masses that extend predominantly North to South, such as Great Britain (Harley, 1975).

The equations relating rectangular coordinates (x,y) and the geographical coordinates (ϕ,λ) for the Transverse Mercator Projection are as follows (Snyder, 1982):

$$\phi = \arcsin\left[\frac{\sin(D)}{\cosh\left(\frac{x}{R}\right)}\right] \qquad \text{eq. 3.2}$$

$$\lambda = \lambda_o + \arctan\left[\frac{\sinh\left(\frac{x}{R}\right)}{\cos(D)}\right] \qquad \text{eq. 3.3}$$

$$D = \frac{y}{R} + \phi_o \qquad \text{eq. 3.4}$$

where ϕ_O,λ_O --------- latitude and longitude of the point of origin respectively in radians.

R --------- Radius of the earth.

x,y --------- rectilinear coordinates.

Y-axis lie along the central meridian λ_O, y increasing northerly and X-axis is perpendicular, through ϕ_O at λ_O, x increasing easterly. Fig. 3.14 shows the relationship between OS grid coordinates and the Transverse Mercator Projection.

For this study, it would have been ideal if the origins of the Transverse Mercator Projection and the OS grid coordinates were the same. But in practice they are different as shown in fig. 3.14. In terms of rectilinear projection coordinates, the origin for the OS grid coordinates is situated at:

$$x_O = -400 \text{ km}$$

$$y_o = 100 \text{ km}$$

relative to the Transverse Mercator Projection.

The origin of the Transverse Mercator map projection is at:

$$\phi_o = 49^o$$

$$\lambda_o = -2^o$$

Therefore, to calculate the geographical coordinates (ϕ,λ) given the grid coordinates of a point, the grid coordinates are first translated with a new origin at (ϕ_o,λ_o) and than using eq's 3.2, 3.3 and 3.4, the geographical coordinates can be found. The following example illustrate the calculations involved.

Example: Given the grid coordinates xg=280 km and yg=170 km of a point, find its latitude and longitude.

Consider fig. 3.15

$xp = xg + xo$ $\qquad$ $yp = yg + yo$

$xp = 280 - 400 = -120$ km $\qquad$ $yp = 170 + 100 = 270$ km

$R = 6378$ km = radius of the earth

$\phi_o = 49^o = 0.8552$ rad $\qquad$ $\lambda_o = -2^o = -0.349$ rad

Using eq.(3.4) $\qquad$ $D = 0.8897$ rad

Using eq.(3.2) $\qquad$ latitude $= 51.4^o$

Using eq.(3.3) $\qquad$ longitude $= -3.73^o$

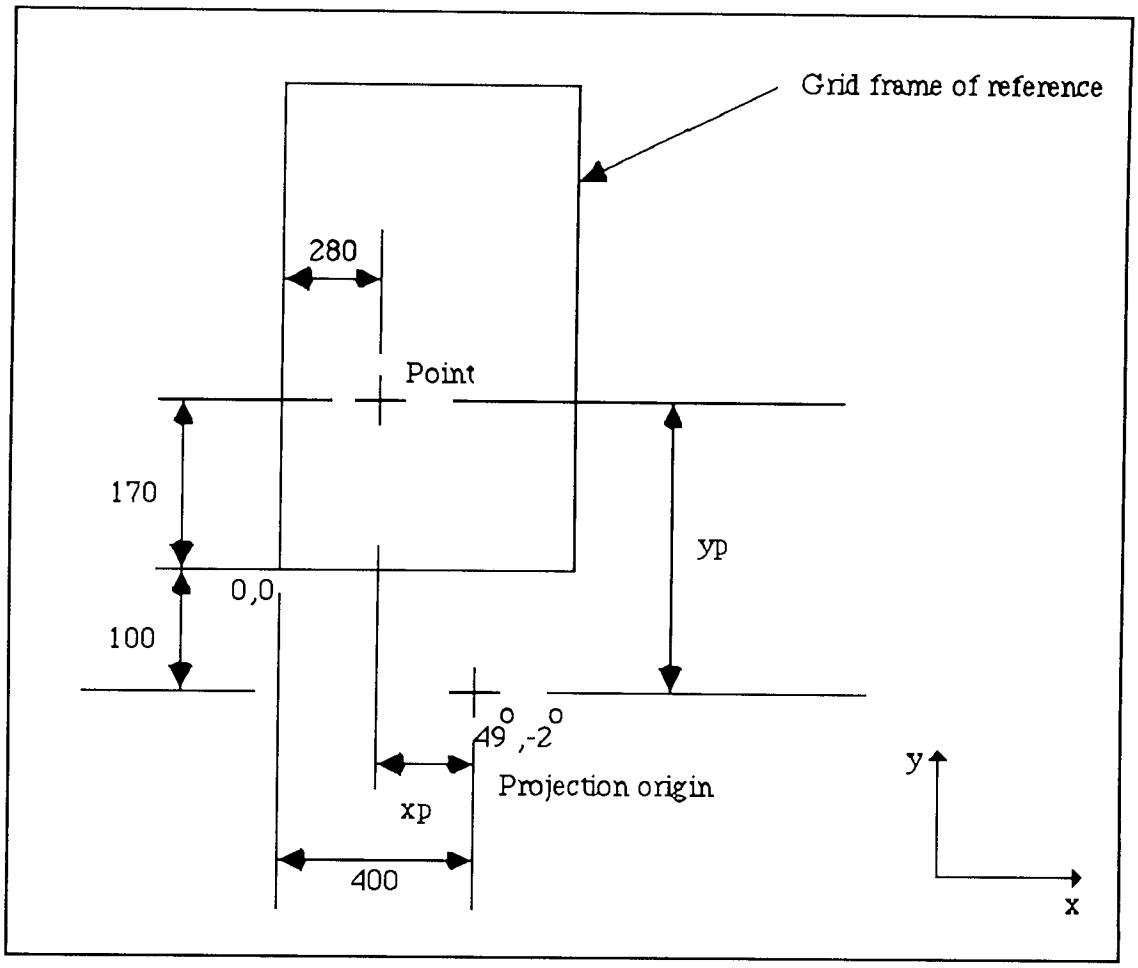

Fig. 3.15 Schematic diagram for calculation of geographical coordinates given the OS grid reference coordinates

3.7.4 The Image Data

The raw Meteosat image data received only provide latitude and longitude information at intervals of 10^{o}. These are superimposed on top of the image data in the case of SDUS images and are provided separately for PDUS images. The Meteosat image can be conceived as a particular kind of projection and to determine the relevant equations of that projections giving the rectilinear coordinates in terms of latitude and longitude, one needs to have an understanding about the scanning mechanism of the satellite.

3.7.5 The Scanning Concept Of the satellite

Fig. 3.16 illustrates the scanning mechanism of the satellite. At each satellite rotation the spin clock delivers a signal to the scanning motor electronics whereby the satellite is rotated 1.25×10^{-4} radians.

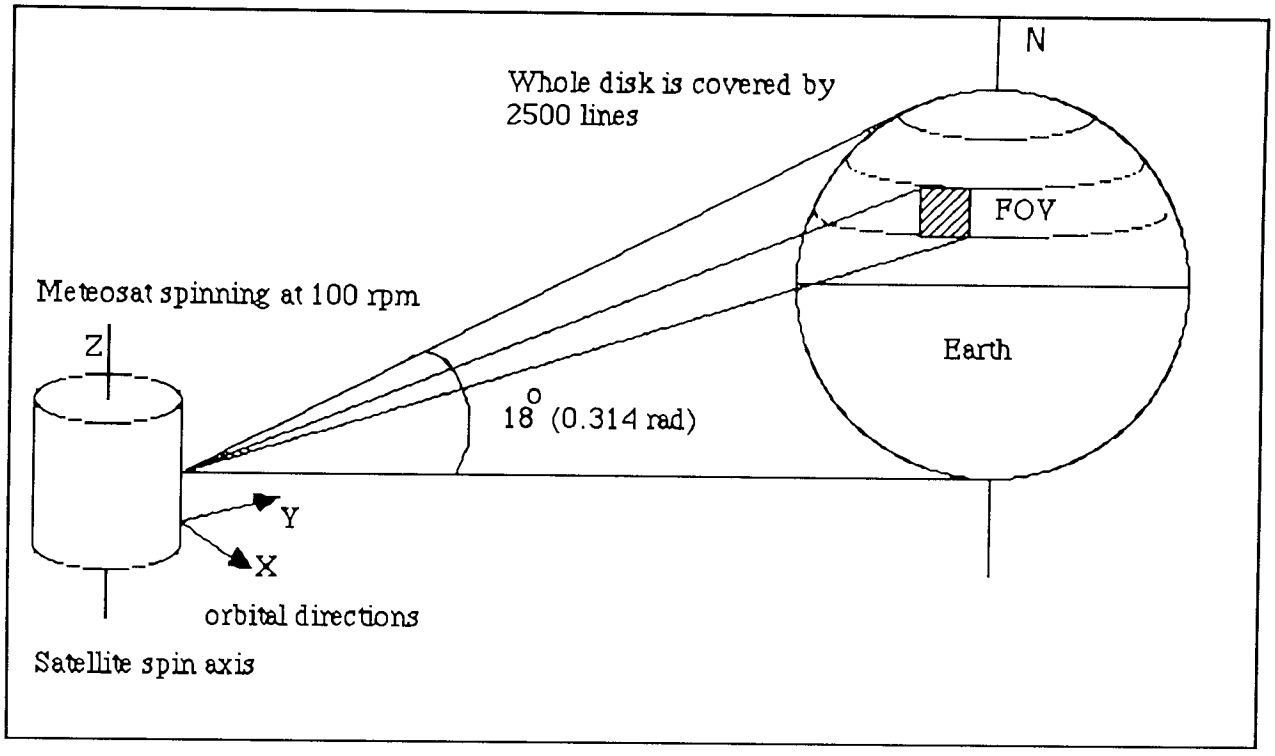

Fig. 3.16 The scanning concept of the Meteosat

By this means, with every rotation of the spacecraft, the telescope scans a new line approximately 5 km north of the previous scan line. The telescope is made to scan through 18^{o} in the S-N direction, giving a full earth scan of 2500 lines in 25 minutes. Following this scan the telescope retraces to its starting position in 2.5 minutes, during which time black-body calibration of the infrared channels are performed. The retrace is followed by 2.5 minutes stabilization period before the next scanning mission can be initiated. Thus, the telescope scans from east to west direction by means of the spinning motion of the satellite and from south to north by means of the stepping mechanism applied to the telescope, and generates a new image in three spectral channels during each half-hour period.

3.7.6 Definition Of Image Coordinates In Terms Of Longitude And Latitude

A pixel in the Meteosat image data received is defined in terms of line number (y value) and row number (x value). In this section equations are derived which define the rectilinear coordinates in terms of latitude and longitude. A pixel can thus be located on the Meteosat image given the latitude and the longitude of a pixel.

Consider Fig. 3.17

$$\text{y-image} = Rs * \theta \qquad \text{eq. 3.5}$$

To find θ consider Δ SUV

$$SU = Re\ SIN(\phi) \qquad \text{eq. 3.6}$$

$$OU = Re\ COS(\phi) \qquad \text{eq. 3.7}$$

$$OT = OU\ COS(\lambda) \qquad \text{eq. 3.8}$$

Substituting eq.(3.7) in eq.(3.8)

$$OT = Re\ COS(\phi)\ COS(\lambda) \qquad \text{eq. 3.9}$$

From fig. 3.17

$$TV = Al + Re - OT \qquad \text{eq. 3.10}$$

Substituting eq.(3.9) in eq.(3.10)

$$TV = Al + Re\left(1 - COS(\phi)\ COS(\lambda)\right) \qquad \text{eq. 3.11}$$

From fig. 3.17

$$UV = \frac{TV}{COS(\alpha)} \qquad \text{eq. 3.12}$$

Substituting eq.(3.11) in eq.(3.12)

$$UV = \frac{Al + Re\left(1 - COS(\phi)\ COS(\lambda)\right)}{COS(\alpha)} \qquad \text{eq. 3.13}$$

From fig. 3.17

$$TAN(\theta) = \frac{SU}{UV} \qquad \text{eq. 3.14}$$

Substituting eq.(3.6)and eq.(3.13) in eq.(3.14)

$$TAN(\theta) = \frac{Re\ SIN(\phi)\ COS(\alpha)}{Al + Re\left(1 - COS(\phi)\ COS(\lambda)\right)} \qquad \text{eq. 3.15}$$

Similarly

$$x\text{-image} = Rs * \alpha \qquad \text{eq. 3.16}$$

$$UT = OU\ SIN(\lambda) \qquad \text{eq. 3.17}$$

Substituting eq.(3.7) in eq.(3.17)

$$UT = Re\ COS(\phi)SIN(\lambda) \qquad \text{eq. 3.18}$$

From fig. 3.17

$$TAN(\alpha) = \frac{UT}{TV} \qquad \text{eq. 3.19}$$

Substituting eq.(3.11)and eq.(3.18) in eq.(3.19)

$$TAN(\alpha) = \frac{Re\ COS(\phi)\ SIN(\lambda)}{Al + Re\left(1 - COS(\phi)\ COS(\lambda)\right)} \qquad \text{eq. 3.20}$$

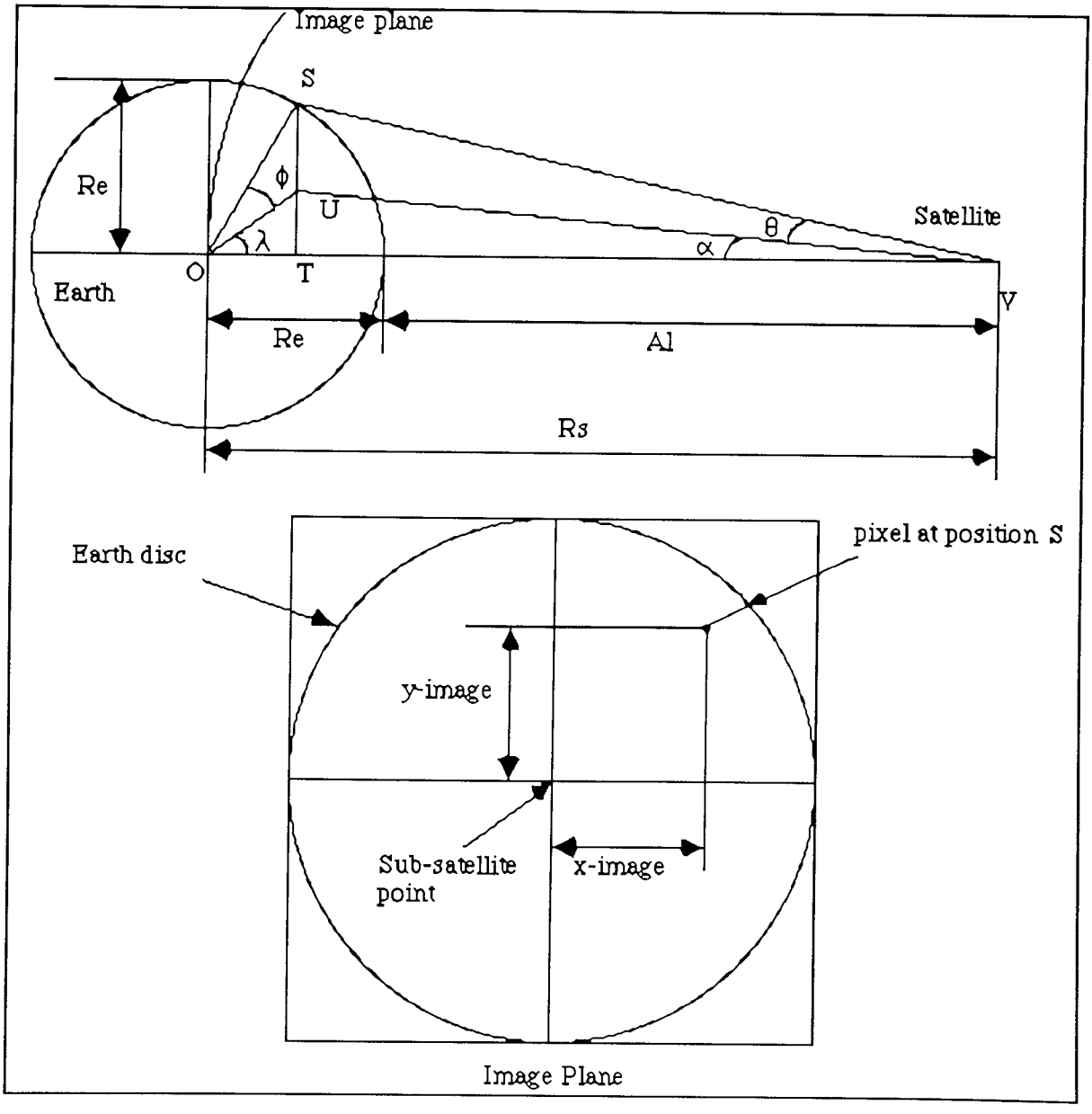

Fig. 3.17 Schematic diagram for the derivation of equations describing the projection of the Meteosat image.

These equations are thus used to integrate the catchment map with the raw images received from the satellite and the whole process is summarised in fig. 3.18. Before such an operation can be performed, the scale values for constants such as the radius of the earth (Re) must be found. Let d^* be the distance (in number of pixels) between any two points on the Meteosat image with known latitudes and longitudes. Scale factor (S) is defined as:

$$S = \frac{d^*}{d} \qquad \text{eq. 3.21}$$

where d is the distance in km and

$$Re^* = Re * S \qquad \text{eq. 3.22}$$

where Re^* is the radius of the earth in pixels.

Value for d can be found using eq.'s 3.2, 3.15, 3.16 and 3.20 with values for Re, Al and Rs in kilometres. These are given in standard textbooks as:

$$Re = 6378 \text{ km} \qquad Al = 35900 \text{ km}$$

$$Rs = Re + Al = 42278 \text{ km}$$

An example of meteosat satellite image projected onto Transverse Mercator Projection is given in fig. 3.19 (see appendix A.1 and A.1.1 for the description of computer routines).

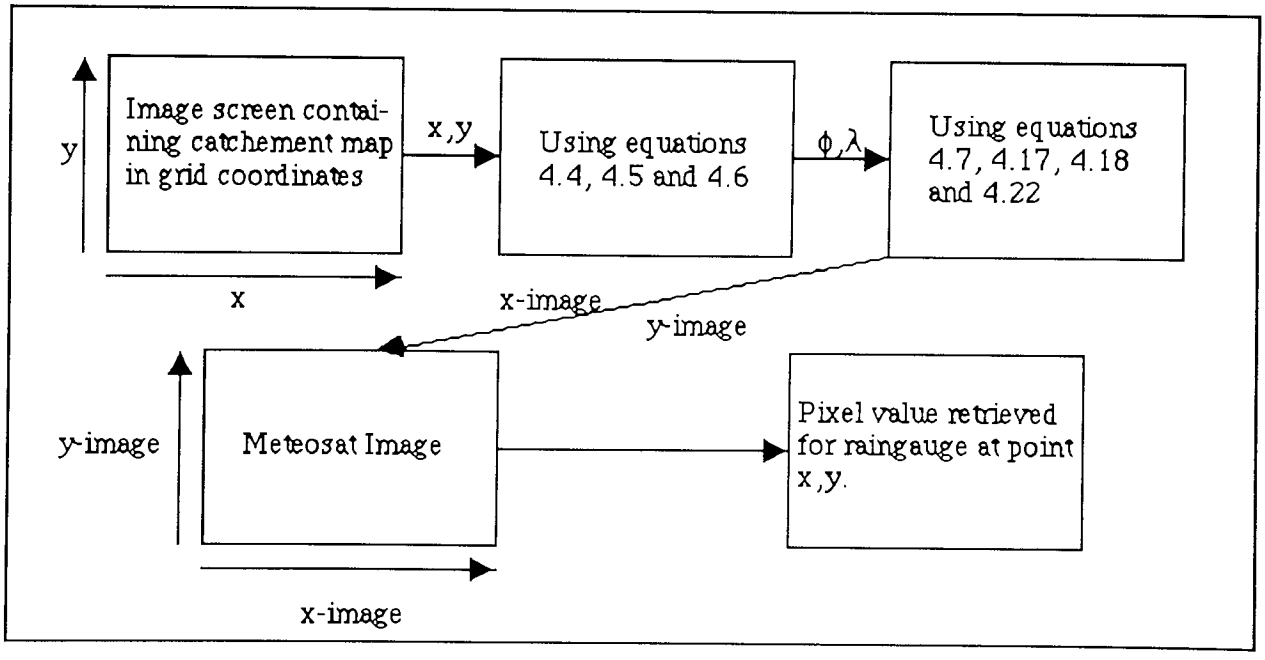

Fig. 3.18 Process of integration of ground-based map and space-borne image data.

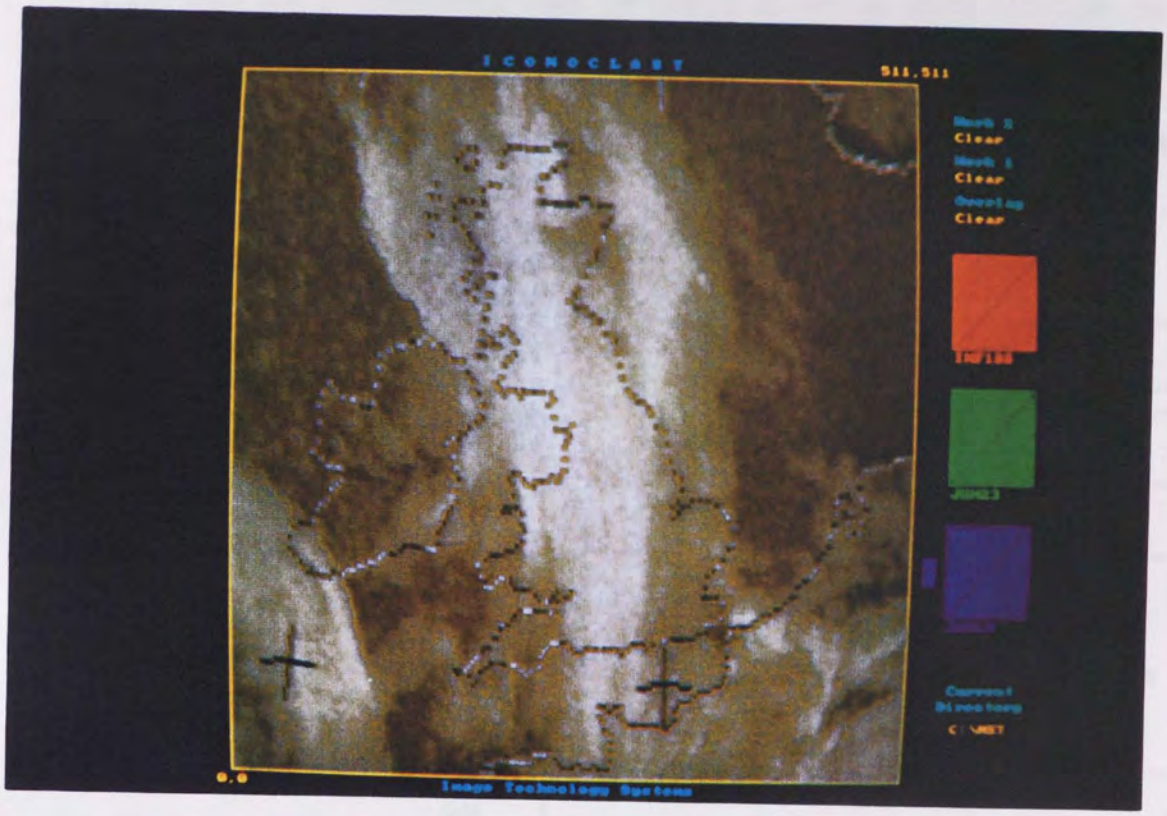

Fig. 3.19 An example of satellite image projected onto Transverse Mercator Projection.

3.8 Hardware And Software Considerations

The last few years have seen a rapid increase in the power and availability of image processing products. With the advent of board level products, professional systems can now be developed on micro-computers. In the field of remote sensing this is demonstrated by the increasing number of IBM PC based image processing systems currently available.

In this research, standard data and image processing were carried out on the following two systems:

* IBM PC (AT)

* Vax Cluster Mainframe

The salient features of the system configuration are (fig. 3.20):

* MICROSOFT C (version 5.0) Compiler - for general software development

* ITS-30 image processing system (Flack, 1989)

* Laser disk drive - principally used for storing of images (each cartridge has a capacity of 200 Mb of memory, and

* RWG PC4000 graphics board consisting of 768 x 768 frame store for image manipulation.

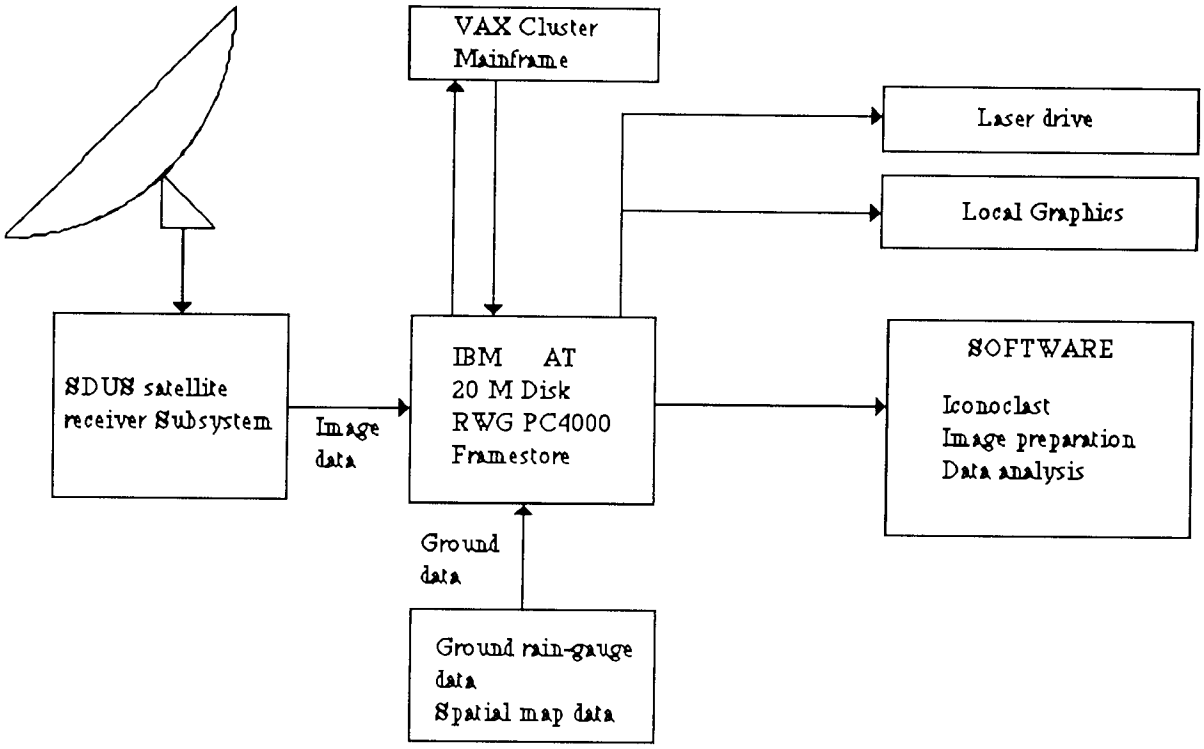

Fig. 3.20 Major system components in hardware and software

3.9 Conclusions

Major contributions of weather satellites are in their effectiveness in providing information, routinely and dependantly, in areas where conventional data are sparse and absent. Their major advantage is in the areal observation of a weather phenomena but depend on the conventional data for calibration and identification. On the other hand, point data source such as a rain-gauge is accurate only at that point and information about the neighbouring areas can only be guessed at. Thus the two forms of data sets are complementary to each other and combined together may be the best means to analyse a highly variable quantity such as rainfall. It has been demonstrated how these two different data sets can be made to be compatible with each other, as a first step towards further analysis. The accuracy of the algorithm was tested by comparing the calculated coordinates with the known data points supplied on the image. The points were located successfully within the 60° latitude and longitude. Beyond that limit and up to the very edge of the earth disk , the accuracy was found to be $\pm$ 1 or 2 pixels. The reason for that could be any one of the following or their combined effect:

* The curvature of the earth increases rapidly above 60° latitude or longitude.

* Rounding off errors due to the integer arithmetic involved.

* Errors arising due to calibrations.

* Earth is not exactly a sphere or an ellipse (Snyder, 1982).

The accuracies obtained were considered sufficient for further analysis.

Chapter 4

4. Preliminary Investigations

4.1 Introduction

Visible and infrared data from geostationary and to a limited extent orbital satellites have been used frequently to estimate rainfall for periods ranging from 30 minutes to monthly estimates (Barrett & Martin, 1981).

Most of the previously mentioned studies (see chapter 2) have concentrated on using radar data to provide 'Ground Truth' for calibrating and verifying satellites estimates of rainfall. However, methods depending on the radar data for calibration may be invalid when extrapolated beyond the radar range (Tsonis and Isaac, 1985). Moreover, Satellite methods are developed and are more significant for data sparse regions where its more likely to find rain gauges than a radar station.

It is therefore intended in this study to use rainfall data from the available network of rain-gauges as ground truth. Reports from the eighty six automatic tipping bucket rain-gauges in the Severn Trent Catchment Area were obtained from the National Rivers Authority (NRA) for the month of June, 1990 for which the satellite data was collected. Emphasis is placed on observing the spectral properties of satellite data over these rain-gauges and how these properties may relate to surface reports of rain/no-rain information. This chapter investigates some of the methods employed by previous researchers as discussed in chapter 2 with a view to assess their applicability and also to gain insight into the nature of satellite data in relation to rainfall information.

4.2 Data Set

The data used in this study consists of Meteosat visible and infrared images obtained as described in chapter 3. Surface rainfall information was obtained on a CCT from NRA for the corresponding image data. It consisted of reports from the eighty six tipping bucket rain-gauges and their positions are shown in fig. 3.13 in chapter 3. Their positions were easily located in the catchment area since these were given in OS grid coordinates. The distribution of rain-gauges is mostly uniform apart from in the Birmingham region where the rain-gauge density is relatively greater than the rest of the catchment. This is typical of most hydrological regimes where the rain-gauges tend to be near the populated areas for easy access and maintenance. Half hour rainfall totals for each gauge were extracted from the rainfall data file corresponding to the half hour interval represented by the satellite data (see chapter 3).

Satellite images were processed as described in chapter 3 with the visible corrected for deviations caused by the changes in solar zenith angle. Only the images in the interval 0800-16.30 GMT were used in the analysis for that reason. For other times, the visible data was found to be unsuitable due to very low solar zenith angles. A routine based on the navigational algorithm described in chapter 3 was written to extract spectral values from visible and infrared images corresponding to the rain-gauges in the catchment area. The spatial resolution of the satellite images at the latitude of the study area is almost twice the value at the sub-satellite point (2.5x2.5 for visible; 5x5 for infrared).

The analysis was carried out for the first six days of the month. Data for the 4th of June was not used since no rainfall and very little cloud cover was observed on that day. After the initial processing the final data format is as follows:

For each image pair and the 86 rain-gauges we have

R [i] = Total half-hour rainfall for gauge i

VIS [i] = Visible spectral value for gauge i

INF [i] = infrared spectral value for gauge i

i = 1,2,3,----------,86

Since only two classes i.e. rain or no-rain were being distinguished, R[i] >0.0 was considered as a raining gauge and R [i] = 0.0 as a not-raining gauge.

4.3 Methodology

In judging the relationship of the satellite data to rain-gauge reports, the two data sets were compared for the two classes of rain and no-rain. The methods employed are as follows:

* Examination of Cospectral plots: These are plots of basic statistical characteristics of visible and infrared spectral values for the two classes of rain and no-rain. These would indicate the ability of the two bands to distinguish between the two classes.

* Examination of Bispectral frequency distribution: Frequency distribution of rain-gauges in the visible/infrared domain are plotted. This is performed separately for both rain and no-rain gauges separately. This is an extension of cospectral plots into two dimensions.

* Examination of Textural properties: Textural measures were also carried out for rain and no-rain gauges in the two bands in an effort to test the existence of any textural differences in the two classes.

* Cloud Area/Catchment Rainfall relationship: This method investigates the relationship between the total 'precipitable' cloud area observed over the catchment with the total catchment rainfall as determined by the rain-gauges. The term 'precipitable' can be defined as cloud area above a certain threshold in the infrared or the visible or both, above which there is a high chance that precipitation is taking place.

4.3.1 Examination of Cospectral plots:

In Remote Sensing, different objects are classified according to their spectral response or signatures in various bands. The spectral response of a particular class is assumed to be normally distributed and are characterized by the values of mean and the standard deviation. In a two class/one band problem, the larger the difference between the means of the two classes and smaller the overlap in the standard deviations, the better would be the classification between the two classes (Curran, 1985; Fraysse, 1980; Mather, 1987). Several researchers in the past have used either visible or the infrared to discriminate between rain and no-rain clouds (see chapter 2). Infrared has been used more extensively than the visible due to its diurnal ability.

4.3.1.2 Results:

To observe the spectral response of rain and no-rain gauges, cospectral plots in both the visible and the infrared bands were drawn and were used to subjectively evaluate the ability of the visible and infrared statistics to identify whether a particular satellite observation is associated with rain or no-rain classes. These are shown in figures 4.1(a-e) corresponding to each of the five days of satellite data and for each half hour image pair. The variation in the spectral response is indicated by the width of the error bar containing the mean (here ± 1 standard deviation). Co-spectral plots indicate the potential overlap between the class spectral or statistical response and show which combination of spectral bands might be best for discrimination. Ideally, the bands with the least amount of overlap will be best for classifying rain and no-rain class systems.

4.3.1.3 Discussion

A number of observations can be made from the examination of the co-spectral plots in figures 4.1(a-e):

1. There is no clear separation between the rain and no-rain gauges in terms of the spectral responses in the visible and infrared spectrum. The separation of the means of the two classes can range from zero to more than one standard deviation.

2. Cloud systems observed for each day occupied the same spectral region in the visible spectrum ($\approx$ 200 count values). However, in the case of the infrared response, the count values varied from approximately 130 for the 2nd of June to 180 for the 1st of June.

3. In a general sense, these plots confirm the observation that raining gauges tend to have higher visible and infrared values. However, on the 1st of June, mean spectral values of the rain gauges were less than the no-rain gauges in the infrared spectrum. This was due to the fact that two separate cloud systems were observed on that day. One developed within the catchment and grew in thickness as shown by the co-spectral plots in the visible in fig. 4.1a. The mean count values increase rapidly from 800 hours onwards. The second cloud system, already fully developed and raining, enters the catchment around 1000 hours. This cloud system possessed lower mean infrared values as shown in fig 4.1a in the infrared by the raining gauges. The two cloud systems merged with one another around 1300 hours.

Clearly, traditional remote sensing techniques of classification, based on the differences in the spectral signatures, cannot be applied to distinguish between rain and no-rain regions within the cloud. Any such attempt would inevitably result in large number of misclassifications. However, these co-spectral plots show that given a raingauge reporting rainfall, there is a greater chance that it would have relatively high visible and infrared values but not vice versa, i.e. given a rain-gauge with high visible or infrared values, it is not guarantied that it would be raining.

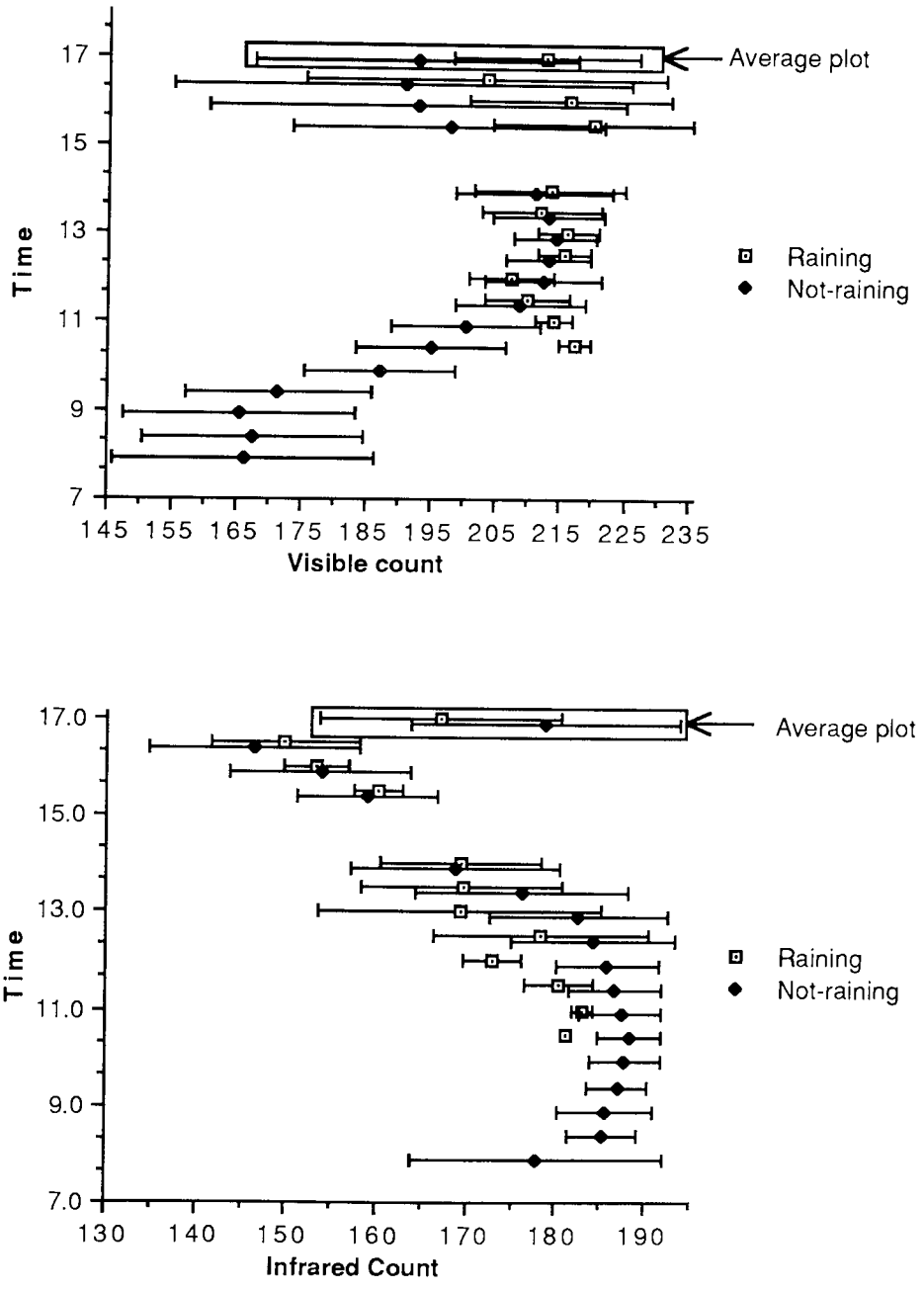

Fig. 4.1a Cospectral plots for the 1st of June in the visible and infrared.

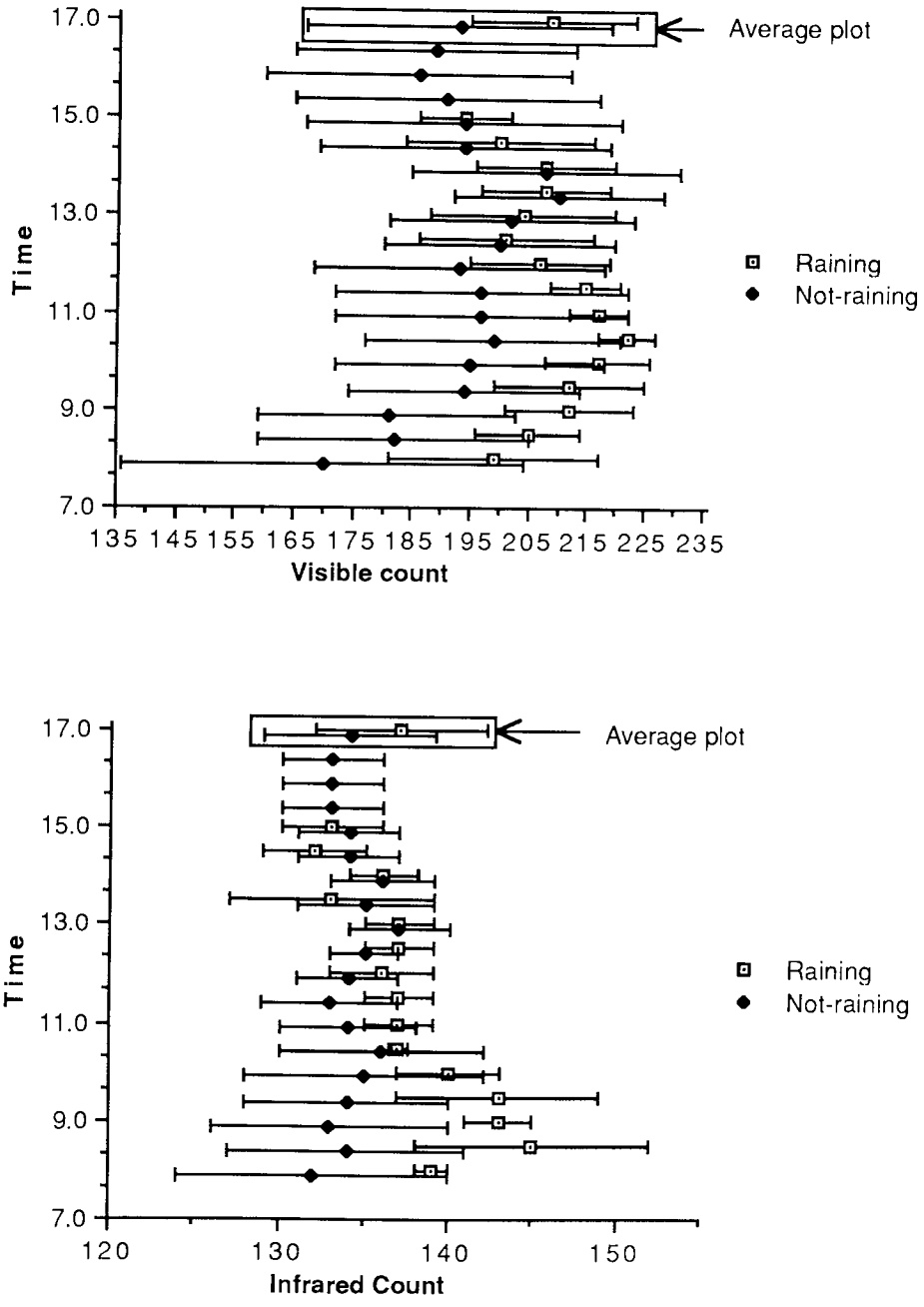

Fig. 4.1b Cospectral plots for the 2nd of June in the visible and infrared.

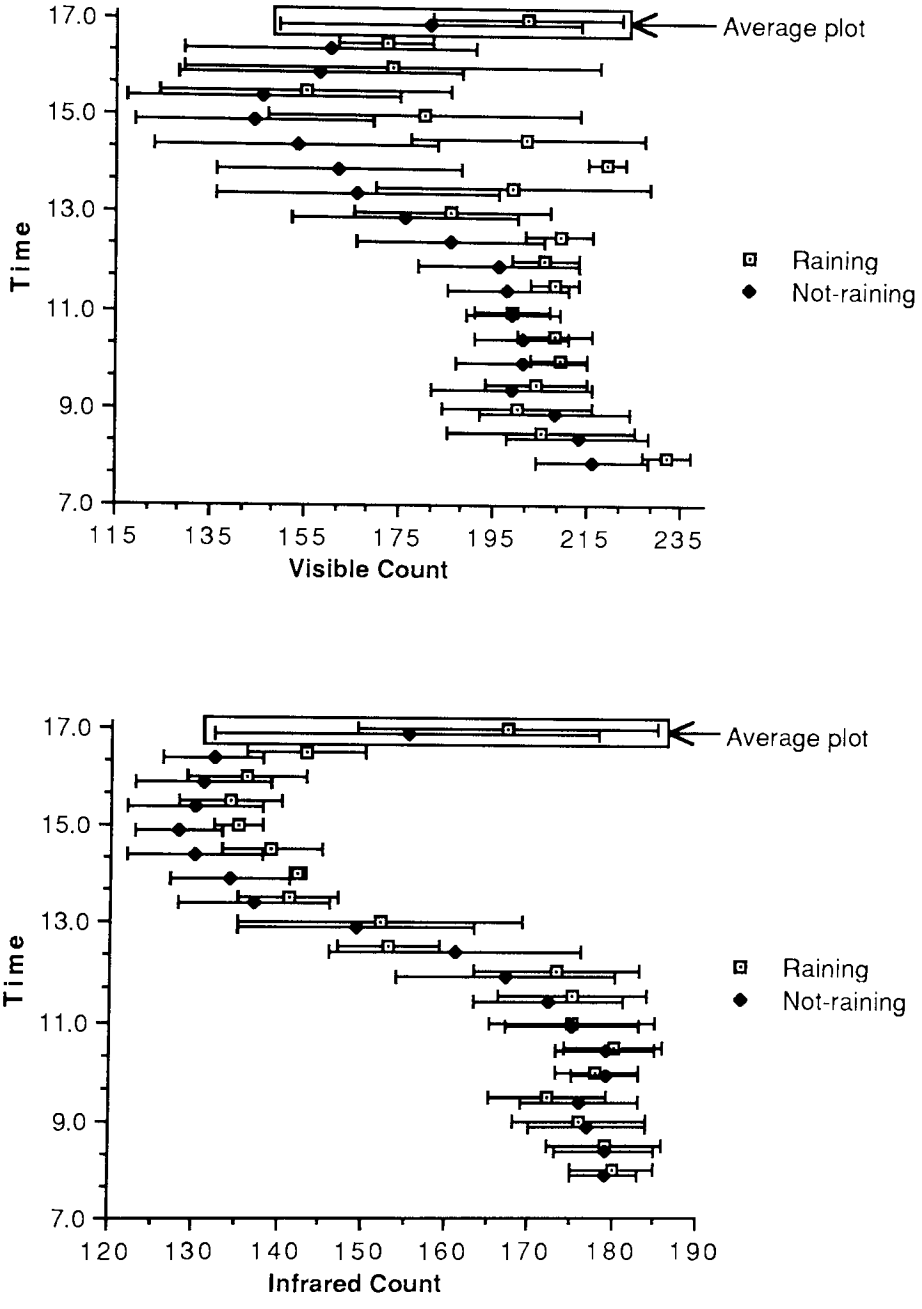

Fig. 4.1c Cospectral plots for the 3rd of June in the visible and infrared.

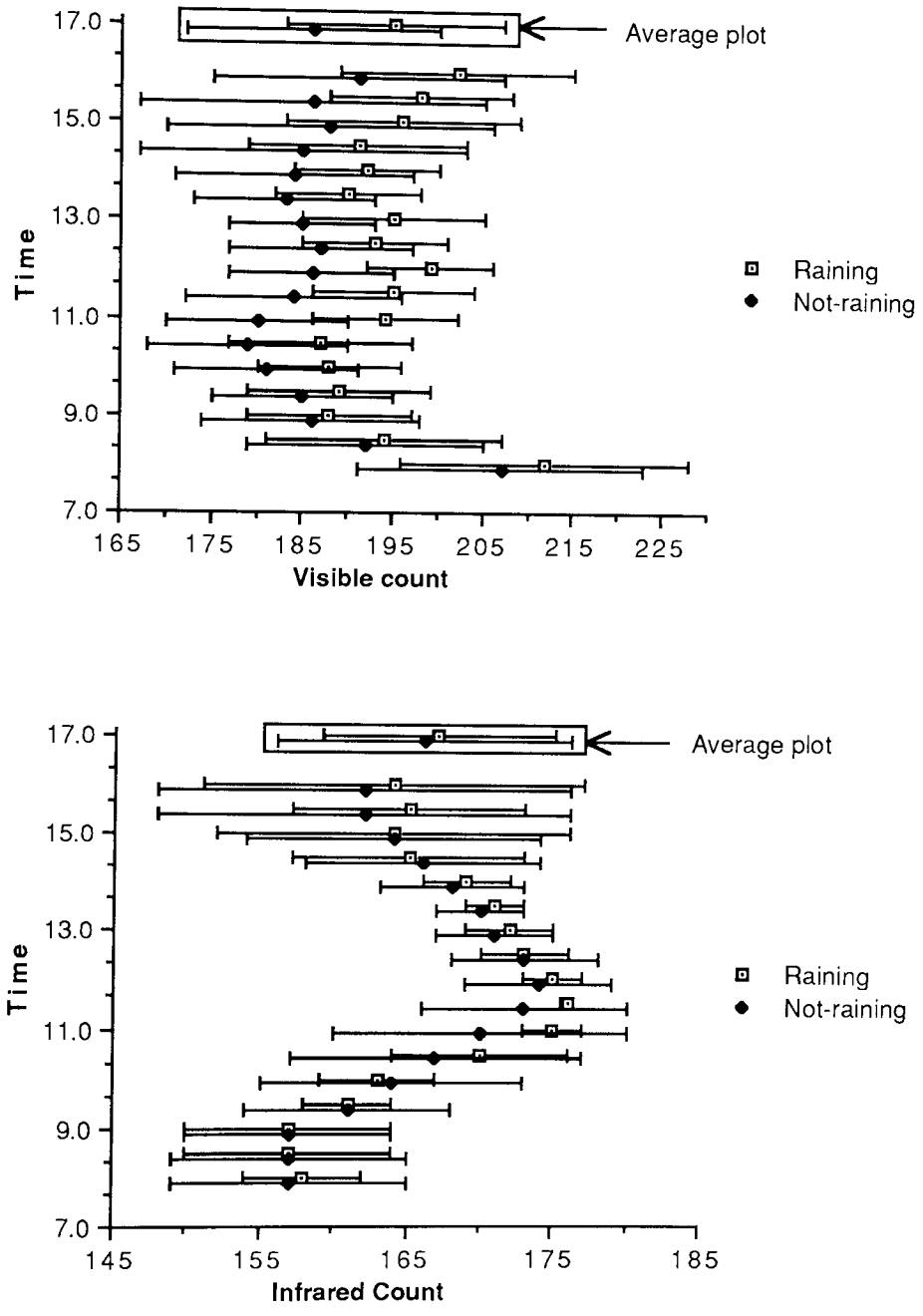

Fig. 4.1d Cospectral plots for the 15th of June in the visible and infrared.

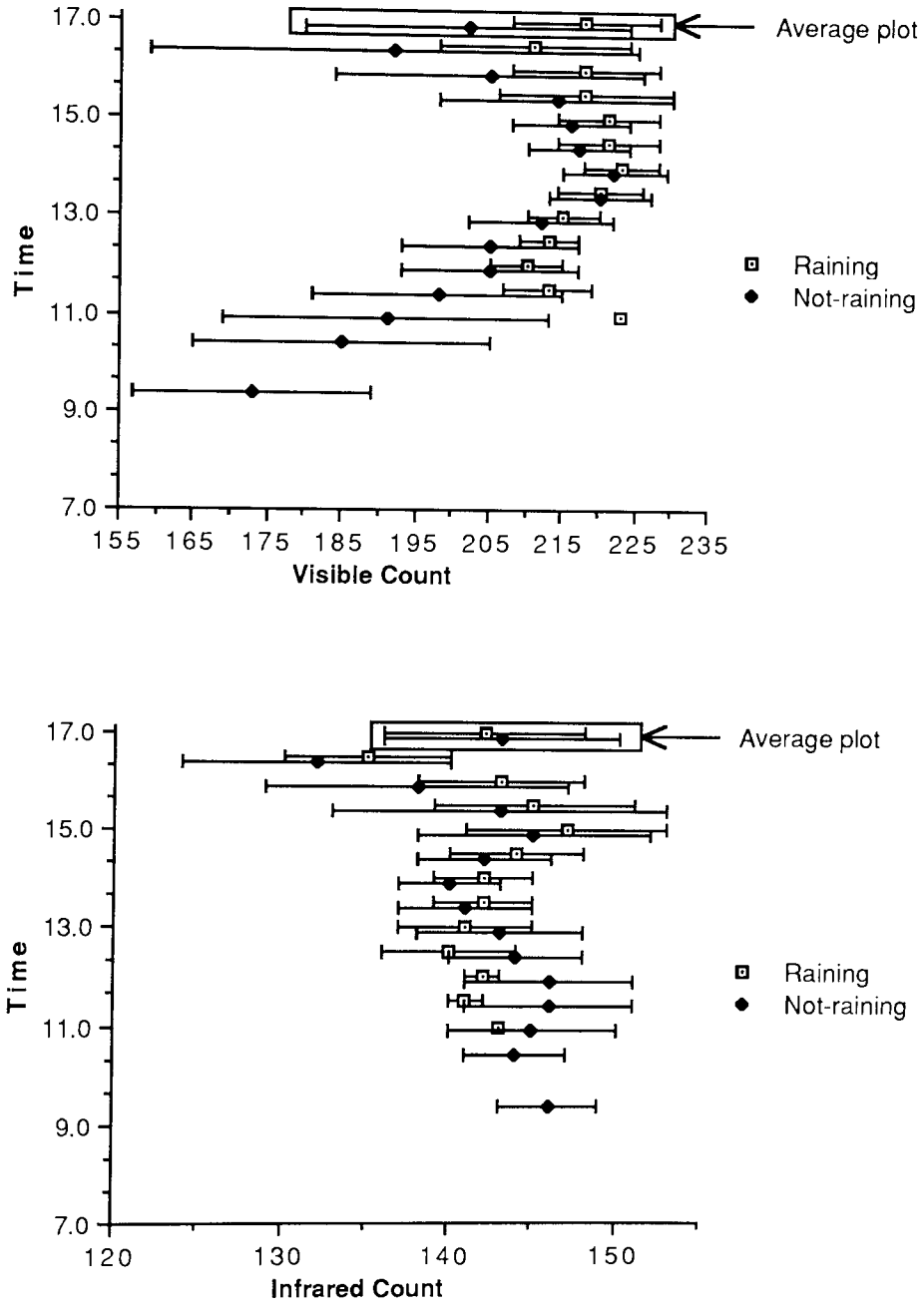

Fig. 4.1e Cospectral plots for the 6th of June in the visible and infrared.

4.3.2 Bivariate Frequency Analysis

4.3.2.1 Introduction

The use of bivariate frequency distributions of visible and infrared data has been used previously in an effort to combine these two separate pieces of information. For example, Lovejoy & Austin (1979a) used this technique to differentiate between rain and no-rain areas; Bellon & Austin (1986) used it in their comprehensive study over Canada; It was also employed by D'Souza (1988) in his study of rainfall estimations over Africa. Tsonis (1984) used this technique together with the spatial characteristics in order to differentiate between various classes that exist in the satellite images. Tsonis concluded that the number of peaks in a frequency distribution is an indication of the number of classes that exhibit different spectral characteristics. The peaks in the distribution were attributed to three main classes, namely: clear skies/no snow cover; clear skies/snow cover and clouds. Rain area or differentiation between raining and not-raining clouds was attempted in a later paper (Tsonis, 1985) in which classification was achieved by determining the location of the peak corresponding to the clouds and cluster analysis. Another investigation was carried out by Coretti et al (1988) over northern Italy with some success.

The basic assumption of the method is that clouds which are both high (very cold in the infrared image) and of large vertical extent (very bright in the visible) are more likely to be raining, so that:

$$R = f\,(\text{Visible, Infrared}) \qquad \text{eq. 4.1}$$

Here R can assume the meaning of rainfall intensity (mm/h) or just the two values Rain/No-rain variable (R/N) for the assessment of the areas with or without precipitation. In this study only R/N is considered since the relationship between intensity and infrared and visible values is quite uncertain (Lovejoy & Austin, 1979b).

In theory, one should use the single pixel infrared and visible values corresponding to the gauge station locations to derive the bivariate frequency distribution. In this case, an uncertainty in time due to the fact that the training set consists of half hourly rainfall totals and not of instantaneous precipitation observations, must be taken into account. This uncertainty in time results in an uncertainty in space if one considers the actual movement of rainfall systems. For these reasons, instead of using single pixel values, a mean of a 3*3 pixel square area centred over the gauge location was used.

4.3.2.2 Results

To derive the frequency distribution, the spectral range (0-255) of the two bands were divided into intervals of eight. The values of all the 8*8 intervals were initialized to zero and were incremented by one whenever the visible and infrared attributes of a gauge fell within the range of a particular interval. For example, a gauge with infrared value of 140 and a visible value of 203 would be assigned to an interval with visible range (200-207) and infrared range (136-143). The procedure was repeated for each image pair over the whole five days and was performed separately for raining and not-raining gauges. Finally, dividing the distribution for the raining gauges by the sum of the raining and not-raining gave rise to the probabilities of presence of precipitation for a certain (visible/infrared) interval. The overall probability (expressed as percentages) distribution is given in fig. 4.2. The shaded region in fig. 4.2 represents area with insufficient data to produce probabilities.

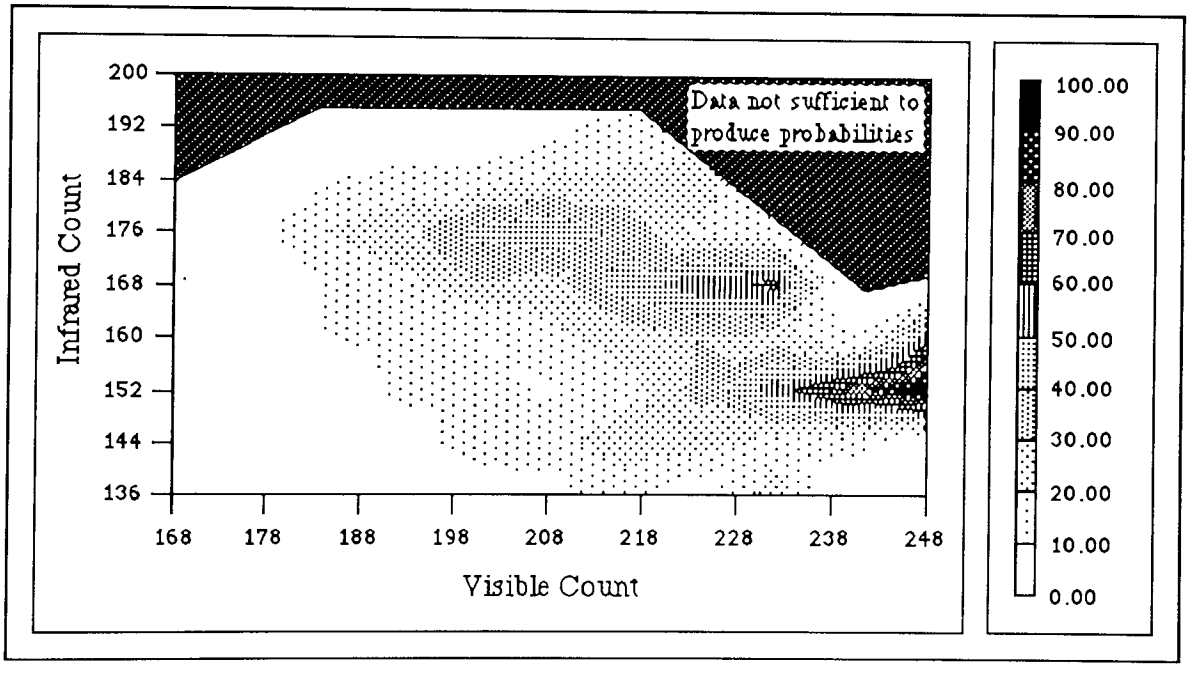

Fig. 4.2 Probability distribution of raining gauges in the visible/infrared domain.

At this point the easiest way to assign the presence or absence of precipitation to a certain pixel would be to check if it lies within the contour in fig 4.2 representing the probability of more than 50%. This would be unrealistic since only a small area in fig. 4.2 is represented by a 50% contour. To circumvent this problem, a method described by Lovejoy and Austin (1979a) was used to select a probability threshold to discern between raining and not-raining pixels. The threshold is defined in such a way that the total number of estimated rainfall cases equals the total number of measured rainfall cases.

Following this method, discrete contours in fig. 4.2 were chosen starting from the contour with the highest probability and their scores in terms of gauges, raining or not-raining, added until it equals the total number of reported rainfall cases. The percentage probability found in this way turns out to be 27 which is incidentally the same as found by Coretti et al (1988) and the 27% contour shown in fig. 4.3 can be used to delineate rain areas from satellite images.

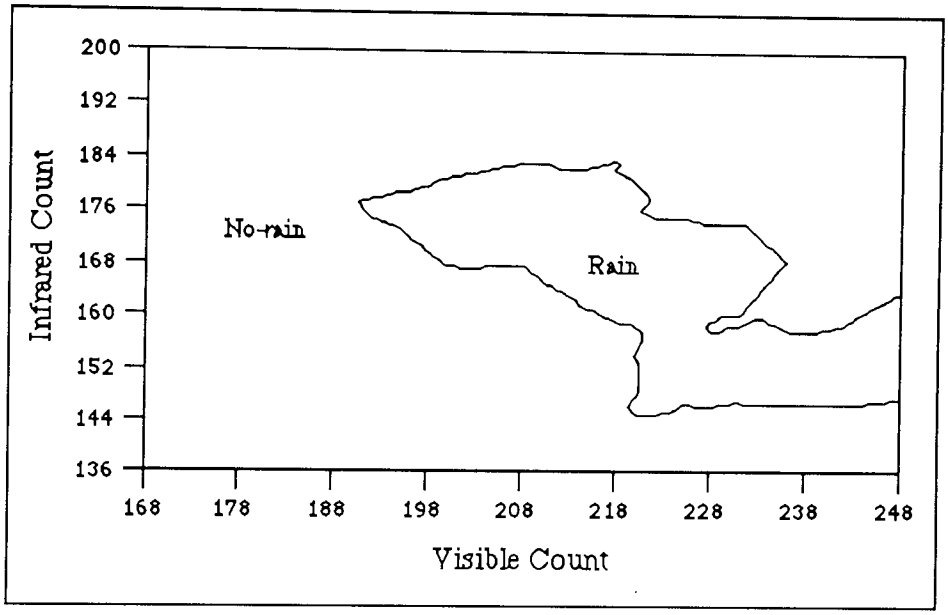

Fig. 4.3 Rain/No-rain classification using bivariate frequency distribution in the Visible/infrared domain.

A quantitative estimate of the effectiveness of the method can be expressed by the statistical indexes (Bellon & Austin, 1986). Given the two classes Rain/No-rain, comparisons with ground truth can be defined in terms of hits H, misses M and false alarms A, from which the following parameters can be defined:

$$\text{Critical Success Index (CSI)} = 100^* \frac{H}{H+M+A} \qquad \text{eq. 4.2}$$

$$\text{Probability of Detection (POD)} = 100^* \frac{H}{H+M} \qquad \text{eq. 4.3}$$

$$\text{False Alarm Ratio (FAR)} = 100^* \frac{A}{H+A} \qquad \text{eq. 4.4}$$

A hit is scored when both the estimated and actual observation show precipitation. A miss is obtained when the estimate is for absence and observation is for presence of precipitation. Conversely, a false alarm is obtained when estimate is for presence of precipitation while the observation show absence.

A perfect method will give CSI = 1, POD = 1, and FAR = 0. However, none of these statistics can be considered as more representative of the success of the method than any other statistics. Each statistics give additional information about the success of the rain area delineation from the satellite data. For example, the POD gives an idea of the ability of the scheme to 'find' the rain. However, a scheme could create five or ten times larger area than the actual and still give a POD of 1. Therefore, high POD should be accompanied by a small FAR in order to be meaningful. The CSI is a compromise score, balancing the need to maximize the number of hits against the disadvantage of generating an unduly large number of false alarms.

The values for CSI , POD and FAR were calculated for each day of analysis used to derive the bivariate frequency distribution. The results are shown in table 4.1 together with the values obtained by other researchers.

4.3.2.3 Discussion

Direct comparisons of results with other studies such as given in table 4.1 may be somewhat misleading. Differences in type of verifying ground data, size of the locality and rainfall systems are prohibitive against such comparisons to be made. For example, better results obtained by Lovejoy & Austin (1979a) and Tsonis & Issac (1986) may be due to the fact that radar data was used and areal rainfall comparisons were made instead of point comparisons. In ADMIT (D'Souza, 1988), different time (daily) and space (continental) scales were involved. Results obtained in this study are slightly worse when compared to the studies by Corretti et al (1988), Bellon & Austin (1986) and Cherna et al (1985) who also used comparisons with point rain-gauge data suggesting that the technique would be more appropriate for convective rainfall storms than storms of frontal origin.

Comparisons in terms of CSI, POD and FAR with conventional methods of obtaining rainfall value at an ungauged point can also be made. Figures 4.4, 4.5, and 4.6 show plots of CSI, POD and FAR respectively as a function of distance from the nearest rain-gauge. These plots were obtained by randomly removing the rain-gauges and comparing the actual value (rain/no-rain) at the rain-gauge with that of an interpolated value using Theissen polygons. Equating the values obtained using satellite data in table 4.1 for this study gives the values for the distances from the nearest rain-gauge as given in table 4.2.

Table 4.1 Comparison of classification accuracy in terms of CSI, POD, and FAR with other studies.

Study	CSI (Range)	POD (Range)	FAR (Range)
*Coretti et. al. (1988)			
Random sample	0.35 (NA)	0.55 (NA)	0.51 (NA)
Convective	0.50 (NA)	0.86 (NA)	0.45 (NA)
*Bellon & Austin (1986)			
Convective	0.54 (0.23-0.82)	0.73 (0.31-1.00)	0.32 (0.18-0.53)
*Cherna et. al. (1985)			
Calibration data	0.44 (NA)	0.63 (NA)	0.39 (NA)
Verification data	0.37 (NA)	0.57 (NA)	0.52 (NA)
**Lovejoy & Austin (1979)			
Convective	0.65 (NA)	NA	NA
Stratiform	0.56 (NA)	NA	NA
**Tsonis & Isaac (1986)			
Convective	0.7 (0.59-0.79)	0.59 (0.33-0.77)	0.3 (0.21-0.4)
Stratiform	0.6 (0.3 0.81)	0.7 (0.58 0.81)	0.4 (0.19-0.7)
Admit (D'Souza,1988)			
Convective (Daily)	0.61 (NA)	0.8 (NA)	0.27 (NA)
*This Study			
Stratiform	0.26 (0.17-0.31)	0.55 (0.34-0.72)	0.66 (0.6-0.79)

* Point raingauge data was used for calibration

** Ground Radar data was used for calibration

Table 4.2 Equivalent mean distances for the nearest rain-gauge for the satellite data according to statistics CSI,POD and FAR.

Satellite Statistic	Distance from the nearest raingauge
CSI	35-40 km
POD	10-15 km
FAR	45-50 km

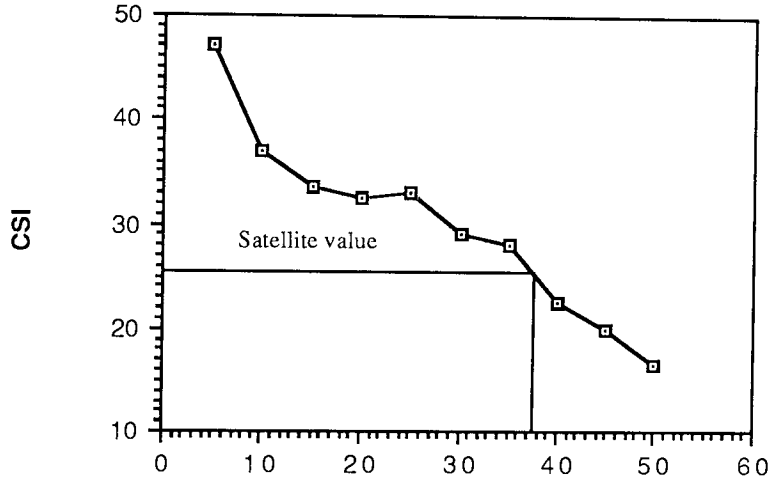

Fig. 4.4 CSI values as a function of distance from the rain-gauges.

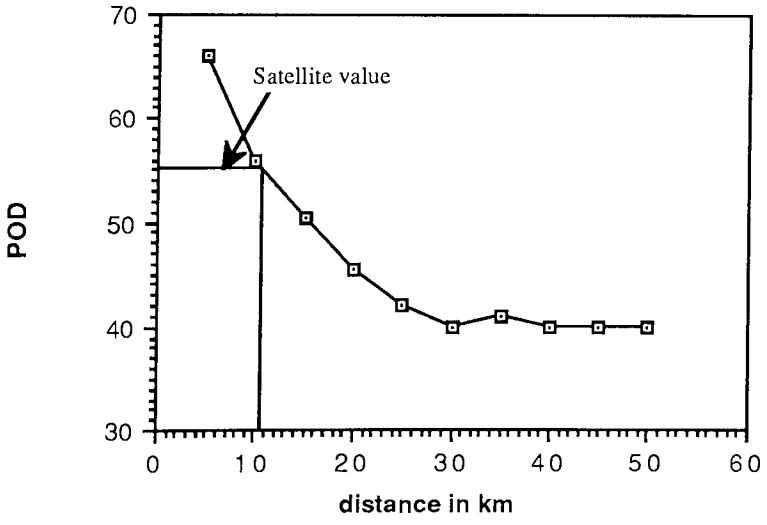

Fig. 4.5 POD values as a function of distance from the rain-gauges.

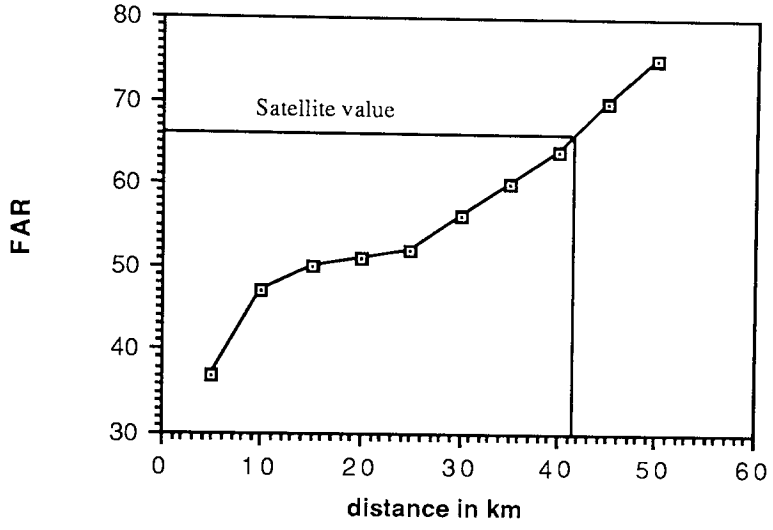

Fig. 4.6 FAR values as a function of distance from the rain-gauges.

In other words, with CSI as the basis, errors involved in determining rainfall at a point 40 km away from a rain-gauge using Theissen polygons are the same as that using satellite data. Lower value obtained using the POD statistics and a higher value for FAR statistics indicates that the satellite data delineates a much larger rain area than the actual rain area. Figure 4.7 shows the percentage of catchment area with the nearest rain-gauge D km distance away for different densities of rain-gauges. It shows that for D=40 km and gauge density as low as 20% of the full network, only 5% of the catchment area is devoid of a rain-gauge in a radius of 40 km. In other words,providing 20% gauge density, satellite data can only be used for that 5% of the catchment area where the accuracy, in terms of CSI, exceeds that of interpolated Theissen field. However, the interpolated field would still have the advantage of assigning actual amounts rather than just establishing rain or no-rain. It is therefore understandable why such a technique would be appropriate for applications such as Forest Fire Management (Bellon & Austin, 1986) in which rain or no-rain information is sufficient to determine wet or dry areas but not for hydrological applications where actual rainfall amounts are required.

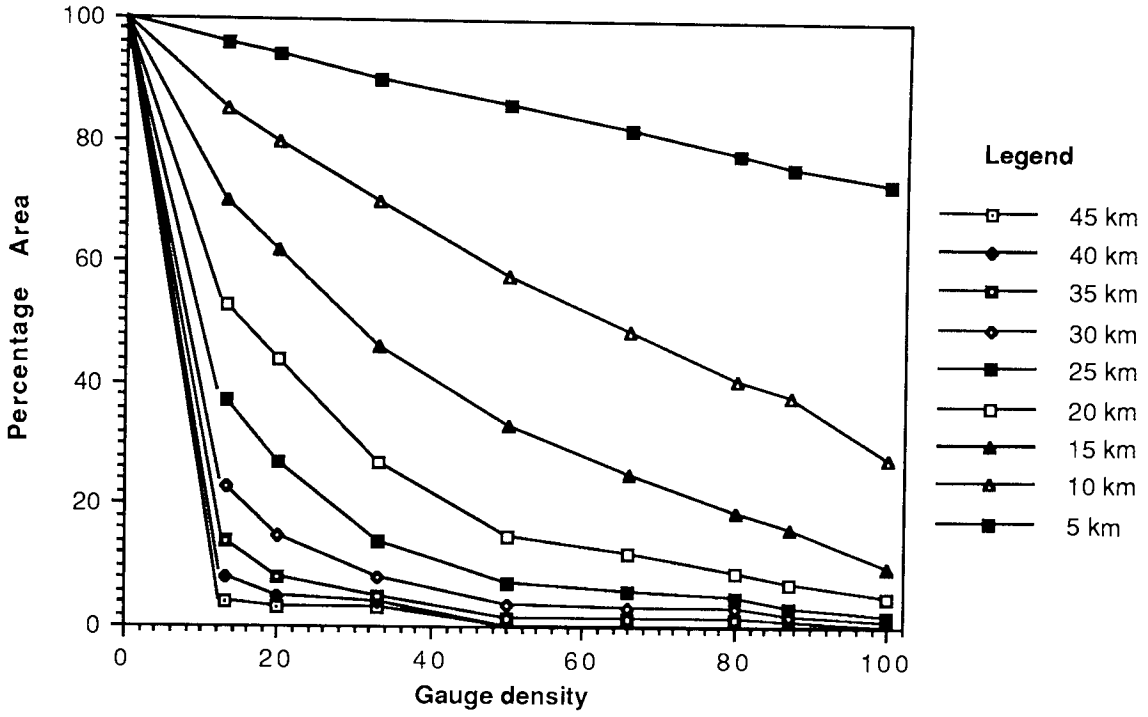

Fig. 4.7 Percentage of catchment area with nearest rain-gauge upto certain distances for different percentage densities of raingauges (relative to the full network).

4.3.3 Texture Analysis

4.3.3.1 Introduction

Textural measurements conducted over an image define the relationship of a pixel with its neighbouring pixels. Wezka et al (1976) gives a comprehensive review of different methods that can be used to derive textural features or measures for terrain classification (see also Haralick et al, 1973). In meteorology, these textural features have been used in addition to radiance features for cloud type identification (see for eg. Parikh, 1977; Parikh & Ball, 1980; Parikh & Rosenfield, 1978, Hawkins, 1980). Their studies showed that additional textural measures did not improve the classification accuracy significantly as achieved by using radiance features alone. The same techniques have been applied to classify cloud areas producing light, moderate or heavy rainfalls (Wu et al, 1985). The method used pattern recognition techniques in which a 'pattern' was described by a feature vector containing various radiance and textural features. These feature vectors were evaluated for each class (light, moderate, or heavy) using training data sets. Maximum likelihood or minimum distance methods were used to assign the feature vectors for unknown data sets to the above mentioned classes. The results showed that higher accuracies are obtained if only two classes, i.e rain and no-rain, are used. Radiance features were found to be much superior to the textural features in the classification scheme.

Earlier investigation using bivariate frequency distribution of radiance values in the visible and the infrared resulted in poor classifications due to large number of not-raining gauges being classified as raining. If there is evidence that the raining gauges are different texturally in any of the two bands then a texture measure can be used to further improve the classification using bivariate frequency distribution. For that purpose a number of texture measures were used on the available data set.

4.3.3.2 Texture Measures

4.3.3.2.1 Standard Deviation of Grey-Level

Fig 4.8 shows a 3*3 image section centred over a gauge. Assume that a raining gauge exhibits a course texture representing higher gradients and a no-rain gauge shows a smooth texture. The mean radiance values in the two cases could well be the same but the standard deviation of radiance values would be higher for the raining gauge than the not-raining gauge. Thus a standard deviation of radiance values in a 3*3 window could be used as a texture measure and is described as:

$$\text{Standard Deviation} = \frac{1}{N}\sum_{N=1}^{9}\left(GL_i - \overline{GL}\right)^2 \qquad \text{eq. 4.5}$$

where GL is the Grey Level or the radiance values of the pixels.

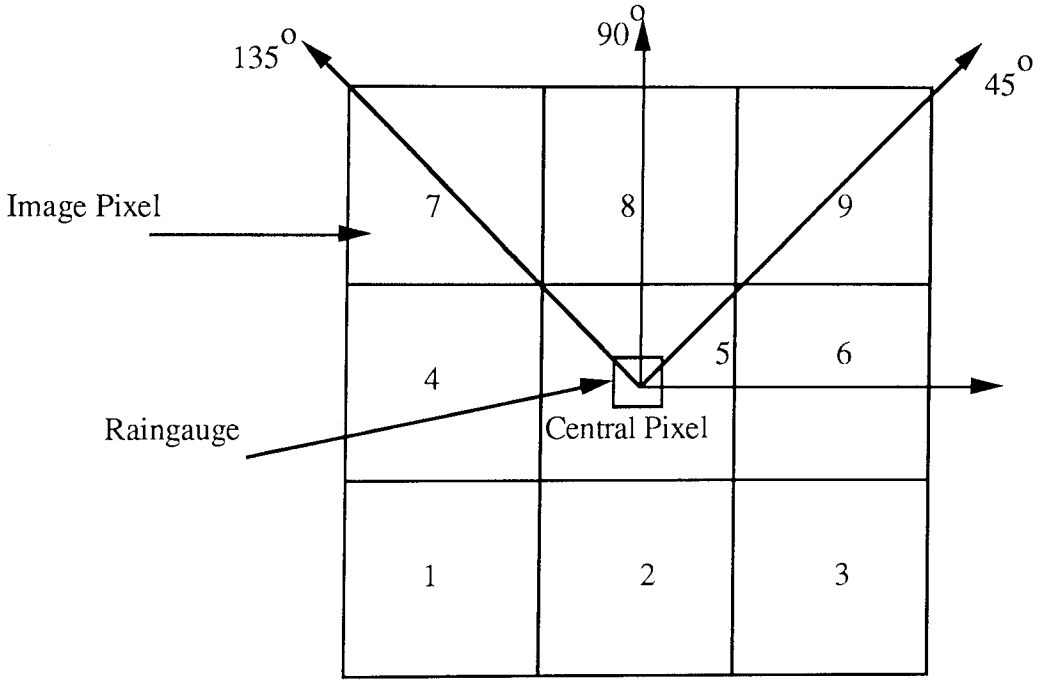

Fig. 4.8 A 3x3 image segment over a gauge location

4.3.3.2.2 Grey-Level Difference Statistics (GLDS):

Texture measures based on GLDS depend on the histograms of the distributions of radiance H(f). Let f(x,y) define the digital image function in fig 4.8. If pairs of pixels are considered within the 3*3 window, the grey level difference is given by the expression:

$$f_d(x,y) = \left| f(x,y) - f(x+d_1, y+d_2) \right| \qquad \text{eq. 4.6}$$

where d is the number of pixels separating the two points and d_1 and d_2 can assume values of 0 or ±d. Different values of d_1 and d_2 give rise to different pairings of f(x,y) and $f(x+d_1,y+d_2)$. For example the central pixel, labelled 5 in fig 4.8, can be paired with eight neighbouring pixels for d=1. These correspond to the directions of 0°, 45°, 90°, and 135° degrees respectively. The grey level difference $f_d(x,y)$ may assume values in the range 0-255.

The histograms H(f) of grey level difference provide a measure of the scale size of the cloud features. If the pixels within a window exhibit smooth texture compared to the selected pixel separation d, then grey level difference $f_d(x,y) = 0$ approximately will be highly probable. On the other hand, if the window is not homogeneous in appearance compared to the pixel separation d, then a larger range of $f_d(x,y)$ is more probable. The histograms H(f) will thus be spread over a larger range of $f_d(x,y)$ as graininess or streakiness increase.

A number of statistical features based on the GLDS, that characterize the shape of H(f) can be calculated. These are described in detail by Wezka et al (1976). One of the statistics called Contrast, measures the local variation of image function f(x,y): if it is small, the grey levels of f(x,y) are quite uniform, while if it is large, f(x,y) has a large range of grey values. The Contrast feature is given by the expression:

$$\text{Contrast} = \sum f_d(x,y)^2 \left[\frac{H(f_d)}{N} \right] \qquad \text{eq. 4.7}$$

where N is the total number of pixel pairs in the window separated by distance d.

4.3.3.3 Results and Discussion

Figures 4.9 (a-e) and 4.10 (a-e) show the results of the texture measures applied to five days of data set for infrared and visible respectively. The measures were conducted only over the gauges classified as raining gauges using the bivariate frequency distribution. The Contrast feature is represented by two sub-features namely the Mean contrast in four directions and the Maximum contrast in four directions. These were calculated for the two separations of d=1 and d=2. For each day of analyses, the distribution of textural values

are given in the form of the mean value and one standard deviation for the classes rain and no-rain. For each of the texture measure there is a large degree of overlap between the two classes of raining and not-raining points making it very difficult to differentiate between the two classes.

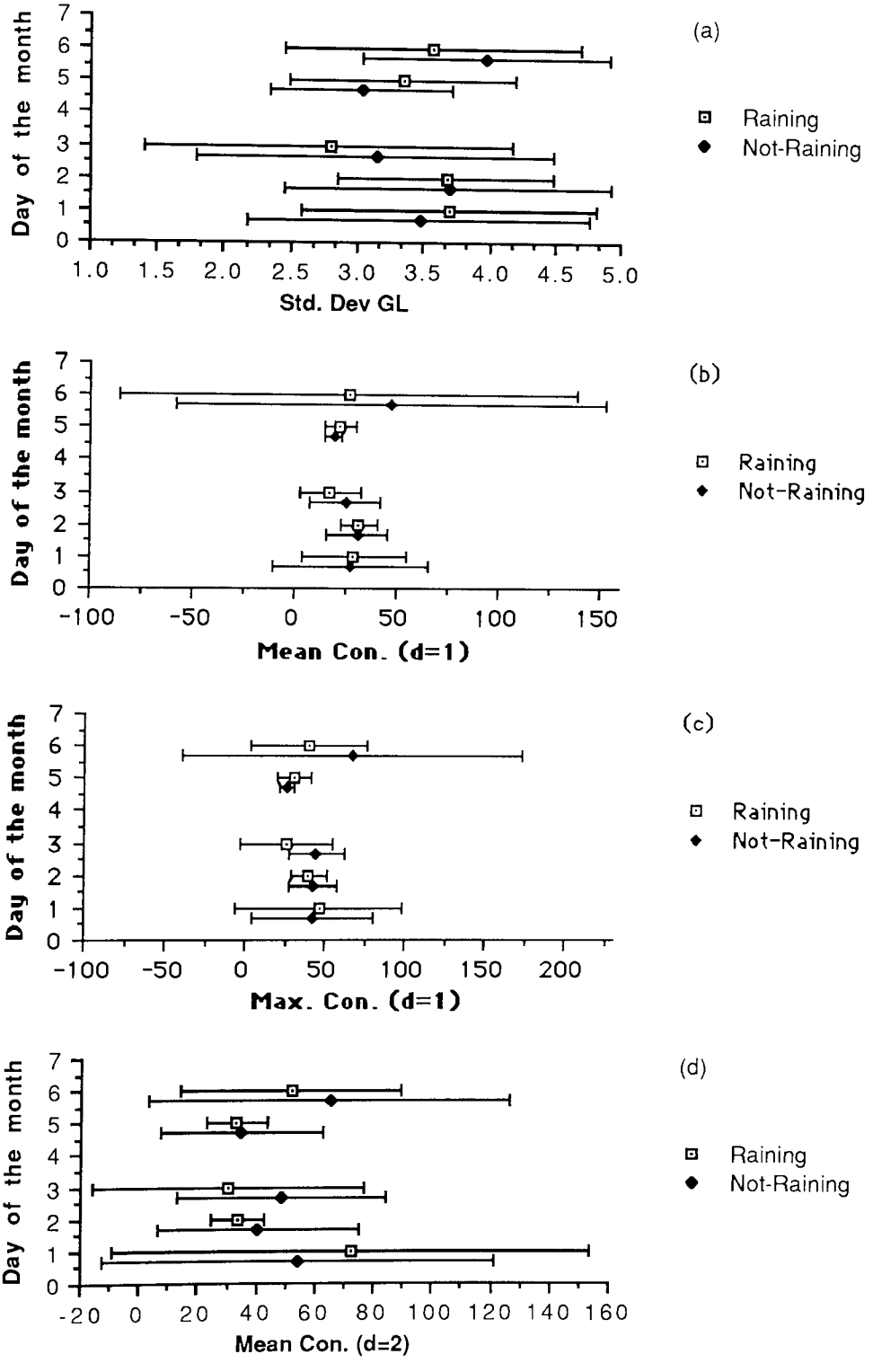

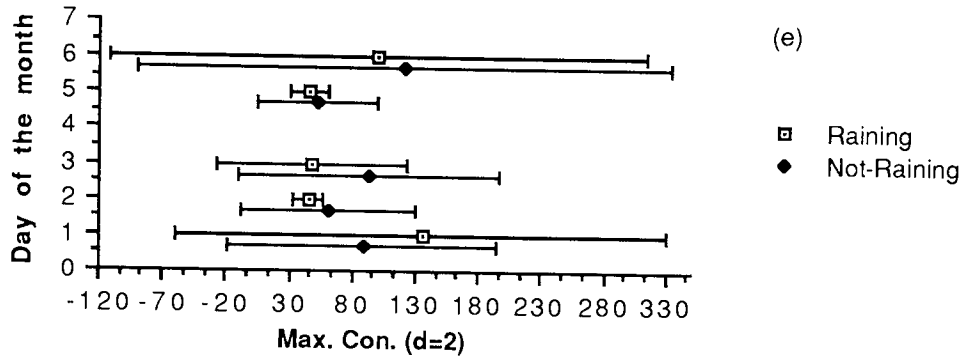

Fig. 4.9(a-e) Plots of textural features for the two classes of raining and not-raining points using the visible images.

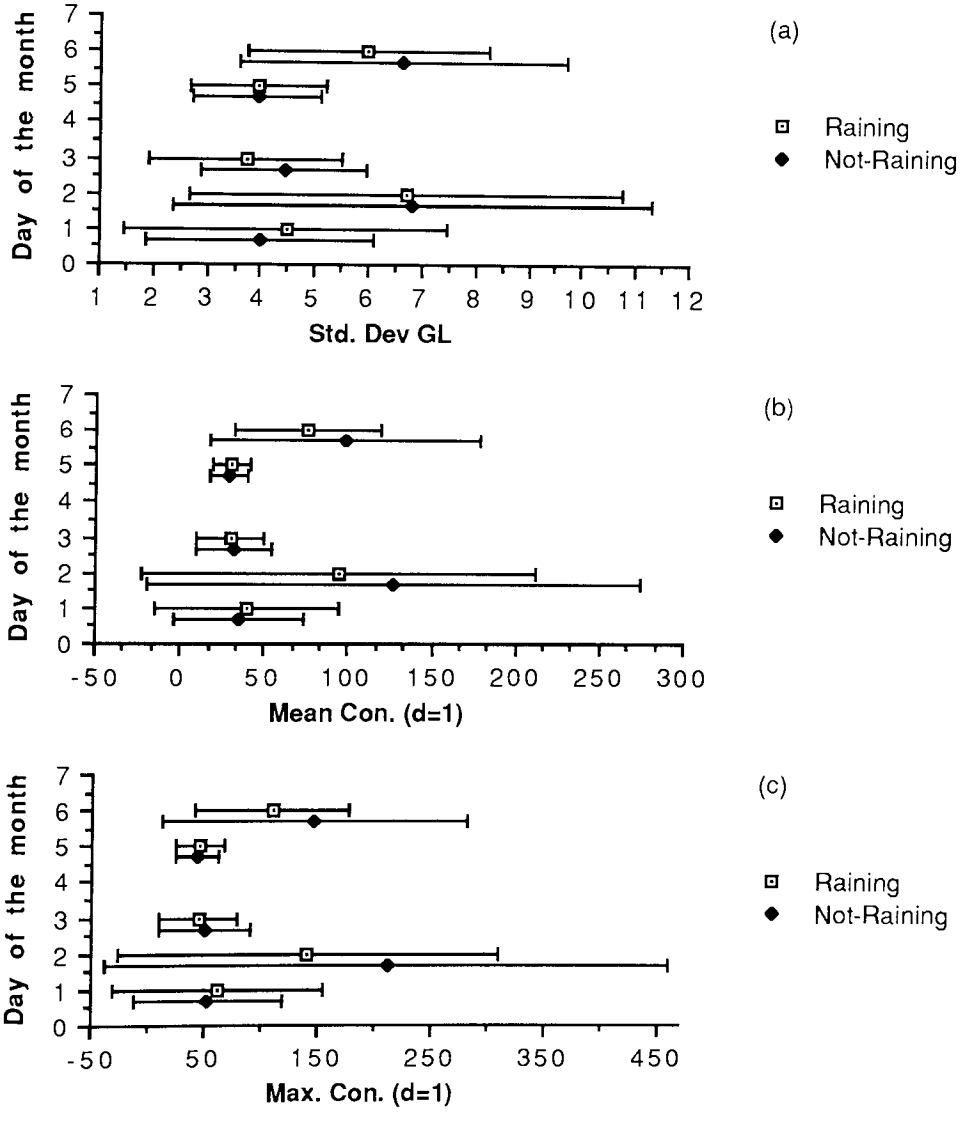

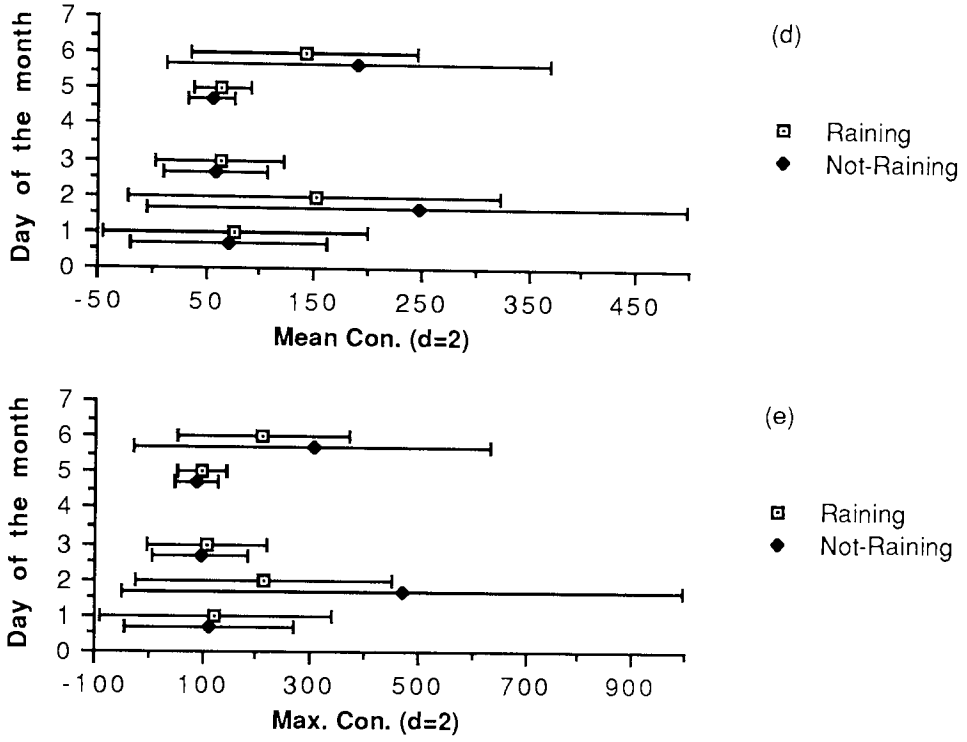

Fig. 4.10(a-e) Plots of textural features for the two classes of raining and not-raining points using the infrared images.

4.3.4 Volumetric Rainfall / Cloud Area Relationship

4.3.4.1 Introduction

In the previous sections, radiance and textural properties derived from satellite data were examined in order to assess their ability in differentiating between raining and not-raining gauges. The analyses showed that point gauge comparisons between satellite observations and gauge reports exhibit large variations. Even if successful rain area delineation is achieved, the problem of assigning rainfall amounts remains.

For most applications, such as in catchment hydrology, exact rainfall amount falling at a point is not required. Instead, a rainfall event is described in terms of total volumetric catchment rainfall (m^3) or mean areal rainfall (mm or inches) falling over a catchment for a specific time period. The value for mean areal rainfall is arrived at using point rain-gauge data and interpolating the values between the gauges. The most common methods for that purpose are the Arithmetic mean and the Theissen polygons.

A scheme which relates a satellite derived parameter with the volumetric catchment rainfall would be highly desirable. The most obvious satellite parameter would be a precipitable cloud area over a catchment since it is reasonable to assume that larger the precipitable cloud area, higher would be the catchment rainfall. Stout et al (1979) investigated the

relationship between the cloud area and the rate of change of cloud area to the volumetric catchment rainfall (see section 2.3.2). Griffith et al (1978) used similar techniques in their study but their algorithm required concurrent radar data. Follansbee (1973) established a relationship between total rainfall and cloud areas associated with three different cloud types usually associated with rainfall such as cumulonimbus, nimbostratus etc. These are identified subjectively on the satellite images.

The following sections investigates the relationship between cloud area and volumetric rainfall for the present data set.

4.3.4.2 Definition of 'Precipitable' Cloud Area

On the infrared satellite images, clouds can easily be distinguished from other features such as land, sea etc (Barrett & Martin, 1981). Some problems are encountered if snow is present on the ground which has the same spectral response as clouds but these too are resolved to some degree by observing the moving nature of the clouds in the sequence of images. A problem arises when within the class labelled 'clouds', one tries to distinguish between raining and not-raining sections of the cloud. Earlier studies adopting this approach have resorted to defining a particular infrared temperature threshold above which clouds are assumed to be producing rain since colder clouds are more likely to produce rainfall than warmer clouds. Definition of such a threshold varies for different studies and for different locations. For example. Stout et al (1979) used a value of 245 K in his study; Arkin (1979) tried a wide range and found 235-240 K to produce the best results; Griffiths et al (1978) and Negri & Adler (1987a, 1987b) found the value of 253 K as suitable for their studies. Similar approach would prove difficult in this study since cospectral plots of figure 4.1 (a-e) show that any threshold would inevitably include most of the not-raining gauges. Moreover, clouds observed for days 1st, 3rd and 5th of June were found to be colder than the clouds observed on the 2nd and 6th of June, making it yet more difficult to arrive at one threshold that is universally applicable.

However, examination of bispectral frequency distribution (section 4.3.2) of all the gauges and of raining gauges for each day show that the peak frequency found in the distribution of raining gauges correspond closely to the peak frequency found in the distribution for all the gauges. In other words, most of the raining gauges occupy the same region defined by the peak frequency and the neighbouring frequencies in the visible / infrared space. The peak frequency (or frequencies since there could be more than one peak frequency) can be defined as the one found in the region enclosed by thresholds of 136 and 192 in the infrared and visible respectively. This is illustrated in table 4.3 which shows the percentage of raining gauges found in the frequencies described by the peak and the neighbouring frequencies. Thus a precipitable cloud area can be defined by the peak and its

neighbouring frequencies in the bivariate frequency distribution of an infrared and visible pair. Cloud area defined in such a way was calculated for each day and for each half hour image pair. The 'cloud area' values were than regressed against the volumetric rainfall totals calculated using rain-gauge readings and Theissen polygons.

Table 4.3 Percentage of raining points belonging to the peak and the neighbouring frequencies in the bivariate frequency distribution for each day of the data set.

Day	Percentage of raining points in the peak
1st of June	74
2nd of June	63
3rd of June	68
5th of June	79
6th of June	59

4.3.4.3 Results

Figures 4.11 (a-e) show the time series of cloud area values and the volumetric rainfall totals for all the five days. The general shape of the graphs corresponding to the two variables relate well to each other except in the case of 2nd of June. Here, the dissimilarity between the two graphs may be due to the suspected orographic influence. The mean altitude for all the 86 rain-gauges is 139 m whereas the mean altitude for the raining gauges on the 2nd of June was found to be 230m which shows a considerable bias towards higher altitude. Also, in the cases of 5th and 6th of June, volumetric rainfall is lagging behind the cloud area whereas on the 3rd of June the opposite is observed, i.e cloud area is lagging behind rainfall. Correlation coefficients between the two variables for each day are given in table 4.4 which shows considerable variation in the values of the coefficients ranging from r=0.2 for the 2nd of June to r=0.88 for the 1st of June. As expected, lagging rainfall behind the cloud area resulted in improved correlations for the 5th and 6th of June and reduced correlations for the 1st and the 3rd.

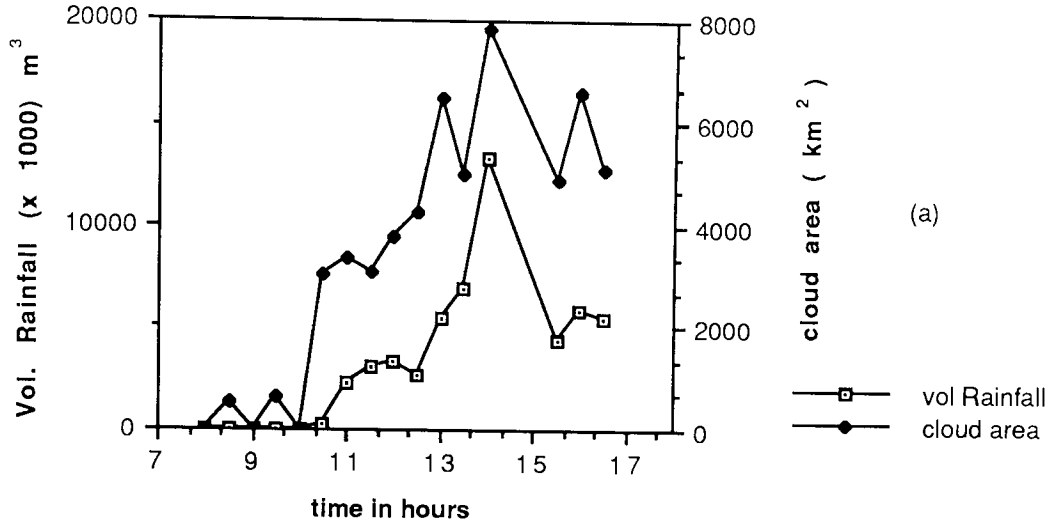
20000
10000
0
8000
6000
4000
2000
0
7
9
11
13
15
17
time in hours
Vol. Rainfall (x 1000) m3
cloud area (km 2)
(a)
vol Rainfall
cloud area

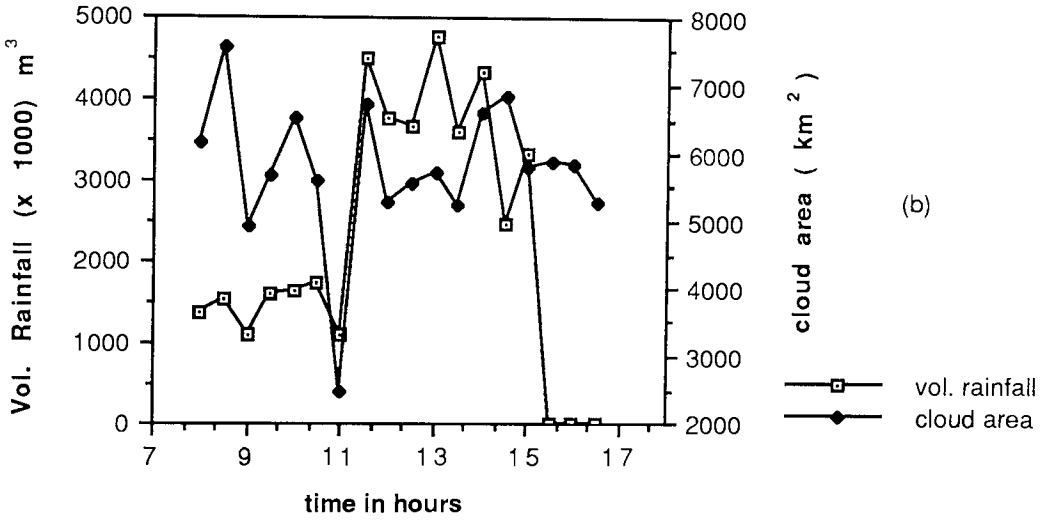
5000
4000
3000
2000
1000
0
8000
7000
6000
5000
4000
3000
2000
7
9
11
13
15
17
time in hours
Vol. Rainfall (x 1000) m3
cloud area (km 2)
(b)
vol. rainfall
cloud area

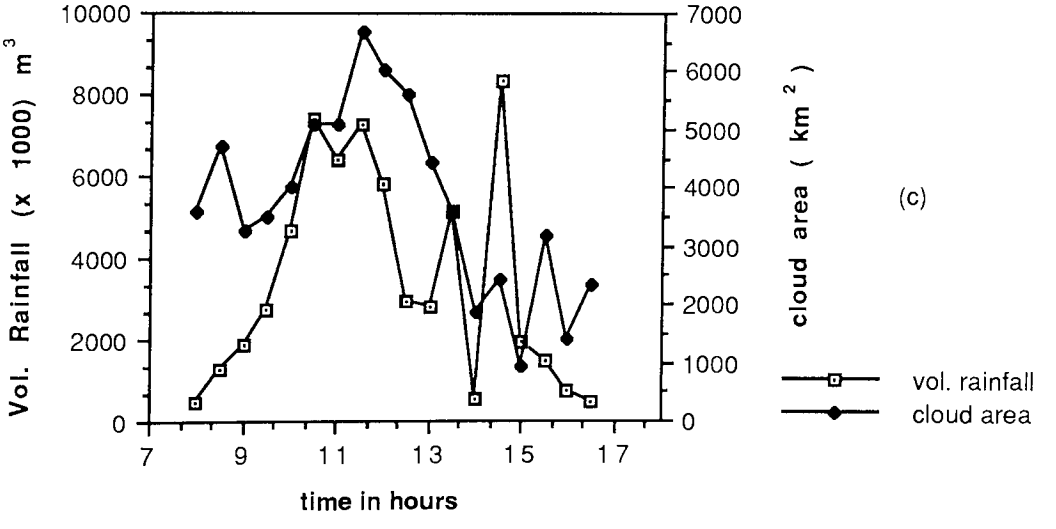
10000
8000
6000
4000
2000
0
7000
6000
5000
4000
3000
2000
1000
0
7
9
11
13
15
17
time in hours
Vol. Rainfall (x 1000) m3
cloud area (km 2)
(c)
vol. rainfall
cloud area

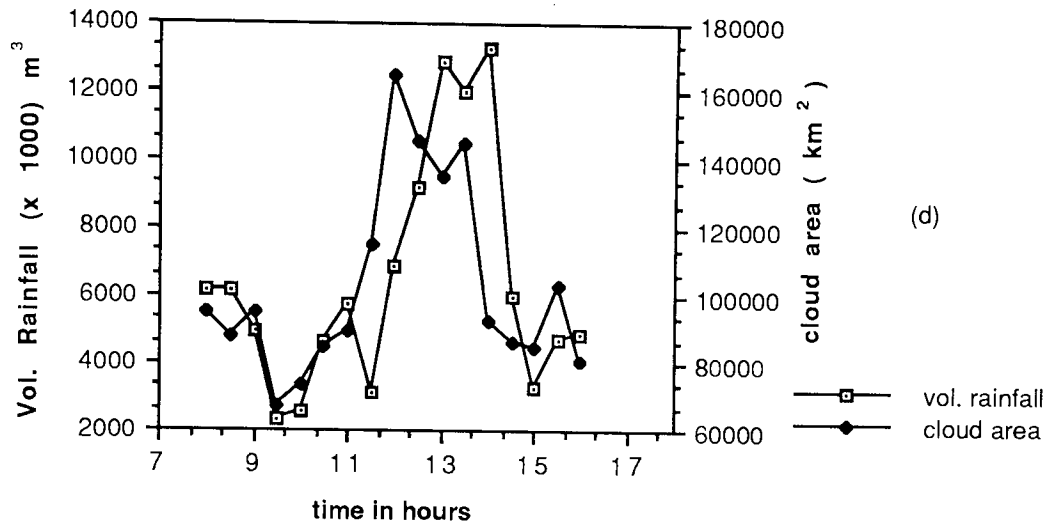

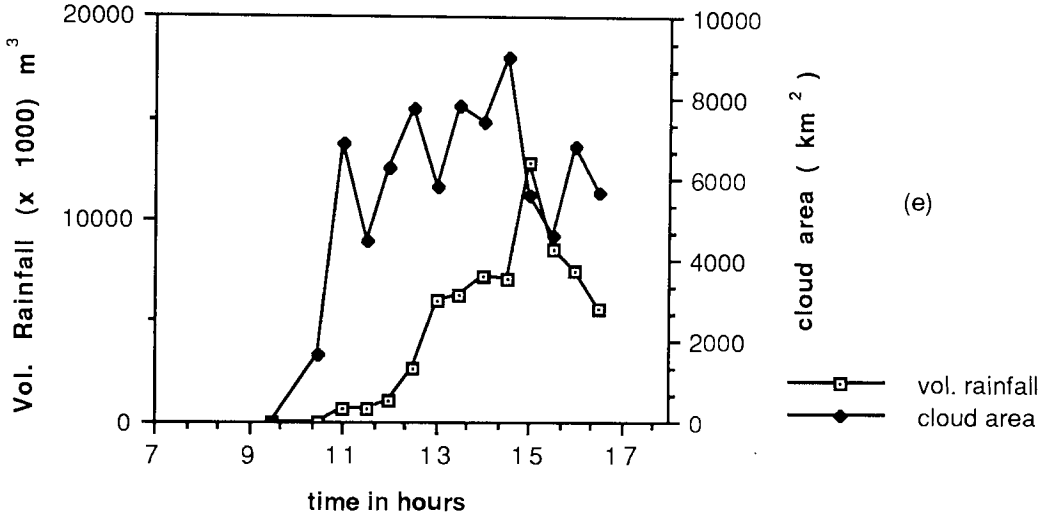

Fig. 4.11(a-e) Time series of volumetric rainfall and observed cloud area for each day of the data set. (a) 1st of June (b) 2nd of June (c) 3rd of June (d) 5th of June (e) 6th of June

Table 4.4 Correlation Coefficients for Cloud Area vs Volumetric catchment rainfall for each day of the data set.

Day	Correlation Coefficients		
	Lag = 0	Lag = 1/2 hour	Lag = 1 hour
1st of June	0.89	0.71	0.81
2nd of June	0.20	0.19	0.16
3rd of June	0.48	0.32	0.29
5th of June	0.57	0.85	0.78
6th of June	0.43	0.70	0.60

Clearly, any regression equation relating cloud area with volumetric rainfall derived for a particular day is not likely to be applicable to a data set for any other day. Therefore, data

from all the five days were combined to give an overall regression as shown in figure 4.12. The correlation coefficient found for this global regression was equal to 0.58. This gave rise to one regression equation shown in figure 4.12 which should be applicable to the five days of the training data set and to any other independent data set. The equation was applied to two independent sets of data corresponding to 11th and 30th of June respectively. The results for these are shown in figures 4.13 and 4.14 respectively.

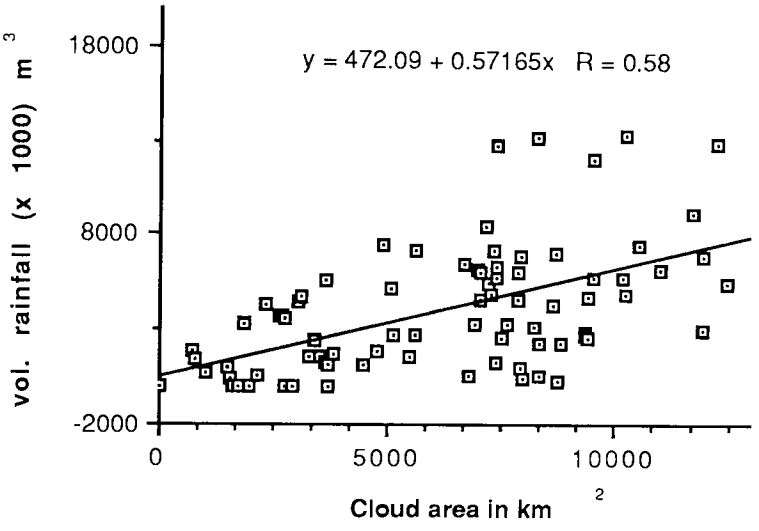

Fig. 4.12 Relationship between the half-hourly cloud area and catchment volumetric rainfall.

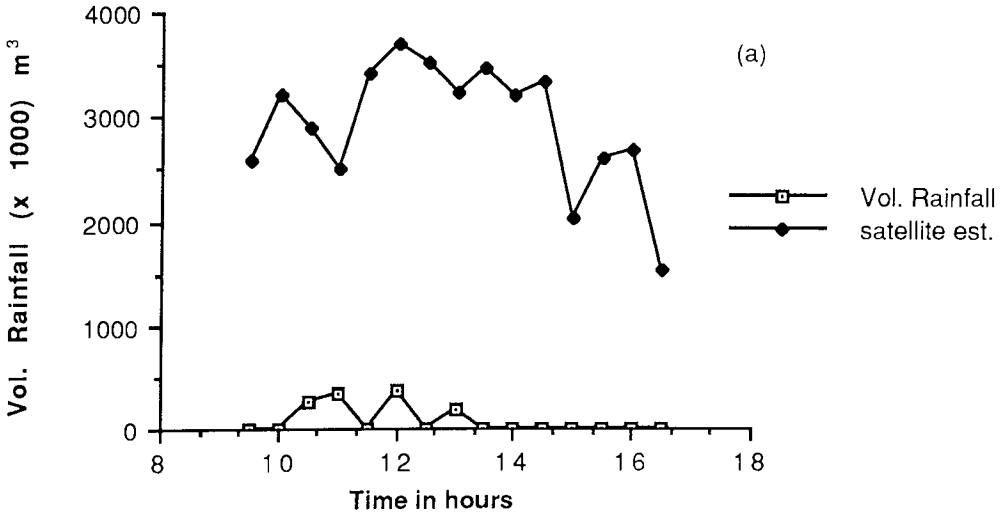

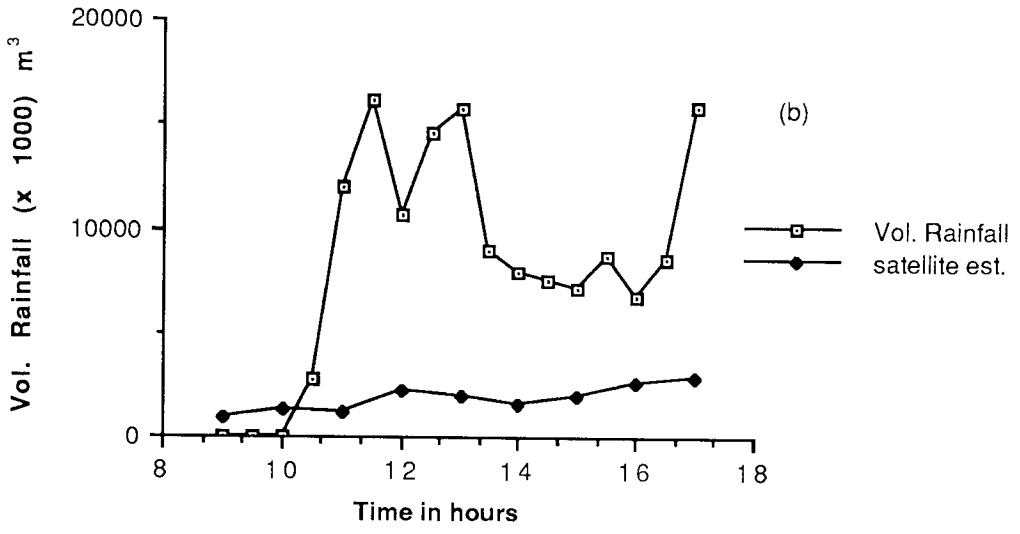

Fig. 4.13 Observed and estimated rainfall using the relationship of fig. 4.12. (a) 11th of June 1990 and (b) 30th of June 1990.

4.3.4.4 Discussion

Considerable variation in the relationship between cloud area and volumetric rainfall does not allow consistent estimates to be made using the satellite data alone. This is clearly shown in the estimates made for independent data sets of 11th and 30th of June, using the equation derived from the training data set of 1st to 6th of June. The algorithm grossly over estimates the rainfall for the 11th of June and grossly underestimates it for the 30th of June. Visual observation of cloud formation for the 30th of June revealed relatively small clusters of clouds, which is a property of convective clouds, and explains the underestimation of rainfall by the algorithm. However, the clouds observed on the 11th of June were similar to the ones in the training data set; i.e of frontal origin, with relatively warmer clouds as found on the 2nd and 6th of June. The algorithm, therefore, produced estimates similar to the rainfall observed on the 2nd of June while in actual fact little or no rainfall was observed by the rain gauges. Discrepancies like these will always be present using such an algorithm. Such algorithms may well have some use in large scale and long term meteorological applications but are unlikely to be reliable enough for hydrological purposes.

4.4 Conclusion

In this chapter, the general relations between rainfall and parameters derived from visible and infrared geosynchronous satellite data have been explored, albeit in a small area of Central England using a 5 day data sample. The objective was to understand these relations

as a first step towards a better visible/infrared rain estimation technique and to understand the limitations of this type of rain estimation.

Estimating rainfall from satellite infrared and visible data has inherent drawbacks, due to the lack of a direct physical connection between the observed radiance (related to the distribution of small, non-precipitating cloud particles) and the precipitation-sized drops falling at the surface. However, there is an obvious correlation between clouds and rain and any satellite based rainfall estimation technique depends on calibrations from conventional ground data. Some general conclusions concerning satellite data/rain interrelations are as follows:

* Visible and infrared data offer slight discrimination between the raining and not-raining areas of the clouds. Poorer results obtained in this study using bivariate frequency distribution as compared to other studies is due to the frontal nature of the clouds observed. However, even if acceptable discrimination is achieved, assigning rainfall amounts to such areas remains a problem.

* There is no evidence that there is any textural difference between the raining and not-raining points.

* Simple cloud area/volumetric rainfall (cloud area defined as the rain area assigned using bivariate frequency distribution) may be of sufficient accuracy to obtain useful results on a longer time scale (decades,monthly). This approach is of questionable value on a smaller time scale such as in this study due to the large variabilities in the cloud area/rainfall relations.

* Although the visible data are helpful in some situations, its unavailability at night and variance due to sun angle variation makes it questionable for inclusion into a technique.

It is acknowledged that a limited data set has been used (total of 83 image pairs) but table 4.1 suggests that even in studies where extensive data sets have been used, results are not that dissimilar. Attempts to calibrate satellite data using rain-gauges or radar information would always give results similar to the ones found in this study and in various other studies (see chapter 3) with varying amounts of successes (in relative terms) and failures. A somewhat different approach may be envisaged in which satellite data can be used as additional information to the already existing information from point rain-gauges for areal rainfall estimates.

Chapter 5

5. Integration of satellite data in areal estimates of catchment rainfall

5.1 Introduction

Rainfall data from the rain-gauges are essentially point data. In hydrological modelling, areal rainfall amounts over a catchment and over some convenient time period are usually required. In order to estimate total catchment rainfall amounts, various interpolation routines are used which attempt to approximate the complex but continuous actual rainfall surfaces. Therefore, the estimated rainfall at ungauged points depends upon the measured rainfall, the number and the spatial distribution of the neighbouring rain-gauges.

In most hydrological and meteorological studies, the configuration of existing rain-gauge network is such that the majority of the rain-gauges are usually located in and around urban areas for easy access and maintenance. Monitoring of rainfall in hydrologically significant remote areas is therefore a considerable problem. Satellite images, with their wide spatial coverage and temporal resolution, were thought to be one possibility to overcome this problem. Satellite derived products could be calibrated using adequate ground-truth data and the derived relationships could than be used to monitor rainfall in data deficient regions. Prime example of such an approach is the FRONTIERS program operated by the Met Office in which satellite data is used to delineate rainfall in regions beyond the range of the radar (Browning, 1987). Much work has been done in that respect (see chapter 2 and 4). Most of the studies have reported some degree of success in differentiating rain/no-rain areas. However, the difficulty lies in the apportionment of rainfall amounts within the classified rain areas. For some applications, such as in Forest Fire Management, knowledge of rain/no-rain regions is sufficient where the prime objective is to produce maps of wet and dry areas (Bellon & Austin, 1986). In others, such as in hydrological rainfall-runoff modelling, actual rainfall amounts are of importance.

In most hydrological regimes, especially in the third world countries, even the best network of rain-gauges fall short of the minimum recommended by the WMO (1965). Obviously, any satellite data calibrated with such ground-truth would be at best as good as the network itself. In view of this, a different approach is tried in this chapter. Satellite data is treated as additional information which could be used to improve upon the rainfall estimates obtained using rain-gauge data alone. Infilling rainfall amounts between the rain-gauges is made to be depended not only on the distances from the nearby gauges but also on satellite observations. One example of a similar approach is the work of Creutin et al

(1986). He sought to combine the satellite estimates using the cloud indexing approach and the isohyetal rain-gauge estimates by using the method of krigging (Delhomme, 1978). He showed that improved areal rainfall estimates can be made for periods of five to ten days by using both sources of information. However, the methodology used in this chapter is different in a sense that no rainfall estimates are made using the satellite data alone. Instead rainfall estimates are based on the combined information of rain-gauges and satellites and compared with the estimates obtained using just the rain-gauges.

5.2 Interpolation methods for estimating Areal Rainfall

Areal Rainfall estimations are calculated using interpolation methods in which rainfall at an unknown point is assumed to be some function of distance from the surrounding gauges. Lack of knowledge about the structure and areal distribution of rainfall have resulted in the evolution of several methods which essentially differ in their assumed relationship between the distance from a rain-gauge and rainfall. The problem therefore reduces to fitting a surface through a set of data points. The most widely used methods for that purpose are the Arithmetic Mean, Theissen Polygons and the Isohyetal Methods. These are all well documented in the literature (Shaw, 1988) and are discussed only briefly here.

The Arithmetic Mean - This is the simplest objective method of calculating the average rainfall over an area. Rainfall is averaged across all gauges of a network and holds a good weighted value on flat watersheds with a uniform gauge distribution. This can be regarded as fitting a horizontal plane surface through the data points. The individual catches should not vary widely from the mean. Mathematically:

$$\overline{R} = \frac{1}{N}\sum_{i=1}^{N} R_i \qquad \text{eq.5.1}$$

where $\overline{R}$ is the mean rainfall, R_i is the rainfall at gauge i and N is the number of gauges.

The Theissen Polygons - This is also an objective method and delineates an area surrounding each gauge according to the minimum distance principal. The catch of the rain-gauge is assumed to be the rainfall amount for that area. The result is the construction of rainfall surface made up of polygons which is discontinuous at the polygons boundaries. The area weighted mean rainfall is generally more accurate than simple averaging for non-uniform networks. Mean rainfall depth in mm's over the catchment is given by:

$$\overline{R} = \frac{1}{A_0}\sum_{i=1}^{N} R_i a_i \qquad \text{eq.5.2}$$

where a_i is the area of the polygon surrounding gauge i and A_0 is the total area of the catchment. $\overline{R}$, R_i and N same as in eq. 5.1.

The Isohyetal Method - This is considered one of the most accurate methods, but it is subjective and dependent on skilled, experienced analysts having a good knowledge of the rainfall characteristics of the region containing the catchment. Lines of equal rainfall are estimated around the rain-gauges and drawn on the watershed. Calculation of mean rainfall is the same as in eq. 5.2 but a_i is the area between two successive isohyets and is measured using a planimeter. R_i is the mean rainfall between the two isohyets.

In addition to these standard methods, there are a number of more sophisticated methods that have also been developed. Akin (1971) applied the concepts of finite element analysis for calculating mean areal depth of rainfall. Hutchinson & Walley (1972) also used finite element techniques in their study of a small catchment in Newzealand, in which they introduced the concepts of using weights based on altitude in addition to the weights generated using distances. Lee et al (1974) used multiquadratic surface equations to define areal distribution of rainfall.

More recently, investigators (Dean & Snyder,1977; Shearman & Slater, 1975) have used a reciprocal-distance weighting technique for objective weather and storm analysis. A weighting technique, using reciprocal distances, proportions information at selected points to produce values at points where information is unknown.

For any point with cartesian coordinates x,y on a catchment, its distance to any rain-gauge i is

$$d_i = \sqrt{(x-x_i)^2 + (y-y_i)^2} \qquad \text{eq.5.3}$$

For weights based on powers of inverse distances, a unitized weight for all gauges affecting a point can be computed by

$$w_i(x,y) = \frac{\frac{1}{d_i^n}}{\sum_i \frac{1}{d_i^n}} \qquad \text{eq.5.4}$$

in which $w_i(x,y)$ is the weighting factor for rain-gauge 'i' with respect to point (x,y); and d_i is the distance as found by eq. 5.3. Values of 1, 2 and 3 have been used for the exponent 'n' in eq. 5.4 in the past. Shearman & Slater (1975) used both the values of 2 and 3 depending on the density of the rain-gauges. However, Dean & Snyder (1977) argued that there has been little attempt to estimate the optimum value of exponent 'n'. For

that purpose, they assumed that the isohyetal method produces rainfall fields which is closest to the actual rainfall field. Their method of defining the optimum value consisted of using a typical isohyetal rainfall pattern with a regular grid superimposed on it. The nodes of the grid represented rain-gauges and their rainfall values were read off from the original isohyetal map. Using just the grid values and eq's. 5.3 and 5.4, the optimum value of the exponent 'n' was found using the algorithm of least square minimisation so that the original isohyetal pattern of rainfall was recreated as closely as possible. In several tests, the optimum values of exponent 'n' varied from 1.5 units to 2.4 units depending upon the original rainfall structure and the grid density used. However, the general rainfall pattern calculated was found to be relatively insensitive to small changes in the value of parameter 'n' and it was decided that the value of n=2 can be used generally as a good approximation to the optimum value for any rainfall event.

5.3 Rain-gauge accuracies for areal rainfall estimation

Many investigators, including Huff (1970), Woodley et al (1975) and Hilderband et al (1979) have researched the accuracy of rain-gauge networks in their ability to estimate mean areal rainfall. Their approaches were similar; each worked with a rain-gauge network for which the gauge spacing was designed to minimize the error in areal rainfall measurements. Empirical relationships were derived which expressed the sampling error in areal rainfall measurements as a function of rain-gauge density. The sampling error in mm of water represents the absolute difference between the best estimate of the true mean of precipitation depth obtained from the maximum density of rain-gauges and the sample mean precipitation calculated from the gauge amounts for less dense network of rain-gauges. Their results show that the sampling error increases with increasing mean rainfall depth and decreases with increasing rain-gauge density, and these results are independent of the method used to calculate mean areal rainfall.

In order to estimate inherent errors in gauge estimates of rainfall, Bellon & Austin (1986) conducted an experiment in which the gauges were removed at random from the network and their rainfall values were estimated using the remaining gauges. Fourteen different rainfall events were used for the experiment. Comparisons of actual and estimated values indicated that even for small distances of 4 to 10 km from the rain-gauge, the absolute difference exceeds 65% of the actual value.

Using several interpolation methods and satellite data, D'Souza (1988) demonstrated that apparent rainfall was assigned to areas where no cloud cover was observed on the evidence of satellite images, indicating that interpolation methods are only effective within the vicinity of the rain-gauges.

5.4 Application of Meteosat data

Fig. 5.1a and 5.1b show the cospectral plots in the infrared and visible bands of the Meteosat images for the 30th of June, 1990. A number of convective cells were observed to pass over the study region during the day. These plots are drawn by observing the pixel values for the two bands over the available rain-gauges. The plots are shown for each hourly image (only hourly data was available) and are drawn separately for the two classes of raining and not-raining gauges. The centre of plots are the mean pixel values found for each class, while the width indicates one standard deviation in both directions. These plots show the degree of separability between the two classes for convective rainfall. There is substantial overlap between the two classes that is more significant due to the larger sample size in the no-rain class. They also show the difficulty in assigning rain area by simple thresholding in the two bands.

Nevertheless, some degree of separability is evident from these spectral plots as compared to cospectral plots of fig. 4.1(a-e) where clouds were of frontal origin. Rain-gauges with high spectral values are relatively more likely to be raining than rain-gauges with low spectral values. In conventional methods rainfall at a point p within a catchment is estimated according to the rainfall values recorded at nearby gauges. These gauges are weighted according to their distances from point p (see section 5.2). With the availability of satellite data, these weights can be further modified on the basis of spectral similarity between point p and the gauges. Thus, rainfall at an unknown point can be estimated using both the spatial distance and the spectral distance as parameters for calculating weights.

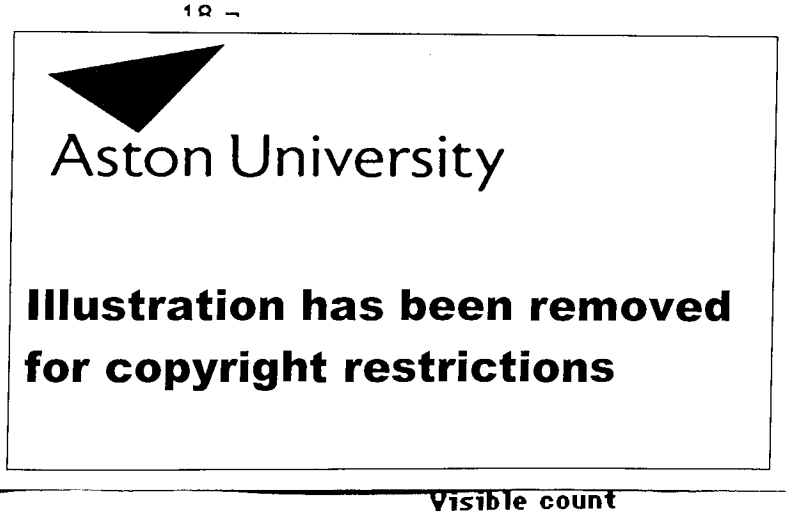

Fig. 5.1a Spectral plots in the visible band for raining and not raining gauges. The sequence of images is from the 30th of June, 1990.

Fig 5.1b Same as fig. 5.1a but for the infrared images.

5.4.1 Formulation of Methodology

In order to use the additional information from the satellite data, eq. 5.3, for the reciprocal distance method, is conveniently modified as follows:

$$d_i = \sqrt{(x-x_i)^2+(y-y_i)^2 + a * (t-t_i)^2} \qquad \text{eq.5.5}$$

where 't' is the spectral count value (range 0-255) over the unknown point and 't_i' is the spectral count value over the corresponding rain-gauge, and 'a' is an empirical coefficient. The distance d_i is measured in km (or any other convenient unit) and the parameter 'a' can be seen as the scaling parameter with units $km^2/count^2$ which converts the spectral counts into equivalent units of distance. This gives a plausible way of combining rain-gauge and satellite data. The weights assigned to nearby gauges in an interpolation routine using eq. 5.5 does not only depends on the interim distances but also on the spectral values observed in the satellite images. The reciprocal distance weighting method was chosen for various reasons:

* It is shown to be preferred over the Theissen Polygons method and conform closely to the Isohyetal method (Dean & Snyder, 1977).

* Oakes & Thrift (1975) in their extensive comparisons of different interpolation methods found this method to be the most reliable.

* It readily lends itself to automation and optimization.

* It is the method used by the Met Office for error checking and infilling missing records (Shearman & Slater, 1975).

Equations 5.4 and 5.5 form the basis of estimating rainfall at any point with rain-gauge and satellite data which can be simply integrated to give the total rainfall falling over a catchment. The values of the two parameters; coefficient 'a' in eq. 5.5 and the exponent 'n' in eq. 5.4 needs to be established. The optimum values of these parameters, a* and n*, determined using least-square minimisation algorithm, would vary between rainfall events, distribution of network rain-gauges, and from catchment to catchment. As mentioned in section 5.2, Dean & Snyder (1977) found the value n=2 as a good approximation to n* to be used generally in rainfall analysis.

5.4.2 Determination of parameters 'a' and 'n' using Least Square minimisation

Data for the analysis concerning Meteosat images and ground rain-gauge data was acquired and processed as explained in chapter 3. Figures 5.6 and 5.7 show the temporal sequence of catchment rainfall for 30th of June, 1990. Clearly, two separate rainfall events affected the catchment with peak rainfalls at 1300 hours and 1600 hours respectively. The first event, starting at approximately 1100 hours and lasting approximately five hours, was chosen for the determination of parameters 'a' and 'n'. Only infrared images were used due to their diurnal availability and unlike visible, does not need correction for the errors in the spectral values due to solar zenith angle.

The accuracy of an interpolated rainfall field can only be determined if compared with the actual rainfall field. However, the actual rainfall field is never known and the next best thing is the rainfall field generated using the maximum number of rain-gauges with which comparisons can be made. In the Severn-Trent catchment area, there are eighty six rain-gauges. Out of these, forty three were chosen at random but ensuring uniform distribution. The accuracy of the interpolated rainfall field, generated using the chosen forty three gauges was than defined by the function:

$$SOSE = \sum_{i=1}^{43} (Re_i - R_i)^2 \qquad \text{eq.5.6}$$

where
- $SOSE$ = sum of square error
- Re_i = estimated rainfall using interpolation at gauge i
- R_i = actual rainfall at gauge i
- i (1-43) = remaining forty three rain-gauges not used in the interpolation procedures

Equation 5.6 therefore provided the means to assess the accuracies involved using different interpolation routines and also served as an objective function for the determination of parameters 'a' and 'n' in eq.'s 5.4 and 5.5. Four different methods were tested (see appendix A.2 for the description of computer programme):

1. Theissen Polygons (TP) - no parameters to be evaluated. Rainfall at the unknown point is simply assigned the rainfall at the nearest rain-gauge.

2. Reciprocal Method (RM) - optimum value of parameter 'n' in eq. 5.4, n*, was determined by minimizing eq.5.6 as an objective function.

3. Satellite Method 1 (SM1) - a* and n*, in eq. 5.4 and 5.5 were determined by minimizing eq.5.6 as an objective function..

4. Satellite Method 2 (SM2) - same as SM1 but with an added constraint that any rain-gauge with an infrared value of less than or equal to 125 was assigned nought rainfall.

Method SM2 was based on the observation given in table 5.1 which shows little rainfall was observed by rain-gauges with infrared count value less than 125. For the rainfall event of 30th of June under consideration, table 5.1 gives the division of rain-gauge readings in percentages observed under increasing spectral values of infrared data. Fig. 5.2 illustrates the method in which the values in table 5.1 were obtained. Given an infrared image superimposed on the catchment map and the corresponding half-hour rainfall recordings from all the rain-gauges, the rain-gauges were first classified according to their spectral values into different spectral intervals. The rainfall readings from the rain-gauges in each interval were than summed and converted into percentages. These percentages were than integrated over the whole rainfall event to give the overall values. On visual inspection of infrared images, regions below the 125 count threshold represented cloud free areas (Elgy & Siyyid, 1991).

Table 5.1 Percentage rain-gauge rainfall observed under different infrared count intervals. Image sequence of 0900 to 1600 GMT, 30-6-90 was used.

Infrared count interval	Gauge percentage Rainfall
count <= 125	2.8
125 < count <= 135	7.0
135 < count <= 145	26.0
145 <count <= 155	22.3
155 < count <= 165	15.3
165 < count <= 175	16.7
175 < count <= 185	9.8
*185 < count <= 195	0.0
*195 < count	0.0

* No cloud in this spectral range was found.

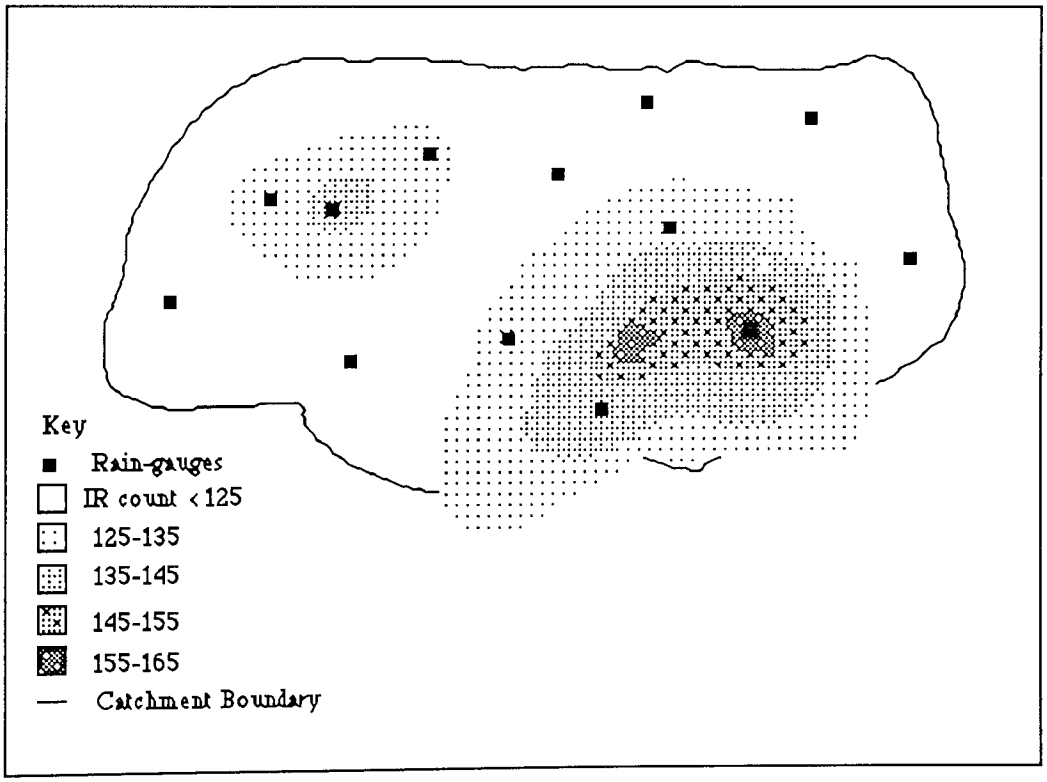

Fig. 5.2 An example of classification of rain-gauges into different intervals of infrared count levels. Rainfall recordings of rain-gauges under each count interval is summed and converted into percentages of the total catchment rainfall (see table 5.1).

5.4.3 Results

The results of the analysis are given in table 5.2. To examine the effect of the distribution of rain-gauges on the values of a* and n*, four different distributions of forty three rain-gauges were used. Salient features of the results obtained in table 5.2 are:

* The value of n* range from 1 to 2.7 units depending on the rain-gauge distribution. The variation is slightly more than that of Dean and Snyder (1977) who found the range in the order of 1.5 to 2.4 units.

* Variation in the value of a* is more pronounced ranging from 5 units for the rain-gauge distributions 3 and 4, to 45 for rain-gauge distribution 2.

* The SOSE is reduced for SM1 and SM2 compared to RM in each of the four rain-gauge distributions. The reduction is however disappointingly low accounting for only about 5% of the SOSE values obtained for RM.

* High SOSE values were obtained for the TP in each of the four rain-gauge distributions.

Table 5.2 Optimum values of parameters 'a' and 'n' in eq. 5.4 and 5.5 and the sum of square error obtained for four different distributions of rain-gauges.

Rain-gauge distributions	Interpolation Method	Parameters a*	Parameters n*	SOSE
1	TP	-	-	626
	RM	-	2.7	585
	SM1	25	2.6	558
	SM2	24	2.6	558
2	TP	-	-	724
	RM	-	1.0	225
	SM1	45	1.1	203
	SM2	38	1.1	199
3	TP	-	-	632
	RM	-	1.5	291
	SM1	5.0	1.6	281
	SM2	6.0	1.5	277
4	TP	-	-	513
	RM	-	2.36	386
	SM1	5.0	2.64	367
	SM2	5.0	2.64	364

In order to establish the general working values of parameters 'a' and 'n', the relationship of SOSE with respect to these parameters are shown in fig. 5.3, 5.4 and 5.5. These graphs show the variation in the SOSE as the parameters 'a' and 'n' are increased. Fig.

5.3 show that the SOSE increases sharply for values of n greater than 2.5 and less than 1. For values of n within that region, the values of SOSE remain close to its minimum. Therefore, the value of n=2 can be taken as a good approximation to n*, confirming the findings of Dean & Snyder (1977).

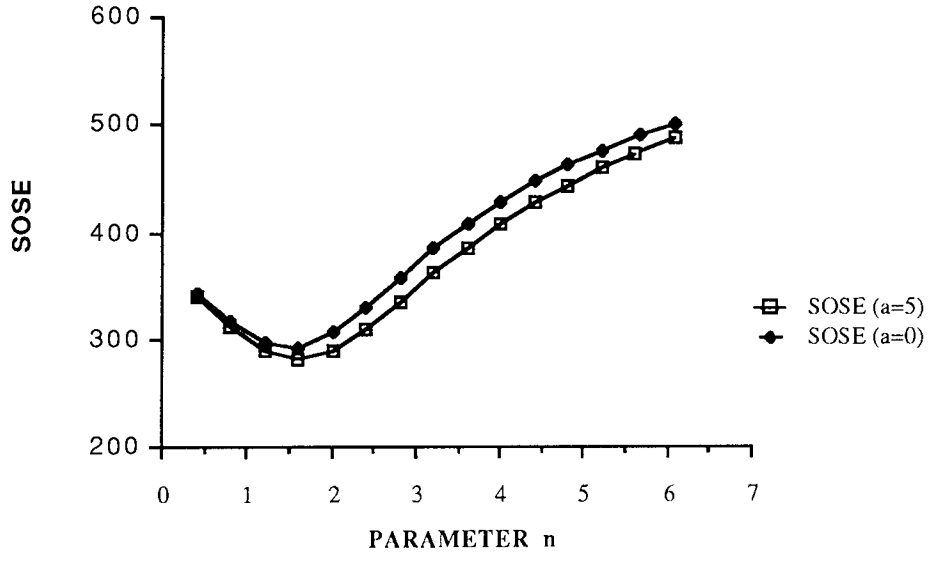

Fig. 5.3 Variation of sum of square error with respect to parameter 'n' (for rain-gauge distribution 3 in table 5.2)

Fig. 5.4 and fig. 5.5 shows the relationship of SOSE with respect to parameter 'a' for two rain-gauge distributions. The graphs are plotted for both n=2 and n*, the optimum value in each case. The value of a* in fig. 5.4 is 5 while in fig. 5.5, a* is equal to 45. However, both graphs are characterized by a sharp reduction in SOSE as 'a' is increased from zero, representing the introduction of satellite spectral information. For values of 'a' greater than 5, SOSE begins to rise slowly in fig. 5.4 while in fig. 5.5 it becomes almost constant. This explains the high value of 45 obtained for a* in this case since SOSE is almost unaffected for 'a' greater than 10. However, most of the reduction in SOSE in fig. 5.4 and 5.5 have resulted for values of 'a' around 5 and is therefore taken as a general working value for parameter 'a'.

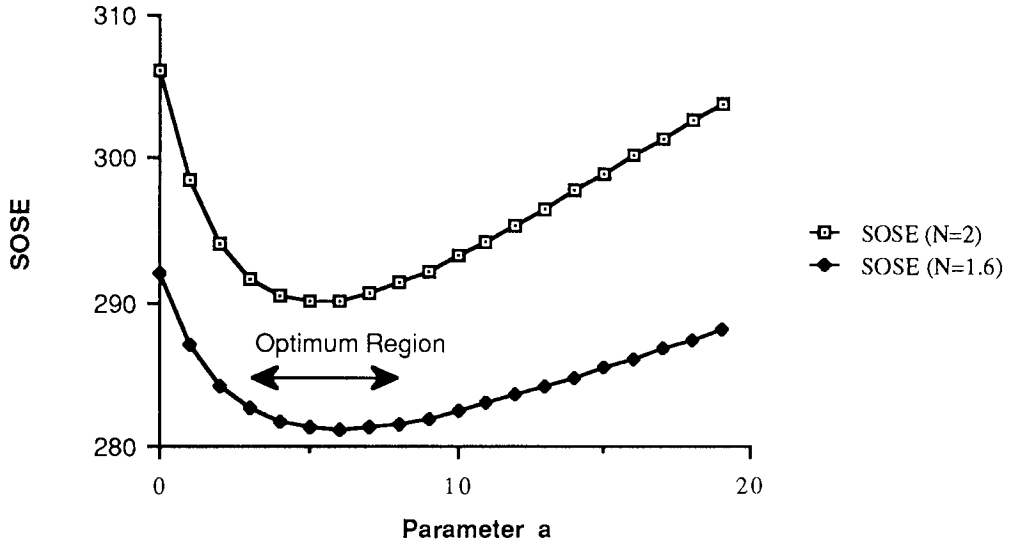

Fig. 5.4 Variation of sum of square error with respect to parameter A (rain-gauge distribution 3 in table 5.2)

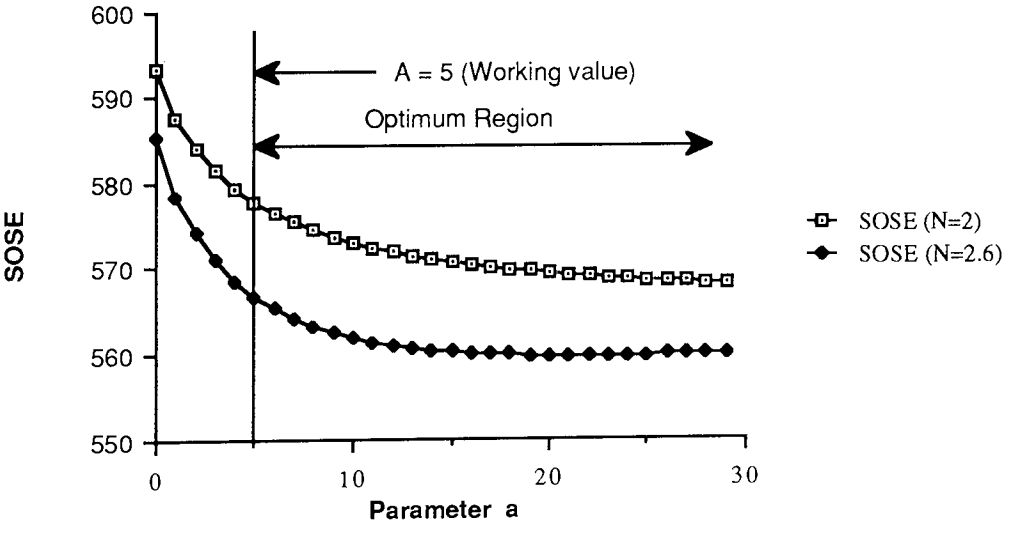

Fig. 5.5 Same as fig. 5.4 but for rain-gauge distribution 1 in table 5.2

In equations 5.3, 5.4 and 5.5 for the reciprocal and satellite methods, rainfall values were calculated using weights from all the available 43 rain-gauges. This is different from the approach used by Dean & Snyder (1977) who arbitrarily used weights from the nearest four rain-gauges for equations 5.3 and 5.4. Oakes & Thrift (1975) have also addressed the problem and used *least square minimisation* algorithm to obtain the optimum number of neighbouring data points. The same method was used in this study. The optimization program was modified to include only the specified number of nearest rain-gauges. Using the reciprocal method and taking the value of parameter 'n' equal to two, SOSE's were calculated for different rain-gauge distributions. The number of rain-gauges affecting a

point was made to increase from 4 upwards. The results are given in table 5.3. The minimum SOSE is reached when about 20 nearest rain-gauges are used. However, use of more than 20 nearest gauges does not affect the minimum since the weights associated with additional rain-gauges are insignificant.

Table 5.3 Relationship between number of neighbouring rain-gauges used to estimate rainfall at a point and the sum of square error (SOSE) obtained for four distributions of rain-gauges.

	Optimum SOSE			
No. of Rain-gauges	*RD 1	RD 2	RD 3	RD 4
4	356	412	595	427
8	302	396	591	284
12	294	394	584	253
16	290	391	585	237
20	289	389	585	230
28	291	387	585	226
36	292	386	585	225

* RD - Rain-gauge distribution

The working values of parameters 'a' and 'n' values were further tested on three independent rainfall sequences comprising of two convective and one frontal system. The results are given in table 5.4. Estimates were obtained for the first two rain-gauge distributions in table 5.2. The results are as expected for SM1 and SM2 when compared to RM:

* The two convective sequences similarly showed a small fall in SOSE for SM1 and SM2 when compared to RM.

* TP again showed high values of SOSE.

* No change is observed in the case of frontal system which was expected due to their homogeneous nature in terms of infrared spectral values.

* Again little rainfall was observed from gauges with infrared value less than 125 in each of the sequences, justifying the use of that threshold in SM2.

Table 5.4 Examination of different interpolation methods in terms of sum of square error for three different image sequences.

Storm type	Date/Time	No of images	Interpolation Method	SOSE (a=5,n=2) *RD1	SOSE (a=5,n=2) RD2	% Gauge rainfall ≤ 125 threshold
**C	30/6/90	13	TP	477	621	0.89
	1700 to		RM	359	512	
	1900		SM1	354	500	
	GMT		SM2	350	500	
C	27/6/90	5	TP	306	492	1.4
	1600 to		RM	218	439	
	1900		SM1	217	429	
	GMT		SM2	208	425	
***F	01/6/90	11	TP	195	179	0.0
	1000 to		RM	138	114	
	1630		SM1	138	114	
	GMT		SM2	138	114	

*RD = Rain-gauge distribution

**C = Convective

***F = Frontal

5.5 Determination of Catchment Rainfall

The analysis above on point rain-gauge data demonstrated the affect of satellite information in areal rainfall estimations. The reduction in SOSE when compared to RM is small and may be rendered insignificant. However, its affect on the integrated rainfall volumes over the catchments should be evaluated.

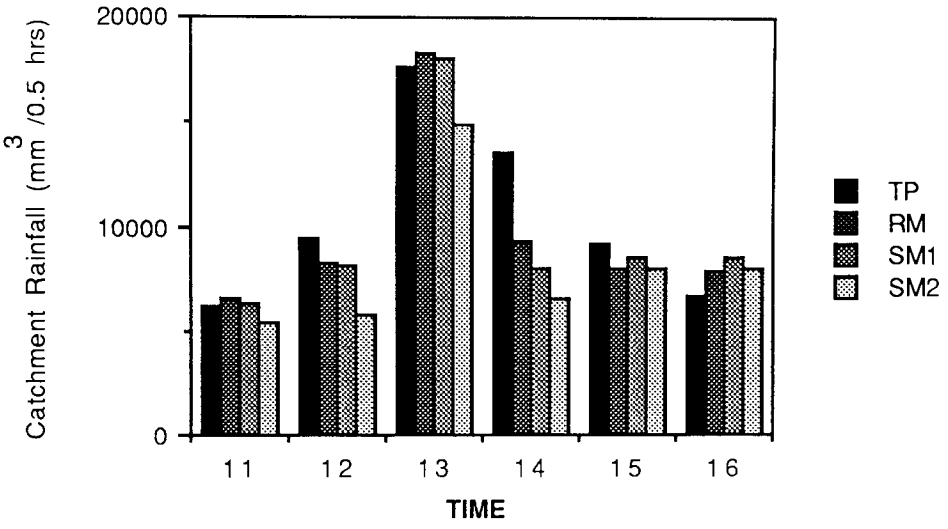

Fig. 5.6 Temporal Variation of catchment rainfall for the convective storm of 30-06-90 using four different methods.This is the data set used to estimate parameters 'a' and 'n'.

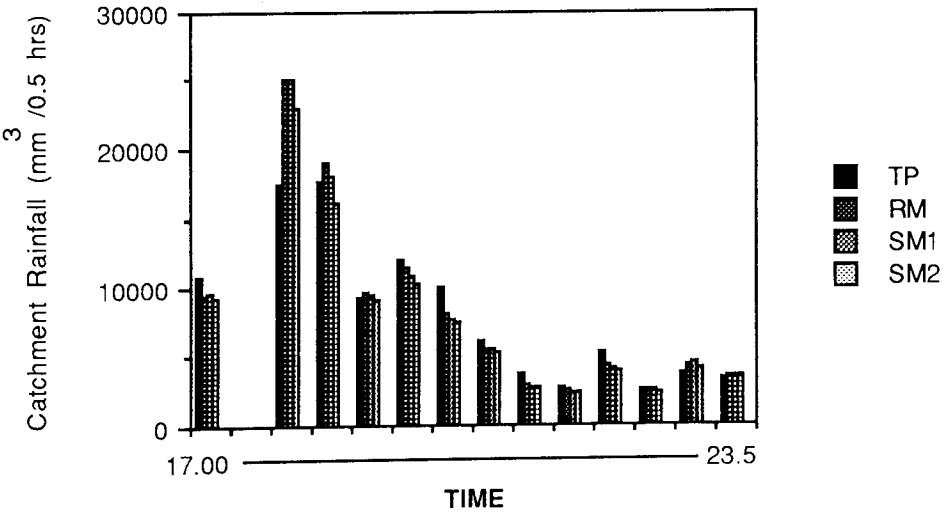

Fig 5.7 Same as fig. 5.6 but for later half of 30-06-90. Image for 17.5 was not available

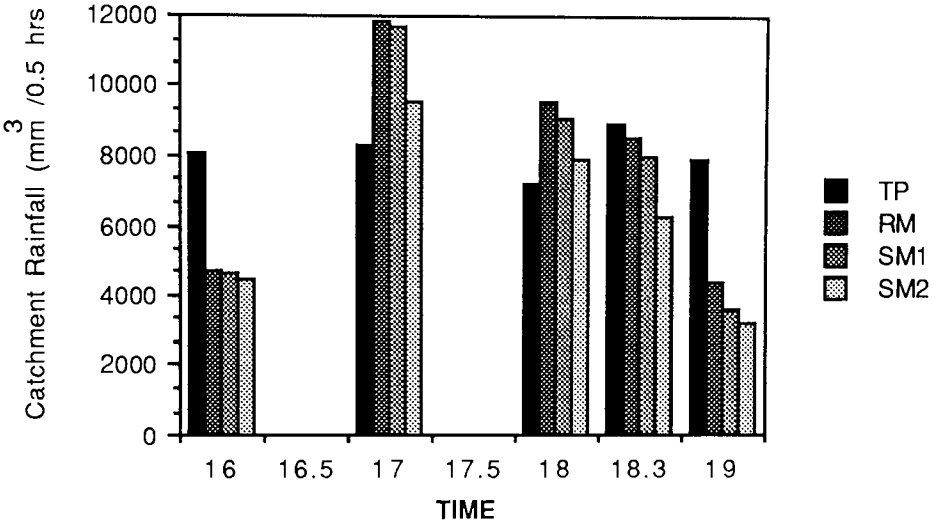

Fig. 5.8 Same as fig. 5.6 but for 27-06-90. Images for times 16.5 and 17.5 were not available.

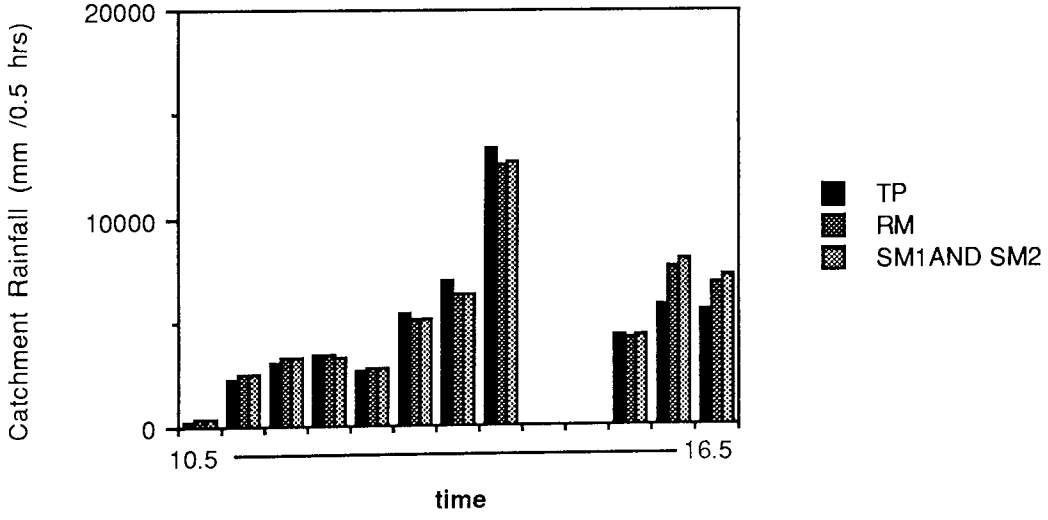

Fig. 5.9 Same as fig 5.6 but for the Frontal storm of 01-06-90. Images for times 14.5 and 15.00 were not available.

Total volumetric catchment rainfalls were estimated for the three image sequences in table 5.4, using the four methods described. The full rain-gauge network of 86 rain-gauges were used in the calculations. Figures 5.6, 5.7, 5.8, and 5.9 show the rainfall totals calculated for each image sequence and their statistical characteristics are given in table 5.5. Table 5.5 also shows the percentage of cumulative rainfall over the whole sequence that is assigned to areas with infrared count values less than 125.

Table 5.5 Comparison of different interpolation methods in terms of total volumetric rainfall over a catchment

Image Sequence	Interpolation Method	Statistics of catchment Rainfall for different events (m^3 / 0.5 hour) Mean	Standard Deviation	Min.	Max.	% Rainfall < 125
30/6/90	TP	8810	5047	2621	17719	07 %
Convectiv	RM	8748	6073	2523	25049	11 %
e 19	SM1	8595	5961	2426	25020	09 %
images	SM2	7765	5308	2327	22874	00 %
27/6/90	TP	8083	0649	7192	08972	06 %
Convectiv	RM	7806	3211	4381	11850	16 %
e 5 images	SM1	7403	3302	3600	11687	14 %
	SM2	6311	2560	3222	09587	00 %
01/6/90	TP	4815	3047	293	13342	00 %
Frontal	RM	4983	3286	366	12542	00 %
11 images	SM1	5048	3326	362	12526	00 %
	SM2	5048	3326	362	12526	00 %

In each of the image sequences in table 5.5; TP, RM and SM1 showed similar catchment rainfall figures with variations between the amounts being less than 5%. The figures for SM2 are consistently less when compared to other methods. This is due to the fact that the other three methods assigned 7% to 11% of their cumulative rainfall estimates to cloud free areas defined by the infrared threshold value of 125. These observations can also be made by examining plates 5.1 to 5.5. Plate 5.1 shows the infrared image of 1300 hours, 30th of June, 1990 superimposed on the catchment boundary. The image is sliced to differentiate between clouded and cloud free areas on the catchment. Plates 5.2 to 5.5 show the corresponding rainfall distributions by TP, RM, SM1 and SM2 respectively. The rainfall distributions according to RM and SM1 are largely similar. The additional satellite information in SM1 made little impact on the general distribution of rainfall when compared to RM. This rainfall distribution is further modified in SM2 in which zero rainfall is assigned to cloud free regions. Rainfall distribution in the case of TP is highly localized as expected.

In the case of frontal rainfall event, there was very little information in the satellite images, as indicated by almost the same values for catchment rainfall for all four methods in table

5.5. This is not unexpected since frontal storms are very uniform in nature and the cloud extent is in the order of 1000 's of km. Consequently, there is very little variation in pixel values which show no discrimination between raining and not-raining gauges (see chapter 4).

5.6 Summary and Conclusions

Reciprocal distance method for estimating areal rainfall over a catchment is modified to make use of additional data available from the half hourly satellite infrared images of the catchment. Observations of the images over rain-gauge locations indicated:

1. A degree of separability between raining and not-raining gauges on the basis of infrared spectral values, provided the rainfall is convective.

2. Virtually no rainfall is observed below an infrared threshold of 125. Areas on the image with infrared values less than 125 may represent anything other than clouds.

Consequently, two methods were developed: SM1 which modifies the conventional reciprocal method by introducing satellite information based on the first observation and SM2 which uses both observations. Direct comparisons between the estimated rainfall and actual rainfall over selected rain-gauge sites showed that the introduction of satellite data reduces the overall error but the reduction is insignificant and have little impact on the integrated rainfall volumes over the catchment area.

It was also observed that the conventional methods, such as Theissen polygons and reciprocal distance for areal rainfall estimation, tend to assign 6% to 14% of estimated rainfall to cloud free regions (table 5.4 and 5.5). Satellite data can be used to delineate such areas and therefore restricts the interpolated rainfall field to clouded areas (such as in SM2). However, such a method would have several disadvantages:

* The rain-gauge network should be able to provide half-hour rainfall values corresponding to the times of the infrared images. In most data deficient regions, rain-gauge recordings are daily or for even longer periods.

* The improvement gained in areal estimates may not justify increased computational costs.

* From hydrological point of view, hourly or half-hourly rainfall totals are significant only in small, heavily urbanized catchments where a short duration high intensity

rainfall can cause flooding within minutes. Meteosat images, with low spatial resolution are more suitable for monitoring larger catchments or areas.

The main conclusion to be drawn from these experimental results is that, single Meteosat images, giving an instantaneous view of the catchment, provide useful and more realistic information on the spatial distribution of catchment rainfall than is possible using conventional methods of interpolation. The SM2 method of restricting interpolation within the defined cloud area introduce a bias of 10% to 15% in areal rainfall estimates which should be compensated for. This factor is important in applications which require highly accurate spatial distribution of short period rainfall but where radar data is not available. However, increased computational and processing cost of satellite data would have to be justified against the increase in accuracy of estimates based on existing rain-gauge network.

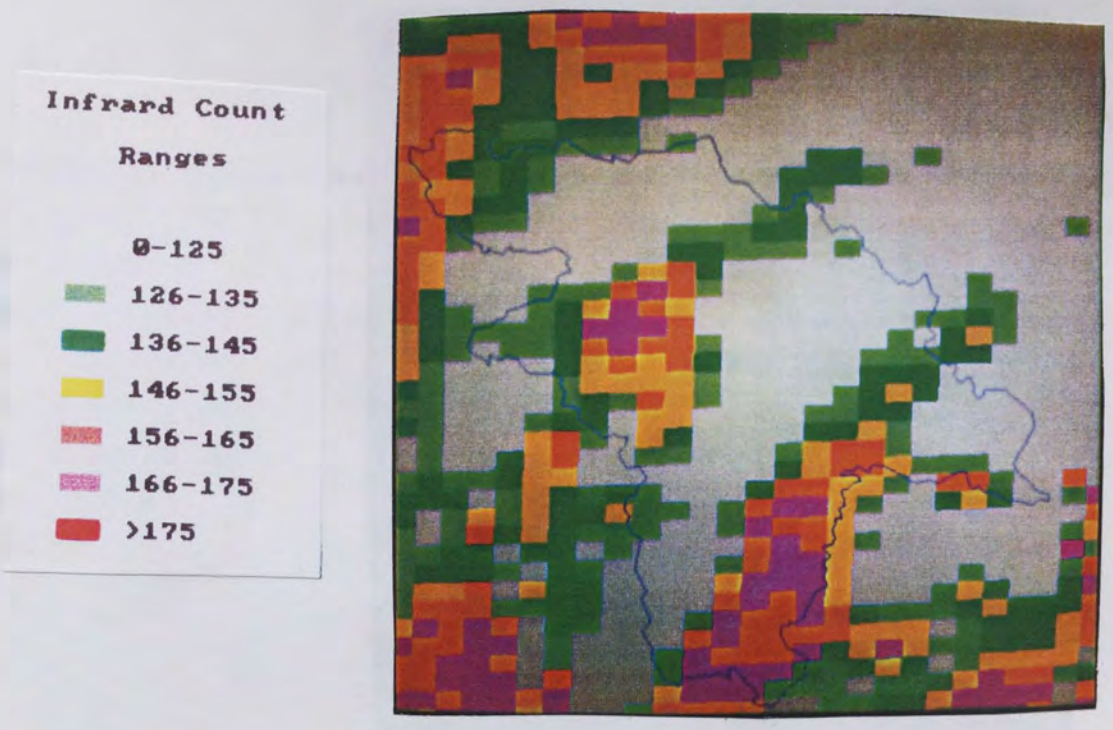

Plate 5.1 False colour infrared image of 1300 hrs, 30th of June, 1990 superimposed on the Severn Trent catchment area.

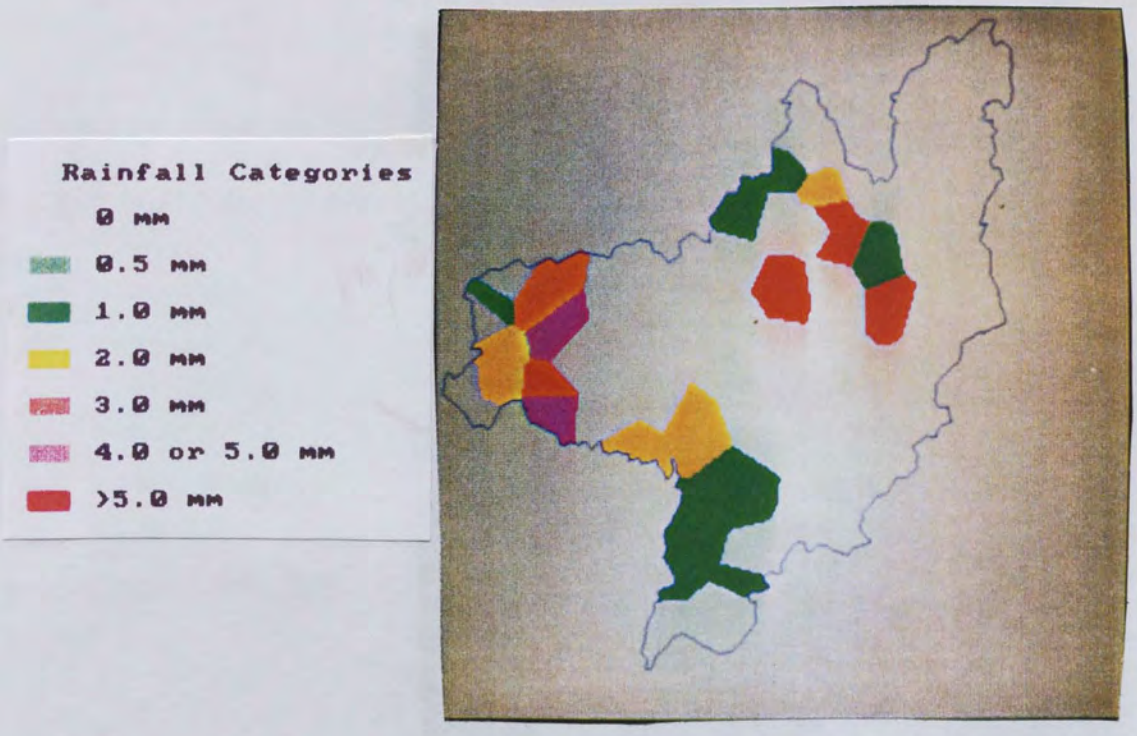

Plate 5.2 Half-hour rainfall distribution according to Theissen Polygons for 1300-1330 hrs, 30th of June, 1990.

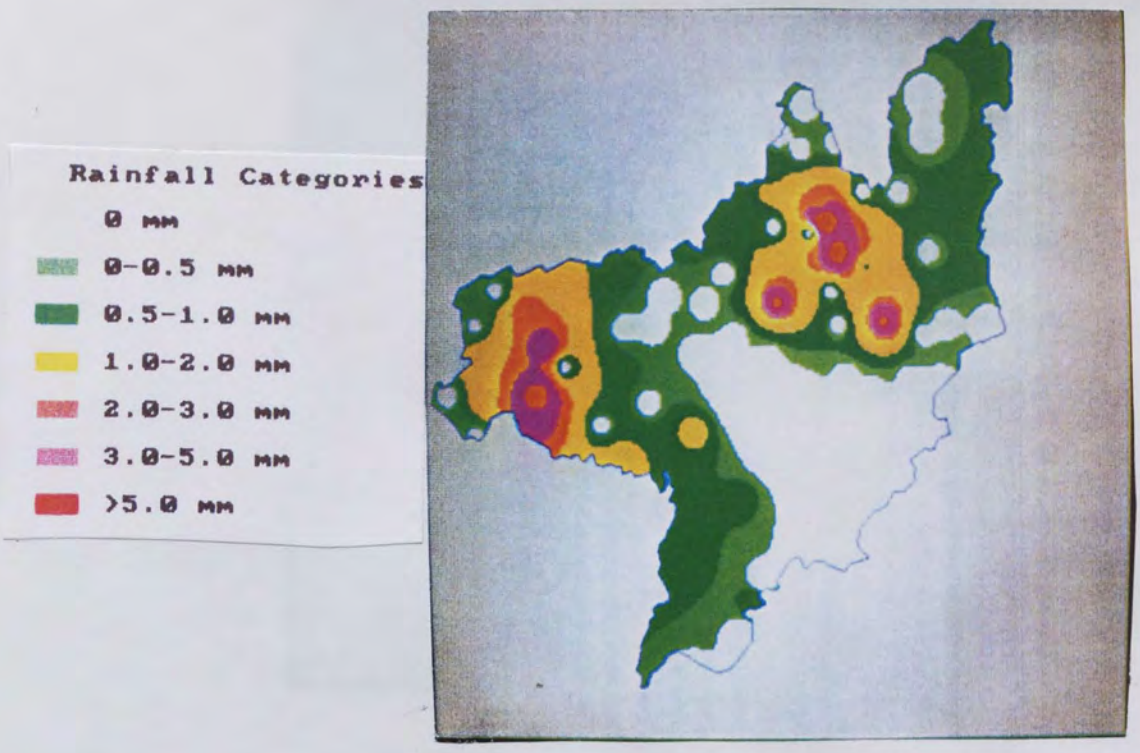

Plate 5.3 Half-hour rainfall distribution according to Reciprocal for 1300-1330 hrs, 30th of June, 1990.

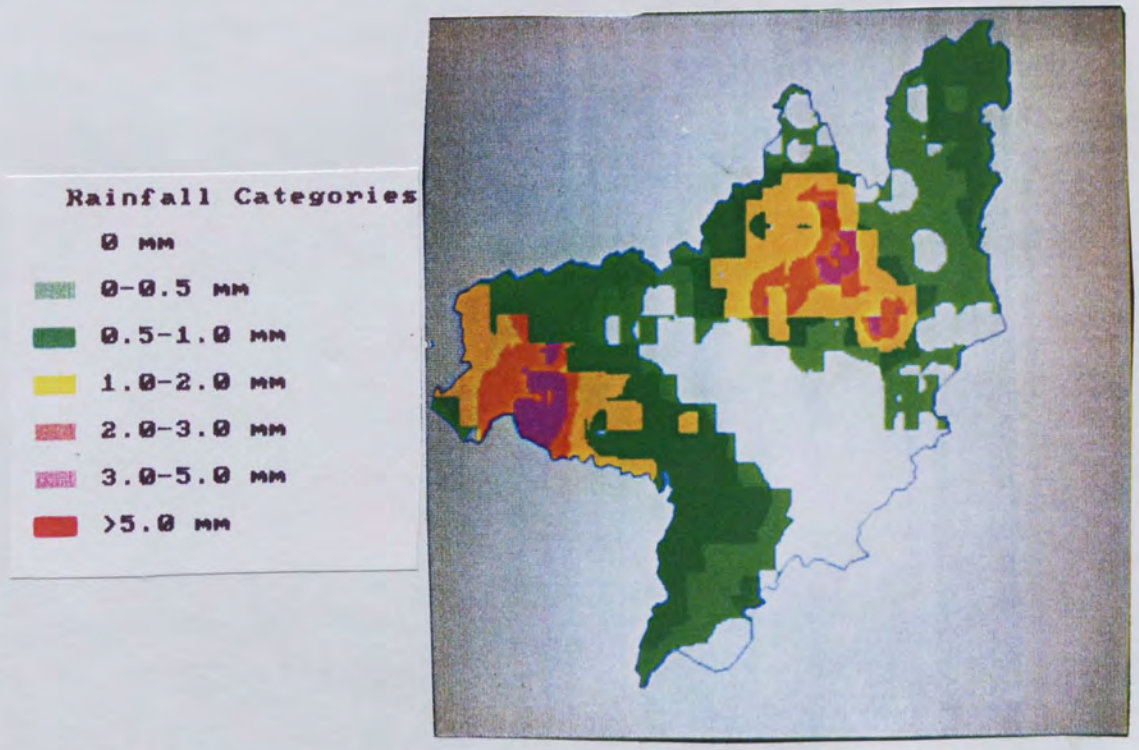

Plate 5.4 Half-hour rainfall distribution according to Satellite Method 1 for 1300-1330 hrs, 30th of June, 1990.

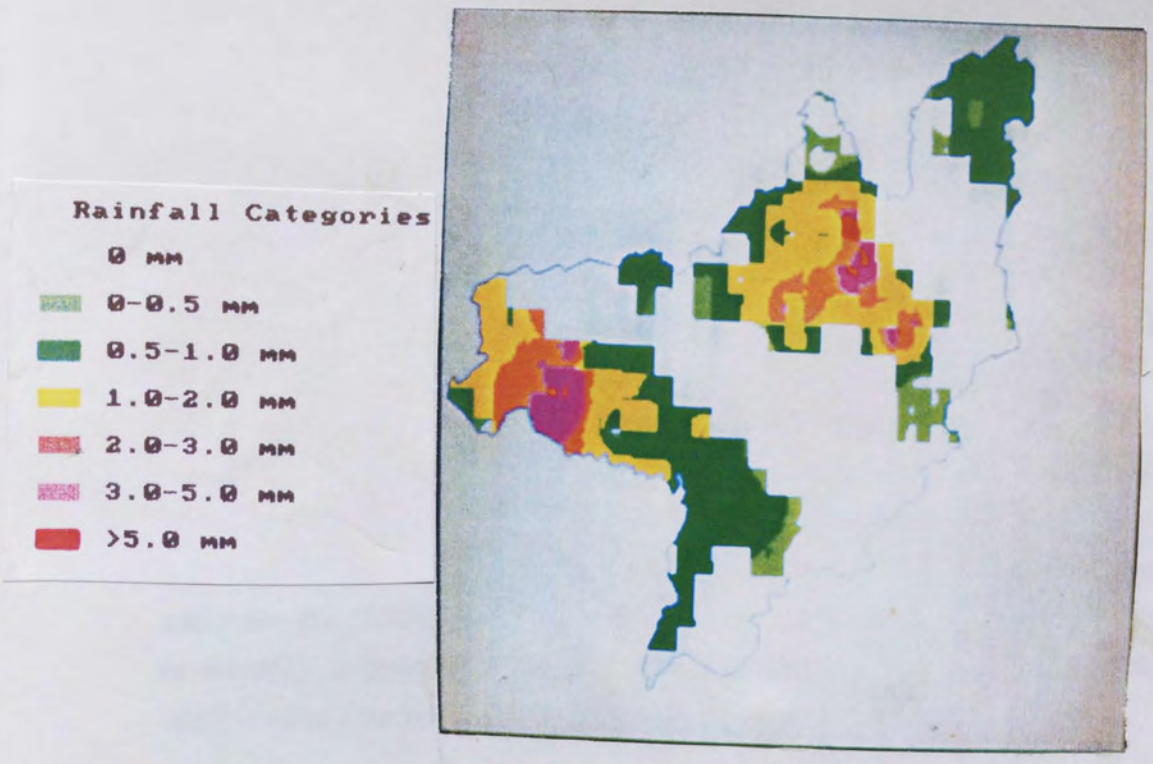

Plate 5.5 Half-hour rainfall distribution according to Satellite Method 2 for 1300-1330 hrs, 30th of June, 1990.

CHAPTER 6

6. Cold Cloud Duration Analysis

6.1 Introduction

In this chapter, a new technique of areal rainfall estimation is investigated with some modifications suggested. The technique is based on satellite data and employs the relationship between duration of cold cloud over a unit area (defined by satellite pixel resolution) and total rainfall falling over that area. A linear relationship between the two variables is assumed the parameters of which are estimated using rain-gauges. The technique has been tested comprehensively over the past few years by other researchers and it has been found that it works best for estimation of rainfall accumulated over 10 day or monthly periods. The variation in the relationship between cold cloud duration and rainfall values for less than 10 days was found to be too large .

In many applications such as hydrology, daily rainfall values are routinely employed. Therefore daily rainfall values and cold cloud durations are used to estimate rainfall. Two modifications to existing techniques are introduced. The first modification essentially turns the model into a Multiple Linear Regression Model from the original simple linear relationship in one variable. Durations of cloud cover relating to different temperature intervals were used as independent variables rather than using one variable based on a subjective threshold temperature. The second modification uses the error field (generated using the known and estimated values at rain-gauge points) to improve the rainfall field generated using multiple regression model.

The study was carried out over two sub-catchments of the Severn Trent Catchment Area. Comparisons of estimated volumetric rainfall values using satellite data and the more established conventional methods such as Arithmetic Mean or Theissen Polygons indicate that there is little difference in the aggregated estimated rainfall and the general distribution of rainfall although there would be discrepancies at point values.

6.2 Back Ground

The theory behind the technique of Cold Cloud Duration for rainfall estimation has been briefly discussed previously in chapter 2 section 2.4.3 and will be elaborated further in this section.

In the Tropics, most of the rain is due to organised convection (thunder storms). These storms which are very frequently associated with ITCZ (Atlantic Intertropical Convergence

Zone), Squall lines or definite convective clusters, produce excessive rainfall at about the time clouds reach their lowest temperature. These could be identified in the thermal infrared imagery of satellites by their high and very cold tops.

Based on this observation, the Tropical Agricultural Meteorology Satellite Project (TAMSAT) at the University of Reading has been investigating the applicability of thermal infrared imagery from Meteosat for the estimation of rainfall in the Sahel region since 1984 (Flitcroft et al; 1986, Chadwick et al; 1986, Dugdale & Milford; 1986). They have developed their technique on the sensible assumption that the longer an area is affected by a thunder storm, the proportionately more rain it will receive. In other words, the longer a cold cloud is observed over an area, the higher the amount of rainfall it receives. A simple model expressing this relationship can be taken as

$$\text{Rainfall} = A * CCD + B \qquad \text{eq. 6.1}$$

Where A and B are regression constants.

Fig. 6.1 Relationship between CCD and rainfall. From Milford and Dugdale, 1986

An example of the relationship for decadal rainfall (10 days accumulations) is as shown in fig.6.1. CCD values are determined on a pixel by pixel basis. Using the Meteosat infrared data, a score is kept of the number of times its temperature drops below a certain threshold temperature. The relationship between CCD and rainfall is established by linear regression using rain-gauge measurements. The choice of the threshold temperature is important and rather subjective depending upon the climatology of the area. It must be high enough so that most precipitating clouds are included but low enough to exclude warmer clouds which are not associated with heavy rainfall.

In Africa, most of the rainfall is observed to take place from clouds colder than -40° C. The method has been applied extensively over various parts of the African continent and the choice of the threshold temperature varied between -40° C to -70° C. Milford and Dugdale (1986) found the threshold value of -60° C as appropriate in their study in the Republic of Niger that spans the Sahel. Huygen, et al (1988) examined different thresholds and found -40° C as the best in terms of higher correlation coefficients in their study over Tanzania. Kumar et al (1988) found a threshold of -50° C as the optimum threshold in a similar study over Kenya.

In addition to the variation in the relationship depicted by eq. 6.1 due to different thresholds, it is also affected when evaluated over different time periods. Huygen et al (1988) found the following relationships for two adjacent periods of 10 day rainfall.

< 1/10 February >	< 11/20 February >
R = 2.3 CCD - 14.9	R = 2.3 CCD - 18.2
r = 0.61	r = 0.84

Similarly Kumar et al (1988) found the following relationships in his study over Kenya:

Month	10 day	Monthly
Jan	R=1.1 CCD + 20.5 (r=0.54)	R=1.5 CCD + 13.2 (r=0.72)
Feb	R=1.0 CCD + 13.5 (r=0.52)	R=1.4 CCD + 11.4 (r=0.71)

where 'r' represent the correlation coefficient.

The regression equations for the 10 day period in the two studies differ largely in their estimation of regression coefficients A and B in eq. 6.1 emphasizing the need for separate calibrations for different areas. Values of A and B also differ for different time periods especially in the case of estimating B. Similar conclusions were also reached by McDougal et al (1988) who showed that both threshold and calibration vary with location and season.

In other words there are no unique values for A and B in eq. 6.1 and it would not be possible to work with a fixed algorithm to estimate the rainfall. The constants in the linear regression equations vary from decade to decade as does even the optimum temperature threshold level. It is therefore inevitable to use the Meteosat images in combination with good quality rain-gauge measurements and recalibrate every decade or whatever time base is used.

Variants of the equation 6.1 with additional variables have also been investigated in a number of studies. Carn et al (1988) modified the equation as follows:

$$R = A * CCD + B * T^{O}MAX + C * LAT + D \qquad \text{eq. 6.2}$$

where $T^{O}MAX$ is the soil surface maximum radiative temperature derived also from infrared images. LAT is the latitude of the point considered, R is the rain-gauge rainfall and CCD is the cold cloud duration at the rain-gauge site.

The use of $T^{O}MAX$ was due to the observations that cumulative rainfall amounts were closely related to corresponding cumulative values of $T^{O}MAX$.

The use of latitude was considered as the practical means to take into account the differences in the physical environment of clouds over West Africa which is related to the latitude. They found that use of additional variables in the multiple linear regression improves the correlation coefficient in a significant manner. However, they were working with monthly rainfall totals.

A similar study was carried out by Rosema (1987) who modified equation 6.1 as:

$$R = A * CCD + B * TE + C * LAT + D \qquad \text{eq. 6.3}$$

where TE is the cloud top temperature in excess of the threshold. Other variables are the same as in eq. 6.2.

Inclusion of cloud top temperature in excess of a chosen threshold was made because of the observation that clouds exhibiting extremely cold temperatures were more often producing high volumes of rainfall.

For a particular study area, eq. 6.1 must be re-evaluated for each day , decade, or whatever time base is used. This put greater emphasis on the value of rain-gauge measurements. Rain-gauges are always required for calibration purposes and a gauge must exist somewhere for any cold cloud duration analysis to work. The whole exercise is essentially an interpolation algorithm for estimating rainfall over a pixel size area where no rain-gauge is available. Its value should therefore be compared against more traditional methods of areal rainfall estimation such as arithmetic mean, Theissen polygons and the reciprocal distance method.

6.3 Modifications To CCD

The first modification to eq. 6.1 addresses itself to the problem of optimum threshold and the second is a technique that is used in adjusting radar estimations for areal rainfall using rain-gauges modified for cloud top temperatures.

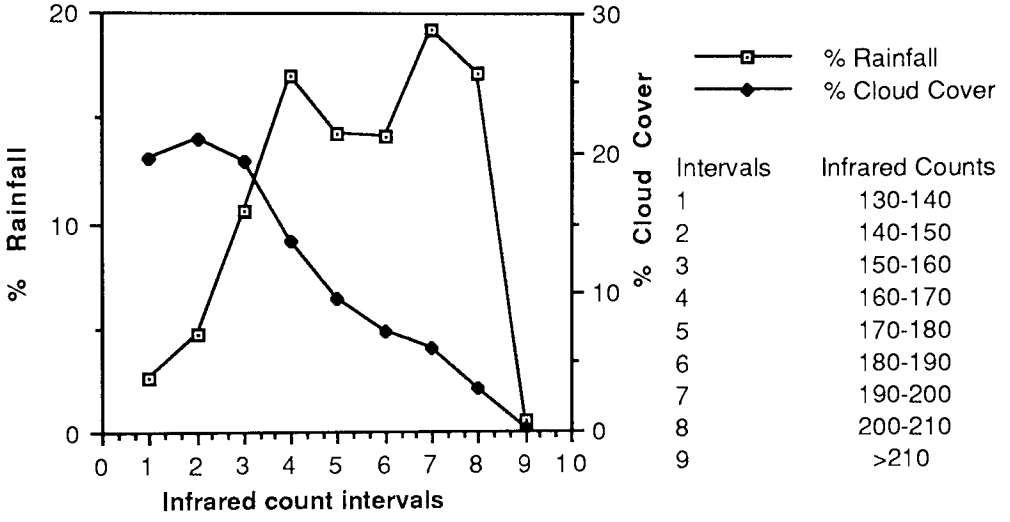

Fig. 6.2 Percentage rainfall and CCD for different count intervals for the whole month calculated from all the rain-gauges.

Fig.6.2 shows the percentage rainfall observed for the month of June, 91 over the river Trent catchment area for a given count interval in the infrared imagery. It also shows the corresponding percentage duration of each of the count interval for the whole month. Values for each count interval were obtained by observing the pixel value over each of the 42 rain-gauges in the Trent region and recording the corresponding half-hour rainfall for each gauge. Raw infrared count values are used instead of temperature values for the following reasons:

* For a given day, radiance values are proportional to raw infrared count values according to the equation (ESOC calibration report, 1991);

$$\text{Radiance} = F * M * (C - C_o) \qquad \text{eq. 6.4}$$

where F is the fine adjustment of gain, M is the MIEC calibration factor, C is the infrared count value and C_o is the reference count value of empty space.

* Although the relationship between radiance and temperature values is essentially non-linear, it is approximately linear in the temperature range where most precipitating clouds are found as shown in fig.6.3.

Temp (°C)

Fig. 6.3 Relationship between radiance and temperature. [From ESOC Calibration Report, 1991]

In fig.6.2 very little rainfall is observed below the count value of 130 and can be taken as the threshold value defining cloud/no-cloud region in the infrared image. Any spurious rainfall found below this threshold is assumed to be due to errors originating from imperfect navigation of image data in both space and time.

Each interval in fig.6.2 above the threshold of 130 represents a cloud layer and contributes some rainfall towards total rainfall. It can be seen that colder clouds are progressively less frequent but produce roughly the same amount of rainfall. In other words higher intensities of rainfall are associated with colder clouds. Assuming that for a given day all pixels defined as clouds (pixel values greater than 130) contribute some rainfall towards the total rainfall at the end of the day, the following equation was tentatively set up:

For a single gauge j;

$$R_j = b_o + \sum_i^n b_i X_{ij} \qquad \text{eq. 6.5}$$

where R = rainfall in mm

X_i = duration of cloud defined by interval i during the day

b_i = regression constants

n = number of intervals or variables

X_i 's are as defined in fig.6.2 above the infrared count threshold of 130. The interval range of 10 was conveniently chosen to define the variables.

In other words, instead of relating the daily rainfall field with a CCD field defined by some optimum threshold, the rainfall field is related to nine successive CCD fields corresponding to different layers of clouds. The whole process is illustrated in fig.6.4.

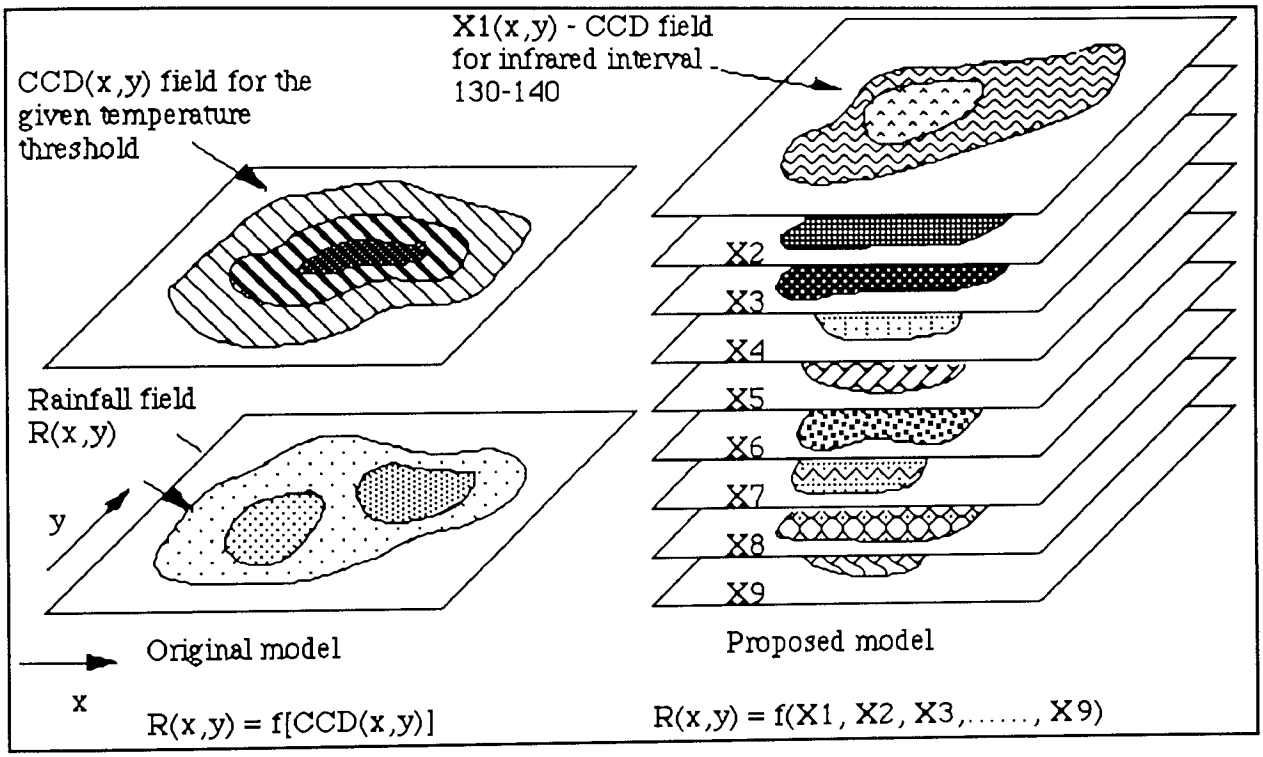

Fig.6.4 Original and modified model for the CCD analysis.

Eq.6.5 constitute a typical multiple regression problem. Values for b_i's are determined using the observations over all the gauges present in the catchment. Also, some of the X_i's may be contributing insignificantly to the overall relationship and should be eliminated. The solution of eq.6.5 and the problem of choosing X_i's are discussed in section 6.4 which explains the theory of multiple regression analysis. In this way clouds layers defined by certain X_i's which are contributing most significantly to the total daily rainfall amounts are automatically selected eliminating the need for defining an optimum threshold as required in eq.6.1.

The rainfall surface produced using CCD's would not produce an exact fit at all data points representing rain-gauge values. To adjust the rainfall field in order to satisfy rainfall values at known data points, a technique is borrowed from rain-gauge/radar studies in which

point rain-gauge values are used to "adjust" rainfall fields estimated using radar (Cluckie & Collier, 1991).

The use of radar for precipitation measurements is not a new idea. It has been considered ever since the inception of the instrument. Its use for rainfall estimation has been discussed in chapter 2. Briefly, if Z is the radar reflectivity of a given storm, than rainfall R is related to reflectivity as:

$$R = a Z^b \qquad \text{eq. 6.6}$$

where a and b are empirical constants

Optimum values of 'a' and 'b' varies in wide ranges and depends upon location, type of rainfall and the number of rain-gauges used for calibrations. Therefore, in practice, exclusive use of radar for rainfall measurements is yet to be achieved. Eq.6.6 is used to provide first approximation to the rainfall rates throughout the radar field, typically using values of a=200 and b=1.6. This rainfall field is than adjusted using calibration factors derived form rain-gauge stations.

Conventionally a radar calibration factor 'c' is defined as the ratio of the rain-gauge rainfall R_g to the radar estimate R_r of rainfall at the rain-gauge site so that:

$$c = \frac{R_g}{R_r} \qquad \text{eq. 6.7}$$

Since 'c' is undefined if $R_r = 0$ or unstable if very small, an alternative version is sometimes used which is :

$$c = \frac{R_g + E_g}{R_r + E_r} \qquad \text{eq. 6.8}$$

where 'E_g' and 'E_r' are positive constants.

Values for 'c' are calculated for each available rain-gauge site and surface-fitting interpolations routines are used to generate a field of 'c' values corresponding to the rainfall field. Each point in the rainfall field is than adjusted by multiplying it by corresponding 'c' value.

For the purpose of this study, rainfall field generated using CCD algorithm R_c simply replaces the radar-rainfall field R_r in eq's.6.7 and 6.8. Typical values for $E_g=E_r=5$ were used.

The idea of using calibration coefficients bears analogy with two well known conventional techniques of areal rainfall estimation namely the Arithmetic mean and the Theissen polygons. If we consider Arithmetic mean (AM) value as the first approximation to the rainfall field, then calibration coefficient 'c' is defined as:

$$c = \frac{R_g}{AM} \qquad \text{eq. 6.9}$$

If a simple surface-fitting technique based on minimum distance algorithm is used to generate field of 'c' values and the AM value accordingly adjusted, than the resultant rainfall field will be the field generated using Theissen polygons with rainfall values satisfied at all known data points. The same is also true for reciprocal distance method if the corresponding surface fitting technique is used. In other words both methods 'improve' the areal rainfall estimates obtained by using simple arithmetic mean as first approximation.

6.4 Theory of Multiple regression

Multiple regression is a general statistical technique used in most research problems where a dependant or a criterion variable depends on more than one independent variable and parameters have to be established. The complexity of most scientific mechanisms is such that in order to be able to predict an important response, a multiple regression model is needed. When this model is linear in the coefficients, it is called a Multiple Linear Regression Model.

For the case of K independent variables X_1, X_2,....., X_k, the general form of the regression is

$$Y' = B_0 + B_1X_1 + B_2X_2 + \ldots\ldots\ldots + B_kX_k \qquad \text{eq. 6.10}$$

where Y' represents the estimated value for Y, B_i are the regression coefficients with B_0 as the Y' intercept. The B_i coefficients are selected in such a way that the sum of squared residuals $(Y-Y')^2$ is minimized. Selection of the optimum B_i coefficients also implies that the correlation between the actual Y values and the Y' estimated values is maximised, while the correlation between the independent variables and the residual values $(Y-Y')^2$ is reduced to zero.

If n is the number of observations of the dependent variable Y, than the actual calculation of B_i values involves the solution of n simultaneous equations using standard matrix algorithms (Draper & Smith, 1966, Nie, 1975).

Following restrictions have to be placed on the sets of observations for the solution of equation 6.10:

1. The number of observations should be greater than the number of regression coefficients to be determined and

2. No one independent variable is a linear combination of any of the remaining independent variables.

In order to carry out efficiently the calculations necessary for multiple regression analysis it is almost essential to have access to the general purpose regression computer routine. NAG statistical library routines were used in this study for the solution of eq. 6.5 on the daily basis.

6.4.1 Adequacy of the model

In many regression equations, the inclusion of all the variables may not prove to be the adequate regression model. In some cases the experimenter using regression analysis is also interested in deletion of variables when the situation dictates that, in addition to arriving at a workable prediction equation, he must find the 'best regression' involving only variables that are useful predictors. There is also some scientific philosophy which dictates that a good model has as few parameters requiring estimation as possible. There are several statistical techniques available which sequentially arrive at the so-called best regression depending on certain criteria (Draper & Smith, 1966).

The most common method used to illustrate the adequacy of the fitted model is to examine a criterion called Coefficient of Multiple Determination (R^2). The total variation in Y (SST) can be partitioned into two independent components, one that is explained by the regression (SSR) and another that is unexplained (SSE) due to residuals; i.e;

$$\begin{array}{ccccc} SST & = & SSR & + & SSE \\ \sum_i^n \left(Y_i - \overline{Y}\right)^2 & = & \sum_i^n \left(Y_i' - \overline{Y}\right)^2 & + & \sum_i^n \left(Y_i - Y_i'\right)^2 \end{array} \qquad \text{eq. 6.11}$$

R^2 is defined as

$$R^2 = \frac{SSR}{SST} \qquad \text{eq. 6.12}$$

The value of R^2 varies between zero and one. Value of one would indicate a perfect relationship while zero indicates no relationship at all. In practice, the value of R^2 is hardly

zero or one and its value is taken as a measure of 'goodness of fit' of the proposed model; i.e.; higher the value of R^2 better is the proposed model.

It can be shown that the value of R^2 nearly always increases with the introduction of one or more variables but the increase may or may not be significant enough to justify the inclusion of the variable(s) in the regression equation. The test for the significance of each variable in the overall regression equation is than carried out by calculating the partial F statistics which is defined as:

$$F = \frac{R^2 - r^2 / 1}{1 - R^2 / n-k-1} \qquad \text{eq. 6.13}$$

Where r^2 is the value of the coefficient of determination obtained with the variable being tested excluded. The value obtained is than compared with a critical value (F_0) in the F distribution statistical tables for 1 and (n-k-1) degrees of freedom. Typical significance levels that are chosen are 95% or 99%. If F is less than F_0 than the variable is rejected otherwise it is accepted. The process is repeated for all the variables and the final equation contains only the accepted variables.

An alternative statistic which has been in considerable use in recent years is the C_p statistic, (Draper & Smith, 1966). This has the form:

$$C_p = \frac{RSS_p}{s^2} - (n - 2p) \qquad \text{eq. 6.14}$$

where RSS_p is the residual sum of squares from a model containing p parameters, p is the number of parameters in the model including the constant term, and s^2 is the residual mean square from the largest equation postulated containing all the variables. It can be shown that a plot of C_p versus p will show up the 'adequate models' as points fairly close to the $C_p = p$ line. Equations with considerable lack of fit, that is, biased equations, will give rise to points above the $C_p = p$ line. The 'best' model is chosen after inspecting the C_p plot. One looks for the regression with a low C_p value about equal to p. This method requires examining all possible regressions and only became practical with the advent of computers.

The advantage of employing C_p values is that it is objective and readily lends itself to computer programming. Standard library routines are available in most statistical packages and libraries such as NAG library routines. Eq. 6.5 is solved using this method and provide the 'best' model for each day depending upon the daily rain-gauge cold cloud durations and associated rainfall (see appendix A.3.1 & A.3.2). The model is than used to

estimate daily rainfall amounts at ungauged points in the catchment from their cold cloud duration values. These are integrated to provide an estimate of total daily rainfall falling over the catchment. The significance of CCD analyses can be tested by comparisons with rainfall estimates from other conventional techniques.

6.5 Data acquisition and processing

6.5.1 Data Acquisition

6.5.1.1 Satellite data

Initially, it was intended that the satellite data would be collected from the SDUS receiver station at the department of Electrical and Electronics Engineering. Unfortunately that system suffered from serious hardware problems in the late 1990 making it impossible to collect any useful satellite images. Consequently, efforts were made to make contacts with various other SDUS or PDUS stations that were in operation all over the country. At some stations, the cost stated for the collection of images was too high, others lacked in storage facilities and at some the system was not operational and some simply did not want to cooperate. In the end, the centre operating at the Imperial College, London kindly agreed to record the satellite infrared images for the month of June,1991 for very little costs. [The centre is run under the guidance of Dr. Chris England (personal communications), Dept. of Atmospheric Physics, Imperial College and the Author is most grateful for his time and cooperation].

The half-hourly satellite data was received in the form of a CCT and was then transferred on to the University computer system for further processing.

6.5.1.2 Rainfall data

The corresponding rainfall data was obtained from the NRA (National Rivers Authority) on the computer disk. It contained readings from all the 83 interrogable rain-gauge stations in the Severn-Trent Catchment Area.

6.5.2 Data Processing

6.5.2.1 Satellite data

It soon became apparent that the quality of the data received was substandard. There were slots of missing data throughout the month with some during the course of every day. Moreover on manual examination of some of the images, it was found that sometime, in the sequence of images, an odd image would contain garbage data. For the purpose of analysis, such images must be identified and eliminated from the full data set. One way

would be to examine each image manually but impractical if 24*48 images were to be examined. One particular aspect of bad images was that a line of data was identical to all the other lines on the image in terms of pixel values. A possibility of finding two identical lines on a correct image is almost nil. This property of bad images was utilized in the automatic screening of bad images from the data set by the computer. To identify a bad image two adjacent lines on an image are compared on the pixel by pixel basis and the process is repeated a number of times throughout the image. This was necessary because in some cases only parts of the image were corrupted. Fortunately the number of missing or bad images were few and sporadic during the course of the day and did not have any major impact on the calculation of cold cloud durations.

For the purpose of CCD analysis, pixel values corresponding to each of the rain-gauges were required. A data file, consisting of time sequences of pixel values for each of the rain-gauges within a catchment area was created for each day of the month. The pixel values were navigated according to the algorithms described in chapter 3. Linear interpolation was used to obtain values for missing or bad data.

6.5.2.2 Rainfall data

Rainfall data files, containing half-hour rainfall values corresponding to the times the images were taken were also created for each day of the month.

These data files formed the data base from which daily rainfall values and the cold cloud durations could be obtained for each of the rain-gauges.

6.5.2.3 Ground data

The study area is again the Severn-Trent catchment area. Analysis of rainfall estimations were carried out over the two smaller sub-catchments namely the Upper-Severn and the Upper Trent respectively as shown in fig. 6.5. The use of smaller catchments provided the opportunity to carry out analysis on different size areas with slightly different climatology. The Upper-Severn region is approximately half the size of the Upper-Trent region and is predominantly mountainous.

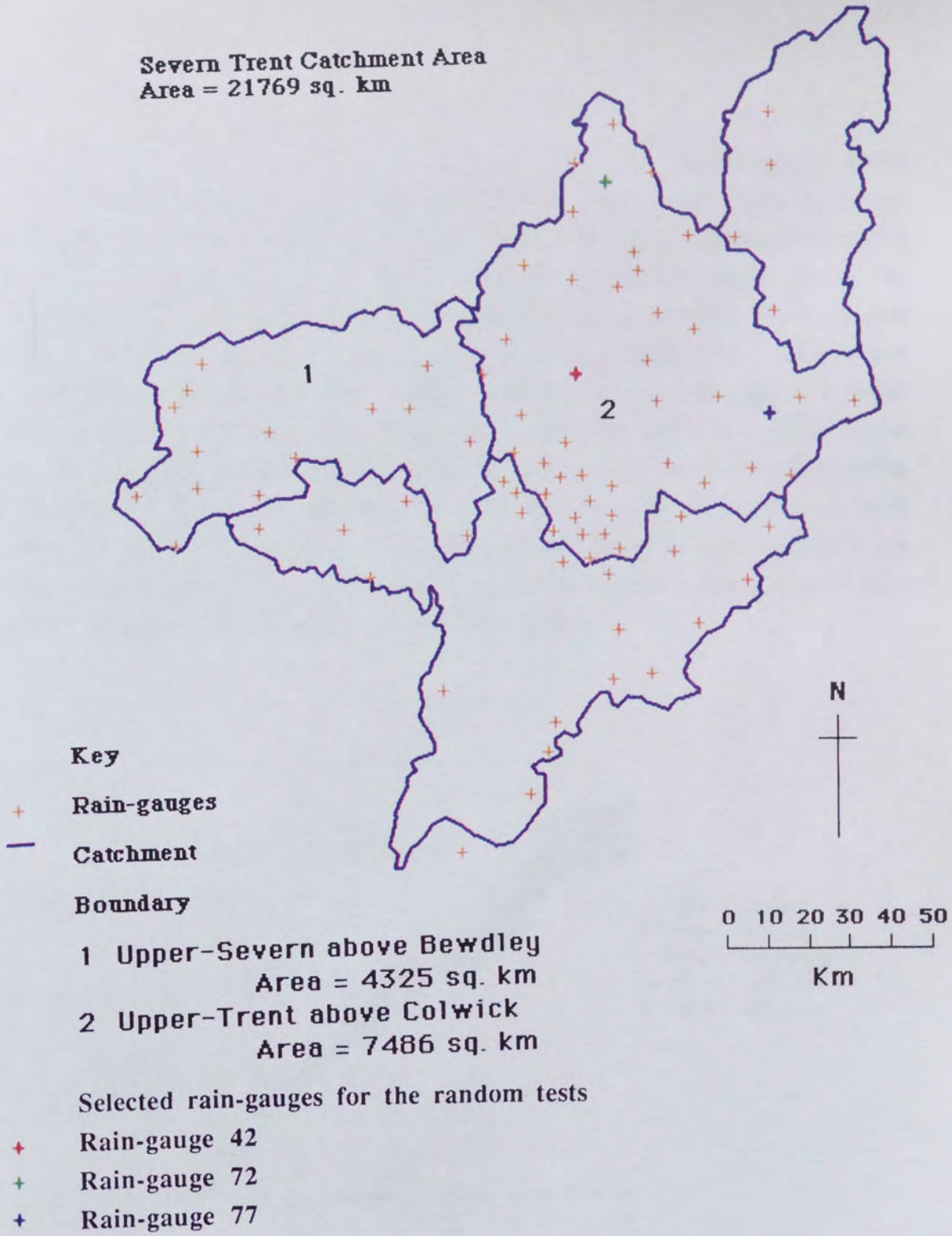

Fig 6.5 Map of catchment boundaries and the position of rain-gauges used.

6.6 Results and Discussion

6.6.1 Selected data

After the completion of all the data processing, daily rainfall estimations in terms of total volumetric rainfall (m^3) for five different methods were carried out separately for the two catchments (see appendix A.4 for the description of computer programme). The rainfall surfaces were repeatedly fitted to smaller number of subjectively selected points. The points were selected to represent uniform distribution over the whole of the catchment. It is assumed that this would approximate the manner in which a hydrologist would distribute the available number of rain-gauges within a catchment using his knowledge of the rainfall distribution. The results for the two catchments are given in fig.6.6 (a-c) and 6.7 (a-d) respectively in terms of cumulative rainfall for the whole month and for different densities of rain-gauges. The results show that the volumetric rainfalls estimated show little variation from method to method. It is also largely unaffected by the reduction in the number of rain-gauges. This may be due to the fact that uniform distribution of rain-gauges was ensured in the subjective selection of rain-gauges.

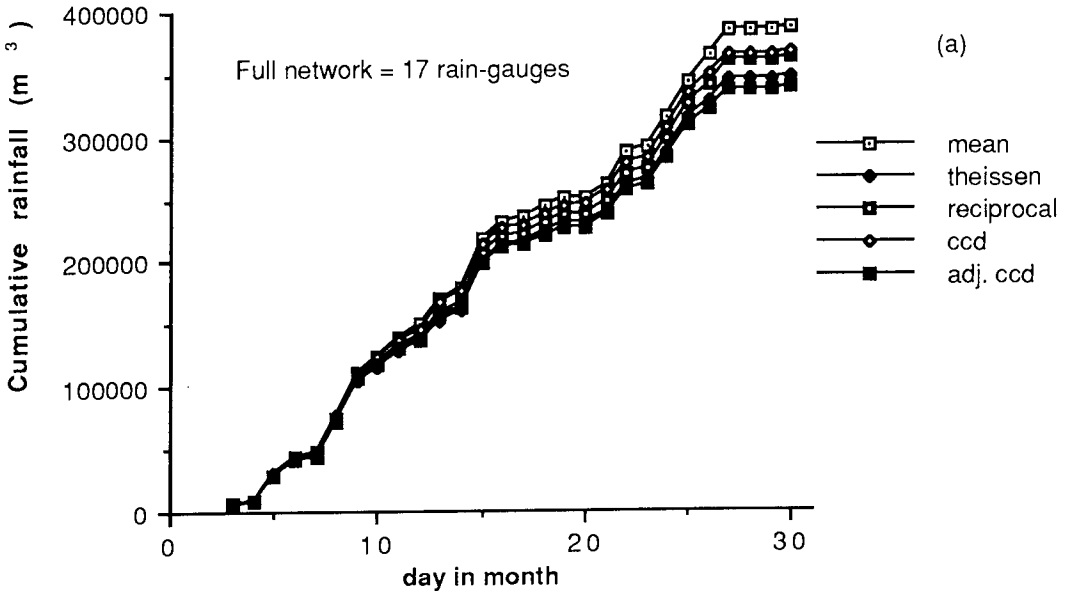

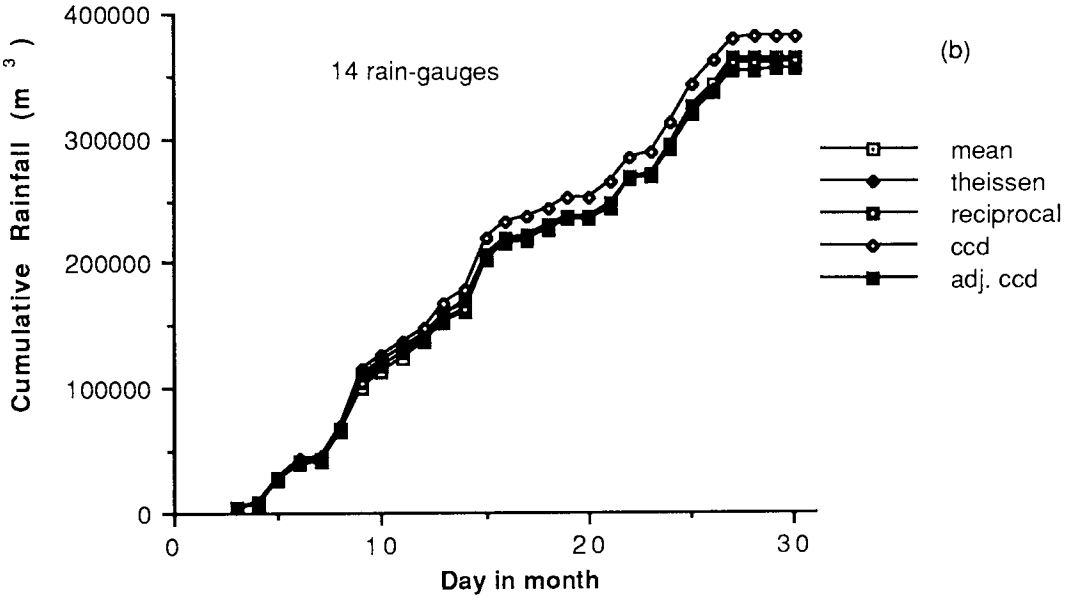

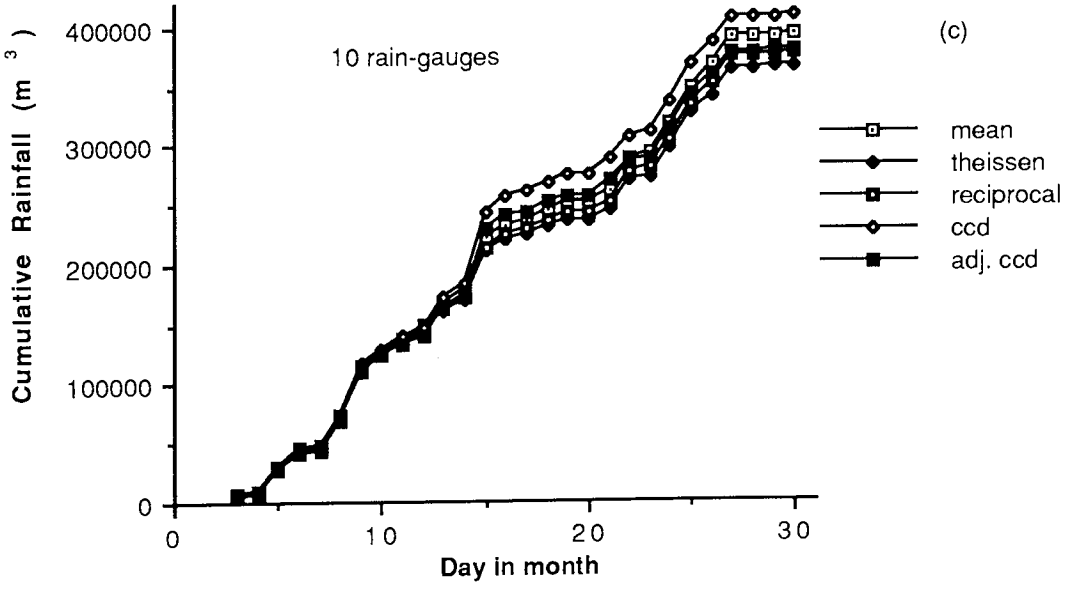

Fig 6.6(a-c) Cumulative rainfall for the Severn region using CCD and conventional methods and for different number of rain-gauges

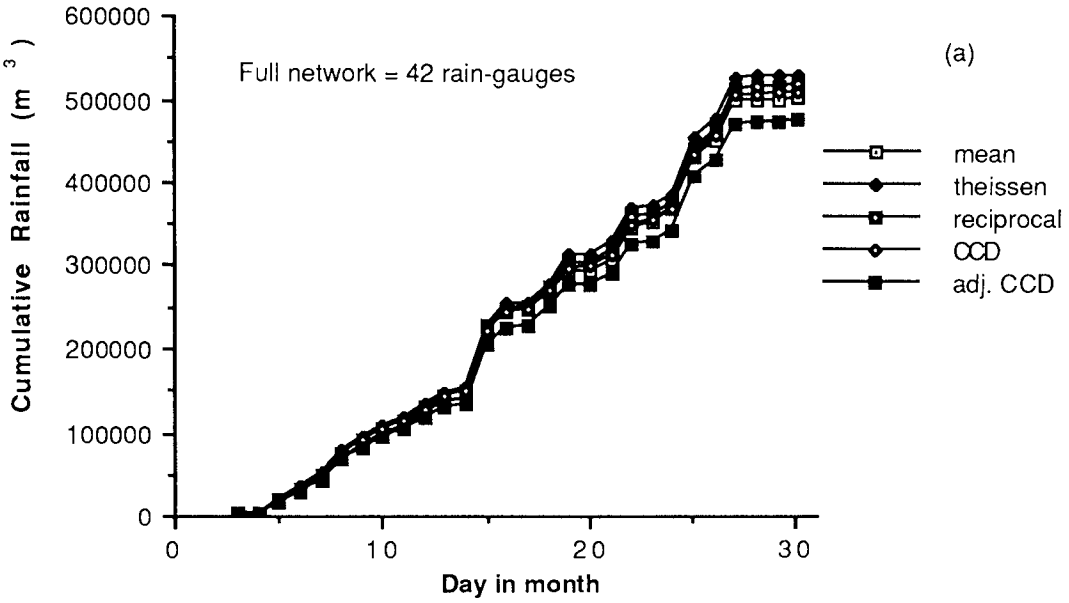
Full network = 42 rain-gauges
(a)
Cumulative Rainfall (m 3)
600000
500000
400000
300000
200000
100000
0
0
10
20
30
Day in month
mean
theissen
reciprocal
CCD
adj. CCD

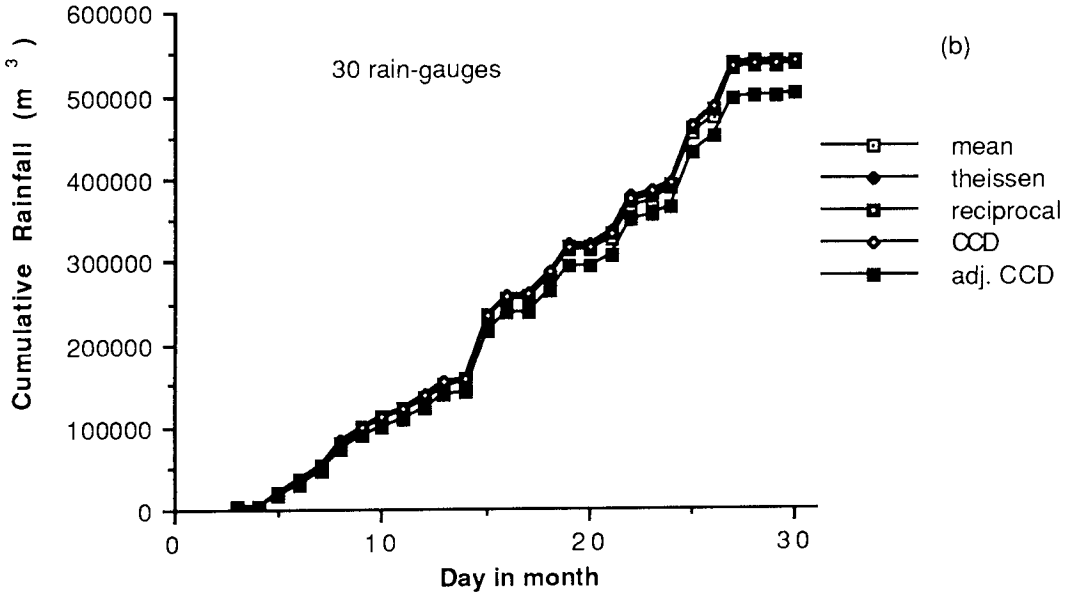
30 rain-gauges
(b)
Cumulative Rainfall (m 3)
600000
500000
400000
300000
200000
100000
0
0
10
20
30
Day in month
mean
theissen
reciprocal
CCD
adj. CCD

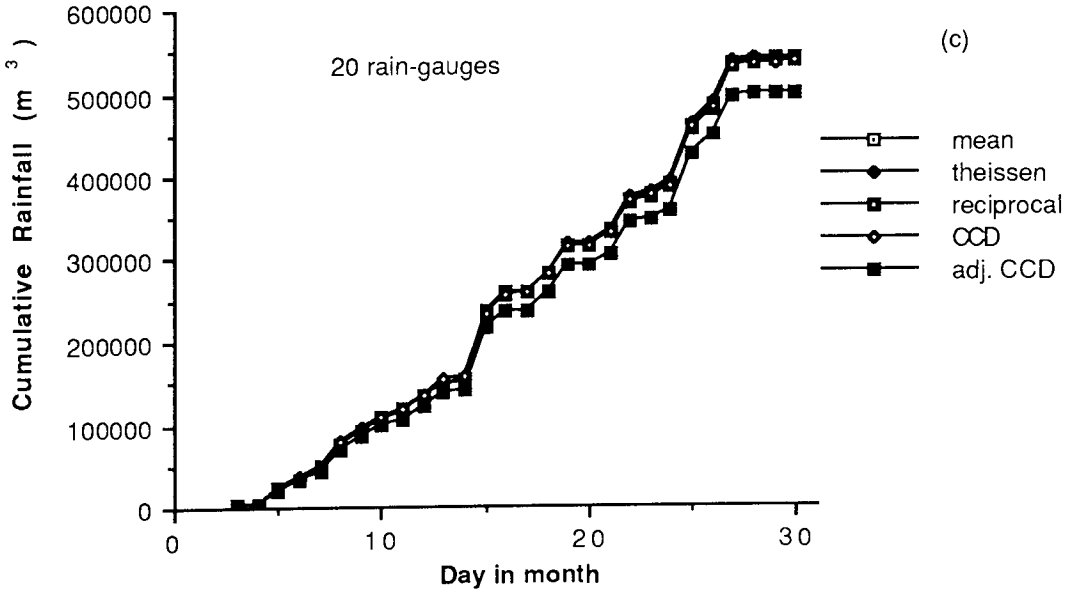
20 rain-gauges
(c)
Cumulative Rainfall (m 3)
600000
500000
400000
300000
200000
100000
0
0
10
20
30
Day in month
mean
theissen
reciprocal
CCD
adj. CCD

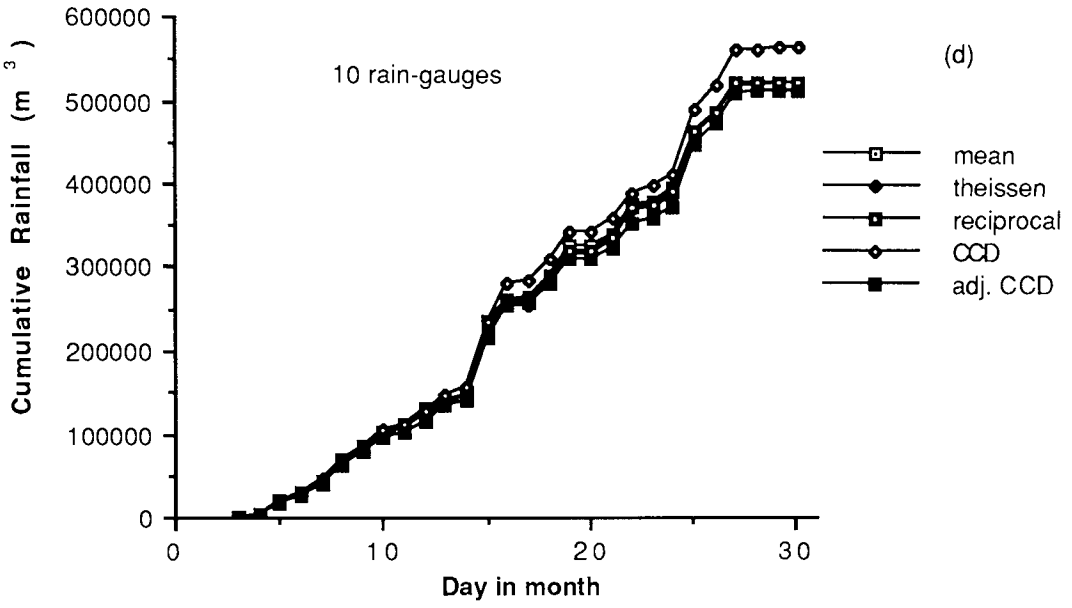

Fig 6.7(a-d) Cumulative rainfall for the Trent region using CCD and conventional methods and for different number of rain-gauges.

Plates 6.1a-c, 6.2a-c, and 6.3a-c shows the rainfall fields generated by various methods for three different days and for three different networks with decreasing number of rain-gauges. The days were selected to represent heavy, moderate and light rainfall events. It can be seen that although volumetric rainfall is approximately the same regardless of the estimating method, the rainfall fields generated do differ in their distribution of rainfall as expected if specific point locations are taken into account. As expected, the CCD method fails to detect extreme values and compensates for small areas of heavy rainfall with larger areas of light or moderate rainfall.When modified using error field, the rainfall field generated looks like a hybrid between reciprocal method and the CCD.

A distinctive feature of the rainfall field as produced by the CCD methods is that they are more 'sporadic' or random in their appearance as compared to artificial boundaries created by Theissen or reciprocal methods. In other words it can be argued that satellite/rain-gauge generated field may be more closer to the 'actual' rainfall distribution than by just using rain-gauges alone.

The use of satellite data would be justified if significant rainfall over part of the catchment, not detected by the rain-gauge network, is identified by using the satellite data. CCD has the ability in theory to extrapolate rainfall beyond the extreme rainfall values given by the rain-gauges but in practice this is difficult. For example, on the 28th of June, little rainfall was reported throughout the catchment except in the extreme East end of the catchment where one gauge reported 5mm of rainfall as shown in plate 6.12a. When that gauge was

removed as in the case of 10 rain-gauges (plate.6.12c), not even CCD analysis was able to detect that rainfall.

6.6.2 Random data

A much more stringent test than the selected data points is the use of randomly chosen rain-gauges. Three rain-gauges from different parts of the Trent catchment area were selected for this exercise and are shown in fig.6.5. Different number of the remaining rain-gauges ranging from 35 down to 10 were randomly selected and used to estimate rainfall at each of the three selected rain-gauges using all of the five methods. For each density of rain-gauges, 15 samples were taken and in each case mean square error (MSE) between the estimated rainfall and recorded rainfall from the three gauges was calculated.i.e. for a particular density of rain-gauges (see appendix A.3.3 for the description of computer programme):

$$MSE = \frac{1}{15*3}\sum_{s=1}^{15}\sum_{i=1}^{3}\left(Re_{i,s} - Ra_{i,s}\right)^2 \qquad \text{eq. 6.15}$$

where Re and Rc are the estimated and recorded rainfall for rain-gauge 'i' and sample 's'.

Results are given in fig.6.8 for the days of 15th, 19th, and 28th of June representing heavy, moderate and light rainfall respectively. With respect to the other methods, a sudden rise in MSE can be noted for the Theissen method on some occasions with the increase in the number of rain-gauges used. The only plausible explanation could be that unlike all the other methods, Theissen method assigns rainfall on the basis of nearest gauge. The effect of introducing or removing a few gauges would have relatively little effect on the other methods but can have a greater effect on the Theissen method.

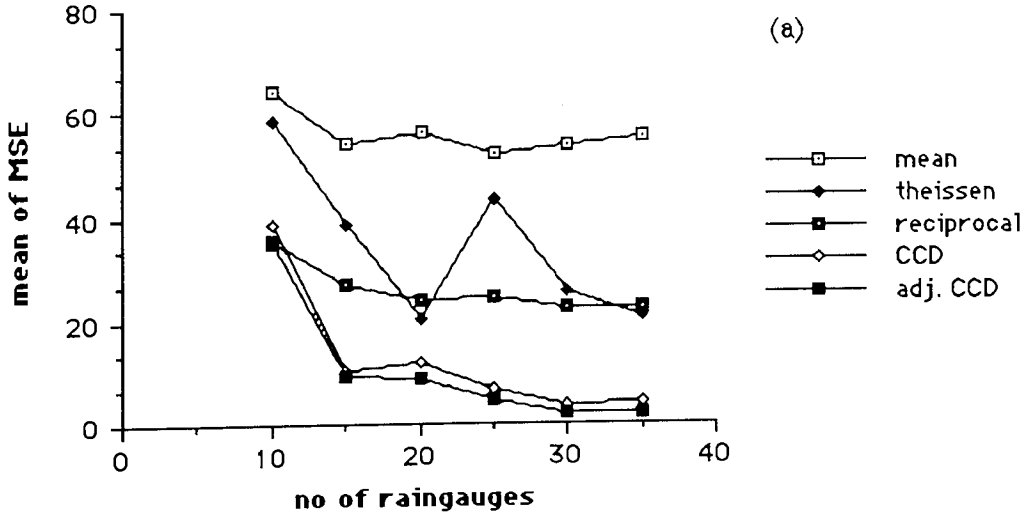

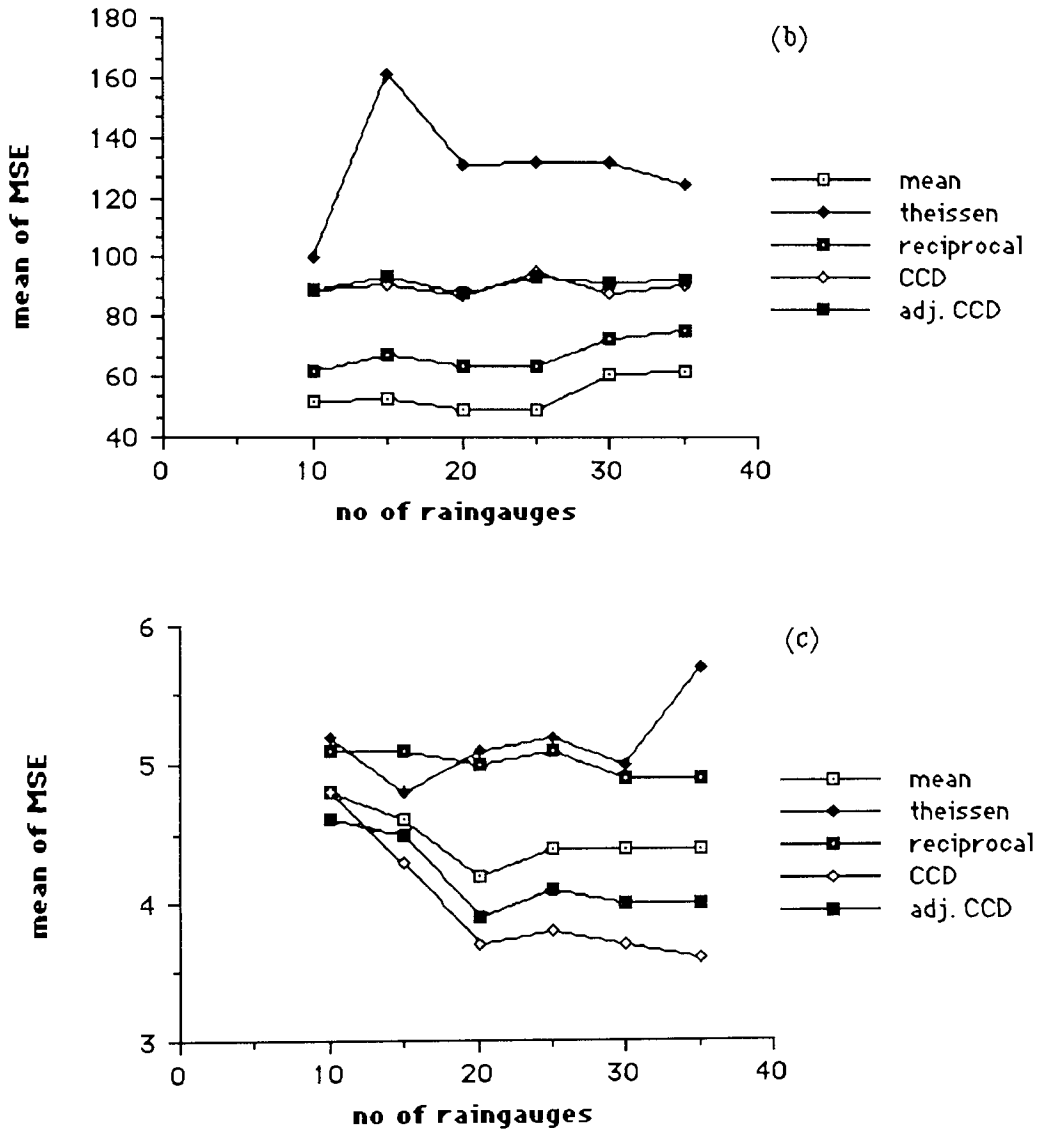

Fig.6.8(a-c) Mean square errors between observed and estimated rainfall obtained for random number of rain-gauges (15 samples) for three different days representing heavy, moderate and light rainfall respectively.

This analysis was carried out for each day of the month starting form the 4th of June. In order to find the best method of areal rainfall estimation, each method was graded on each day according to its MSE value. For example according to the results obtained for the 19th of June in fig.6.8b, the five methods were graded as follows:

Method	Grade
Arithmetic Mean	1
Reciprocal	2
adj. CCD	3
CCD	4
Theissen	5

Summation of grade values over all the days gave the following values for each of the method:

Method	Total
Arithmetic Mean	79
Reciprocal	50
adj. CCD	80
CCD	92
Theissen	89

This shows that in terms of mean deviations between estimated and observed point rainfall, reciprocal method is the best on the average followed by arithmetic mean and the adjusted CCD with Theissen and CCD coming last. This result can be explained if one examines the nature of each method. In the cases of reciprocal method and the arithmetic mean, large differences between observed and estimated rainfall would be less frequent than in the cases of Theissen since information from all the gauges is used rather than the nearest gauge. The results obtained for CCD and adjusted CCD indicate that on the daily basis the method can be used for estimating total rainfall. However, the differences between measured and estimated rainfall at a point is of the same order of magnitude as other conventional methods of determining total rainfall.

6.7 Conclusions

An elaborate method of areal rainfall estimation over areas of the order of thousands of square kilometres has been investigated based on daily rainfall gauges and half-hourly satellite infrared images. The modifications made to the Cold Cloud Duration technique

enabled the method to be applied objectively over any area. Once again, as in the case of half hour estimates in chapter 5, major differences between the CCD and other conventional methods were in the spatial distribution of catchment rainfall rather than in volumetric estimates.

A surprise result of the random tests conducted (section 6.6.2) was that the method of Arithmetic mean was found to be the second best method of estimating catchment rainfall after the Reciprocal method while the method of Theissen polygons was found to be the worst in terms of mean square errors. However, in practice Theissen polygons method is usually preferred over the Arithmetic mean since it gives better distribution of rainfall and provides weights to overcome spatial bias inherrent in rain-gauge distribution. This further emphasize the importance of rainfall distributions obtained using CCD or adjusted CCD. Another positive result obtained in the random tests clearly demonstrate the successful use of error fields in reducing the score obtained by CCD from 92 to 80 points.

The distribution of rainfall over a catchment using CCD or adjusted CCD may be more realistic than what can be obtained from conventional methods and could be used as an input to distributed hydrological models. Such models have extensive data requirements and until recently were confined to small experimental catchments. Current research is focussed on adopting such models to accept conventional data as well as satellite data (France et al, 1986; Goodison et al, 1985a, 1985b, Chander & Fattorelly, 1991, Einfalt & Denoeux, 1991). This would enable such models to be used on catchments deficient in conventional data.

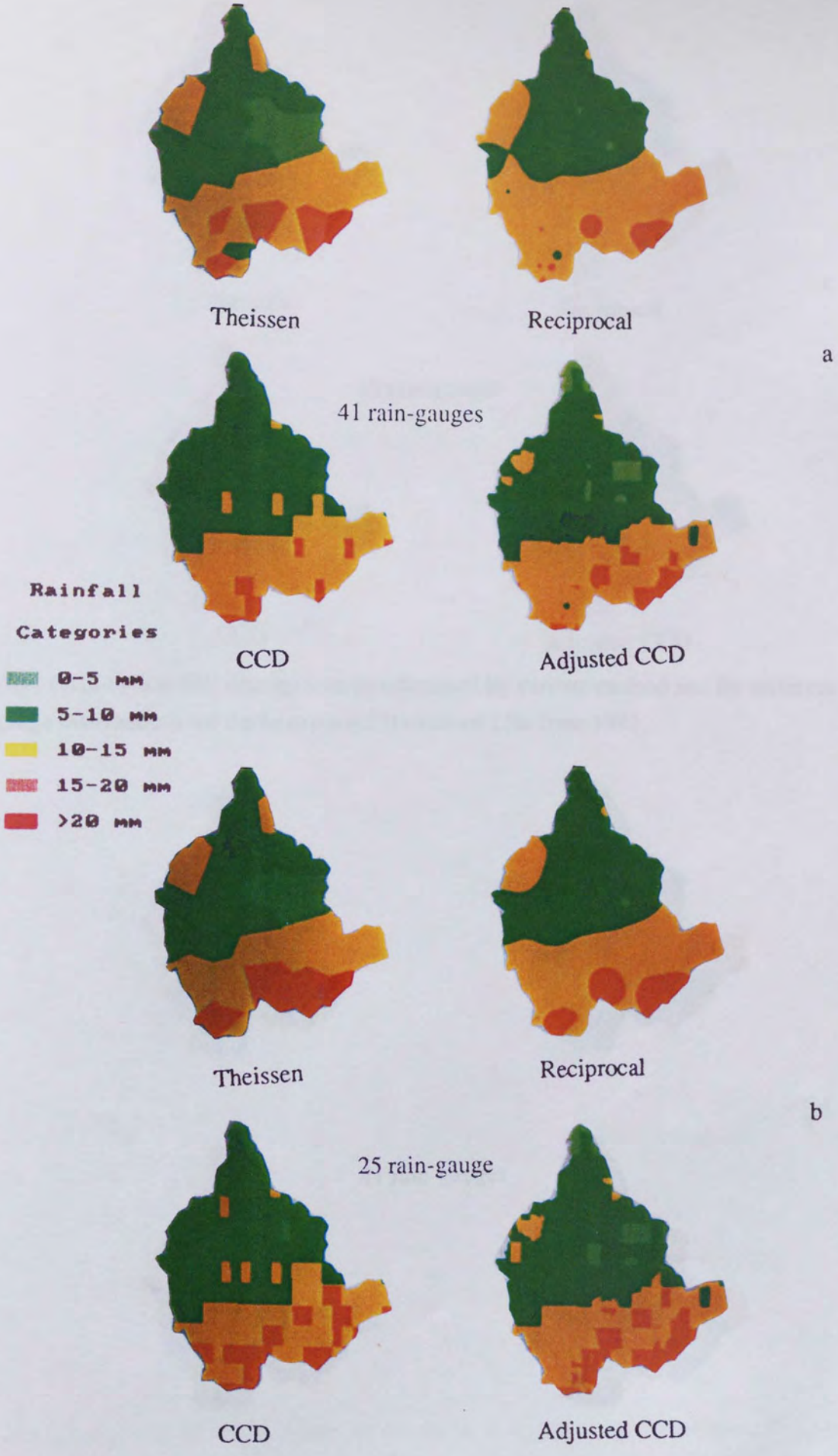
Theissen
Reciprocal
a
41 rain-gauges
Rainfall
Categories
0-5 mm
5-10 mm
10-15 mm
15-20 mm
>20 mm
CCD
Adjusted CCD
Theissen
Reciprocal
b
25 rain-gauge
CCD
Adjusted CCD

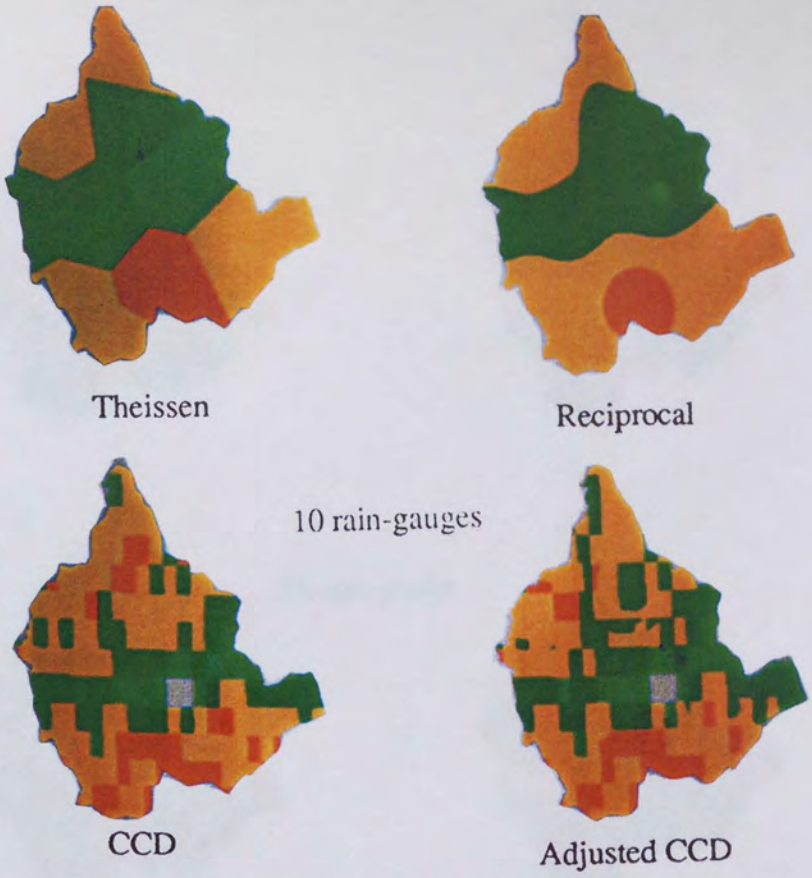

Plate 6.1(a-c) Rainfall distributions as calculated by various method and for different rain-gauge distributions for the heavy rainfall event of 15th June 1991.

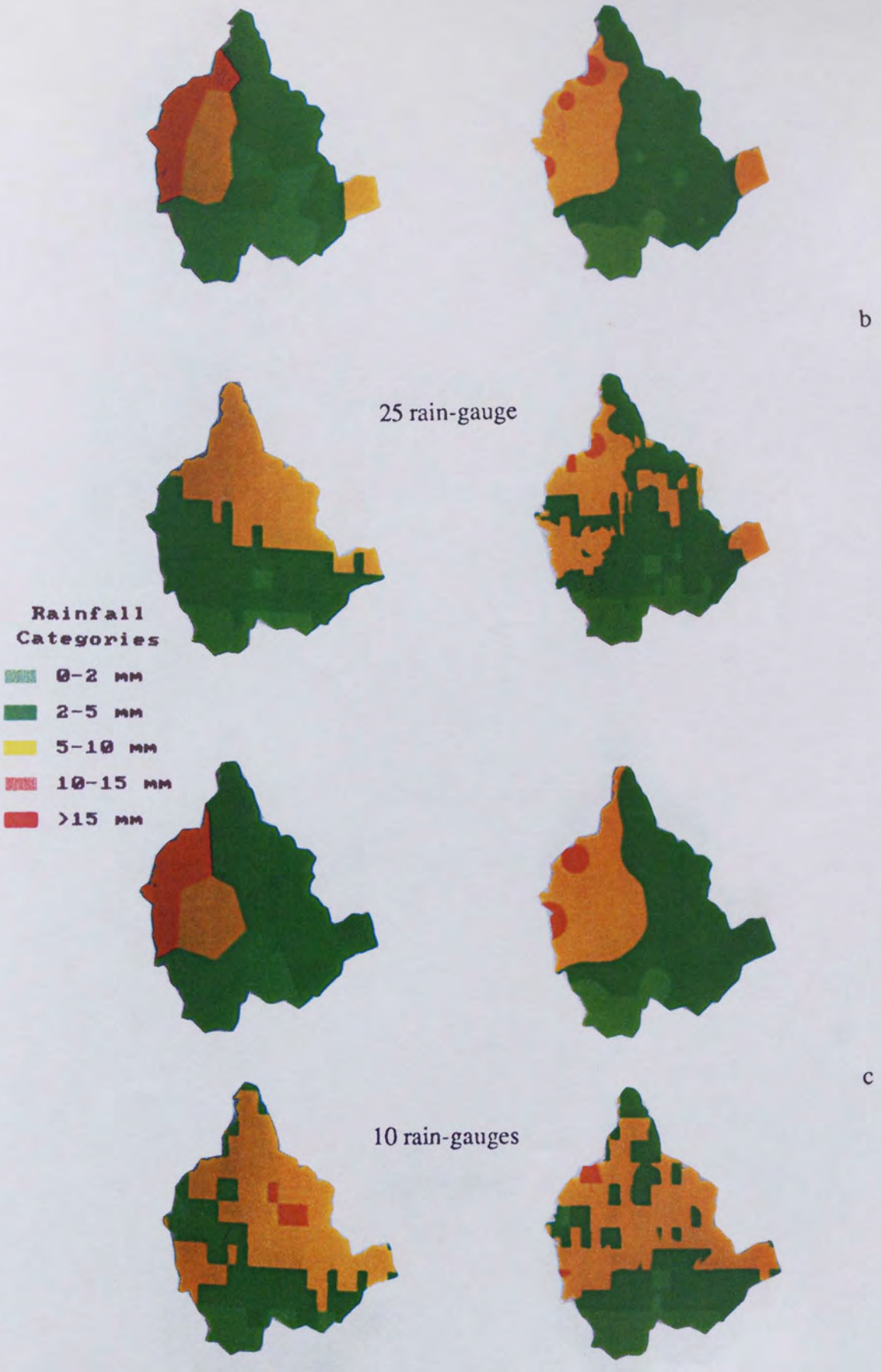

Plate 6.2(a-c) Rainfall distributions as calculated by various method and for different rain-gauge distributions for the moderae rainfall event of 19th June 1991.

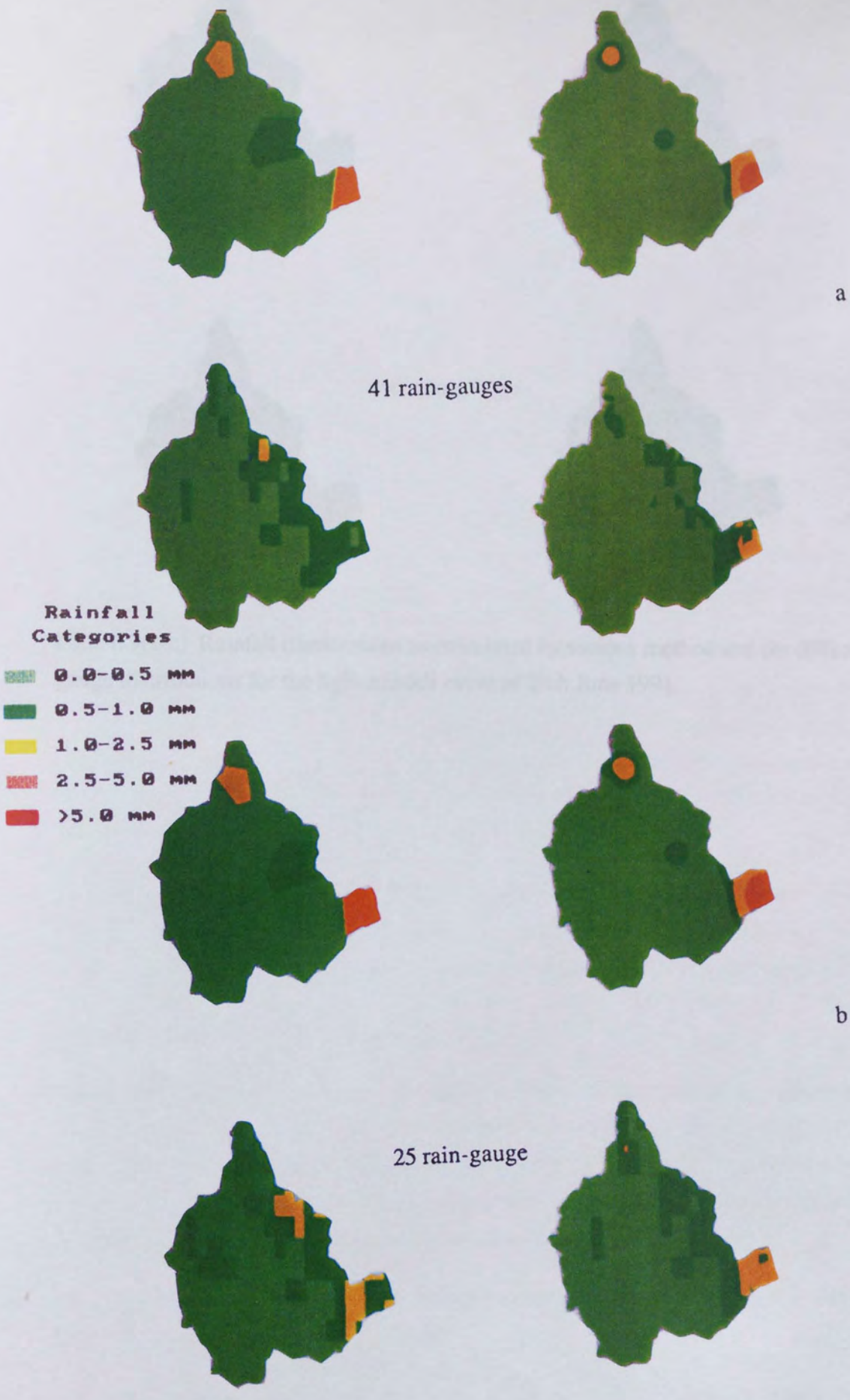
a
41 rain-gauges
Rainfall
Categories
0.0-0.5 mm
0.5-1.0 mm
1.0-2.5 mm
2.5-5.0 mm
>5.0 mm
b
25 rain-gauge

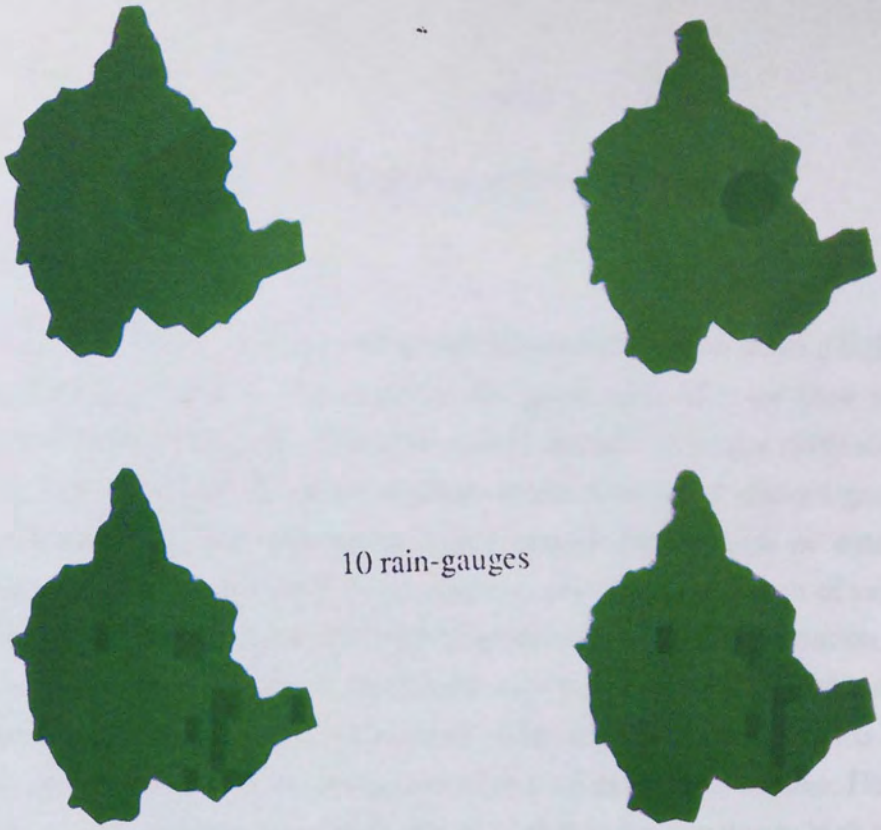

Plate 6.3(a-c) Rainfall distributions as calculated by various method and for different rain-gauge distributions for the light rainfall event of 28th June 1991.

Chapter 7

7. Hydrological Investigations

7.1 Introduction

In developing countries the scarcity of hydrologic information poses a difficult problem to the hydrologists who is interested in the generation of river-flow series or runoff prediction through the use of rainfall-runoff models. A major difficulty is due to the unreliable rainfall information arising from scarce network of rain-gauges and inability to use more sophisticated physically based model due to lack of data from remote, inhospitable areas. Under such circumstances, new data in the form of satellite images of the catchment may provide the hydrologists with useful information. Geostationary satellites, with high temporal resolution, can provide valuable information on cloud formation and thus indirectly on rainfall. Alternatively, radar can also be used in data sparse regions to assist in the estimation of rainfall extent and volume. However, only the most developed countries have been able to exploit radar data due to high operational costs and specialized knowledge.

This chapter investigates the potential of information from geostationary satellite imagery as an input to rainfall-runoff model. A simple linear multiple regression model was used with river-flow data, rainfall data and satellite images as its only data requirements. Daily values were used since this is the highest frequency time interval in which data is generally available to the hydrologists in many underdeveloped regions.

Two sub-river basins of different characteristics located in the Severn-Trent catchment area were selected for study. Results from both indicated that the introduction of satellite information improves the suggested model in terms of defined statistical criteria.

7.2 Use of satellite data in applied Hydrology

Modern planning techniques (eg. operation research methods) for design and operation of water resources systems require a thorough knowledge of the relevant hydrological processes. Usually conventional hydrological rainfall-runoff models are fed with input data from a classical observation network of rain-gauges. Although satellite data can never replace such conventional networks, it has three distinct advantages:

* Satellites provide data with higher spatial and temporal resolution compared to conventional point measurements.

* It provide the means of accessing remote areas where no measurements exist.

* It can be used to infill missing areas of data (see chapters 5 and 6)

On the other hand, it is at a disadvantage since it cannot observe rainfall directly and therefore relies on conventional data sources for calibrations.

Two important problems, differing considerably in their data requirements, that are frequently encountered in the field of Water Resources Management are:

* Design of Water supply system (eg. for municipal and industrial supply, irrigation, hydro-power etc.).

* operation of Water resources systems and flood protection measures.

The first problem requires hydrological data of long duration (many years) and an aggregation scale running into months. This requires a long-term rainfall-runoff model with a long time series of monthly rainfall data as model input.

The second problem require short-term forecasts in real time (hourly) or near real time (daily) depending on the individual application.

Although the present study emphasizes the use of satellite data for rainfall estimations, surface runoff is also affected by various other catchment characteristics such as land cover, land use, soil type, soil moisture and evapotranspiration. Most hydrological models take account of all or some of these factors in order to forecast future flows. Some of these catchment characteristics can also be assessed using satellite images. Data from the high resolution orbital satellites (eg. Landsat) is generally used for land use classification and delineation of drainage network. Classification is based on the fact that different features on the catchment have different spectral response in the visible, infrared and near-infrared sensors (see for eg. Flach, 1989; France et al, 1986, France & Hedges 1989; Downy et al, 1989; Groves et al, 1985). Microwave channel can also be used to assess the soil moisture content (Schmugge et al 1979). Table 7.1 gives a summary of hydrological variables that are currently or potentially available from satellite data.

Table 7.1 Hydrological parameters currently or potentially determined using satellite data (from Groves et al, 1985)

Physical or hydrological data	Satellite	Sensor
Land use, drainage networks, snow cover, groundwater recharge and discharge areas, impervious data, vegetation species, water extent and geology.	Landsat	TM or MSS
	Polar Orbitor	AVHRR
Precipitation, cloud cover and movement, solar radiation, surface and canopy temperatures and high altitude winds.	Geostationary satellites	Visible, Infrared or both
Soil moisture and snow water equivalent.	Nimbus 5, 6, 7	Microwave

7.2.1 Generation of long-term rainfall-runoff data using satellite data

The design of a water supply reservoir system (eg. based on large dam) requires a long time series of river flow data in order to evaluate the water supply reliability. Such data is very often not available or in some cases is available for only short period (1-3 years). Satellite data from the orbital satellites which have been available for many years can provide the means to extend such short term data by relating satellite observations to available rainfall data (see also section 7.5).

One of the very first such studies were undertaken by Davis et al (1971). They used cloud indexing approach for rainfall estimation (see section 2.2) over three river basins in north-western Montana using images from the polar-orbital satellites. The cumulative rainfall estimates agreed well with the estimates from both rain-gauge and radar studies.

Another example of the use of cloud indexing method (see section 2.2) is the study over the Mekong river basin in south-east Asia (Follansbee, 1973). Since no conventional rainfall data was available from the northern half of the basin, a simple cloud indexing method employing a fixed weighting system for different categories of clouds was

organized using APT images from NOAA satellites. The resulting estimates of mean monthly areal rainfall served as input to the rainfall-runoff model for river discharges and floods and related well with observed values from the established network of 79 rain-gauges.

Kruger et al. (1985) demonstrated the use of satellite data for the generation of long term rainfall design data. Preliminary studies based on two years of satellite data and relating cloud indices directly to the observed runoff suggested that such a method is suitable to reduce the problems occurring in the planning of water resources projects based only on short term hydrological data (Strubing & Shultz, 1985).

Creutin et al. (1986), in his study of water resources investigations in the Middle-East, also sought to utilize satellite data to complement the available sparse network of rain-gauges. A novel approach of cokriging (a simple extension of kriging when several measurements sets are available) was used to combine rain-gauge estimates with that of satellite estimates. The study concluded that rainfall depth assessment using satellites produce coherent results provided that the time step considered is large enough (15 days to a month) and also by using the process of cokriging to combine both satellite and rain-gauge estimates, statistically optimum rainfall values can be obtained at non recording points. Again cloud indexing method (see section 2.2) was used to produce satellite estimates of rainfall.

In addition to producing long term rainfall estimates, satellites have been more successfully used to determine snow cover and have been used in river basin studies in which runoff is predominantly dependent on snow melt (Kite, 1991; Rango et al, 1985; Dey & Goswami, 1985).

7.2.2 Real time applications

Water resources systems (eg. dams for water supply, irrigation etc. or for flood protection) have to be operated in real-time. Particularly for highly dynamic processes, eg. flood events, it is necessary to have a real time forecast of the event. Another application where small time scales are required is the design of flood protection measures. Total flood duration usually ranges from several hours to days and the knowledge of several events is required for real time applications. Such data is not always available in conventional terms and satellite data can be used to determine flood producing rainfalls over the relevant catchment area.

Grosh et al. (1973) directly related the frequency and the areal extent of bright clouds observed in the visible channel of the geostationary satellite ATS III with the observed

stream runoff. The study was conducted in Surinam and was initiated due to the lack of conventional data from remote inaccessible areas. He found useful relationship between the two variables which were adequate under the circumstances.

Scofield and Oliver (1977) technique (see section 2.3.3) for rainfall estimation was primarily devised as guidance information to the forecaster for flash flood forecasting and warnings. In the early 1980's hydrologists at the National Weather Service West Gulf Forecast Centre, USA, set up an operational experiment to test the utility of satellite data as input into a river forecast model. Preliminary results indicated that for routine predictions, satellite data may not be necessary but they can serve as critical inputs for severe rainstorms at night when the gauge network is largely inactive (Clark & Morris, 1986).

Similarly, Rott (1986) used cloud cover indices for estimation of daily runoff based on Meteosat data for large catchments in Central Europe. Cloud indices were directly related to river runoff for three separate rainfall events. Results indicated that useful runoff forecasts can be made for large basins on the daily basis.

Kite (1991) also used a daily rainfall runoff model specifically designed to make use of satellite data as model input by deducing the physical parameters of the catchment based on satellite data. It used Landsat data for land-use classifications of the basin and NOAA / AVHRR data to provide estimates of snow and cloud cover. The model provided comparatively better results when estimates of snow cover using satellite data were used. On the other hand, incorporation of cloud cover in the model did not improve the results in any way. It was observed that no significant relationship existed between observed cloud cover and daily rainfall.

Hardy et al (1988) applied the technique of Cold Cloud Duration of rainfall estimation as input to a general rainfall runoff model. The study was carried out over the catchment area of the River Baise which is a tributary of river Senegal in Africa. To produce daily rainfall values, the technique was modified such that average cold cloud durations over the catchment were used instead of point values. The Pitman Rainfall-runoff model was used. It was calibrated using data from the rain-gauges. The model was than rerun on an independent data set with input based on CCD and rain-gauges. It was found that results produced using CCD rainfall estimates as input were better than results produced using the rain-gauges. Although the results demonstrate the utility of satellite information, it is not clear that it is 'superior' to rain-gauge information since the model was calibrated on rain-gauge information. Ideally, comparisons should be made from models calibrated separately on both sets of input data (this point is further discussed in section 7.3.2).

Most of the research effort of using satellite data has been directed towards the estimation of daily rainfall. Shorter time periods are required for the monitoring of small urban catchments where the runoff response time is of the order of hours. Radar data has been used comprehensively in that respect. Radar can provide rainfall estimates for as short a duration as 15 minutes (Collinge & Kirby, 1987, Cluckie & Collier, 1991). Satellite data, on the other hand, show poor relationship with hourly rainfall estimates (Griffith et al, 1981; D' Souza, 1988). Furthermore, only geostationary satellite data is available at high temporal resolution but suffers from low spatial resolution (5x5 km at sub-satellite point) and therefore unsuitable for the monitoring of small hydrological regimes. This was confirmed in an exploratory study carried out over two small catchments of River Izaak Walton (catchment area 83 km^2) and River Perry (catchment area 164 km^2) in the Severn-Trent region. It was found that at the latitude of the study area, the whole catchment could be defined by only one or two pixel and at that spatial and temporal resolution there is no relationship between the rainfall observed at ground level and the pixel value due to the natural variability of rainfall. Such errors are largely compensated for large areas and time scales as will be shown in sections 7.8 and 7.9.

In summary satellite data has been used for the generation of long term river flow records for design purposes and on the daily basis for hydrological forecasting applications. Emphasis has been placed upon the use of satellite data alone so that data sparse regions can be effectively monitored. The information content of satellite data has been clearly demonstrated. What is required is to assess quantitatively the significance of satellite data in relation to the existing conventional network. A 'sparse network' is usually a justification for the use of satellite data but it is a relative term. Depending on the type of rainfall, catchment morphology and the distribution of rain-gauges, a high density of rain-gauges may still be considered inadequate in some areas while in others it may be more than necessary. In chapter 6 it was shown how a largely reduced number of rain-gauges still gave rainfall estimates within few percent of the rainfall value from the full network.

7.3 Influence of rainfall estimation errors on Rainfall-runoff modelling

To improve the modelling of rainfall-runoff process by improving the input data, consideration should be given first to the effect on rainfall-runoff model performance of erroneous rainfall measurements. This serves to clarify the potential value of satellite-derived measurements of rainfall to flood forecasting and rainfall-runoff model design. It is important to understand the influence of these errors on rainfall-runoff model performance if an appreciation of the potential value of satellite rainfall data is to be gained. The following examines the relation of model structure to rainfall input errors, and the error introduced by using a lumped, areal average, rainfall input.

7.3.1 Effect of the Structural form of the model

Singh and Woolhiser (1976) in their simulation studies showed that the effect of errors on rainfall measurements used as input to a rainfall-runoff model will depend on the model's structural form. They demonstrated how a non-linear rainfall-runoff model tends to amplify the errors so that a linear model calibrated on data simulated from a non-linear model may perform better than the true non-linear model when the rainfall input is in error. Singh (1977) demonstrated that even if rainfall is known exactly, the errors introduced in conversion to rainfall excess (effective rainfall) may mean that a linear model may out-perform a non-linear one. However, experience using actual data suggests that in many circumstances, non-linear models provide improved performance, presumably because amplification of errors by non-linear models is less deleterious than the use of linear models to represent the non-linear rainfall-runoff process in these situations.

7.3.2 Effect of using lumped, areal average, rainfall

Basin average rainfall estimated by a single rain-gauge measurement or as an average of measurements from a small number of rain-gauges will have a greater variance than rainfall averaged over a much larger number of points within the basin. This error, associated with rain-gauge network-derive estimates of basin average rainfall, may be termed a space-sampling error and is a major cause of bias in runoff prediction (Troutman, 1982, 1983). In practice this bias is compensated for by calibrating the rainfall-runoff model by least-squares using the areal estimates of rainfall from the rain-gauge network. However, if a model is calibrated in this way and then used operationally for flood forecasting using satellite-derived areal average rainfall, there will be doubts about the output, on account of the statistical properties of satellite estimates being different from the rain-gauge estimates. This serves to emphasize the importance of calibrating rainfall-runoff models using the data source whose utility is being investigated. Ideally an operational system should accommodate a range of model calibrations appropriate to various possible configurations of rain-gauges and satellite observations, thereby catering for all possible scenarios of data availability.

7.4 The study basins

The Severn-Trent catchment Area is composed of three main drainage basins which are: 1) the River Severn drainage basin on the west of the catchment, 2) River Trent basin in the North and, 3) the River Avon drainage basin in the south-east which is also a tributary of river Severn.

The hydrological studies presented in this chapter were carried out separately for the Upper-Severn basin and the Upper-Trent basin. The corresponding river-flow gauging stations are located at Bewdly (4325 sq. km drainage area) for the Upper-Severn and in Colwick (7486 sq. km drainage area) for the Upper Trent. The two river regimes reveal significant differences in their catchment characteristics and rainfall-runoff regimes. The main part of the Upper-Severn basin lies in the Welsh mountains. The Upper-Trent basin is mainly low lying except in the north of the basin which comprises of the high grounds of the Pennines. This difference in the altitude is reflected in the average annual rainfall totals of the two basins with Upper-Severn (average 1400m) receiving almost twice the amount of rainfall than Upper-Trent (average 800m).

7.5 The Basic Concept

A variety of rainfall-runoff models exist, ranging from complete conceptual and physically based models to simple regression models (Anderson &Burt, 1985; Weeks & Hebbert, 1980; Singh, 1989). The accuracy of runoff calculations is not necessarily dependant on the complexity of the model, more important is the quality and availability of the input data.

The investigations in this study focussed on the possibility of satellite data as input for runoff modelling in conjunction with the available conventional data. During the summer months, snowmelt in the river basin can be considered insignificant. This suggests as one possibility for runoff simulations that the areal rainfalls are derived from the satellite data and that this rainfall data is used as input to the runoff model. This process introduces two sources of errors by 1) the transformation of satellite data into rainfall and 2) the relation of rainfall to runoff. Plus algorithms used to transform satellite parameters into rainfall estimates generally work well for large space and time scales (see chapter 2). Their use for generating long term rainfall-runoff records have already been demonstrated in which they are not used as an alternative to conventional data (see section 7.2.1). For real-time operational use such a method would be of limited value since reliable rainfall estimates from a network of conventional rain-gauges would be required to calibrate the satellite information. A second possibility exists in which areal satellite data and point rain-gauge information could be combined in such a way that better estimates of areal rainfall could be obtained. Chapters 5 and 6 investigated this possibility and it was found that satellite improved areal rain-gauge estimates were similar to the ones produced using traditional interpolation routines. Significance of including satellite data in such cases is difficult to prove objectively. Therefore in this study a third and a more direct approach is used which relates satellite derived data on the clouds (cloud indices) and the available conventional data directly to daily runoff volumes using multiple regression analysis.

7.6 The Daily Satellite Cloud Variable

Various methods have been applied for estimating rainfall volumes based on visible and/or infrared satellite imagery by relating parameters associated with clouds such as cloud temperature, area, rate of change of temperature, etc. with observed rainfall from a network of rain-gauges or ground based radar (see chapter 2). Fractional cloud coverage, given by the area of the cloud above a certain temperature threshold is one of the simplest form of cloud indices used as predictor for rainfall volumes or rates (Arkin, 1979). In mid-latitudes, the relationship between cloud top temperature and precipitation reveals considerable variability depending on the synoptic situation and on cloud type.

Among more direct approaches, relating satellite derived cloud indices directly to observed river flow, Rott (1986) used

$$CI = \frac{A}{N} \sum_{j=1}^{N} (T_a - T_c)^{\frac{1}{3}} \qquad \text{eq. 7.1}$$

to calculate the cloud index (CI) where Ta is the threshold temperature above which the probability for precipitation is assume to be zero. Tc is cloud top temperature averaged over the area, N represents the number of Meteosat images and A is an empirical constant. The exponent 1/3 is arbitrarily used as a weighting factor, indicating a certain increase of rainfall intensity with decreasing cloud top temperature.

Kruger et al. (1982) in their application for generating long-term rainfall records using historical data from an orbital satellite used three coldest range of 'grey-levels' of the grey scale contained in the images to define a cloud index as follows:

$$CI = 0.5 \sum_{k=1}^{2} \sum_{i=1}^{3} B\,(T_i)_{k,l}^{a_i} \qquad \text{eq. 7.2}$$

where $B(Ti)_{k,l}$ is the fractional cloud cover for the grey-level range i, image k (NOAA produces two images per day) and 'a_i' is the calibration coefficient determined for each grey-level range by using available rain-gauge data, and l is the number of day.

In the above mentioned studies, the objective was to establish a technique so that rainfall-runoff model can be operated using the satellite data alone. Simple indexing techniques based on cloud top temperatures and areal extent which enables automatic data analysis were developed for the purpose of this study since it is important for operational applications. Because of the size of the river basins under investigation and the resolution of infrared image pixels which doubles in the mid-latitudes (10x10 km), something like

60-80 infrared pixels would cover the whole basin. A composite image made up of all the half-hourly infrared images was created for each day which represents the structure and movement of clouds throughout the day. The first line of the composite image represents the first image received in a day and the last line represent the final image in a 24 hour cycle. A normal histogram of such an image would produce peaks as shown in fig. 7.1. These peaks are attributed to clouds at different altitude and at the lower end of the scale, they represent cloud free areas. Area under the peak represents the duration that particular peak has affected the catchment. Separation boundaries of such peaks are easily determined using unsupervised classification algorithm on one band. Three different cloud indices are defined based on such histograms:

1. $CI_1 = T$

   where T is the mean cloud grey level of the highest peak (coldest)

2. $CI_2 = \frac{1}{N}\sum_{i=1}^{N} T_i A_i$

   where T_i and A_i are the mean cloud grey-level and relative size of the i th peak found in the histogram

3. $CI_3 = \frac{1}{N}\sum_{i=1}^{N} T_i$

   where T_i is the mean grey-level of the i th peak found in the histogram.

Cloud index CI_1 only makes use of the coldest peak while CI_2 and CI_3 utilize all the peaks found in the histogram. Fig. 7.2 gives a schematic diagram of the construction of daily composite images.

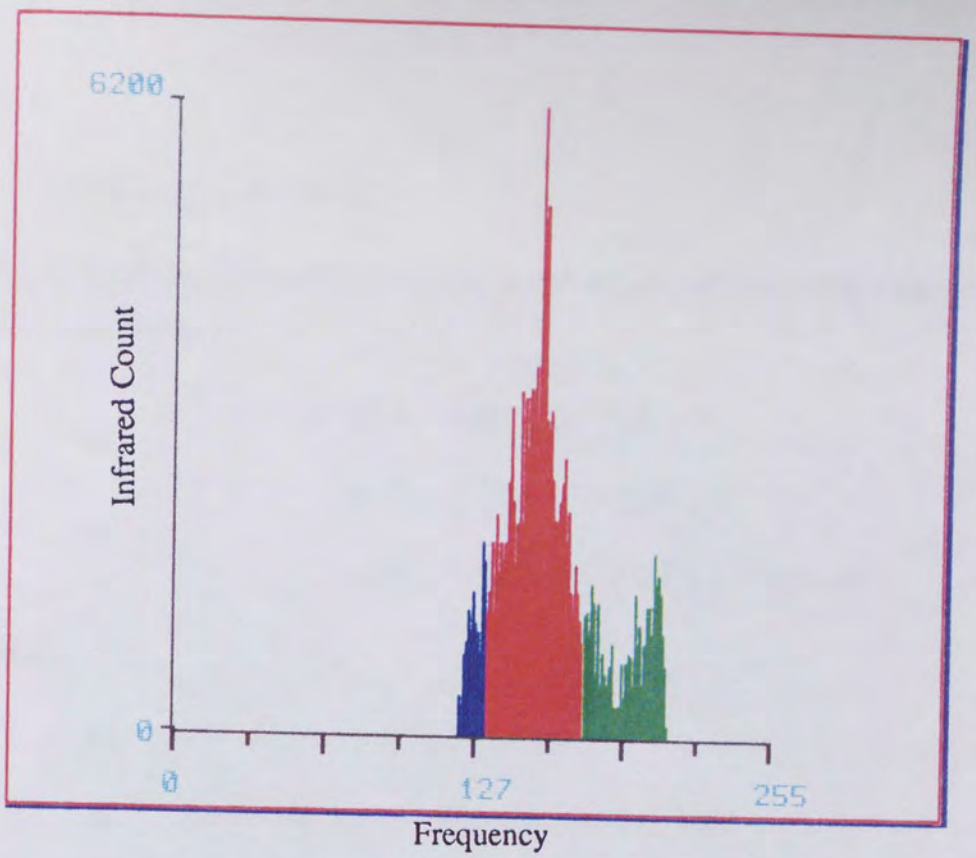

Fig. 7.1 Example of a histogram produce for the composite images.

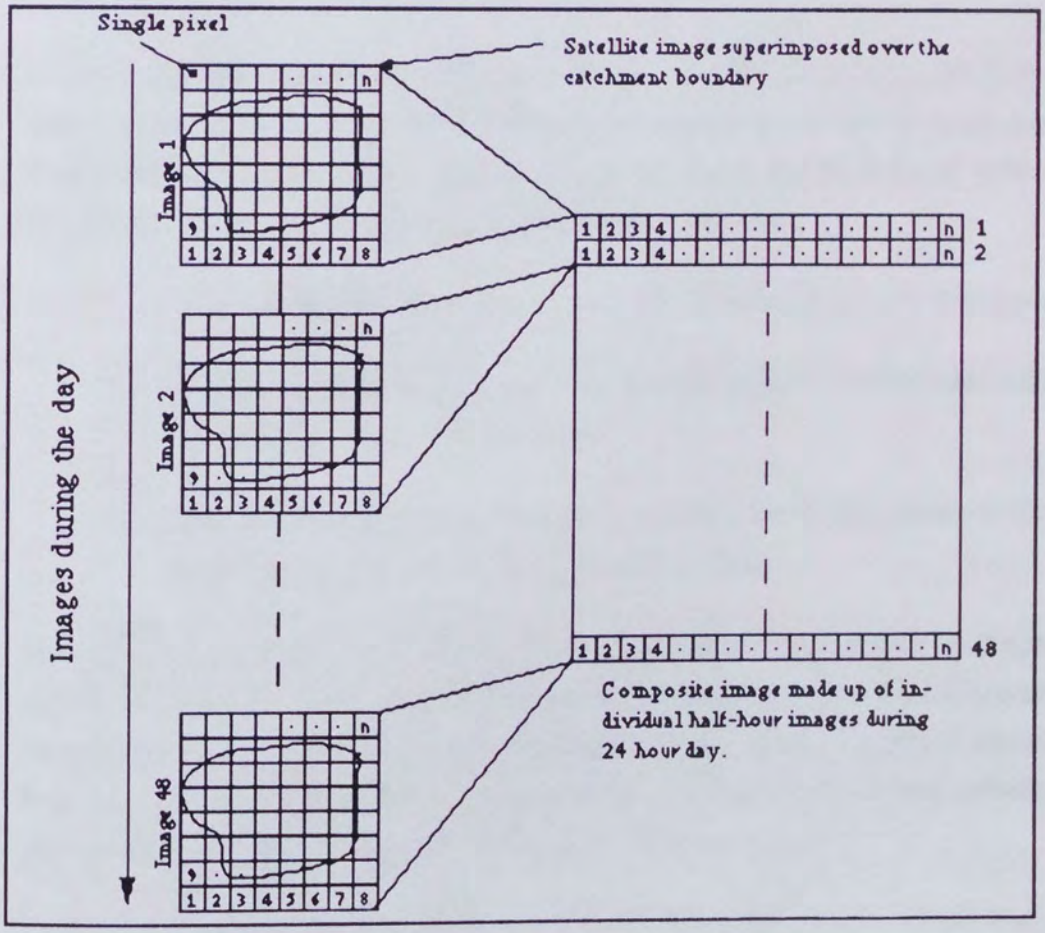

Fig. 7.2 A schematic diagram showing the construction of daily composite images.

7.7 The Rainfall-runoff Model

The Rainfall-Runoff model developed is the simple linear multiple regression function of the following form:

$$q_t = a_1Q_{t-1} + a_2Q_{t-2} +..+ a_pQ_{t-p} +$$

$$b_1R_{t-1} + b_2R_{t-2} +..+ b_qR_{t-q} +$$

$$c_1CI_{t-1} + c_2CI_{t-2} +..+ c_sCI_{t-s} + \text{constant} \qquad \text{eq. 7.3}$$

where:

qt = generated flow at time t

Q_t = the actual or recorded flow at time t

R_t = Rainfall measured at time t from the rain-gauges

CI_t = Cloud index for time t

A similar transfer fumction model was used by Cluckie & Owens (1987) in their study using radar estimates of rainfall and can be seen as a numerical approximation to a traditional Unit hydrograph model subject to the same assumptions of system linearity. The choice of the model depended on the following criteria:

* It has minimum data requirements unlike a more physically based model
* It takes total rainfall as input rather than the effective rainfall which is difficult to define in real time situations, and
* The objective of the exercise is to estimate the significance of satellite input which can be seen more clearly in a linear model.

Equation 7.3 represents a classic multiple regression model, theory and application of which has already been demonstrated in the previous chapter. The F statistics for the significance test can be used for each of the variables in eq. 7.3. The F statistics at 95% level of significance is carried out in three stages corresponding to three different inputs of previous river-flow, catchment rainfall and the cloud indices.

In the first stage it is assumed that the river flow data is the only information available and therefore the model is calibrated on previous flow data only. The value for p in eq. 7.3 for the flow variables is arbitrarily chosen to be equal to 3 initially and eq. 7.3 becomes:

$$q_t = a_1Q_{t-1} + a_2Q_{t-2} + a_3Q_{t-3} + \text{constant} \qquad \text{eq. 7.4}$$

Coefficients a_i (i=1-3) in eq. 7.4 are calculated using least square minimisation and the significance of each variable is tested using the F statistics (see section 7.8.3).

In the second stage, rainfall data is also made available in the form of average daily areal rainfall estimates from the full network of rain-gauges and the rainfall variables in eq. 7.3 are added to the optimized equation from stage 1. These rainfall variables are tested for their significance as in stage 1 with q=3. The optimized equation in terms of number of variables is also calibrated with rainfall estimates using only one gauge from the network. This gives a rough measure of the effect of sparse network of rain-gauges on rainfall-runoff model. Moore (1977) investigated the effect of using several rain-gauges located in and around a basin as inputs to a multiple-input transfer function model. Data from up to six rain-gauges was used for a small (33.9 sq. km) basin and the results indicated that inclusion of more than two gauges, either as separate inputs or as a single average value failed to improve forecasts of hourly flow. It was argued that a gauge, or set of gauges, should not be chosen for use in flood forecasting in terms of how well it estimates the basin average rainfall, but rather on the strength of its association with observed river flows. Siting of a single gauge in the vicinity of the contributing area of storm runoff (for example, located near the basin outlet) could be superior for flood peak forecasting than a dense network designed to obtain a good estimate of basin average rainfall. This is actually an admission of our inadequacy in modelling and understanding of the hydrologic processes in the catchment.

Similarly in the third stage, satellite gathered information is made available in the form of daily cloud indices and are introduced and tested for significance in the optimized equation derived at the end of stage 2. The whole procedure and the results for two basins are presented in the following section.

7.8 Case Study 1: The Upper-Trent River basin

7.8.1 General description and hydrology

The River Trent basin above Colwick is composed of four major basins corresponding to its main tributaries and drains a total area of approximately 7486 sq. km. The major basins are associated with rivers Dove and Derwant, Soar, Tame, and the Upper Trent itself. The respective positions of these basins in the Severn-Trent catchment area are given in fig. 7.3.

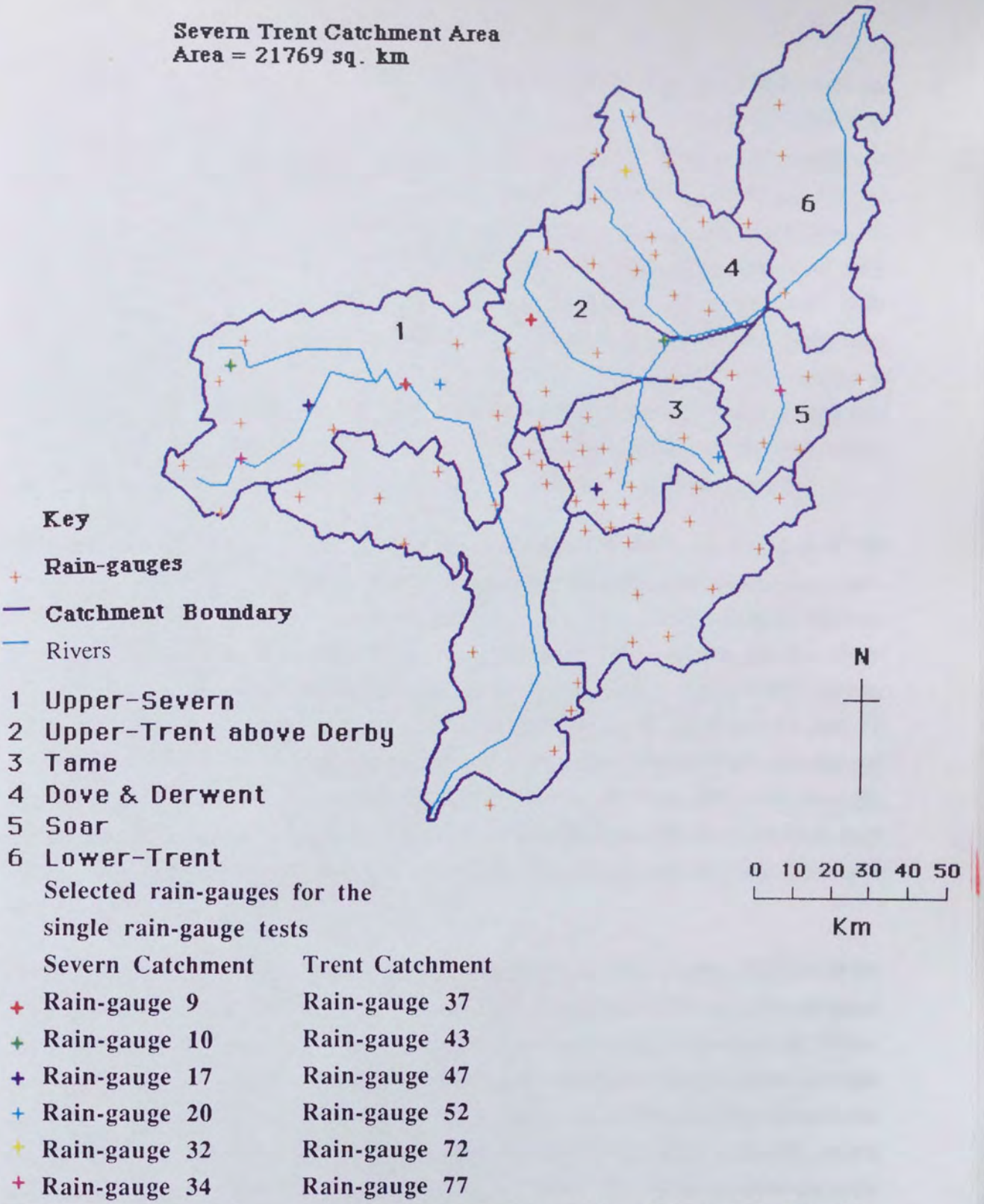

Fig 7.3 Map of Upper Trent catchment above Colwick and Upper Severn above Bewdely with respective rain-gauges.

The Upper-Trent extends from its source north-east of Stoke to its confluence with the river Derwant and is some 115 km long and drains an area of 1750 sq. km. The river flows firstly south through Stoke-on-Trent and then south-east before turning north-east through Burton-on-Trent and then east into the Lower-Trent.The mean altitude of the area is about 100 m although the maximum of 355 mm is found in the north. Other than the upper reaches above Stoke, the rivers in the basin have low land characteristics, flowing generally in wide bottomed valleys with flat gradients. Rainfall in the area show little variation in its pattern with all areas receiving drier springs than other seasons. Long-term rainfall distribution show the effect of altitude increasing northwards with increase in altitude. The urban areas of the West Midlands to the south of the basins tends to generate summer thunderstorms which often travel northwards to progress along the Trent valley towards the east midlands (STWA, Upper Trent basin Report of Survey, June 78)

The head waters for both the rivers Derwant and Dove rise at the southern end of the Pennines and both flow for much of their length through sparsely populated upland areas. The River Derwant, which has a catchment area of 1200 sq. km, rises on Howden Moor at an altitude of 630 m and then flows south for a distance of 70 km, joining the river Trent 15 km to the south west of Nottingham. The River Dove, draining an area of 900 sq. km, rises on Axe Edge near Buxton at an altitude of 430 m and flows south-east for over 50 km before joining the river Trent 5 km north-east of Burton on Trent, 23 km upstream of Derwant/Trent confluence. The mean altitude of the basin is about 300 m and average annual rainfall is 970 mm ranging from 1600 mm in the Peak district to 700 mm near derby. The rainfall variation is largely associated with the altitude (STWA, Dove and Derwant River Basin Report of Survey, 1978)

River Soar drains a catchment area of 1360 sq. km and its source is located at 20 km to the south-west of Leicester, at an altitude of 140 m. The river flows northwards for a distance of about 52 km joining the River Trent at Radcliffe on Soar having fallen through 110 m. The highest point in the basin is Bardon Hill in Charnwood Forest which reaches a height of 279 m but otherwise there is little variation in altitude across the area. Compared to the other catchments in the Severn-Trent region, the Soar is one of the driest, receiving around 650 mm of rainfall annually. The rainfall distribution shows little variation across the basin except at the high ground (STWA, River Soar Basin Report of Survey, 1978).

River Tame drains an area of 1470 sq. km of the densely populated area of the West Midlands which is also heavily industrialized. The river rises in the Black country and flows eastwards through Birmingham. It then flows northwards and eventually joins River Trent. The basin lies in the altitude range of 50 to 270 m although the greater part of its area is on a flattish plateau between 100 to 200 m. Rainfall in the basin is fairly evenly

distributed however the greatest rainfall intensities tend to be associated with summer storms. The average annual rainfall amounts decrease steadily from approximately 760 mm over the high ground in the south-west to about 660 mm in the northern part of the basin (STWA, River Tame Basin Report of Survey, 1976).

7.8.2 Data set

Rainfall data consists of the same data used for CCD analysis (see chapter 6), i.e. daily areal rainfall estimates from the 42 rain-gauges. Values obtained using the reciprocal distance method were used. The corresponding daily flow data of River Trent at Colwick was also obtained from the NRA. Daily satellite cloud indices were also evaluated as described in section 7.6. These were available from the 4th of June since no data was available for the first and second of June while for the 3rd of June satellite images were only available for the second half of the day. Fig.'s 7.4, 7.5 and 7.6 show the time series of river-flow, rainfall, and the cloud indices respectively.

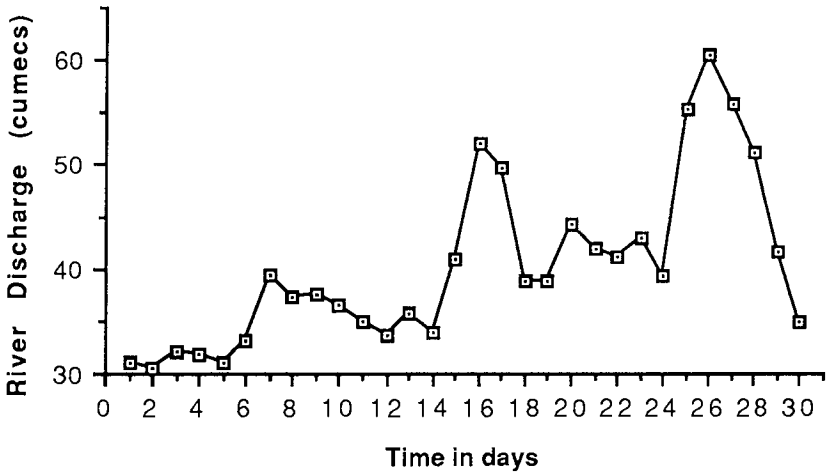

Fig. 7.4 Daily flows for the month of June of Trent catchment area.

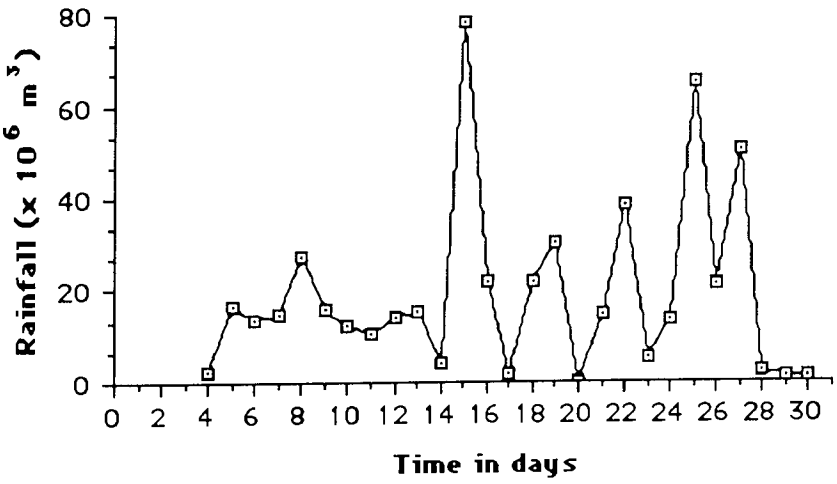

Fig. 7.5 Daily rainfall data for the month of June of Trent catchment area.

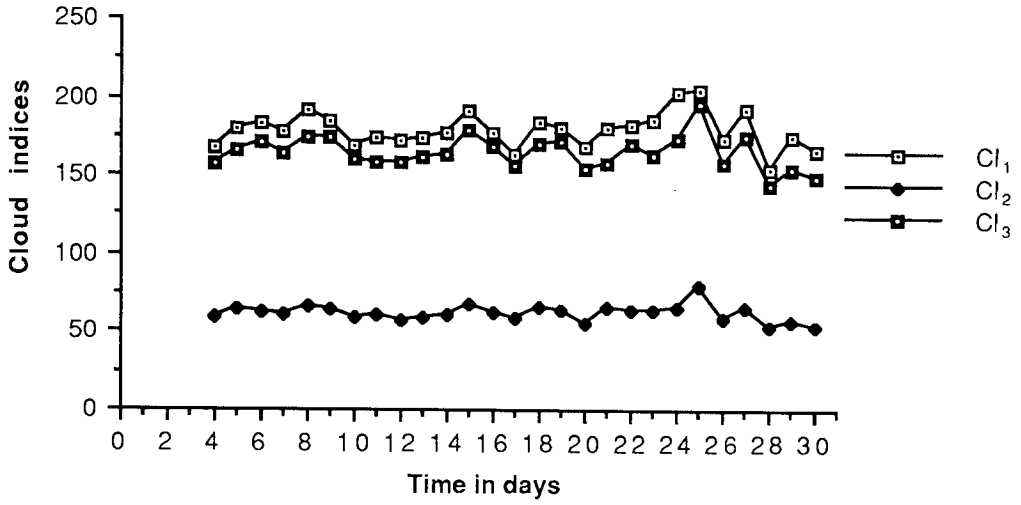

Fig. 7.6 Daily satellite cloud indices for the Trent catchment area.

7.8.3 Results

The results are given in the form of different stages in the development of the linear Rainfall-runoff model as described in section 7.7.

Stage 1 : Only river flow records are available

Proposed Model(s) : As in eq. 7.4

Significance Tests : F statistics for each variable in the model is used to define its significance in the model. The F statistics is defined as:

$$F = \frac{R^2 - r^2 / 1}{1 - R^2 / n-k-1} \qquad \text{eq. 7.5}$$

where R^2 is the coefficient of determination of the model with all the variables, r^2 is the coefficient of determination without the variable being tested in the model, n is the number of data values and k is the number of variables in the model. In other words it measures the increase in the explained variation if the variable under test is included in the model with respect to decrease in the degrees of freedom in the model. The significance of that increase is than evaluated by comparing the calculated F statistics against the critical values in the F distribution tables. If the calculated value is greater than the critical value than the variable is accepted in the model, otherwise it is rejected. The results are given in table 7.2

Table 7.2 Significance tests for each of the variable in eq. 7.4

variable	n	k	R^2	r^2	Critical $F_{0.05}$ (1,n-k-1)	F calculated	verdict
Q_{t-3}	26	3	0.60	0.59	4.3009	0.59	not significant
Q_{t-2}	26	2	0.59	0.52	4.2793	3.92	not significant
Q_{t-1}	26	1	0.52	0.00	4.2597	26.0	significant

In table 7.2, Q_{t-1} is the only variable which is significant in the proposed model. Therefore, the proposed linear model with the given data becomes:

$$q_t = 0.71Q_{t-1} + 12.14 \qquad \text{eq. 7.6}$$

The resulting hydrograph for the same data set is given in fig. 7.7 which, as expected from such a model, follows the same general shape as the observed hydrograph but with a one unit time shift. It also over-estimates low flows and under-estimates peak flows.

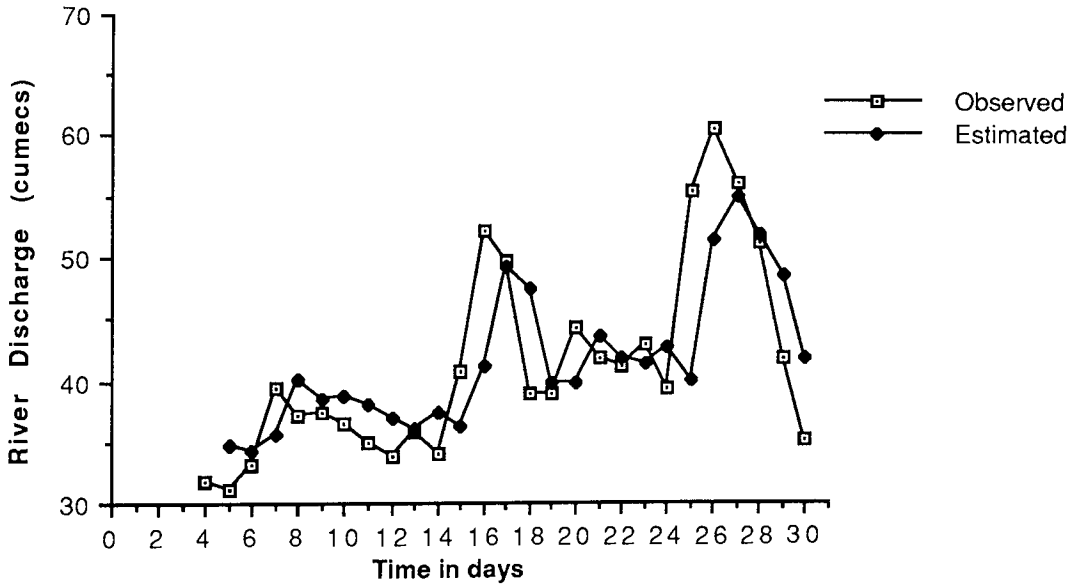

Fig. 7.7 Recorded and modelled streamflow at Colwick using eq. 7.6

Stage II : Rainfall data from the full network is now also made available

Proposed Model : $q_t = a_1Q_{t-1} + b_1R_{t-1} + b_2R_{t-2} + b_3R_{t-3} + \text{constant}$ eq. 7.7

Significance Tests : Results for the significance tests for each of the new rainfall variables are given in table 7.3.

Table 7.3 Significance tests for each of the rainfall variable in eq. 7.7

variable	n	k	R^2	r^2	Critical $F_{0.05}(1,n-k-1)$	Partial F	verdict
R_{t-3}	24	4	0.69	0.67	4.3808	1.23	not significant
R_{t-2}	24	3	0.67	0.67	4.3513	0.00	not significant
R_{t-1}	24	2	0.67	0.47	4.3248	12.7	significant
$*R_{t-1}$	26	2	0.71	0.55	4.2793	14.33	significant

* Consideration of R_{t-3} means that data values from the 7th of June upwards could only be used for calibration giving n=24. With Rt-2 and R_{t-3} eliminated and using only R_{t-1}, data from the 5th of June could be used for calibration giving n=26.

In table 7.3, only R_{t-1} was found to be significant in the linear model described by eq. 7.7 which becomes:

$$q_t = 0.57Q_{t-1} + 0.18R_{t-1} + 14.18 \qquad \text{eq. 7.8}$$

The resulting hydrograph using eq. 7.8 is as shown in fig. 7.8. The introduction of the rainfall variable have resulted in removing most of the lag that was observed in fig. 7.7. where simply previous day flow was considered and explains the increase in regression coefficient from 0.55 to 0.71. The model agrees with the observed river flow in general except on days 8 to 12 where low flows are over-estimated and on day 25 where high river-flow is significantly under-estimated. On that basis it appears that the rain-gauge network has under-estimated the catchment rainfall on day 24 and therefore failed to detect the rise in river-flow on day 25.

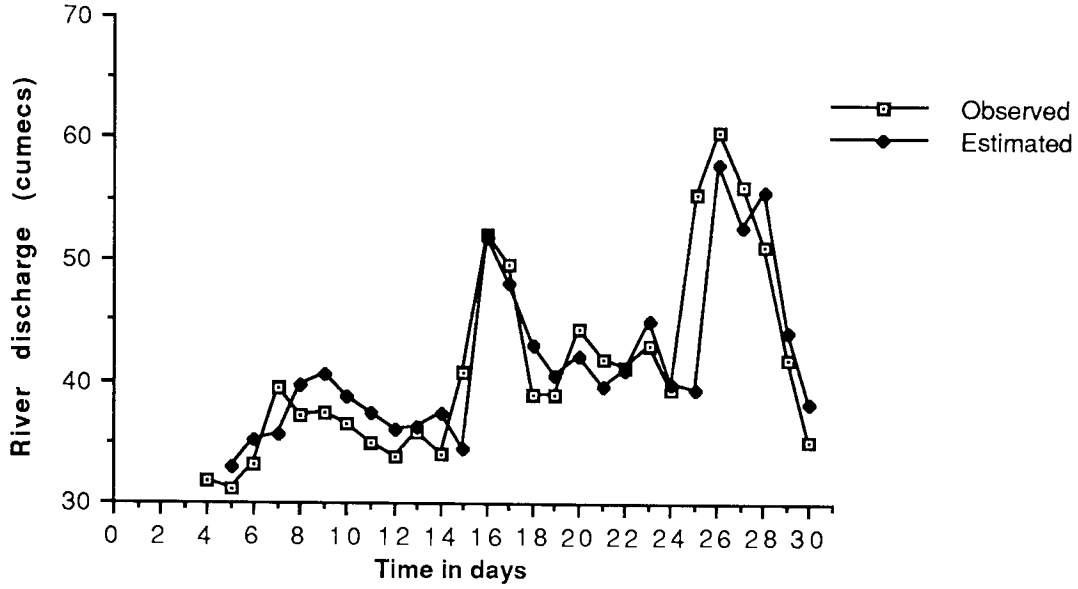

Fig. 7.8 Recorded and modelled streamflow at Colwick using eq. 7.8

Stage III: Satellite data in the form of different cloud indices is now available

Proposed Model: $q_t = a_1Q_{t-1} + b_1R_{t-1} + c_1CI_{t-1,i} + \text{constant}$ eq. 7.9

where i takes the value of 1,2 or 3 for the three cloud indices defined in section 7.6. $CI_{t-2,i}$ and $CI_{t-3,i}$ were not considered since when rainfall inputs were considered in stage II only R_{t-1} was found to be significant. Table 7.4 show the results for each of the cloud indices in terms of their significance in eq. 7.9.

Table 7.4 Significance tests for each of the cloud index in eq. 7.9

Cloud index	n	k	R^2	r^2	Critical $F_{0.05}$ (1,n-k-1)	Partial F	verdict
$CI_{t-1,1}$	26	3	0.80	0.71	4.3009	9.90	significant
$CI_{t-1,2}$	26	3	0.73	0.71	4.3009	1.83	not significant
$CI_{t-1,3}$	26	3	0.76	0.71	4.3009	4.58	significant

In table 7.4, it can be seen that the inclusion of two of the cloud indices in eq. 7.9 increases the proportion of explained variation significantly in the runoff response. In terms of R^2 and partial F statistics, $CI_{t-1,1}$ has the largest influence with R^2 increasing from 0.71 to 0.80 and shall be considered in further analysis. Eq. 7.9 becomes:

$$q_t = 0.63Q_{t-1} + 0.06R_{t-1} + 0.29CI_{t-1,1} - 38.11 \qquad \text{eq. 7.10}$$

The resulting hydrograph is given in fig. 7.9. The peak flow of days 25 and 26 and the low flows of days 8 to 12 are better estimated than in fig 7.8. However, the peak flow of day 16 is slightly under-estimated and the simulated hydrograph also show a false peak for day 9. This is due to the high value of cloud index observed for day 8 but the cloud system only produced relatively moderate catchment rainfall (see fig.7.5 and 7.6). Such over-estimations are always likely with satellite data but in hydrological terms it is far more important to predict peak flows accurately than over-estimations as in the case for day 25.

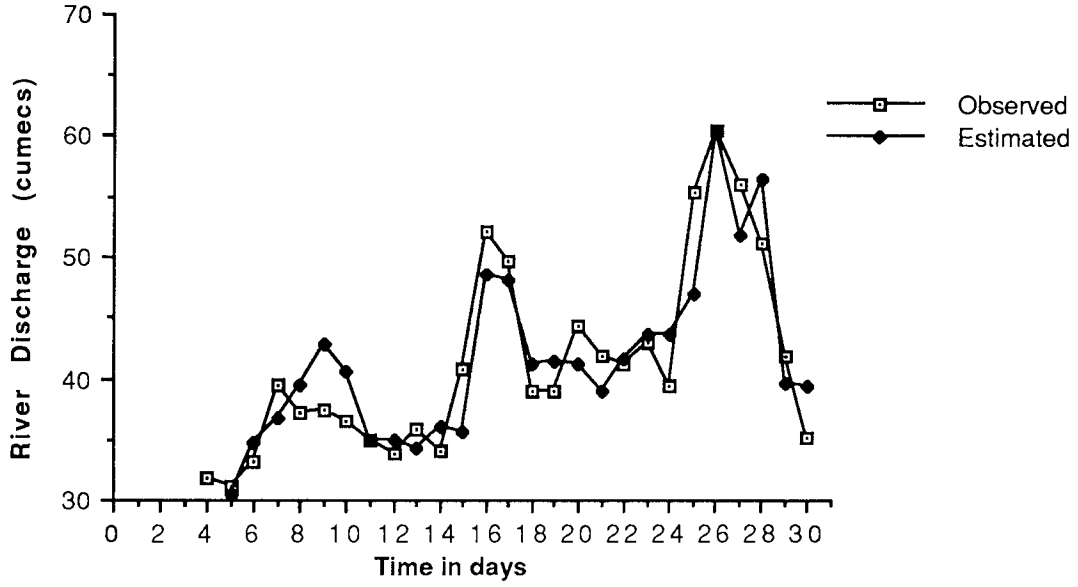

Fig. 7.9 Recorded and modelled streamflow at Colwick using eq. 7.10

Interestingly, the rainfall coefficient in eq. 7.10 has a very low value of 0.06, suggesting that it may not be significantly greater than 0. The significance of the rainfall variable in eq. 7.10 was investigated for all three cloud indices and the results are given in table 7.5. The results indicate that the high R^2 obtained in eq. 7.10 was largely due to the cloud index and that the rainfall variable become insignificant against the satellite cloud indices.

The model using CI_1 is

$$q_t = 0.67Q_{t-1} + 0.36CI_{t-1,1} - 50.83 \qquad \text{eq. 7.11}$$

and the resulting hydrograph is given in fig. 7.10. The hydrograph is almost identical to the one in fig. 7.9 as expected. The only difference is that the peak flow of day 16 is even further under-estimated with the removal of rainfall term. It is therefore recommended that for best results satellite and rain-gauge data should be used together.

Table 7.5 Significance tests for rainfall variable R_{t-1} in eq. 7.10 for each of the cloud index.

Cloud index	n	k	R^2	r^2	Critical $F_{0.05}$ (1,n-k-1)	Partial F	verdict
$CI_{t-1,1}$	26	3	0.80	0.79	4.3009	1.10	not significant
$CI_{t-1,2}$	26	3	0.73	0.71	4.3009	1.63	not significant
$CI_{t-1,3}$	26	3	0.76	0.75	4.3009	0.92	not significant

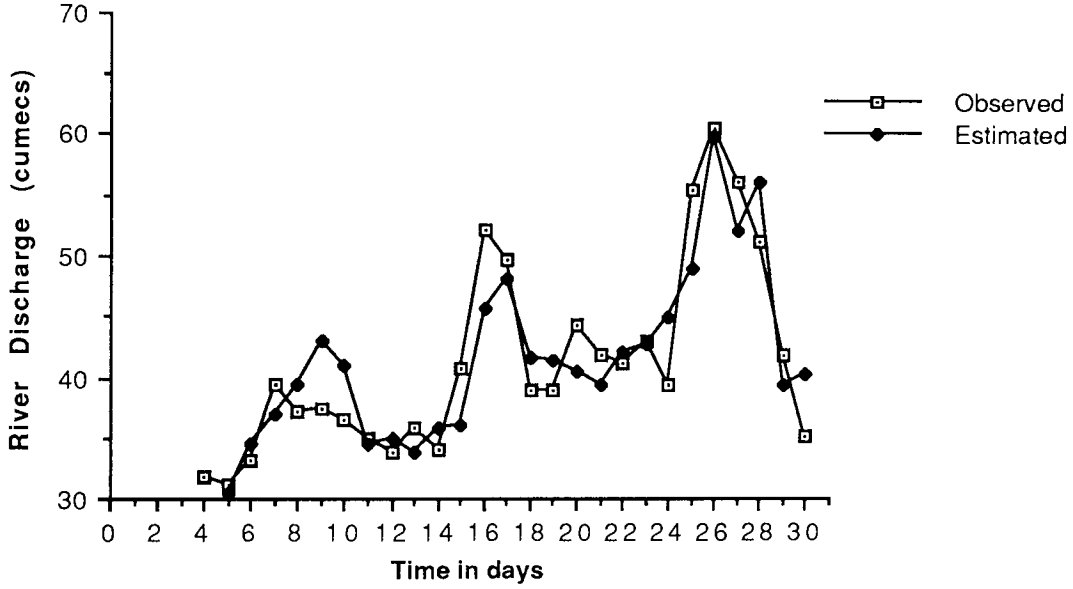

Fig. 7.10 Recorded and modelled streamflow at Colwick using eq. 7.11

So far in the analysis, areal rainfall estimates from the full network of rain-gauges were considered (42 in total). In table 7.6, results of runoff model calibrations are presented in which catchment rainfall estimates are based on single rain-gauge readings representing a case for sparse networks. Up to six different rain-gauges are used. Effect of using cloud index $CI_{t-1,1}$ is also examined. The position of these rain-gauges are as shown in fig. 7.3. As expected, satellite cloud index becomes the dominant variable when introduced. However, the R^2 values obtained for single rain-gauges are only slightly less than the full network of rain-gauges (R^2 = 0.71). This confirms the findings of Moore (1977) who showed that the increase in the density of rain-gauges does not necessarily improve rainfall-runoff relationships. The resulting hydrographs with and without the satellite data are given in fig.'s 7.11, 7.12, 7.13 and 7.14 for rain-gauges 47 and 72 respectively. Rain-gauge 47 show as good a correlation (R^2 = 0.72) with observed river-flow as from the full network (R^2 = 0.71) and produced a similar hydrograph (fig. 7.8). Rain-gauge 72, on the

other hand, showed no correlation with the observed river-flow and the hydrograph produced is similar to the one in fig. 7.7 which uses previous flows only. Other rain-gauges showed R^2 values falling in between these two extremes.

Table 7.6 Results of significance tests using single gauge values and satellite index.

$q_t = a_1Q_{t-1} + b_1R_{t-1} + \text{constant}$			$q_t = a_1Q_{t-1} + b_1R_{t-1} + c_1CI_{t-1,1} + \text{constant}$			
Rain-gauge No	R^2	* S.E.E	R^2	S.E.E	Critical $F_{0.05}(1,22)$	Partial F
37	0.62	5.09	0.82	3.56	4.3009	24.44
43	0.64	4.94	0.81	3.65	4.3009	19.68
47	0.72	4.38	0.82	3.58	4.3009	12.22
52	0.70	4.54	0.80	3.77	4.3009	11.00
72	0.53	5.69	0.81	3.71	4.3009	32.42
77	0.66	4.74	0.80	3.70	4.3009	14.3

* Standard error of estimate

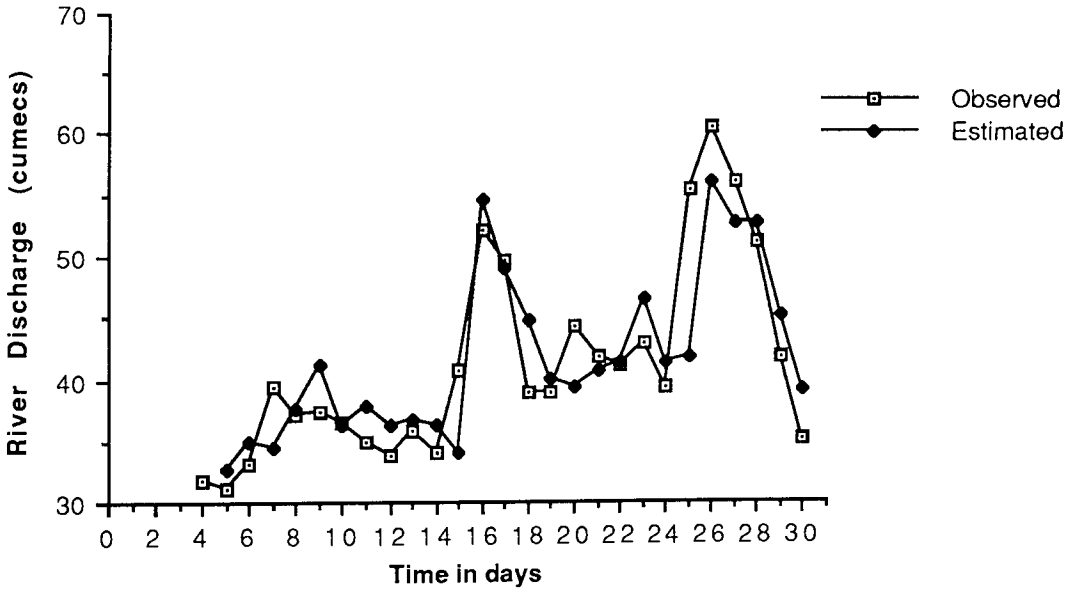

Fig. 7.11 Recorded and modelled streamflow at Colwick using data from rain-gauge 47 only.

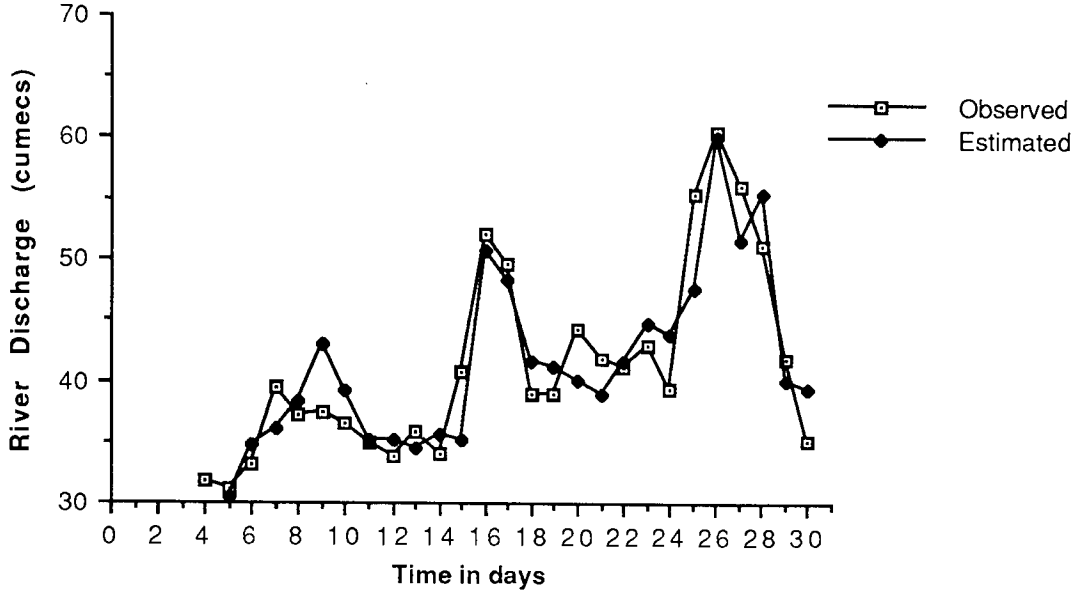

Fig. 7.12 Recorded and modelled streamflow at Colwick using data from rain-gauge 47 and the satellite data.

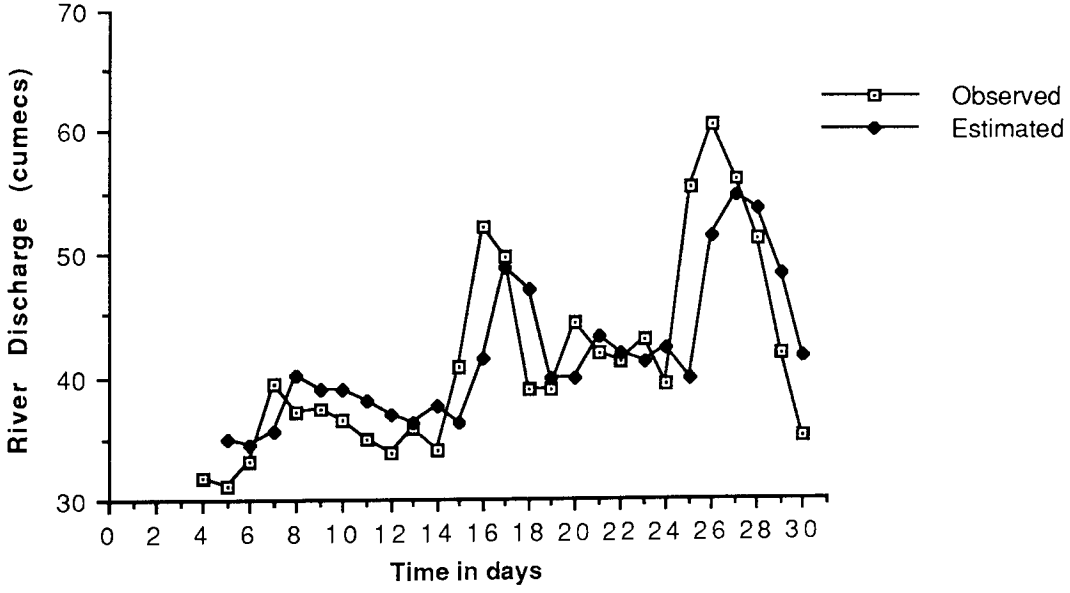

Fig. 7.13 Recorded and modelled streamflow at Colwick using data from rain-gauge 72 only.

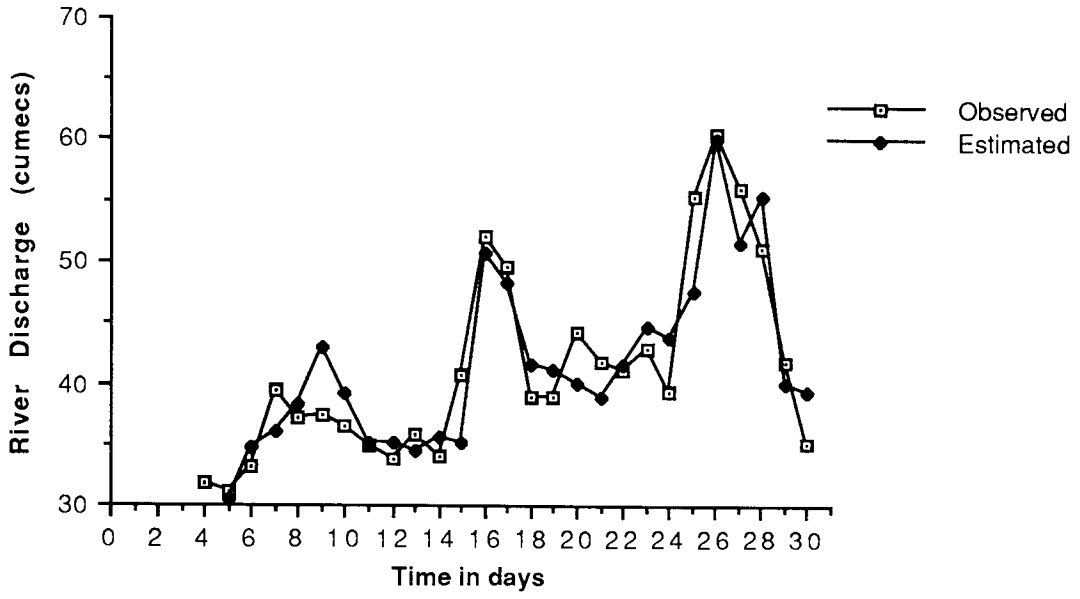

Fig. 7.14 Recorded and modelled streamflow at Colwick using data from rain-gauge 72 and the satellite data.

Traditionally, cloud indices are derived and related to observed areal rainfall estimates from ground data. These cloud indices can be used to estimate rainfalls in data sparse regions and than used as input to general rainfall-runoff models. This two step method will be investigated using simple linear relationships and the results are given in table 7.7.

Step I: $$R_{t,estimate} = c\ CI_{t,i} + constant \qquad \text{eq. 7.12}$$

where i = 1,2,3 with respect to the three variables.

Step 2: $$q_t = a_1 Q_{t-1} + b_1 R_{t-1,estimate} + constant \qquad \text{eq. 7.13}$$

Table 7.7 Values for the coefficient of regression (R^2) for eq. 7.12 and 7.13.

Cloud Index	Step I							Step II	
	*FN	G-37	G-43	G-47	G-52	G-72	G-77	*FN	G-37
$CI_{t,1}$	0.46	0.09	0.19	0.37	0.45	0.12	0.36	0.80	0.79
$CI_{t,2}$	0.58	0.18	0.31	0.43	0.54	0.08	0.43	0.71	0.71
$CI_{t,3}$	0.64	0.24	0.30	0.43	0.54	0.14	0.47	0.75	0.75

* FN = full network

A number of things can be said about the results in table 7.7. Firstly, the R^2 values in step II indicate that in the case of simple linear model, transforming cloud indices into rainfall estimates and using derived rainfall estimates to predict river flow is the same as relating cloud indices directly to river flows. Secondly, using such a procedure, one would choose $CI_{t,3}$ instead of $CI_{t,1}$ since it showed highest correlation of 0.64 with the full network in step I. Thirdly, in step I, very low correlations were obtained between cloud indices and catchment rainfall in the case of single gauges suggesting that satellite data may get rejected if there is a sparse network of rain-gauges. However, such an approach has an advantage in cases where more sophisticated rainfall-runoff models are used which cannot take cloud indices directly. Cloud indices can be transformed into rainfall units using a simple linear model of step I and the estimated rainfall values can be used as input to a general rainfall-runoff model (see Hardy et al, 1988).

7.9 Case Study 2: The Upper-Severn River basin

7.9.1 General description and hydrology

The River Severn upstream from the gauging station at Bewdly drains an area of 4325 sq. km and is 200 km long from its source in the Welsh mountains up to Bewdly. Initially, it flows generally northeast and into England before turning southwards to reach the sea eventually in the Bristol Channel. The elevation of basin decreases eastwards from a maximum height of 827 m in the northwest. The high ground also extends from the Welsh Hills into the Border land on the right bank of the river, in the area to the south of Shrewsbury and to the west of Bewdly. The upland part of the catchment above Montford is characterized by high annual rainfalls (1000-2500 mm) with winter precipitation occurring, in part, as snow. The annual rainfall in the area between Montford and Bewdly is approximately 700 mm (STWA, River Severn Basin Report of Survey, 1978).

7.9.2 Data set

Data set was processed similarly as in case 1 for the Trent river basin. Time series of river-flow, rainfall and the cloud indices are given in fig's 7.15, 7.16 and 7.17 respectively.

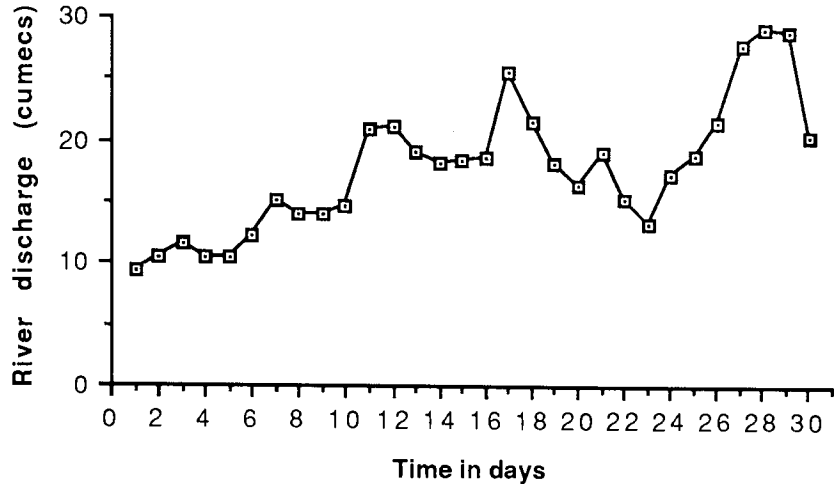

Fig. 7.15 Daily flows for the month of June of Severn catchment area.

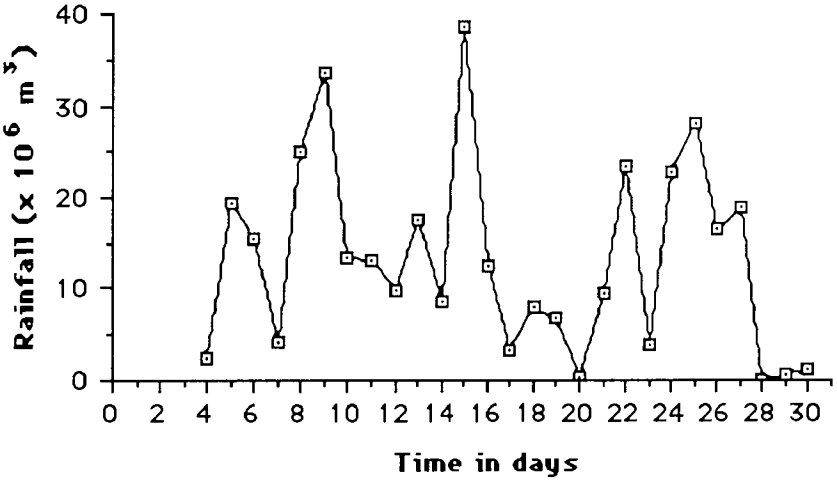

Fig. 7.16 Daily rainfall data for the month of June of Severn catchment area.

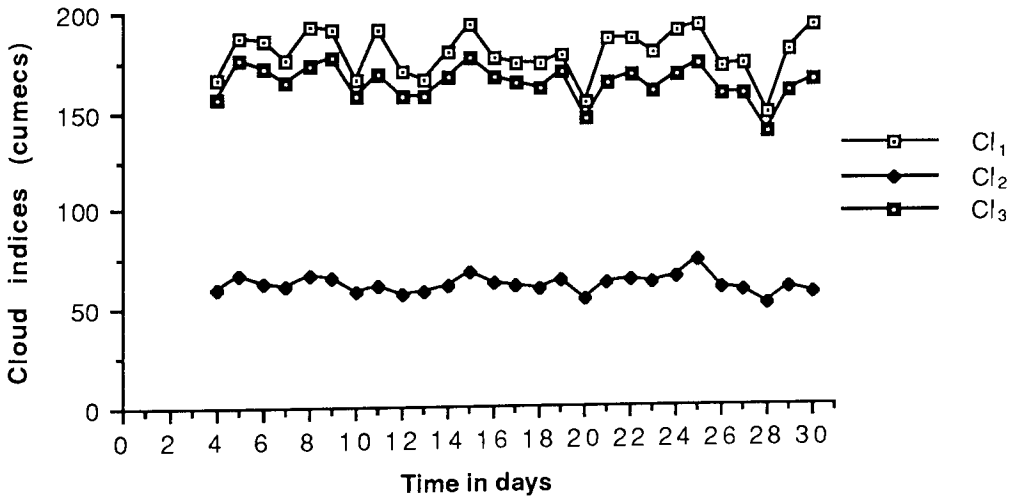

Fig. 7.17 Daily satellite cloud indices for the Severn catchment area.

7.9.3 Results

The results were obtained in the same way as for case 1. Therefore only the relevant tables produced at different stages of the analysis are given.

Stage 1 : Only river flow records are available

Proposed Model : As in eq. 7.4

Significance Tests : F statistics for each variable in the model are presented in table 7.8.

Table 7.8 Significance tests for each of the variable in eq. 7.4 for the Severn region

variable	n	k	R^2	r^2	Critical $F_{0.05}(1,n-k-1)$	F calculated	verdict
Q_{t-3}	27	3	0.64	0.64	4.2793	0.00	not significant
Q_{t-2}	27	2	0.64	0..62	4.2597	1.30	not significant
Q_{t-1}	27	1	0.62	0.00	4.2417	44.44	significant

In table 7.8, Q_{t-1} is the only variable which is significant in the proposed model. Therefore, the suggested linear model would become:

$$q_t = 0.70Q_{t-1} + 6.17 \qquad \text{eq. 7.14}$$

The resulting hydrograph is as shown in fig. 7.18, and as expected, was of the same shape as the observed hydrograph but with a one unit time shift generally over-estimating low flows and under-estimating peak flows.

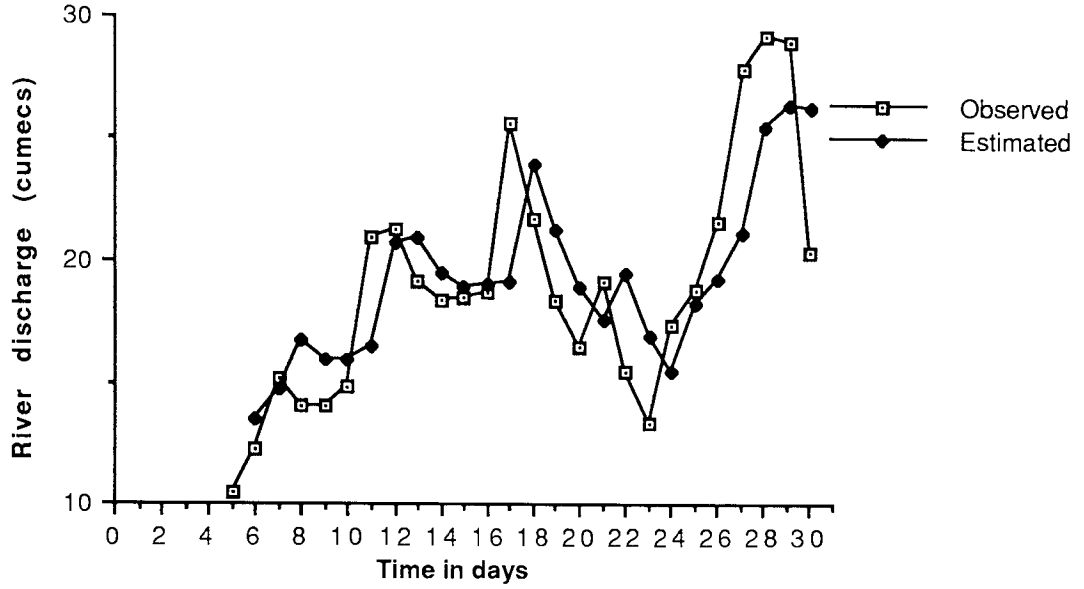

Fig. 7.18 Recorded and modelled streamflow at Bewdly using eq. 7.14.

Stage II : Rainfall data from the full network is now also made available

Proposed Model : As in eq. 7.7

Significance Tests : Results for the significance tests for each of the new rainfall variables for the Severn region are given in table 7.9.

Table 7.9 Significance tests for each of the rainfall variable in eq. 7.7 for the Severn region

variable	n	k	R^2	r^2	Critical $F_{0.05}$ (1,n-k-1)	F calculated	verdict
R_{t-3}	24	4	0.83	0.83	4.3808	0.00	not significant
R_{t-2}	24	3	0.83	0.51	4.3513	37.647	significant
R_{t-1}	24	3	0.83	0.82	4.3513	1.18	not significant
*R_{t-2}	25	2	0.83	0.55	4.3009	42.70	significant

* Consideration of R_{t-3} means that data values from the 7th of June upwards could only be used for calibration giving n=24. With R_{t-1} and R_{t-3} eliminated and using only R_{t-2}, data from the 6th of June could be used for calibration giving n=25.

In table 7.9, only R_{t-2} was found to be significant in the linear model described by eq. 7.7 and therefore the suggested linear model becomes:

$$q_t = 0.74Q_{t-1} + 0.24R_{t-2} + 1.84 \qquad \text{eq. 7.15}$$

The resulting hydrograph is as shown in fig. 7.19. A lag of two days between the observed rainfall and observed river-flow is understandable since the length of river Severn is almost twice the length of river Trent where a lag of one day was observed. The peak flows of days 11, 12, 17 and 29 were very well matched but the peak flows of days 27 and 28 were under-estimated.

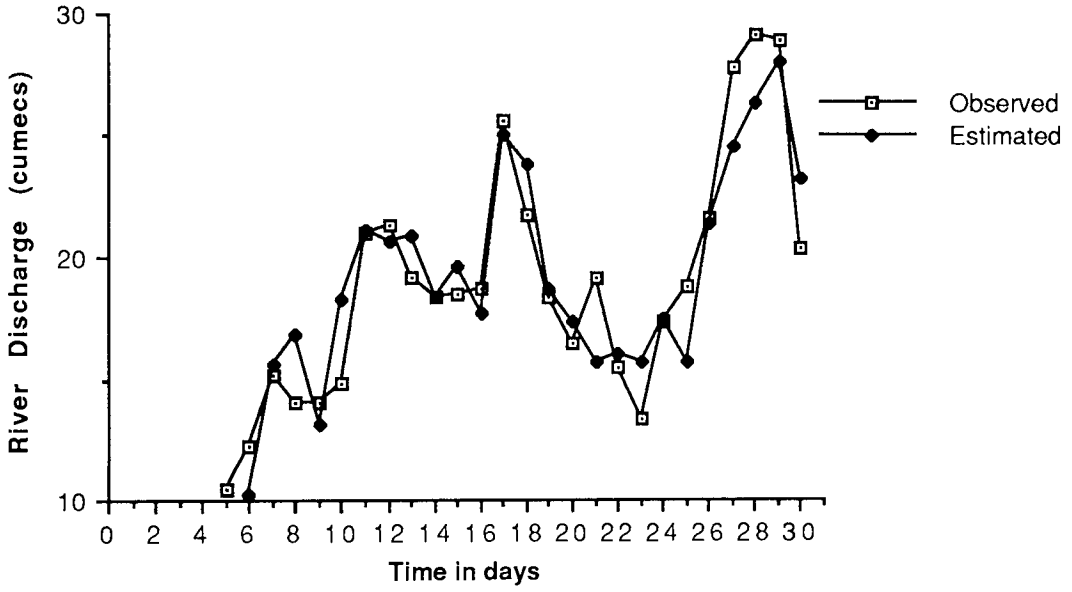

Fig. 7.19 Recorded and modelled streamflow at Bewdly using eq. 7.15

Stage III : Satellite data in the form of different cloud indices is now available

Proposed Model : $q_t = a_1Q_{t-1} + b_1R_{t-2} + c_1CI_{t-2,i} + \text{constant}$ eq. 7.16

Significance tests : These are given in table 7.10.

$CI_{t-2,i}$ were only used due to the lag of two days observed in the relationship between rainfall and river-flow in the previous stage.

Table 7.10 Significance tests for each of the cloud index in eq. 7.16 for the Severn region

Cloud index	n	k	R^2	r^2	Critical $F_{0.05}$ (1,n-k-1)	Partial F	verdict
$CI_{t-2,1}$	25	3	0.83	0.83	4.3248	0.00	not significant
$CI_{t-2,2}$	25	3	0.85	0.83	4.3248	2.80	not significant
$CI_{t-2,3}$	25	3	0.83	0.83	4.3248	0.00	not significant

The derived equation using $CI_{t-2,2}$,which showed the highest R^2 value of 0.85 is

$$q_t = 0.81Q_{t-1} + 0.17R_{t-2} + 0.26CI_{t-2,2} - 14.54 \qquad \text{eq. 7.17}$$

and the resulting hydrograph is shown in fig. 7.20.

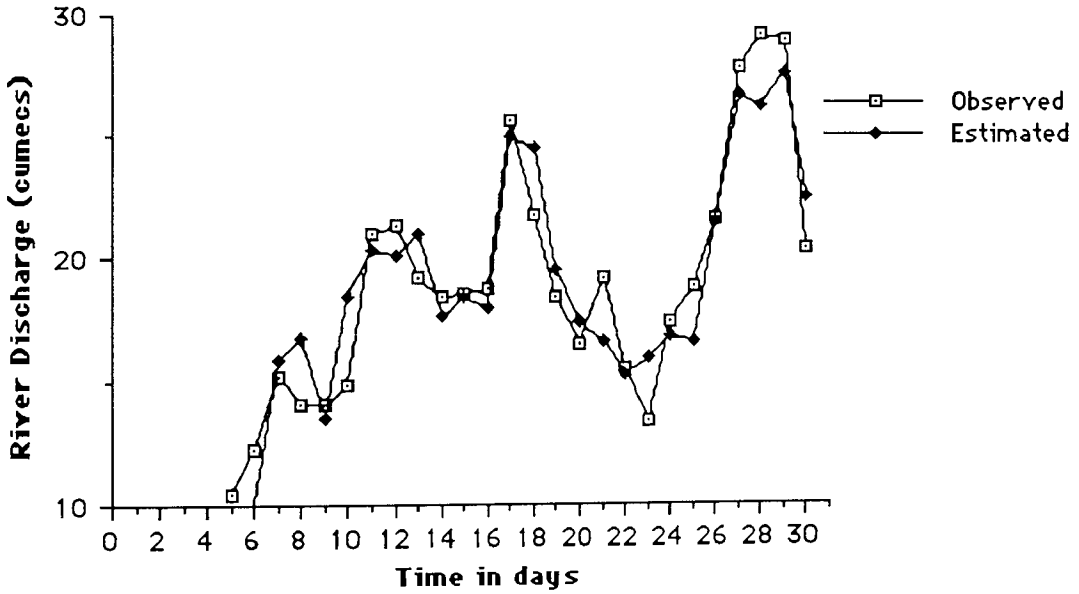

Fig. 7.20 Recorded and modelled streamflow at Bewdly using eq. 7.17

In this case, the introduction of satellite cloud indices in the linear model does not alter the relationship significantly because of the high regression coefficient ($R^2 = 0.83$) existing due to the rainfall variable but it does improve upon the estimated flow of day 27. In order to assess the significance of cloud indices to river-flow, the model was re-evaluated without the rainfall variable. Cloud indices with a lag of one day were also included in the model to give a clearer picture.

Proposed Model: $q_t = a_1Q_{t-1} + b_1CI_{t-1,i} + c_1CI_{t-2,i} + \text{constant}$ eq. 7.18

Significance tests : These are given in table 7.11.

Table 7.11 Significance tests for each of the cloud index in eq. 7.18 for the Severn region

Cloud index	n	k	R^2	r^2	Critical $F_{0.05}$ (1,n-k-1)	Partial F	verdict
$CI_{t-1,1}$	25	3	0.72	0.71	4.3248	0.75	not significant
$CI_{t-2,1}$	25	3	0.72	0.58	4.3248	10.5	significant
$CI_{t-1,2}$	25	3	0.80	0.79	4.3248	1.05	not significant
$CI_{t-2,2}$	25	3	0.80	0.58	4.3248	25.2	significant
$CI_{t-1,3}$	25	3	0.74	0.72	4.3248	1.62	not significant
$CI_{t-2,3}$	25	3	0.74	0.58	4.3248	12.9	significant

In table 7.11, cloud indices with a lag of one day were not significant as expected. All three cloud indices with a lag of two days were found to be significant in the relationship and the highest regression coefficient of 0.80 was achieved with the second cloud index. The proposed model becomes:

$$q_t = 0.89Q_{t-1} + 0.57CI_{t-2,2} - 32.93 \qquad \text{eq. 7.19}$$

and the resulting hydrograph is given in fig. 21. Although a good value for the correlation coefficient is achieved, the peak flows are generally under-estimated apart from the peak flow on day 27.

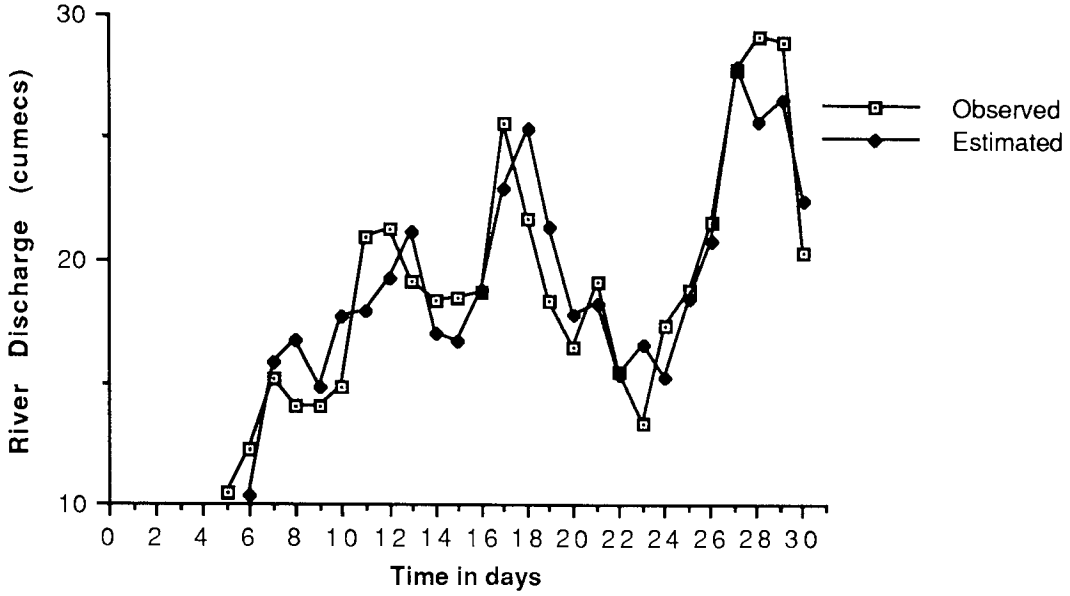

Fig. 7.21 Recorded and modelled streamflow at Bewdly using eq. 7.17

The effect of using satellite cloud index when rainfall estimates are from only one gauge were investigated and the results are given in table 7.12. The position of these rain-gauges are also shown in fig. 7.3. The results again were similar to the results obtained for the river Trent in case 1. The regression coefficients obtained using single gauge rainfall estimates (average 0.75) were only slightly less than using rainfall estimates from the full network of gauge (17 in total). The resulting hydrographs for the two of the rain-gauges are given in fig.'s 7.22, 7.23, 7.24 and 7.25 for rain-gauge only and rain-gauge with satellite data respectively. The introduction of the satellite cloud indices were found to be significant for all the rain-gauges. The major contribution of the satellite data was the improved river-flow estimate for day 27. It appears that the rainfall on day 25 responsible for the increase in river-flow on day 27 was under-estimated by the rain-gauge network. Comparison of fig's 7.20 / 7.21, 7.22 / 7.23 and 7.24 / 7.25 shows that the combined use of rainfall estimates from the rain-gauges and the satellite data produced the best results.

Table 7.12 Results of significance tests using single gauge values and satellite cloud index for the Severn region.

$q_t = a_1Q_{t-1} + b_1R_{t-2} + \text{constant}$			$q_t = a_1Q_{t-1} + b_1R_{t-2} + c_1CI_{t-2,2} + \text{constant}$			
Rain-gauge No	R^2	* S.E.E	R^2	S.E.E	Critical $F_{0.05}(1,22)$	Partial F
9	0.70	2.72	0.80	2.24	4.3248	10.5
10	0.67	2.86	0.82	2.14	4.3248	17.5
17	0.81	2.14	0.85	1.94	4.3248	5.8
20	0.74	2.51	0.81	2.18	4.3248	7.7
32	0.78	2.30	0.84	2.02	4.3248	7.9
34	0.78	2.30	0.85	1.96	4.3248	9.8

* Standard error of estimate

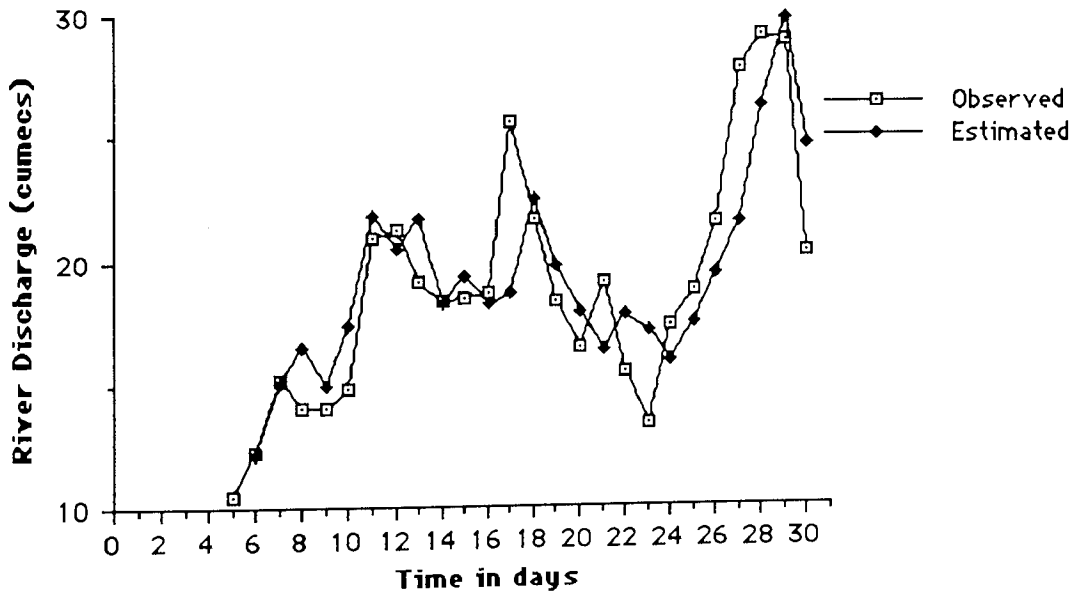

Fig. 7.22 Recorded and modelled streamflow at Bewdly using data from rain-gauge 10 only.

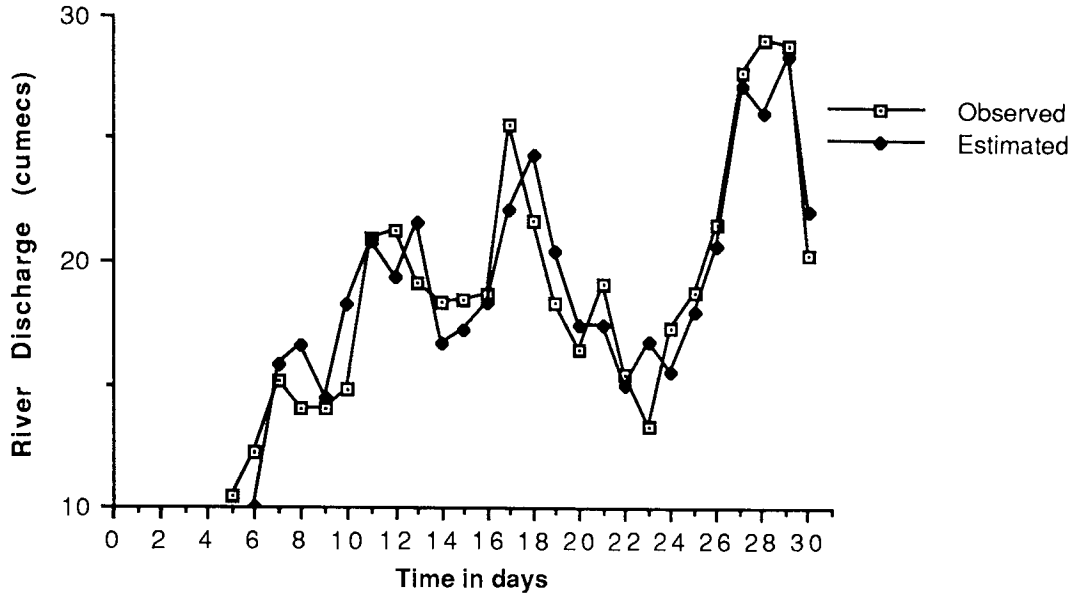

Fig. 7.23 Recorded and modelled streamflow at Bewdly using data from rain-gauge 10 and the satellite data.

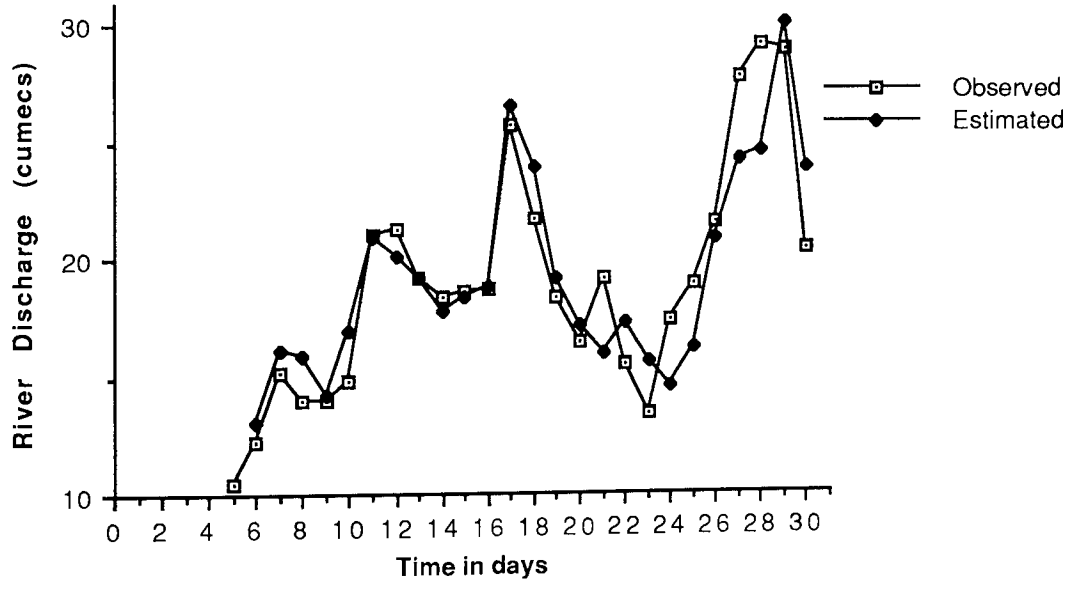

Fig. 7.24 Recorded and modelled streamflow at Bewdly using data from rain-gauge 17 only.

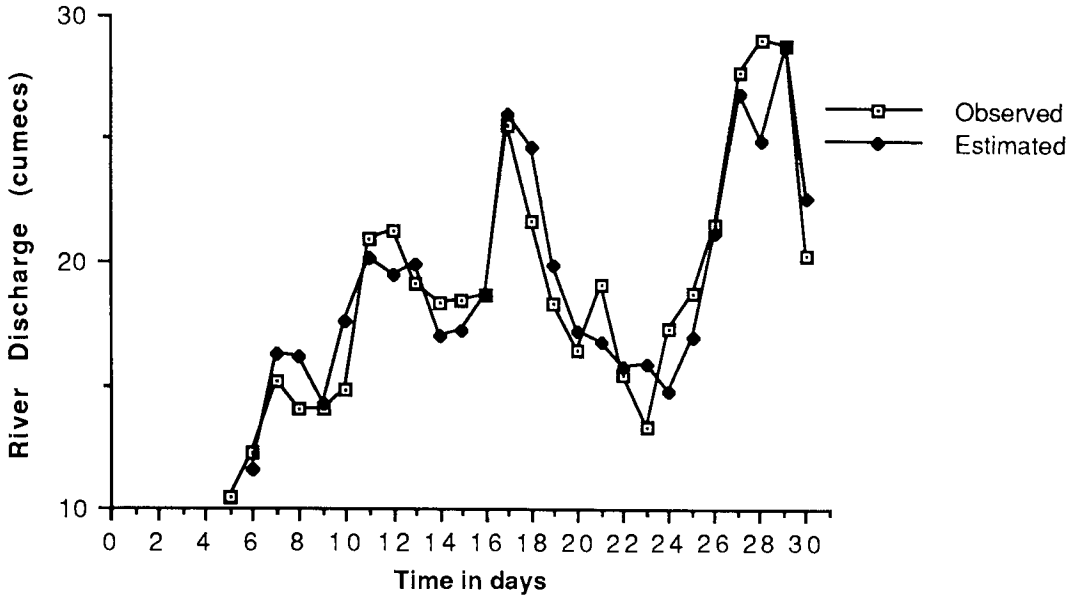

Fig. 7.25 Recorded and modelled streamflow at Bewdly using data from rain-gauge 17 and the satellite data.

Table 7.13 give the results for the two step procedure in which rainfall is first related to observed cloud indices and than the estimated rainfall is used as input to the rainfall-runoff model. Results are again similar to the ones obtained in case 1 for the Trent region with low regression coefficients for the relationship between cloud indices and observed rainfall. In this case however, the result would be a decrease in the value of explained variance achieved using the full network of rain-gauges from 0.83 to 0.79 if satellite data is used.

Step I: $$R_{t,estimate} = c\ CI_{t,i} + constant \qquad \text{eq. 7.20}$$

where i = 1,2,3 with respect to the three variables.

Step 2: $$q_t = a_1 Q_{t-1} + b_1 R_{t-2,estimate} + constant \qquad \text{eq. 7.21}$$

Table 7.13 Values for the coefficient of determination (R^2) for eq's. 7.18 and 7.19

Cloud Index	Step I							Step II	
	*FN	G-9	G-10	G-17	G-20	G-32	G-34	*FN	G-9
$CI_{t,1}$	0.35	0.26	0.14	0.20	0.28	0.22	0.18	0.71	0.71
$CI_{t,2}$	0.51	0.43	0.13	0.37	0.45	0.29	0.34	0.79	0.79
$CI_{t,3}$	0.46	0.37	0.16	0.29	0.37	0.22	0.27	0.72	0.72

* FN = full network

7.10 Discussion

Two case studies are presented in which the use of satellite derived cloud parameters as an additional information is investigated in a simple linear rainfall-runoff model. Partial F statistics at 95% significance level were used as a standard to establish the significance of satellite information. Daily values for the whole month were used in the analysis. In the case of river Trent basin, satellite data was found to be significant even when rainfall estimates were derived from the full network of rain-gauges (table 7.4). In contrast, they had virtually no effect in the second case for the Severn basin when rainfall was estimated from full network (table 7.10). This was due to the finding that higher correlation existed between the rainfall estimates and river-flow in the Severn region ($R^2 = 0.83$) than in Trent region ($R^2 = 0.71$). Better estimates of areal rainfall in the Severn region may be due to the distribution of rain-gauges which is more uniform in the Severn region than in the Trent region, where most rain-gauges are concentrated around the Birmingham area. In the cases where areal rainfall estimates were based on single rain-gauge values, cloud indices were significant for both river basins (table 7.6 and 7.12) in terms of increased R^2 values and reduced standard errors.

An interesting observation from these results is the relation of recorded river flow to estimates of areal rainfalls based on one and the full network of rain-gauges respectively. For the Trent basin, the average R^2 value for eq. 7.8 using single rain-gauge estimates is 0.65 while with full network it is 0.71, an increase of only 0.06 units (table 7.6). Similarly, for the Severn basin, the average R^2 value for eq. 7.14 using single rain-gauges is 0.75 while with full network it is 0.83, an increase of 0.08 (table 7.12). These results

confirms the findings of Moore (1977) who found similar results in his investigation over a small catchment (see section 7.7).

Cloud indices produced high R^2 values for both catchments when related to recorded river-flows without the rainfall estimates from the rain-gauges (0.80 for the Trent basin and 0.79 for the Severn basin). However, poor R^2 values were noted when cloud indices were related to areal rainfall estimates (table 7.9 and table 7.13) in the two step procedure. This gives weight to the argument that satellite derived products should be related directly to the river-flows if the objective is to produce improved river-flow estimates rather than to improve mean catchment rainfall. This also explains the results of Hardy (Hardy et al, 1988) (see section 7.2.2) if we consider the average CCD over a basin as another form of cloud index. Poor correlations exist between CCD and observed rain-gauge rainfalls but nevertheless, better results were obtained for river-flow estimates when rainfall estimates based on CCD were used as compared to the results when rain-gauges were used. It has been demonstrated that depending on the present number and configuration of rain-gauge network in a catchment, satellite information may be or may not be useful, but to establish that, one must relate the satellite information directly to recorded river flows.

It is not clear at present why poor correlations exist between the cloud indices and rain-gauge rainfall estimates yet both variables contribute significantly in improving river-flow estimates. One likely explanation is that cloud indices, in addition to providing some information on areal rainfall, may also be giving some indication of evapotranspiration taking place over the catchments.

The black-box rainfall runoff model used in this chapters was calibrated using multiple regression techniques. A number of other mathematical or empirical techniques can also be used for model parameter estimation (Mimikou, 1983). Cluckie & Owens (1987) used recursive least square algorithm for the estimation of parameters and in addition used a real time correction factor to scale the rainfall parameters to further improve the performance of their model.

Finally, there is a question of costs associated with using satellite data. The costs can be divided into two groups. Firstly, there are costs associated with preliminary studies which establishes the significance of satellite data for river-flow estimates for a given catchment, based on the techniques described in this chapter. These include the cost of purchase of satellite data for specific period and the cost of hire of necessary image processing hardware and software. Secondly, based on the results of preliminary studies, the costs of actual purchase of the whole system must be compared against the costs of improving and maintaining the present rain-gauge network to give equivalent improvement in river-flow

forecasts. Table 7.14 gives a general guide to the actual costs involved in the acquisition of satellite data.

Table 7.14 Approximate costs of the equipment and data sets at 1992 prices.

	Costs in £'s
Purchase of Meteosat Satellite Images	0-100's
Purchase charges for a general image processing system	12000-15000
Purchase charges for SDUS receiver station	6000
Purchase charges for PDUS receiver station	17000-20000
DCP (Transmitter & antenna)	3600
Computer System (hardware for DCP opertaions)	10000
Cost of a rain-gauge (operating and maintenance costs not included)	400

7.11 Conclusions

Although this study was performed using only one month of data set, it does give some insights into the rainfall-runoff process and the value of satellite data for such purposes. First of all is the relationship between runoff and areal averaged rainfall. Runoff does not depend only on rainfall but also on other complex factors such as evaporation, infiltration, permeable and impermeable surfaces etc., which are only some of the many variables. Even if the basin rainfall can be determined exactly, it does not guarantee exact determination of runoff generated as a result. Secondly, satellite data should be used as an independent variable in the rainfall-runoff model rather than to be used as improving the areal rainfall estimates. Thirdly, there is no unique satellite parameter that can be applied in all situations. River basins are unique with respect to their size, morphology, topology, rainfall regimes, response times etc. and therefore prompt hydrological studies of their own. Each of the two basins studied showed affiliation with a different cloud index and therefore its necessary that for a given hydrological situation, a number of satellite parameters should be tried and the suitable one chosen.

Chapter 8

8. Discussion and Conclusions

8.1 Summary of Research

Remote Sensing can be an effective data source in hydrological studies (Deutch et al, 1979). A number of important hydrologic processes can be modelled using remotely sensed data (section 7.2). Of these, rainfall is perhaps the most important and the most difficult to measure component and can be viewed as the 'driving force' in hydrological models. Rain-gauges are used to measure point rainfall. Rain-gauges can provide reasonably accurate measurements at pre-selected points within a river basin but the spatial integrity is lacking when these point measurements are interpolated to provide estimates of areal distribution. This is especially true for convective storms where even a dense network of rain-gauges may not adequately represent the spatial structure of storm. Unfortunately, many areas of the world are inadequately equipped with rain-gauges, falling short of the minimum recommended by the WMO (WMO, 1965). Rain-gauges are also subject to vandalism, especially in remote areas. A further complication is that for most countries the network of gauges is state operated and relies heavily on volunteer observers. Clearly there are more potential observers in the major centres of population, which also tend to be the lowland areas, whereas very few may be found in the remote areas of the country. As a result the actual distribution of rain-gauges tend to be heavily biased towards the major centres of populations and often away from the areas where detailed information on precipitation would be of great benefit. All these factors contribute significantly to the cost of rain-gauges and are the reason why most areas of the world are still devoid of good rain-gauge networks. Satellites provide access to such areas in the form of infrared, visible and microwave images at a fraction of the cost.

Much work has been directed towards estimating rainfall using satellite data so that rainfall estimates can be made over rain-gauge deficient areas. However, most of the satellite techniques developed were found to be highly region specific, i.e. algorithms developed over test areas with good ground truth data for calibration could not be readily applied over rain-gauge deficient areas. They also tended to ignore the existing rain-gauge data which were only used for calibration or verification purposes. This research looked specifically at methods of combining rain-gauge and satellite data, to improve rainfall estimates and consequently river-flow forecasts, so that satellite information could be readily applied wherever deemed necessary. The approach was based on similar lines as Radar data which is used for rainfall estimation with real-time calibrations using rain-gauge data. Radar data,

although highly sophisticated and reliable, suffers from high costs and limited spatial coverage, which has mostly limited its widespread use in developed countries.

As a first step, the relationship between satellite observed cloud fields in the visible and infrared spectrum and the corresponding point rain-gauge rainfall over a catchment were studied in the light of some of the techniques preferred by previous researchers (chapter 4). These preliminary investigations confirmed the observation that rainfall tends to fall from relatively colder (high infrared values) and thicker (high visible values) clouds. Given a rain-gauge reporting the presence of rain, it is likely that it would have high infrared and visible pixel values but given a satellite image pixel with high infrared and visible value, there is no guarantee that it would be raining underneath. The investigations also uncovered some of the shortcommings of such techniques in that they may be adequate for a certain region and certain applications (detection of Locust swarms breeding areas or forest fires) but not for hydrological purposes.

In an effort to improve upon the rain-gauge estimates of rainfall, methods were developed to take into account both the rain-gauges and the satellite information. Half-hour as well as daily rainfall accumulations were investigated (chapters 5 and 6). Similar results were obtained in terms of catchment average rainfall in comparison with other conventional methods but differences were noted in the spatial distribution of rainfall. This could be of great significance for smaller catchments or in distributed rainfall-runoff models.

In a further analysis, satellite derived cloud indices were directly related to observed river flows using multiple regression techniques. Two different river basins were used in the analysis. A simple blackbox linear rainfall-runoff model was used to establish the significance of satellite data (chapter 7).

8.2 Integration of satellite data with conventional rainfall data

To a practising hydrologist, a major objective is to forecast river flows as accurately as possible using all the information at his disposal. Areal rainfall estimates are made by interpolating point rain-gauge readings using one of several interpolation methods. Satellites, providing spatial information about the catchment in the form of infrared radiation at pixel resolution, could be used to assist in the interpolation process.

In order to investigate such a possibility, two algorithms were devised: one for half hour rainfall accumulations using individual infrared images and the other to accommodate accumulations relating to longer durations such as daily rainfall. Major differences between the satellite based methods and other conventional methods were found in the spatial distribution of catchment rainfall. Conventional methods produced artificial rainfall

boundaries depending upon the number and distribution of rain-gauges and tended to assign 10% to 14% of rainfall to cloud free areas (table 5.5). Satellite assisted interpolation and CCD analyses produced rainfall boundaries influenced by the size and position of the clouds observed. In the case of half-hour convective rainfall, the instantaneous storm centre and extent is identifiable from the satellite images which is sometimes not possible from the rain-gauge network (plates 5.1 to 5.5). Such visual displays are invaluable in short-term forecasting of heavy rainfall events, for although there is little information of the intensity of rainfall, they give at the very least a qualitative display of the spatial extent and movement of storm area. Similarly, CCD analysis for daily rainfall provides information on the spatial distribution of rainfall based on both rain-gauge data and satellite cloud data (plates 6.1a-c to 6.3a-c). Such information is important in physically based distributed hydrological models and in the assessment of wet and dry areas. The introduction of error field, based on comparison with known point rain-gauge measurements, was also shown to reduce overall errors in CCD estimates.

Up to now the focus was to improve the accuracy of estimated basin-averaged rainfall with the assistance of satellite data which would automatically improve the output of the rainfall-runoff model. In a further analysis, instead of relating satellite data to basin rainfall, a multiple regression model was set up with river flow as the dependent variable and basin rainfall, previous flow measurements and satellite derived cloud indices as the independent variables. The relationships were studied over two different catchments of River Trent and River Severn respectively. The inclusion of satellite cloud indices were found to be significant in the Trent basin, but not in the Severn basin, although they were significant when rainfall estimates were based on single rain-gauges.

Important points from the multiple regression analysis were:

* High R^2 values of 0.8 and 0.79 were obtained for both the Trent and Severn catchments respectively when cloud indices were related directly to the river-flows without the rainfall estimates from the rain-gauges. On the other hand, the relationship between rain-gauge rainfall estimates and the cloud indices was found to be poor for both catchments (table 7.7 and 7.13). These results give weight to the argument that in studies where the prime objective is to improve river-flow estimates, satellite data should be related directly to the river-flow rather than indirectly via trying to improve estimated rainfall.

* Mean areal rainfall over a catchment is an important parameter in any rainfall-runoff model. However, improving the mean areal rainfall estimates by increasing the density of rain-gauges would not necessarily improve river flow estimates due to modelling inaccuracies. Catchment rainfall estimates based on single rain-gauge

values will be different from the estimates based on full network but the reason why some of the rain-gauges showed good relationship with the observed flow is that they have managed to detect days with heavy rainfall giving rise to peak river-flows. However, with sparse networks based on single or few rain-gauges, there is a greater likelihood that a significant rainfall event would be missed or a moderate, isolated rainfall event over exaggerated. This is evident in fig.'s 8.1 to 8.4. Fig. 8.1 which show the comparison of rainfall estimates based on rain-gauge 47 with the estimates from the full network. Although there are deviations in the actual estimated amounts, major rainfall events are well matched and therefore rain-gauge 47 shows a good relationship with the observed river-flow in the Trent catchment area (R^2 = 0.72). On the other hand, in fig. 8.2, rain-gauge 72 grossly overestimates the observed rainfall on day 27 and therefore gives poor relationship with observed river-flow (R^2 = 0.53). Similarly, in the Severn region, rain-gauge 10 gives poor relationship (R^2 = 0.67) with observed river-flow as compared to rain-gauge 17 (R^2 = 0.81) as evident in fig.'s 8.3 and 8.4.

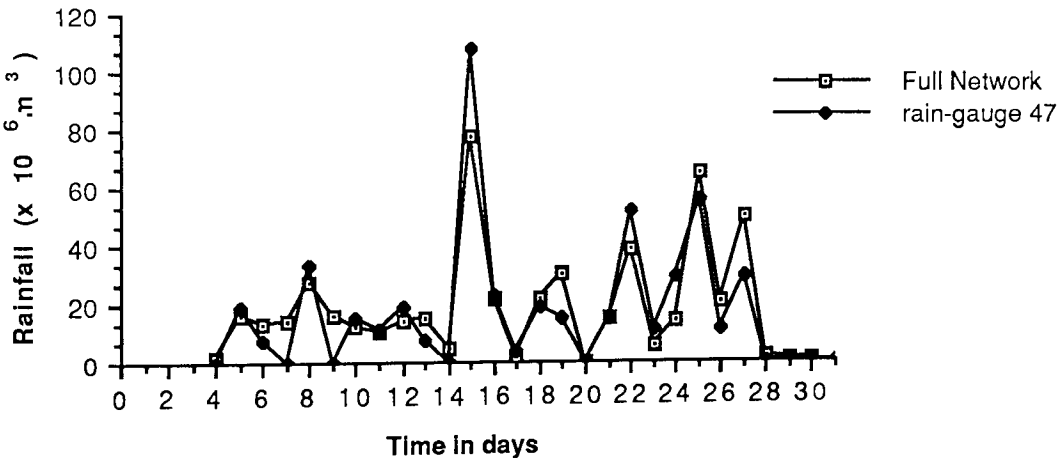

Fig 8.1 Comparison of rainfall estimates using rain-gauge 47 with that of using full network in the Trent region

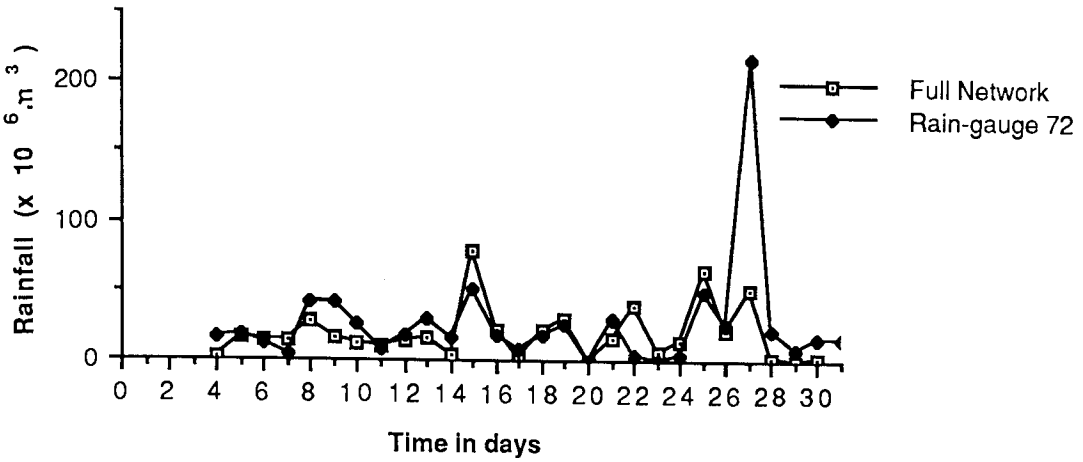

Fig 8.2 Comparison of rainfall estimates using rain-gauge 72 with that of using full network in the Trent region.

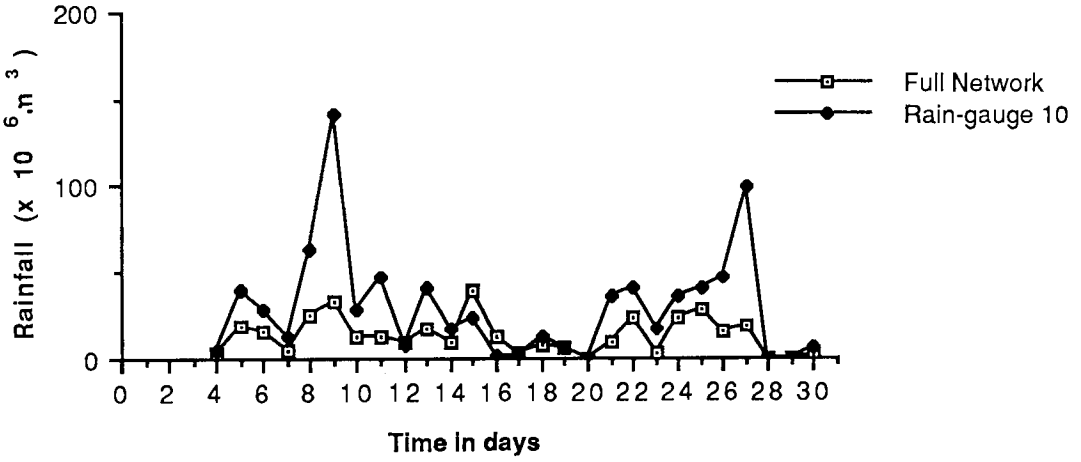

Fig 8.3 Comparison of rainfall estimates using rain-gauge 10 with that of using full network in the Severn region.

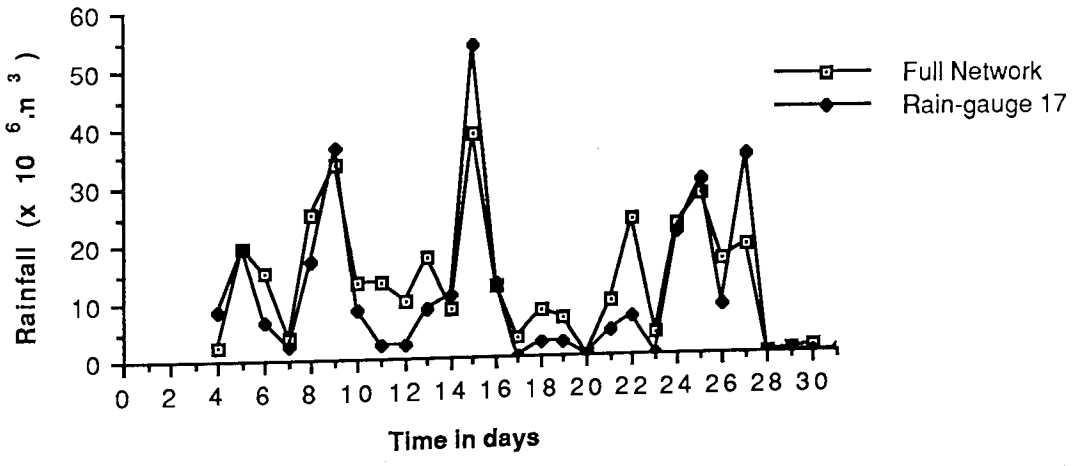

Fig 8.4 Comparison of rainfall estimates using rain-gauge 17 with that of using full network in the Severn region.

Based on the results of the analysis in chapter 7, a practising hydrologist is offered a simple methodology to establish the significance of satellite cloud data to his/her catchment requirements in the light of existing rain-gauge network. The decision to use the satellite data can be made on the results of pilot studies based on few months of relevant data. For example, in the Trent region, satellite data showed a better relationship with the observed river-flow than the rainfall estimates from the full network of 42 rain-gauges. This was not true for the Severn region where, although satellite data showed good relationship with the observed river-flow, but was not better than the rainfall estimates from the full rain-gauge network. Better rainfall estimates in the Severn region as compared to the Trent region may be due to the distribution of rain-gauges within the catchment. In the Severn region, rain-gauges are distributed more uniformly than in the Trent where rain-gauges are concentrated around the Birmingham area. Therefore, satellite data may be recommended for the Trent region but not for the Severn region. Such methodology has certain advantages in that:

* Rainfall-runoff models are based on simple regression.

* No calibrations are required for the satellite data with the ground based rainfall data.

* The methodology can be readily deployed over any catchment suitably covered by a geostationary satellite with minimum image processing requirements.

* Raw infrared count values are used instead of the normal temperature values. This makes it possible to use both SDUS as well as PDUS images.

* The problem of assessing effective rainfall can be avoided.

On the question of the economics of such a methodology, it is dependent on factors such as the reliability of satellite data, costs of acquisition and processing and the benefits gained in terms of the overall improvement in the accuracy and reliability for the defined purpose. This can only be provided after initial studies have been carried out over the study area and shown to be successful. These should be compared against the costs of more standard methods such as improving the rain-gauge network or using radar data.

8.3 Problems encountered

Some of the problems encountered in this work arose due to the dynamic nature of the rainfall event. Standard remote sensing techniques are designed and effectively employed to monitor and assess variables which are static in nature or change slowly over time. For example, the assessment of drainage pattern and slope factors in a catchment using remote sensing techniques need only be done once and monitoring vegetation damage or

deforestation may require seasonally or annually assessment. Catchment rainfall needs to be monitored continuously and this requires extensive data processing.

The acquisition of Meteosat satellite images was another problem. The in-house SDUS satellite receiver had a number of hardware and software problems and although every effort was undertaken to resolve them, only a limited number of image sequences were captured. Efforts were made to acquire satellite data from other institutions but this proved difficult and because of the costs involved limited the amount of data acquired. For future research purposes, a single PDUS receiver station broadcasting over Super Janet would be a very useful addition to UK satellite reception.

Another drawback associated with Meteosat images is their low resolution. At 60^{o} latitude, the area represented by a pixel increases from 5x5 km at sub-satellite point to approximately 8x8 km. This makes it extremely difficult to study small catchments quantitatively when only few pixels effectively cover the whole catchment. Also, the visible data could not be used effectively because of its unavailability at night time and problems with the pixel brightness during the day-time due to changing solar zenith angle.

There were also problems associated with the rain-gauge rainfall data supplied by the NRA. On some occasions there was confusion with the code numbers of individual rain-gauges with two rain-gauges given the same code. On one occasion a rain-gauge reported no rainfall while the other surrounding rain-gauges were reporting heavy rainfall. These errors were notified to the NRA and were consequently rectified.

Problems were also encountered with the selection of rainfall-runoff models to test any improvement in river-flow variance in relation to improved rainfall estimates. Hydrological models range from very simple lumped regression models to highly complex, physically based, distributed models and from purely deterministic models to highly sophisticated stochastic models. Most hydrological studies tend to generate their own hydrological models to suit their own data requirements and availability. Since the objective of the exercise was to determine the utility of satellite data, a simple multiple-regression model with minimum number of parameters was used in this study. The intention was to study the suitability of Meteosat data rather than the suitability of hydrological models.

8.4 Future recommendations

It is expected that the encouraging initial results obtained with the introduction of satellite data would lead to better river-flow forecasts for a given catchment. However, these results should be further substantiated and verified with applications over a number of

different catchments, preferably over the African continent and other tropical regions and using more sophisticated rainfall-runoff models.

Currently, greater emphasis is placed on the restructuring of hydrological models to better exploit the superior spatial data of remote sensing systems, especially radar data (Cluckie & Collier, 1991). This factor can also be exploited using satellite data in cases where radar data cannot be justified economically.

Regression models were used in this thesis to investigate the utility of satellite data. Cluckie & Owens (1987) has shown how radar and rain-gauge data can be combined using a Transfer function rainfall-runoff model. Such models can also be further investigated using satellite data in place of radar data.

The temporal resolution of Meteosat images provide an effective means of tracking storm movement in real-time. Coupled with few strategically placed real-time rain-gauges providing information on rainfall intensities, a storm movement through the catchment can be charted in real-time and its effect on areal rainfall estimates investigated.

Relative humidity plays an important role in many rainfall systems. Knowledge of this factor and other related meteorological variables and synoptic charts may be important in determining whether a particular cloud system is rain-bearing or not.

Possibilities also exists in applications where, for one reason or another, daily rainfall amounts need to be disaggregated into hourly amounts or some other convenient time step. Existing methods are purely statistical in nature where the duration of a storm during the day is calculated using depth-duration relationships. Hourly rainfall is estimated from the daily amount using an assumed distribution function (Pitman, 1976). The duration of storm can be easily estimated by examining the satellite image sequences, especially where rainfall is predominantly convective from well defined convective clouds. There is also an added benefit in cases where two or more storms have affected the catchment during the day. However, satellite data would be of little use as far as the temporal distribution of rainfall is concerned since rainfall rates cannot be inferred from the satellite data.

Studies of cloud cover in the visible also enable one to assess the amount of solar radiation incident at ground level at pixel resolution. This has important applications in agriculture, for example, length of growing period, and is a major factor in the determination of potential evaporation at ground level.

Rapid technological advances and decreasing computational costs will no doubt encourage the utilization of satellite data for hydorlogical applications. Improvements in the

Microwave technology with increased spatial resolution and satellite based active radar will surely open new avenues for the space-borne rainfall estimation systems.

8.5 Conclusions

It is evident from even a cursory review of observational data and analyses that precipitation is a very complex phenomenon and conventional means of measuring it are inadequate in most parts of the World. In such cases satellite data can be of great value for the estimation of the relevant hydrological data. A single approach is described by which the utility of satellite data can be assessed for a given catchment. This approach has shown that satellite data can serve as model input not only for the determination of river-basin characteristics but also for dynamic hydrological processes.

The most important general findings from this research were that:

1. The spatial coverage of satellite data combined with point rain-gauge values provide better information on the spatial distribution of rainfall within a catchment especially in the case of convective rainfall. Convective storms are particularly difficult to monitor using rain-gauge networks as they can be very localized.

2. Total catchment rainfall values are not greatly influenced by the method used to calculate them. Both conventional and satellite assisted methods produce similar overall values but are differently distributed over the catchment.

3. It has been demonstrated that adjustment techniques used in Radar studies using rain-gauges can also be used in satellite based Cold Cloud Duration analysis to improve upon the initial distribution of rainfall. This could be important in some studies.

4. It has also been shown how satellite data can be incorporated in a conventional method of areal rainfall estimates so that interpolated values not only depend on the distance from the nearest rain-gauges but also on the evidence of satellite data in terms of infrared count values and also on the physical evidence of clouds.

5. In case of rainfall-runoff models, it was found that satellite derived cloud indices show good relationships with the measured river flow. A better way of improving river-flow estimates would be to relate it directly with the cloud indices. This was shown in the case of two separate catchments differing in topology and a methodology is described using simple multiple regression analysis how one can assess the utility of satellite data for his or her catchment.

In conclusion, satellite data has the potential to be of great benefit in large hydrological regimes supporting inadequate network of rain-gauges, both in terms of assessing the spatial distribution of rainfall as well as improving river-flow forecasting.

This thesis provides plausible means of combining satellite data with the traditional point rain-gauge data as well as means for investigating the suitability of satellite data as additional input to rainfall-runoff models. The algorithms presented are by no means universal, and in the opinion of the author deserves further attention and testing, especially as input to distributed rainfall-runoff models.

Future developments, particularly in the field of computer processing and storage are expected to reduce the costs of remote sensing systems and data acquisition which should see a rise in the use of such techniques in the poorer regions of the world.

REFERENCES

Adler, R.F & Mack, R.A, 1984, Thunderstorm cloud height-rainfall rate relations for use with satellite rainfall estimation techniques, Journal of Climate and Applied Meteorology, 23, 280-295

Akin, J.E., 1971, Calculation of mean areal depth of precipitation, Journal of Hydrology, 12 (1971), 363-376

Anderson, M.G. & Burt,T.P., 1985, Hydrological Forecasting, John Wiley & Sons, Chichester,

Arkin, P. A., 1979, The relationship between fractional coverage of high cloud and rainfall accumulations during GATE over the B-scale array, Monthly Weather Review. 107, 1382-1387

Arkin, P.A. & Meisner, B.N., 1987, The relationship between large-scale convective rainfall and cold cloud over the Western Hemisphere during 1982-84, Monthly Weather Review, Vol. 115, January 1987, 51-74

Arkin, P.A., 1988, The global precipitation climatology project, In proceedings of the 7th meteosat scientific users' meeting, Madrid, 27-30 Sep. 1988, EUM P04, 227-230

Atlas, D. & Thiele, O.W. (editors), 1981, Precipitation measurements from space, workshop report, NASA, Goddard Space Flight Centre, Greenbelt, Maryland 20771

Augustine, J.A.; Griffith,C.G.; Woodley,W.L. & Meitin,J.G., 1981a, Insights into errors of SMS-inferred GATE convective rainfall, Journal of Applied Meteorology, 20, May, 1981, 509-520

Augustine, J.A.; Meitin, J.G.; Griffith, C.G. and Woodley, W.L., 1981b, An objective evaluation of the Griffith/Woodley rain estimation technique, In preprints of the 4th conf. on hydrometeorology, Oct., 1981, Reno, NV, American Meteorological Society, 3409.552, 134-140

Barrett, E. C. & Curtis, L. F., 1974, Environmental Remote Sensing: Applications and Achievements, Edward Arnold (Publishers) Ltd, 309pp

Barrett, E. C. & Curtis, L. F., 1982, Introduction to Environmental Remote Sensing, Chapman & Hall, New York,2nd Edition, 352pp

Barrett, E. C. & Martin, D. W., 1981, The Use of Satellite Data in Rainfall Monitoring, Academic press. London, 340pp

Barrett, E. C., 1970, The estimation of monthly rainfall from satellite data, Monthly Weather Review. 98, No. 4, 322-327

Barrett, E. C., 1973, Forecasting daily rainfall from satellite data, Monthly Weather Review. 101, 215-255

Barrett, E. C., 1974, Climatology from Satellites. Methuen, London, 418pp

Barrett, E. C.; D'Souza, G.; Kidd, C. & Palmer, H., 1989a, Rainfall monitoring by Passive microwave satellite, radar & rain-gauges: Results from Kenya and The British Isles, Annual report to the U.S Department of Commerce, 79pp

Barrett, E. C.; Kidd, C. & Bailey, J.O., 1987, The Use of SMMR data in suppor of the Bristol/NOAA Interactive scheme (BIAS) for satellite-improved rainfall monitoring, Annual report to the U.S Department of Commerce, 77pp

Barrett, E. C.; Kidd, C. & Palmer, H, 1989b, A passive microwave satellite technique for rainfall monitoring over the British Isles and surrounding seas, Final report to the Department of Enviroment, 57pp

Barrett, E.C., 1977a, Mapping rainfall from conventional data and weather satellite imagery across Algeria, Libya, Morocco and Tunisia, Consultants report, W/K 4647, FAO, Rome, 55pp

Barrett, E.C., 1977b, Monotoring precipitation: a global strategy for the 1980's , In monitoring enviromental change by Remote Sensing (Genderen,J.L. & W.G. Collins, eds.), Remote Sensing Society, (UK), 53-58

Barrett, E.C., 1979, Satellite rainfall estimation by cloud indexing methods for desert locust surveys and control, In Satellite Hydrology (eds. Deutsch,M; Weisnet,D.R. & Rango,A.), proceedings of the AWRA symposium on Satellite Hydrology, Sioux Falls, S.D., June 1979, 92-100

Barrett, E.C., 1986, Estimation of precipitation from AVHRR & METEOSAT data over Africa, In proceedings of the twentieth international symposium on remote sensing of enviroment, 4-10 of dec. 1986, Nairobi, Kenya, 235-254

Barrett, E.C. & D'Souza, G., 1985, An objective monitoring method for African rainfall based on Meteosat Visible and Infrared images, In Proc. of the ISLSCP Conf., Rome, Italy, 2-6 Dec., 1985 (ESA SP-248, May 1986), 305-313

Barrett, E.C. & D'Souza, G., 1986a, The development of an objective range of dry day products for drought monitoring by meteosat over Africa, Final report to Earsel, ESA contract No. 6137/84/D/JS(SC), 71pp

Barrett, E.C. & D'Souza, G., 1986b, ADMIT: An objective technique for broad scale rainfall monitoring by geostationary satellites, In proceedings of the twentieth international symposium on remote sensing of enviroment, 4-10 of dec. 1986, Nairobi, Kenya, 955-964

Barrett, E.C. & Herschy, R.W., 1986, A European perspective on satellite remote sensing for hydrology and water management, In Hydrologic Applications of space technology (Proceedings of the Cocoa Beach Workshop, Florida, August 1985). IAHS Publ. no. 160., 3-12pp

Barrett, E.C. & Kidd, C., 1988, Intercomparisons of passive microwave rainfall algorithms over land, In Remote Sensing: Moving towards the first century, IGARSS'88, 12-16 Sep, 1988, Edinburgh, UK, ESA SP-284, 253-254

Barrett, E.C. & Power, C.H., 1986, Satellite cloud and rainfall assessment in the Western Sahel, In proceedings of the twentieth international symposium on remote sensing of enviroment, 4-10 of dec. 1986, Nairobi, Kenya, 943-954

Barrett, E.C.; Beaumont, M.J. & D'Souza, G., 1988, Hierarchical system for operational rainfall monitoring by meteosat, In proceedings of the 7th meteosat scientific users' meeting, Madrid, 27-30 Sep. 1988, EUM P04, 393-407

Barrett, E.C.; D'Souza, G. & Power, C.H., 1986, Comparison of two meteosat based satellite rainfall monitoring techniques applied to part of the Western Sahel, In proceedings of the 6th meteosat scientific users' meeting, Amsterdam, 25-27 Nov. 1986, Vol. II, EUM P01, NA

Bellon, A. & Austin, G.L., 1986, On the relative accuracy of satellite and raingauge rainfall measurements over Middle Latitudes during daylight hours, Journal of Climate and Applied Meteorology, 25, No. 11, 1712-1713

Beven, K.J., Warren, R. & Zaoui, J., 1980, SHE: Towards a methodology for physically based distributed forecasting in hydrology, Proc. Oxford Symp., IAHS publ. no. 129, 133-137

Browning, K.A., 1987, Towards the more effective use of radar and satellite imagery in weather forecasting, In Weather Radar and Flood forecasting (eds.Collinge,V.K. & Kirby,C), John Wiley & Sons (pub.), 1987, 239-270

Callis, S.L. & LeComte, D.M., 1987, Operational use of satellite imagery to estimate rainfall in the Sahelian countries of Africa, In Preprints, 18th Conf., on Agriculture and Forest Meteorology, West lafayette, American Meteorological Society, Boston, MA, USA, 160-163

Carn, M; Dagorne, D.; Guillot, B. & Lahuec, J.P., 1988, Rainfall estimation over the Western Sahel using meteosat imagery, In proceedings of the 7th meteosat scientific users' meeting, Madrid, 27-30 Sep. 1988, EUM P04, 247-251

Chadwick, A.F.; Dugdale, G.; Traore, A.F. & Milford, J.R., 1986, Operational rainfall mapping over the Sahel, In proceedings of the 6th meteosat scientific users' meeting, Amsterdam, 25-27 Nov. 1986, Vol. II, EUM P01, NA

Chander, S. & Fattorelli, S., 1991, Adaptive grid-square-based geometrically distributed flood forecasting system, In Hydrological Applications of Weather Radar, Cluckie, I.D. & Collier, C.G. (editors), Ellis Horwood, Chichester, 424-439

Cherna, E.; Bellon, A.; Austin, G.L. & Kilambi, A., 1985, An objective technique for the delineation and extrapolation of thunderstorms from GOES satellite data, Journal of Geophysical Research, 90, 6203-6210

Clark, D. & Morris, D.G., 1986, The NOAA satellite precipitation estimate program - with preliminary results of an operational test using estimates in a hydrologic river forecast model, In Hydrologic Applications of space technology (Proceedings of the Cocoa Beach Workshop, Florida, August 1985). IAHS Publ. no. 160., 41-46

Cluckie, I.D. & Collier, C.G. (editors), 1991, Hydrological Applications of Weather Radar, Ellis Horwood, Chichester, 644pp

Cluckie, I.D. & Owens, M.D., 1987, Real-time rainfall-runoff models and use of weather radar information, In Weather Radar and Flood forecasting (eds.Collinge,V.K. & Kirby,C), John Wiley & Sons (pub.), 1987, 171-190

Collinge, V. & Kirby, C. (editors), 1987, Weather Radar and Flood Forecasting, John Wiley & Sons, 296pp

Coretti, C.; Desiato, F.; Telespazio, C.G. & Bergamini, V.A., 1988, Rainfall estimate over Northern Italy based on meteosat images, In proceedings of the 7th meteosat scientific users' meeting, Madrid, 27-30 Sep. 1988, EUM P04, 253-259

Crawford, N.H. & Linsley, R.K., 1966, Digital Simulation in Hydrology, Stanford Watershed Model 4, TR39, Department of Civil Engineering, Stanford

Creutin, J.D.; Lacomba, P. & Obled, C.H., 1986, Spatial relationship between cloud cover and rainfall fields; a statistical approach combining satellite and ground data., In Hydrologic Applications of space technology (Proceedings of the Cocoa Beach Workshop, Florida, August 1985). IAHS Publ. no. 160., 81-90

Curran, P. J., 1985, Principles of Remote Sensing, Longman, London, 282 pp

D'Souza, G. & Barrett, E. C., 1988, A comparative study of candidate techniques for U.S heavy rainfall monitoring operations using Meteorological satellite data, Final report to the U.S. Department of Commerce, 39pp

D'Souza, G. , 1988, Rainfall estimation over Africa using satellite data, Unpublished Phd Thesis, University of Bristol, UK, , 273pp

D'Souza, G.; Ahindukha,J. & Ahago,V., 1988, Rainfall estimation over Kenya using meteosat imagery, ground-based radar and raingauge recorders, In Remote Sensing: Moving towards the first century, IGARSS'88, 12-16 Sep, 1988, Edinburgh, UK, ESA SP-284, 249-250

Davis, P.A.; Weigman,E.J. & Serebreny,S.M., 1971, Estimation of precipitation over flathead drainage basin using meteorological satellite photographs, Final report, Contract 14-06-D-7407, Stanford research institute, Menlo Park, California, 59pp

Dean, J.A & Snyder, W.M., 1977, Temporally and Arealy Distributed Rainfall, Journal of Irrigation and Drainage Division, June 1977

Delhomme, J.P., 1978, Kriging in Hydrosciences: Advance Water Resources, 1(5), 251-266

Desboise, M., Seze, G. & Szejwach, 1982, Automatic classification of clouds on meteosat imagery: Application of high-level clouds, In Journal of Applied Meteorology, vol. 21, 401-412

Deutch, M.; Weisnet, D.R. & Rango, A., 1979, Satellite Hydrology: Proceedings of the AWRA Symposium on Remote Sensing, Sioux Falls, South Dakota, 730pp

Dey, B. & Goswami, D.C., 1985, Application of remote sensing for seasonal runoff prediction in the Indus basin, Pakistan, In Hydrological applications of remote sensing and remote data transmission (ed. by Goodison,B.E), IAHS publication No. 145, 637-645

Doneaud, A.A.; Miller, J.R. & Johnson, L.R., 1987, The Area-Time-Integral technique to estimate convective rain volumes over areas applied to satellite data - A preliminary investigation, Journal of Climate and Applied Meteorology, 26, Nov. 1987, 156-169

Downey, I.D, Petch, J.R. & Walters, D., 1989, Estimation of hydrological model parameters from digitized aerial colour infrared photography, In Remote sensing for operational applications, Technical contents of the 15th Annual conference of the Remote sensing society (compiled by Barrett,E.C. & Brown,K.A.), Uni. Of Bristol, 13-15 Sep. 1989, 93-100

Draper, N. & Smith, H., 1966, Applied Regression Analysis, John Willey & Sons, Inc., Newyork

Dugdale, G. & Milford, J.R., 1986, The use of meteosat data to evaluate rainfall in tropical Africa, In proceedings of the twentieth international symposium on remote sensing of enviroment, 4-10 of dec. 1986, Nairobi, Kenya, 499-506

Dugdale, G.; Milford, J.R. & Rowell, D.P., 1986, Using meteosat data to relate rainstorms over the West African Sahel to data on the scale of the ECMWF grid, In proceedings of the 6th meteosat scientific users' meeting, Amsterdam, 25-27 Nov. 1986, Vol. II, EUM P01, NA

Dugdale, G.; Milford, J.R.; Stephenson, J. & Williams, J.B., 1989, Operational installations of the Bradford-Reading meteosat PDUS in Africa, In Remote sensing for operational applications, Technical contents of the 15th Annual conference of the Remote sensing society (compiled by Barrett,E.C. & Brown,K.A.), uni. Of Bristol, 13-15 Sep. 1989, 113-122

Einfalt, T. & Donoeux, T., 1991, Never expect a perfect forecast, In Hydrological Applications of Weather Radar, Cluckie, I.D. & Collier, C.G. (editors), Ellis Horwood, Chichester, 452-458

Elgy, J. & Siyyid, A.N., 1991, Combining Satellite and rain-gauge data for areal estimates of rainfall, In Proceedings of the International Conference UDT '91, Dubrovnik, Yugoslavia, 5-14pp

ESA, 1980, Meteosat High Resolution Image Dissemination, Meteosat System Guide, Vol. 9

ESA, 1981, Meteosat WEFAX Transmission, Meteosat System Guide, Vol. 4

ESOC, 1990, Meteosat-3 calibration report, issue 7, April to June 1990

ESOC, 1991, Meteosat-4 calibration report, , April to June 1990

Ferroro, R.R., Alishouse, J.C & Fiore, J.V., 1988, Comparison of Weather Radar and Satellite based Passive Microwave Observations of Rainfall over Land and Oceans, 3rd conf. on Satellite, Meteorology and Oceanography, February 1-5, American Meteorological Society

Flach, J.D., 1989, River basin Surveillance Using Remotely Sensed Data - A Water Resource Information Management System, PhD Thesis, University of Aston, Dept. of Civil Engineering

Flack, J.D., Chidley, T.R.E. & Siyyid, A.N., New possibilities for precipitation estimation for river basin managers in developing countries, In Weather Radar and Flood forecasting (eds.Collinge,V.K. & Kirby,C), John Wiley & Sons (pub.), 1987, 171-190

Flitcroft, I.D.; Mcdougall, V.; Milford, J.R. & Dugdale, G., 1986, The calibration and interpretation of meteosat based estimates of Sahelian rainfall, In proceedings of the 6th meteosat scientific users' meeting, Amsterdam, 25-27 Nov. 1986, Vol. II, EUM P01, NA

Follansbee, W.A. & Oliver, V.J., 1975, A comparison of infrared imagery and video pictures in the estimation of daily rainfall from satellite data, NOAA technical memorandum NESS 62, Washington,D.C., 14pp

Follansbee, W.A., 1973, Estimation of average daily rainfall from satellite cloud photographs , NOAA technical memorandum NESS 44, Washington,D.C., 39pp

Follansbee, W.A., 1976, Estimation of daily precipitation over china and the USSR using satellite imagery, NOAA technical memorandum NESS 81, Washington,D.C., 30pp

Fowler, M.G.; Burke, H.K.; Hardy, K.R. & Tripp, N.K., 1979, The estimation of rainrate over land from spaceborne passive microwave sensors, In Satellite Hydrology

(eds. Deutsch,M; Weisnet,D.R. & Rango,A.), proceedings of the AWRA symposium on Satellite Hydrology, Sioux Falls, S.D., June 1979, 101-108

France, M.J. & Hedges, P.D., 1989, The appropriate use of remotely sensed satellite data for water resource assessment and modelling, In Remote sensing for operational applications, Technical contents of the 15th Annual conference of the Remote sensing society (compiled by Barrett,E.C. & Brown,K.A.), uni. Of Bristol, 13-15 Sep. 1989, 147-154

France, M.J.; Chidley, T.R.E. & Collins, W.G., 1986, Extraction of hydrological parameters from landsat thematic mapper imagery, In proceedings of the twentieth international symposium on remote sensing of enviroment, 4-10 of dec. 1986, Nairobi, Kenya, 1165-1174

Fraysse, G., 1980, Remote Sensing Application in Agriculture and Hydrology, A A Balkema, Rotterdam, 502 pp

Garcia, O., 1981, A comparison of two satellite rainfall estimates for GATE, Journal of Applied Meteorology, 20, 430-438

Goodison, B.E. (editor), 1985, Hydrological Applications of Remote Sensing and remote data Transmission, IAHS Publication No. 145., 684pp

Goodison, B.E.; Langham, E.J. & Athanassiadis, D., 1985a, Radarsat and Msat: proposed Canadian satellite systems with hydrological applications, In Hydrological applications of remote sensing and remote data transmission (ed. by Goodison,B.E), IAHS publication No. 145, 75-85

Goodison, B.E.; Whiting, J.M.; Wiebe, K. & Cihlar, J., 1985b, Operational requirements for water resources remote sensing in Canada: now and in the future, In Hydrological applications of remote sensing and remote data transmission (ed. by Goodison,B.E), IAHS publication No. 145, 647-657

Griffith, C.G. & Woodley, W.L. , 1973, On the variation with height of the top brightness of precipitating convective clouds, Journal of Applied Meteorology, 12, Sep., 1973, 1086-1089

Griffith, C.G.; Woodley, W.L. & Augustine, J.A., 1981, Satellite rain estimation in The U.S. High Plaines , Journal of Applied Meteorology, 20, 53-66

Griffith, C.G.; Woodley, W.L.; Grube, P.G.; Martin, D.W.; Stout, J. & Sikdar, D.N., 1978, Rain estimation from geosynchronus satellite imagery-visible and infrared studies, Monthly Weather Review. 106, 1153-1171

Griffith, C.G., 1987a, The estimation from satellite imagery of summertime rainfall over varied space and time scales, NOAA technical memorandum ERL ESG-25, April, 87, 102pp

Griffith, C.G., 1987b, Comparison of gauge and satellite rain estimates for the coastal U.S. during August, 1979, Journal of Geophysical Research, 92, 9551-9566

Griffith, C.G.; Augustine,J.A. & Woodley,W.L., 1985, Real time inference of convective rainfall from satellite data, In Hydrological applications of remote sensing and remote data transmission (ed. by Goodison,B.E), IAHS publication No. 145, 281-287

Griffith, C.G.; Woodley, W.L.; Browner, S.; Teijeiro,J.;Maier, M.; Martin, D.W.; Stout,J. and Sikdar,D.N., 1976, Rain estimation from geosynchronus satellite imagery during daylight hours, NOAA technical report ERL 356-WMPO 7, Boulder, Col., 106pp

Grosh, R.A.; Weinman, J.A. & Van Scherpenzeel, 1973, Cloud photographs from satellites as a hydrological tool in remote equatorial regions, Journal of hydrology. 18, 147-161

Groves, J.R.; Ragan,R.M. & Clapp,R.B., 1985, Development and testing of a remote sensing based hydrological model, In Hydrological applications of remote sensing and remote data transmission (ed. by Goodison,B.E), IAHS publication No. 145, 601-611

Haralick,R.M.; Shanmugam,K. & Dinstein,I., 1973, Textural features for image classification , IEEE transactions on systems, man and cybernatics, Vol. SMC-3, Nov. 1973, 610-621

Hardy,S.; Dugdale,G.; Milford,J.R. & Sutcliff,J.V., 1988, The use of satellite derived rainfall estimates in water management, In proceedings of the 7th meteosat scientific users' meeting, Madrid, 27-30 Sep. 1988, EUM P04, 261-266

Harley, J.B., 1975, Ordanance Survey Map - a Descriptive Manual, Ordnance Survey, Southampton

Hawkins, R.S., 1980, A clustering technique for satellite imagery anlysis, U.S. Airforce Geophysics Laboratory , Bedford, Massachusetts

Hielkema,J.U.; Barrett,E.C.; Harrison,A.R.; Colella,G. & Petricono,A., 1986, Operational rainfall monitoring of Africa using low resolution meteosat observations, In proceedings of the 6th meteosat scientific users' meeting, Amsterdam, 25-27 Nov. 1986, Vol. II, EUM P01, NA

Hildebrand, P.H., Towery, N. & Snell, M.R., 1979, measurement of convective mean rainfall over small areas using high density rain-gauges and radar, J. of Applied Meteorology, 18, 1316-1326

Hogg, W.G., Hanssen, A.J., Niitsou, A. & Polaravapu, V.L., 1988, Midlatitude evaluation of some satellite rainfall estimation techniques, 3rd conf. on Satellite, Meteorology and Oceanography, February 1-5, American Meteorological Society

Huff, F.A., 1970, Sampling errors in measurements of mean precipitation, J. of Applied Meteorology, 9, 35-44

Hutchinson,P. & Walley,W.J., 1972, Calculation of areal rainfall using finite element techniques with altitudinal corrections, Bulletin of the International Association of Hydrological Sciences, XVII, 3, 10/1972, 259-272

Huygen,J.; Simons,W. & Berkhout,J.A.A., 1988, Estimation of rainfall over zambia, using meteosat data and raingauge measurements, In proceedings of the 7th meteosat scientific users' meeting, Madrid, 27-30 Sep. 1988, EUM P04, 231-241

Ingraham,D.; Amorocho,J.; Guilarte,M. & Escalona,M., 1977, Preliminary rainfall estimates in Venezuela and Columbia from GOES satellite images, In preprints, 2nd conf. on hydrometeorology, Toronto,25-27 Oct. 1977, 316-323

Kilonsky,B.J. & Ramage,C.S., 1976, A technique for estimating Tropical open-ocean rainfall from satellite observations, Journal of Applied Meteorology, 15, Sep., 1976, 972-975

Kite,G.W., 1991, A watershed model using satellite data applied to a mountain basin in Canada, Journal of Hydrology, 128 (1991), 157-169

Kruger, L.R.; Strubing, G. & Schultz, G.A., 1982, Satellite data as the basis for the estimation of rainfall and runoff, In Advances in Hydrometry (Proceedings of the Exeter Symposium, July 1982)., 273-284

Kruger,L.R.; Harboe,R. & Schultz,G.A., 1985, Estimation of convective rainfall from satellite data, In Hydrological applications of remote sensing and remote data transmission (ed. by Goodison,B.E), IAHS publication No. 145, 273-279

Kumar,O.S.R.U.B.; Ogallo,L.J. & Ouma,G.O., 1988, Relationship between cold cloud duration and rainfall over Southern Tanzania, In proceedings of the 7th meteosat scientific users' meeting, Madrid, 27-30 Sep. 1988, EUM P04, 305-308

Lee,B.G. & Chin,R.T. , 1983, Classification of rain cells in satellite imagery, IEEE Conf. on computer vision and pattern recognition, Washing DC, 405-406

Lee,B.G.; Chin,R.T. & Martin,D.W., 1985, Automated rain-rate classification of satellite images using stastical pattern recognition, IEEE transactions on geoscience and remote sensing, Vol. GE-23, No.3, May 1985, 315-323

Lee,P.S.; Lynn,P.P. & Shaw,E.M., 1974, Comparison of multiquadratic surfaces for the estimation of areal rainfall, Hydrological sciences bulletin, XIX, 3, 9/1974, 303-317

Lovejoy,S. & Austin,G.L., 1979a, The sources of error in rain amount estimating schemes from GOES visible and infrared satellite data, Monthly Weather Review, Vol. 107, August 1979, 1048-1054

Lovejoy,S. & Austin,G.L., 1979b, The delineation of rain areas from visible and infrared satellite data for GATE and mid-latitudes, Atmospheric-Ocean 17(1) 1979, 77-92

Maling, D. H., 1973, Coordinate Systems and Map Projections: London, George Phillip & Son, Ltd.

Manikiam,B., 1986, Rainfall estimation from satellite data-A review, Vayu Mandal, July-December 1986, 10-14pp

Martin,D.W. & Howland,M.R., 1986, Grid History: A geostationary satellite technique for estimating daily rainfall in the tropics, Journal of Climate and Applied Meteorology, 25, 184-195

Mather, P. M., 1987, Computer processing of Remotely-Sensed Images - An Introduction, John Wiley & Sons, Chichester, 352 pp

Mcdougall,V.D.; Saunby,M.; Dugdale,G. & Milford,J.R., 1988, Relationship between rainfall and cloud top temperature in tropical Africa - seasonal and regional effects, In proceedings of the 7th meteosat scientific users' meeting, Madrid, 27-30 Sep. 1988, EUM P04, 297-303

Mcginnis,D.F.; Asce,A.M.; Scofield,R.A.; Schneider,S.R. and Berg,C.P., 1979, Satellite as an aid to water resource managers, Preprints 3486, American Society of Civil Engineers Convention and Exposition, Boston, 2-6 April, 21pp

Milford,J.R. & Dugdale,G., 1986, Applications of meteosat data in agriculture and hydrology, In proceedings of the 6th meteosat scientific users' meeting, Amsterdam, 25-27 Nov. 1986, Vol. II, EUM P01, NA

Mimikou, M., 1983, Kalman Filter Empirical Fitting on Monthly Rainfall-Runoff Responses, 93-112, Nordic Hydrology, Vol. 14, No. 2

Mishra,D.K.; Kalsi,S.R. & Jain,R.K., 1988, The estimation of heavy rainfall using INSAT-!B satellite data, Mausam, (1988), 39, 4, 383-392

Moore, R.J., 1977, Rain-gauge network requirements for real-time flow forecasting, In O' Connell, P.E., Beven, M.A., Gurney,R.J., Jones,D.J. & Moore,R.J., Methods for evaluating the U.K. rain-gauge network, Institute of hydrology, Report No. 40, 168-182, 190-205

Moses, J.F., 1983, Interactive adjustment of automatic satellite derived precipitation estimates, 5th conf. on Hydrometeorology, American Meteorological Society, Oct. 17-19, Tulso, Okla

Moses,J.F. & Barrett,E.C., 1986, Interactive procedures for estimating precipitation from satellite imagery, In Hydrologic Applications of space technology (Proceedings of the Cocoa Beach Workshop, Florida, August 1985). IAHS Publ. no. 160., 25-39

Negri,A.J.; Adler,R.F. & Wetzel,P.J., 1984, Rain estimation from satellites: An examination of the Griffith-Woodley technique, Journal of Climate and Applied Meteorology, 23, 102-116

Negri,J.A. & Adler,R.F., 1987a, Infrared and Visible satellite rain estimation. Part 2: A cloud definition approach, Journal of Climate and Applied Meteorology, 26, Nov. 1987, 1553-1564

Negri,J.A. & Adler,R.F., 1987b, Infrared and Visible satellite rain estimation. Part 2: A cloud definition approach, Journal of Climate and Applied Meteorology, 26, Nov. 1987, 1565-1576

Nie, N.H.; Hull, C.H.; Jenkins, J.G.; Steinbrenner, K. & Bent, D.H., 1975, SPSS : statistical package for social sciences, McGraw-Hill Book Company, 675pp

Oakes, J. & Thrift, N., 1975, Spatial Interpolation of Missing data: An empirical comparison of some different methods, Computer Applications, Vol. 2, No. 3 & 4

Parikh,J.A. & Ball,J.A., 1980, Analysis of cloud type and cloud amount during GATE from SMS infrared data, Remote Sensing of Enviroment, Vol. 9, No. 3, May 1980, 225-245

Parikh,J.A. & Rosenfield,A., 1978, Automatic segmentation and classification of infrared meteorological satellite data, IEEE transactions on systems, man and cybernatics, Vol. SMC-8, Oct. 1978, 736-743

Parikh,J.A., 1977, A comparative study of cloud classification techniques, Remote sensing of enviroment; 6, 67-81

Pitman, W.V., 1976, A mathematical model for generating daily river flows from meteorological data in South Africa, Report No. 2/76, Hydrological Research Unit, University of Witwatersrand Johannesburg, 56 pp

Rango,A., 1985a, A survey of progress in remote sensing of snow and ice, In Hydrological applications of remote sensing and remote data transmission (ed. by Goodison,B.E), IAHS publication No. 145, 347-359

Rango,A.; Engman,E.T.; Jackson,T.J.; Ritchie,J.C. & Paetzold,R.F., 1985b, Hydrological research in the AgRistars programme, In Hydrological applications of remote sensing and remote data transmission (ed. by Goodison,B.E), IAHS publication No. 145, 579-589

Richard,F. & Arkin,P., 1981, On the relationship between satellite observed cloud cover and precipitation, Monthly Weathet Review, 109, 1081-1093

Rosema, A. 1987, A study of meteosat based rainfall mapping in the sahel region. Consultants report GCP / INT / 432 / NET, FAO, Rome, Italy.

Rott,H., 1986, Estimation of daily runoff based on meteosat data, In Hydrologic Applications of space technology (Proceedings of the Cocoa Beach Workshop, Florida, August 1985). IAHS Publ. no. 160., 321-329

Salim, M., 1989, The design of Real-Time Nowcasting system for Lacalised Weather, Phd Thesis, University of Aston, 203pp

Schmugge, T.J., Jackson, T.J. & McKim, H.L., 1979, Survey of In-situ and Remote Sensing methods for soil moisture determination, In Satellite Hydrology (eds. Deutsch,M; Weisnet,D.R. & Rango,A.), proceedings of the AWRA symposium on Satellite Hydrology, Sioux Falls, S.D., June 1979, 333-352

Scofield,R.A,, 1986, Satellite convective and extratropical cyclone cloud categories associated with heavy precipitation, In Hydrologic Applications of space technology (Proceedings of the Cocoa Beach Workshop, Florida, August 1985). IAHS Publ. no. 160., 47-57

Scofield,R.A. & Oliver,V.J., 1977, A scheme for estimating convective rainfall from satellite imagery, NOAA technical memorandum NESS 86, Washington,D.C., 47pp

Scofield,R.A., 1981, Analysis of rainfall from flash flood producing thunderstorms using GOES data, In Proceedings of the IAMAP Symposium, Hamberg, 25-28 Aug., 1981 (ESA SP-165, June 1981), 51-58

Scofield,R.A., 1985, Satellite-derived precipitation estimates for hydrological application, In Hydrological applications of remote sensing and remote data transmission (ed. by Goodison,B.E), IAHS publication No. 145, 259-271

Scofield,R.A., 1987, The NESDIS Operational Convective Precipitation Estimation Technique, Monthly Weather Review, Vol. 115, 1773-1792

Severn Trent Water Authority, 1980, Dove and Derwent River Basin, Report of Survey

Severn Trent Water Authority, December 1976, River Tame Basin, Report of Survey

Severn Trent Water Authority, December 1977, River Severn Basin, Report of Survey

Severn Trent Water Authority, June 1978, Upper-Trent Basin, Report of Survey

Severn Trent Water Authority, June 1979, Lower-Trent Basin, Report of Survey

Severn Trent Water Authority, October 1978, River Sour Basin, Report of Survey

Shaw, E.M., 1988, Hydrology In Practice, Second edition, Van Nostrand Reinhold (International) Co. Ltd., 539pp

Shearman, R.J. & Slater, P.M., 1975, An objective rainfall interpolation and mapping technique, Hydrological Sciences Bulletin, Vol. 20, No. 3, 353-363

Singh V.P., 1989, Hydrologic Systems, Watershed modelling, Vol. 1 and 2, Prentice Hall Inc

Singh, V.P. & Woolhiser, D.A., 1976, Sensitivity of linear and nonlinear surface runoff models to input errors, In Journal of hydrology, 33, 301-318

Singh, V.P., 1977, Sensitivity of some runoff models to errors in rainfall excess, In Journal of hydrology, 33, 301-318

Snidgers,F.L., 1988, An evaluation of techniques for monitoring of rainfall over the Western Sahel using meteosat PDUS data, In proceedings of the 7th meteosat scientific users' meeting, Madrid, 27-30 Sep. 1988, EUM P04, 275-282

Snyder, J.P., 1982, Map Projections Used by the U.S. Geological Survey, U.S. geological Survey Bulletin 1532

Spayd,L.E., 1986, Future applications of GOES satellite VAS data to estimating and forecasting heavy precipitation, In Hydrologic Applications of space technology (Proceedings of the Cocoa Beach Workshop, Florida, August 1985). IAHS Publ. no. 160., 71-79

Spencer, R.W. & Goodman H.M., 1988, The 1982-1983 ENSO Global convective precipitation Anamoly derived from Nimbus-7 SMMR 37 GHz Scattering measurements, 3rd conf. on Satellite, Meteorology and Oceanography, February 1-5, American Meteorological Society

Stout, J.E.; martin, D.W. & Sikdar, D.N., 1979, Estimating GATE rainfall with geosynchronus satellite images, Monthly Weather Review. 107, 585-598

Strubing,G. & Shultz,G.A., 1985, Estiamtion of monthly river runoff data on the basis of satellite imagery, In Hydrological applications of remote sensing and remote data transmission (ed. by Goodison,B.E), IAHS publication No. 145, 491-497

Sumnar, G., 1988, Precipitation: process and analysis, John Wiley & Sons, 455pp

Tamayo,J.; Segarra,D. & De La Rubia,J., 1988, Evaluation od SDUD WEFAX data by means of high resolution meteosat images, In proceedings of the 7th meteosat scientific users' meeting, Madrid, 27-30 Sep. 1988, EUM P04, 417-420

Troutman, B.M., 1982, An analysis of input errors in precipitation-runoff models using regression with errors in the independent variables, Water Resources Research 18 (4) 947-964

Troutman, B.M., 1983, Runoff prediction errors and bias in parameter estimation induced by spatial variability of precipitation, Water Resources Research 19 (5) 791-810

Tsonis,A.A. & Isaac,G.A., 1985, On a new approach for instantaneous rain area delineation in the mid-latitudes using GOES data, Journal of Climate and Applied Meteorology, 24, Nov, 1985, 1208-1218

Tsonis,A.A., 1984, On the separability of various classes from the GOES visible and infrared data, Journal of Climate and Applied Meteorology, 23, Oct., 1984, 1393-1409

Tsonis,A.A., 1987, Determining rainfall intensity and type from GOES imagery in the mid-latitudes, Remote sensing of enviroment, 21, 29-36

Turpeinen, O.M.; Abidi, A. & Belhouane, W., 1987, Determination of rainfall with the ESOC Precipitation Index, Monthly Weather Review. 115, 2699-2706

Turpeinen,O.M., 1986, Validation of the ESOC precipitation index, In proceedings of the 6th meteosat scientific users' meeting, Amsterdam, 25-27 Nov. 1986, Vol. II, EUM P01, NA

Weeks, W.D. & Hebbert, R.H.B., 1980, Comparicon of rainfall-runoff models, Nordic Hydrology, Vol. 11, 7-24

Weiss, M. & Smith, E.A., 1987, Precipitation discrimination from satellite infrared temperatures over the CCOPE mesonet region., Journal of Climate and Applied Meteorology, 26, 687-697

Weszka,J.S.; Dyer,C.R. & Rosenfield,A., 1976, A comparative study of tecture measures for terrain classification, IEEE transactions on systems, man and cybernatics, Vol. SMC-6, No. 4, April 1976, 269-285

Whitney,L.F. & Herman,L.D., 1979, A statistical approach to rainfall estimation using satellite data, In Satellite Hydrology (eds. Deutsch,M; Weisnet,D.R. & Rango,A.), proceedings of the AWRA symposium on Satellite Hydrology, Sioux Falls, S.D., June 1979, 139-143

WMO, 1965, Guide to Meteorological Instruments and Observing Practices, Repoprt No. 8

Woodley, W.L.,Olsen, A.R., Herndon, A. & Wiggert, V., 1975, Comparison of gauge and radar methods of convective rain measurements, J. of Applied Meteorology, 14, 909-928

Woodley,W.L.; Griffith,C.G. & Augustine,J.A., 1979, Rain estimation over several areas of the globe using satellite imagery, In Satellite Hydrology (eds. Deutsch,M;

Weisnet,D.R. & Rango,A.), proceedings of the AWRA symposium on Satellite Hydrology, Sioux Falls, S.D., June 1979, 84-91

Woodley,W.L.; Griffith,C.G.; Griffin,J.S. & Stromatt,S.C., 1980, The inference of GATE convective rainfall from SMS-1 imagery, Journal of Applied Meteorology, 19, 388-488

Wu,R.; Weinman,J.A. & Chin,R.T, 1985, Determination of rainfall rates from GOES satellite images by a pattern recognition technique, Journal of atmospheric and oceanic technology, Vol. 2, Sep. 1985, 314-330

Wylie,D.P., 1979, An application of a geostationary satellite rain estimation technique to an extratropical area, Journal of Applied Meteorology, 18, Dec., 1979, 1640-1648

Appendix A

This appendix details some of the computer programmes developed during the course of this thesis. The programmes are written both in 'C' and 'FORTRAN 77' and compiled using the Microsoft C Compiler and the C and Fortran compiler on the VAX main frame.

A.1	Geometric Transformations
Programme name:	TMPROJ.C
Location:	C:\Met on the IBM PC in the Remote Sensing Unit
Description:	For each pixel in a 512 x 512 screen window, the programme locates the corresponding pixel on the meteosat image in terms of x and y image coordinates. The programme uses the inverse Transverse Mercator Projection equations to obtain the geographical coordinates (Longitude and Latitude) of a given point (chapter 3 section 3.7.3). The geographical coordinates are used to obtain the x and y coordinates on the meteosat image (chapter 3 section 3.7.6).
Input:	None
Output:	A file containing the x and y image coordinates for the full 512 x 512 screen window.
Comments:	The programme is slow to run on the PC ($\approx$ 2 hours) but relatively fast on the VAX mainframe. Some global variables need to be initialized according to the area of interest and scale requirements.

A.1.1 Geometric Transformations Continued

Programme name: TMPROJ1.C

Location: C:\Met on the IBM PC in the Remote Sensing Unit

Description: Since the original programme was slow to run, it could not be used repeatedly as in the case where several images needs to be processed. The image coordinates calculated are the same for different images and therefore needs to be calculated only once. This programme retrieve these coordinates whenever required. Since only read and write commands are required, the process is fast and efficient.

Input: Output files of programme TMPROJ.C

Output: Image file containing the Tranverse Mercator Projection of the area of interest of Meteosat image.

Comments: None

A.2 Least Square Minimization

Programme name: LSQUARE.FOR

Location: VAX / CLUSTER Mainframe under CHIDLEYTRE.SID

Description: The programme optimize the coefficients of a given function using least square minimization algorithm. The given function calculates the weights assigned to each available gauge for an ungauged point. The weights are influenced by the distance of a raingauge from a point as well as the spectral information inherrent in the satellite images. The function is optimized by removing half the rain-gauges and comparing the actual and calculated rainfall values. The whole procedure is explained in more detail in chapter 5, section 5.2 and section 5.4.1

Input: A file containing coordinates of rain-gauge points and their respective rainfall values.

Output: Optimized coefficients of the objective function.

External Routines: 'E04FDF' NAG Library Routine for Least Square Minimization.

Comments: None

A.3 Multiple Regression

A.3.1 Model Adequacy

Programme name: BEST_MODEL.FOR

Location: VAX / CLUSTER Mainframe under CHIDLEYTRE.PSUD

Description: The programme uses different combinations of all the independent variables within the regression equation and outputs the best model according to the Cp criteria (see section 6.4.1.

Input: Rainfall values of known rain-gauges and their respective cold cloud durations for an event (daily rainfall).

Output: Significant independent variables.

External Routines: 'G02ECF' NAG Library Routine that uses the Cp algorithm.

'G02EAF'NAG library that calculates the residual sum of squares.

Comments: None

A.3.2 Calculation of Coefficients

Programme name: REG.FOR

Location: VAX / CLUSTER Mainframe under CHIDLEYTRE.PSUD

Description: This programme produces the coefficients of independent variables for the given regression equation and the calibration values for the adjusted CCD method.

Input: Rainfall values of known rain-gauges and their respective cold cloud durations for an event (daily rainfall). Also the output from the BEST_MODEL.FOR.

Output: Coefficients of independent variables and calibrations values for each known rain-gauge.

External Routines: 'G02DAF' NAG Library Routine that calculates the coefficients of independent variables.

Comments: None

A.3.3 Random Testing

Programme name: R_TEST.FOR

Location: VAX / CLUSTER Mainframe under CHIDLEYTRE.PSUD

Description: This programme produces random sequences of different number of rain-gauges form a given set of known rain-gauges. These different sequences of rain-gauges are than used to estimate rainfall at three different points within the catchment. The estimated rainfall is compared to the actual rainfall that has fallen at that point. The programme uses different methods of estimation and statistically investigates their accuracies.

Input: Rainfall values of known rain-gauges and their respective cold cloud durations for an event (daily rainfall).

Output: Mean square error for each rainfall estimation method at each of the three points.

External Routines: 'G02ECF' NAG Library Routine that uses the Cp algorithm.

'G02DAF' NAG Library Routine that calculates the coefficients of independent variables.

Comments: None

A.4 Rainfall Estimations

Programme name: DAILY_RAIN.C

Location: VAX / CLUSTER Mainframe under CHIDLEYTRE.PSUD

Description: This programme estimates the total catchment rainfall according to arithmetic mean, reciprocal, theissen, CCD and adjusted CCD respectively. It also stores the estimated rainfall value for each point in the calchment and presents this information of rainfall distribution as an image.

Input: Rainfall values of known rain-gauges and cold cloud durations of all points within the catchment. Also the output from the REG.FOR.

Output: Estimated daily rainfall according to different methods and their distributions

External Routines: None

Comments: None